The Effect of Thermal Degradation on the Crystallisation and Mechanical Properties of PEEK-Glass Fibre Composites

by

Andrew Martin Parkes

A thesis submitted to the University of Birmingham for the degree of

DOCTOR OF PHILOSOPHY

School of Metallurgy and Materials

College of Engineering and Physical Sciences

University of Birmingham

February 2018

ACKNOWLEDGEMENTS

I would like to express my sincere gratitude to everyone who has supported me during my PhD. I would like to thank my family and friends for all of their advice and encouragement.

I would also like to give special thanks to my supervisor, Dr. Mike Jenkins for his guidance, and Frank Biddlestone for his invaluable technical assistance and advice.

Abstract

To prevent the formation of ice on aircrafts, de-icing systems are incorporated into various structures. These can consist of composite structures, made functional through the addition of a heating system. To maintain control over the production of these systems, the composite must be formed in stages, the first of which is the impregnation of the glass fibres with the thermoplastic matrix (PEEK). Although there is a significant body of literature describing the infusion of PEEK into fibre reinforcement, there are many inconsistencies regarding the selection of hold temperature, time and pressure. This work sought to identify a set of optimum process conditions for the infusion of PEEK into a glass fibre fabric. The key considerations were the effect of process conditions on degradation and subsequent crystallisation of PEEK.

Thermogravimetric analysis (TGA) of poly(ether-ether-ketone) (PEEK) showed minimal weight loss due to degradation through extensive holds at T_m^0 (395^{o}C). However Differential Scanning Calorimetry (DSC) analysis indicated high levels of degradation through a decrease in overall crystallinity (X_c). The repeatability of DSC analysis was determined through the use of thermal cycling through a range of temperatures from above melt (350^{o}C) to above T_m^0. The number of runs obtainable, from a sample of PEEK before the effects of degradation occurred, decreased when hold temperature increased. However, a distinct change in degradation rate was observed above 380^{o}C. Results show that multiple runs of PEEK can be obtained at 380^{o}C, without the effects of degradation, while ensuring the removal of residual nuclei in the melt. Furthermore, the effect of degradation was demonstrated at temperatures significantly lower than those

previous reported in the literature, and can be observed due to the appearance of a second cooling endotherm.

The process of degradation affects the chemical structure of PEEK. Through Fourier-transform infrared spectroscopy (FTIR) of PEEK the effect of degradation can be measured in the variation in the height of peak 1653cm^{-1} (crystalline phase) and 1648cm^{-1} (amorphous phase). As the amount of nuclei available for crystallisation decreases the amorphous peak will increase in ratio in comparison to the crystalline peak.

Flash DSC, a novel thermal analysis technique, allowed analysis of thermal cycling of PEEK unachievable in conventional DSC. The fast heating and cooling rates available allowed the removal of any degradation caused in the heat/cool cycle, allowing only degradation caused by hold time at final temperature. Results showed comparability to conventional DSC analysis with an increase in degradation over 380^{o}C.

Hot press manufacturing was used to produce PEEK/Glass fibre laminates. Literature showed no definitive set of process conditions for laminate production. Recommended values for hold temperature, hold time and hold pressure were inconsistent. It was found that hold temperature of 380^{o}C, combined with 200 PSi pressure and 60 minute hold times produced laminates with the best mechanical properties. Ultimate tensile strength was showed to increase from 110 to 145 MPa as processing temperature was increased. A similar increase was observed through the process of pre-drying. The increase in mechanical properties shown when hold temperature and hold time were increased indicated that controlled thermal degradation of PEEK in laminate production

could increase mechanical properties due to the removal of previous nuclei in the melt, thus increasing nucleation from the fibre mat.

Table of Contents

Glossary of Terms

PEEK	Polyetheretherketone
GF	Glass Fiber
DSC	Differential Scanning Calorimetry
TGA	Thermogravimetric Analysis
FTIR	Fourier Transform Infrared Spectroscopy
Flash DSC	Flash Differential Scanning Calorimetry
SEM	Scanning Electron Microscopy
Tg	Glass Transition Temperature
ΔH_f	Heat of Fusion
ΔH_c	Heat of Crystallisation
X_c	Overall Crystallinity
T_m^0	Equilibrium Melting Temperature
T_{upper}	Upper value for ΔH_f measurement
T_{lower}	Lower value for ΔH_f measurement

1 Chapter 1: Introduction

1.1 Polymer Morphology

The origin of this thesis began with an industrial investigation into the processing conditions of PEEK and glass fiber for use in hot press production. During the research for this thesis it was discovered that there is a wide range of conditions recommended in the literature and these are dependent on the final properties needed from the PEEK/glass fiber laminate. Furthermore it was found that during processing the thermal stability of PEEK is affected due to degradation, and processing temperatures and times have a large effect on the extent of degradation and the following crystallisation in PEEK to temperatures below discussed in previous literature. This has been investigated in this thesis in regards to the extent of degradation caused by processing and the affect degradation has on the thermal analysis of PEEK using a variety of thermal analysis techniques. These results have then been discussed in the processing of PEEK/Glass fibre laminates and the effect that degradation may have.

Polymers are long, sometimes branched chain molecules, constructed from repeating units known as monomers, covalently bonded together. A semi-crystalline polymer consists of two phases; a crystalline phase consisting of layers of ordered material and an amorphous interlayer, the two phase model is shown in Figure 1-1. Polymers can be divided into a number of classes including, thermoplastics, elastomers and thermosets. In addition to linear chains, polymers

can be branched (with side chains extending from the backbone), cross-linked (with short interconnections between chains). Network structures can also form when the backbones are linked by branches [1].

Semi-crystalline thermoplastics are linear (or branched) polymers, which melt under the application of heat. 100% crystallinity is seldom (if ever) reached; therefore polymers always contain an amorphous region.

Amorphous polymer chains generally display coiling due to C-C bond rotation and there is 360-degree rotation through trans and gauche conformations, this is illustrated in Figure 1-2. The mobility of the polymer chains is highly temperature dependent. In the liquid state there is concerted C-C bond rotation, but as the temperature decreases, mobility reduces. There is a progressive reduction in chain motion until a temperature is reached at which there is no further long-range motion. This temperature is termed the glass transition temperature. The three-phase model of a semi crystalline polymer is shown in Figure 1-3.

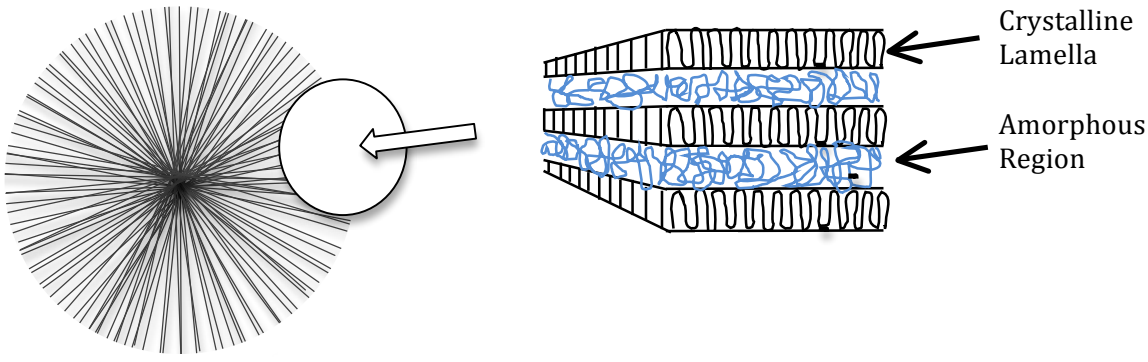

Figure 1-1: The amorphous and semi-crystalline phases of a polymer spherulite.

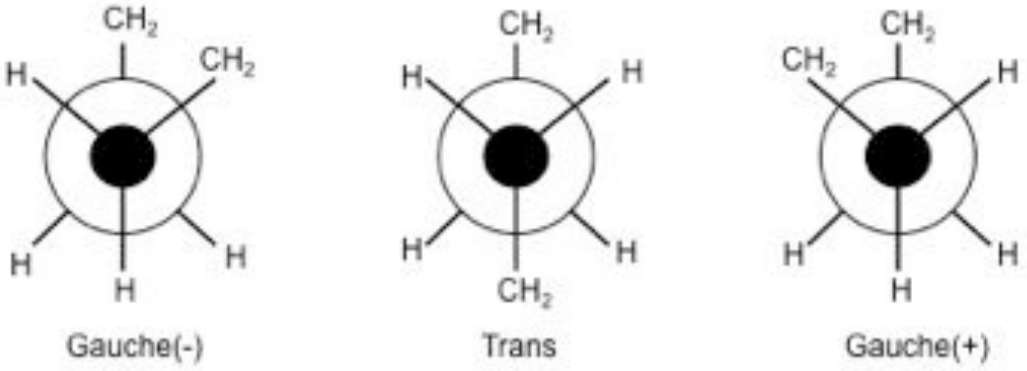

Figure 1-2: A schematic example of chain conformation.

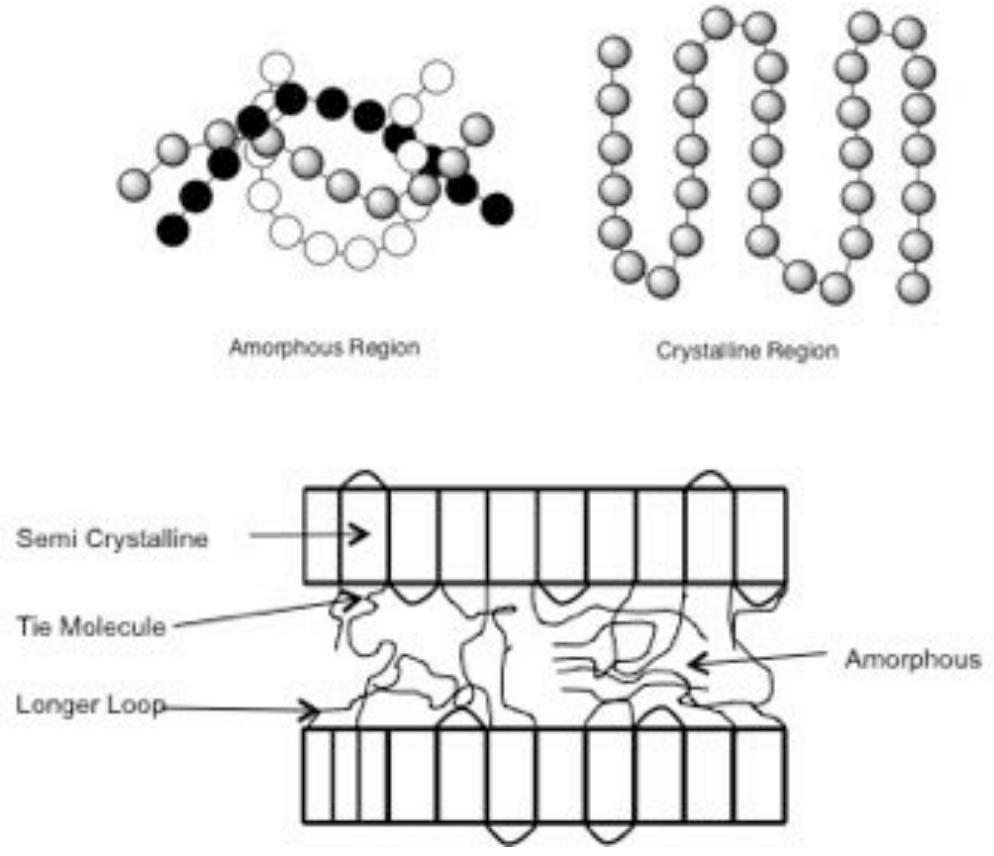

Figure 1-3: Schematic examples of crystal morphology.

Degree of crystallinity is an important characteristic of a polymer, as it determines mechanical properties, such as yield stress and impact resistance [2]. The two-

phase nature of the material allows deformation of the amorphous fraction of the polymer thereby increasing the toughness [3].

With increasing crystallinity, lamellae are organised via extensive branching into 3D superstructures known as spherulites. The small angle branching and splaying microstructure most commonly gives arise to the spherical shape [4]. Two types of spherulitic morphologies are shown in Figure 1-4. In Type A crystalline lamellae initiate from a central nucleus, and grow a varying speeds in all directions. Each crystal lamellae nucleate independently and the spherical symmetry extends to the centre of the spherulite. In Type B the spherical shape is obtained by continuous branching and fanning out from a single lamella crystal, however the centre shows unidirectional growth, which goes through a wheatsheaf stage [5].

Lamellae will radiate outward; generally chain folding direction will be transverse to growth direction. Mechanical properties are improved by the role of the tie chains between the lamellae; these act as bridging units, which are both interlamellar and interspherulitic in origin [6].

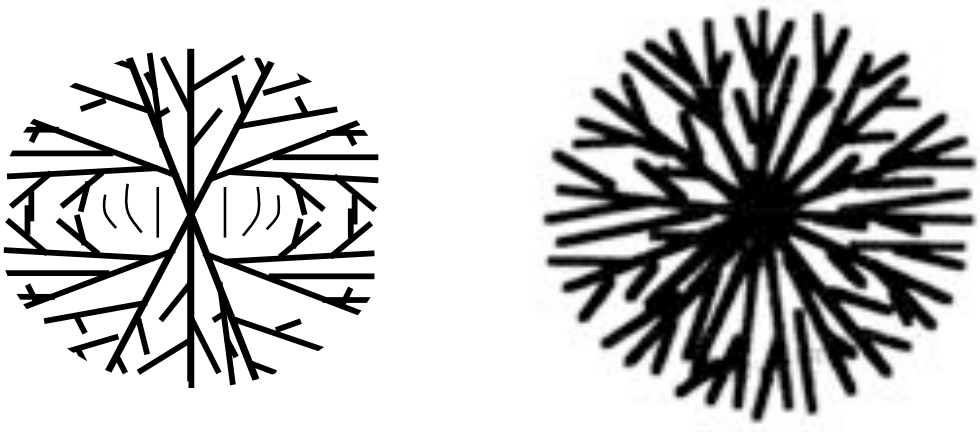

Figure 1-4: Two forms of spherulite formation. Type A - right, Type B – left (adapted from Price, 1959).

Spherulites can be characterised in terms of their birefringence, where they can be divided into four categories. Negatively birefringent are the most common type of spherulites found in polymers with a refractive index greater along the transverse direction than the growth direction [7]. Positively birefringent is when refractive index along radial direction exceeds the index along the transverse direction. These spherulites are less common, as the polarisability along the chain direction usually exceeds that of the other two principal directions [7]. Zero birefringence occurs when the optic axis of the spherulites is parallel to the viewing direction [8, 9]. Finally Chain-extended spherulites have been observed in some high-pressure crystallisation, specifically polyethylene [10].

Polymers are often shown as a two-phase model, describing polymers consisting of a clear ordered crystalline phase and a disordered amorphous phase, and that any transition phases between the two are minimal. However, many polymers show a

three-phase structure; due to a development of a rigid amorphous phase, which sits between the true amorphous phase and its crystalline region [11-13].

The three-phase model introduces an interphase between the crystalline and amorphous regions. Magill [9] showed the formation of three-dimensional crystals, requires chain folding, therefore surface energy where chain folding takes place, in the basal plane, will be different than in the lateral plane. Different types of chain folds (tight folds, loose loops and free ends) will give rise to an interphase between the crystals and the free melt [14]. This interphase has been widely discussed as the Rigid Amorphous Phase or Rigid Amorphous Fraction (RAF) (Figure 1-5). Results from Suzuki et al., Grebowicz et al. [15, 16] and Huo and Cebe [17] suggest that not all amorphous chains relax at Tg, therefore the Rigid Amorphous Fraction was introduced [15]. RAF described a portion of amorphous chains that do not relax at normal Tg, not coinciding with the expected behaviour of either the amorphous or crystalline phase, with the three-phases being mobile amorphous, rigid amorphous and crystalline phase. The amorphous layer is less mobile due to being constrained by surrounding crystals. RAF describes that interphase layer as closer to the amorphous region than the crystalline phase; this validated by work from Huo and Cebe [17] that observes the density of RAF to be close to the amorphous phase. However Bonnet et al. [18] used TMDSC and TMA measurements to describe the interphase layer as closer to the crystalline phase; this was described as the Pseudo-Crystalline phase.

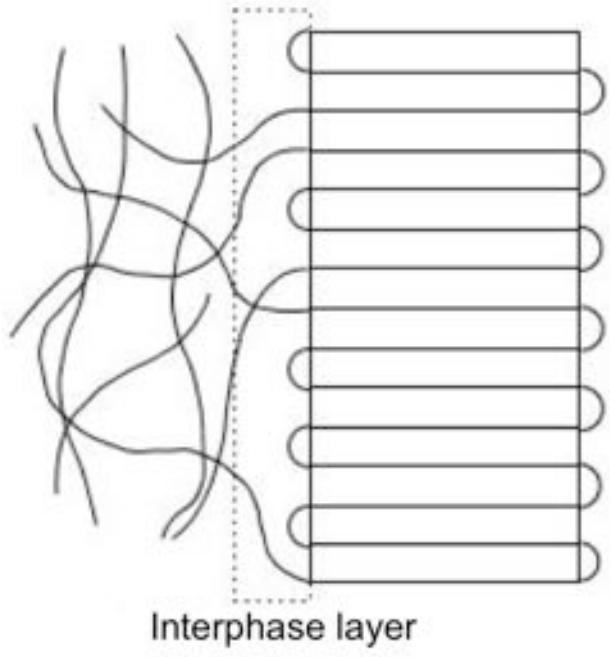

Figure 1-5: Schematic of interphase layer in polymers.

1.2 Crystallisation in Polymers

As an initially amorphous crystallisable polymer is heated through its glass transition temperature (Tg), crystallisation occurs. Factors affecting the extent of crystallisation include presence of orientation and melt temperature; furthermore molar mass and the presence of nucleating agents can all affect crystallisation [1]. When the repeat units of polymer chains are symmetrical and there are Van der Waals forces operating between the chains, crystallisation occurs more readily, when chains are branched and have high molar mass, the process of crystallisation is inhibited as chain movement and reptation is reduced, and chains get tangled easily [19].

Polymer chains begin to form an ordered structure initiated from nuclei, also occurring on cooling. Due to the formation of a more stable crystalline phase, Gibbs

free energy (ΔG) will decrease, resulting in a thermodynamic driving force, causing crystallisation. Formation of the nuclei occurs in two ways, homogenous nucleation, where small nuclei form randomly throughout the melt due to chain entanglements. If there are no existing nuclei, formation of nuclei occurs spontaneously, therefore for this to occur $\Delta G < 0$. Nucleation can also form heterogeneously, where nucleation occurs on foreign bodies such as dust particles, followed by growth of spherulites, as described above; the size of the spherulites is determined by the crystallisation temperature. Crystallisation may also derive from Self-nucleation; occurring due to pre-existing residual nuclei that may have survived the initial melt [19]. For spherulites to be roughly similar in size, all nuclei must begin forming at the same time/temperature. This is called Athermal nucleation and will occur during isothermal crystallisation. Thermal nucleation occurs when nuclei form at different temperatures thus creating spherulites of varied size.

In order for a polymer to crystallise, there must be a formation of a small amount of crystalline material due to fluctuations in density or order in the super cooled melt [20]. The forming of these primary nuclei is called primary nucleation (homogenous or heterogeneous). Secondary nucleation (heterogeneous) is the result of continuous crystallisation on the growth surface due to the addition of extra polymer molecules. Tertiary nucleation describes nucleation occurring along an existing crystal edge involving two crystal faces. (Figure 1-6).

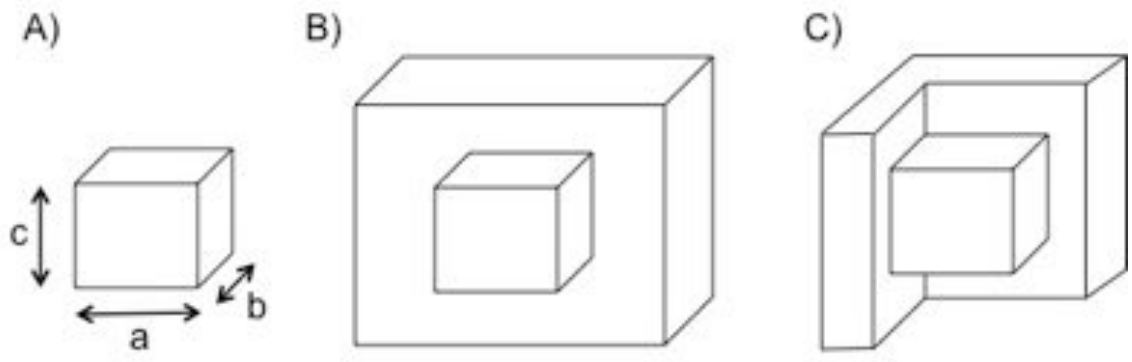

Figure 1-6: Primary (A), Secondary (B), and Tertiary crystal nuclei (C). (Adapted from Huang et al. 94)

1.2.1 Isothermal Crystallisation and the Avrami Equation

Isothermal crystallisation is a process of holding a polymer for a period of time at a constant temperature, thus allowing crystals to grow. Melt crystallisation involves heating above a material's melting point and then fast cooling to the desired hold temperature, allowing for isothermal holds at high temperatures (around T_m). Cold crystallisation involves heating an amorphous sample to the desired hold temperature, this used for hold's at lower temperatures (around T_g).

Models describing the development of crystallinity have been developed by authors, such as Avrami. The Avrami equation as shown is Equation 1-1 [21] can be used for analysis of isothermal crystallisation.

$$1 - \frac{X_t}{X_\infty} = \exp\left(-Zt^n\right)$$

Equation 1-1

Where X_t/X_∞ is the relative crystallinity at time t, Z relates to a composite kinetic parameter containing nucleation and spreading rates, and n is a mechanistic constant, which describes the mechanisms of both nucleation and crystal growth. Descriptions of various n values are shown in Table 1-1.

n value	**Crystallisation Mechanism**
4	Homogenously nucleated spheres
3	Heterogeneously nucleated spheres
3	Homogenously nucleated discs
2	Heterogeneously nucleated discs
2	Homogenously nucleated rods
1	Heterogeneously nucleated rods

Table 1-1: Crystallisation and growth mechanisms for different values of n (Avrami exponent).

Both the n and Z values can be derived from the gradient and intercept of the line when Equation 1-2 is plotted against log time (nlogt + logZ).

$$ln[-ln(1-\frac{X_t}{X_\infty})] = nlnt + lnk$$

Equation 1-2

When the Avarmi equation is applied to polymers there are six assumptions made [19].

1. The rates of nucleation and growth increase with time in a linear fashion
2. No secondary crystallisation occurs
3. The volume remains constant during crystallisation
4. The impingement of crystallites causes growth to cease
5. Crystals keep their original shape (n) until impingement occurs
6. There is no induction time before crystallisation

Z values can be determines using Equation 1-3.

$$Z = \frac{Ln\,2}{(t_{1/2})^2}$$

Equation 1-3

As stated above, Avrami analysis assumes no secondary crystallisation occurs. Theories of secondary crystallisation will be discussed further later, however there is debate regarding when secondary crystallisation takes over from primary, or if these two processes occur concurrently. Figure 1-7 shows the change in growth of primary to secondary crystallisation over time. This describes that as process time

increases a shift from primary crystal growth to secondary crystal growth occurs. Therefore kinetic analysis is rendered somewhat unsatisfactory due to the difficulties in resolving the two processes of crystallisation.

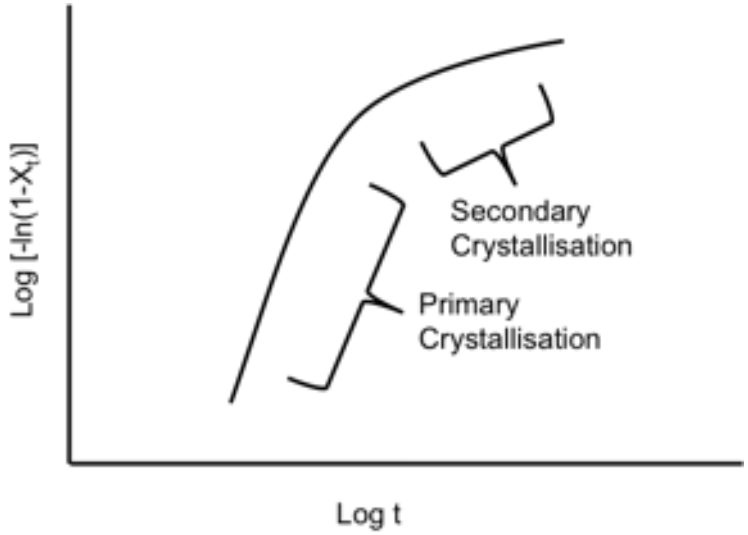

Figure 1-7: Schematic of change in growth from Primary and Secondary Crystallisation over time.

Banks et al. [22] proposed a differential form of the Avrami equation using isotherms of polyethylene in terms of a two time separate stages. Equation 1-4 shows stage 1, where $X_{p,t}$ describes the crystallinity formed by primary processes at a time t, and $X_{p\infty}$ is the total crystallinity formed by the primary process. $X_{p\infty}$ is adjusted to yield a constant n value over the primary process.

$$X_{p,t} = X_{p\infty}(1 - \exp\{Z_{p,t}\}) \qquad \text{Equation 1-4}$$

Values of n were obtained from Equation 1-5, where several $X_{p\infty}$ values were used in an iterative manner to find the conditions under which n remained constant for the longest period of time.

$$n = -t\left(\frac{dX_{p,t}}{dt}\right)\left(X_{p\infty} - X_{p,t}\right)\ell n\left[\frac{X_{p\infty}}{1-X_{p,t}}\right]^{-1} \qquad \text{Equation 1-5}$$

Using this approach, a sharp transition from primary to secondary crystallisation was observed.

1.2.2 Non-isothermal Crystallisation

Non-isothermal crystallisation is the process of allowing crystal growth with a constant heating or cooling rate. This process holds increased industrial interest over isothermal crystallisation as it closely mirrors industrial conditions. Changes in cooling rates greatly effect development of crystallinity. A slower cooling rate will give rise to a higher crystallisation temperature [23]. According to Hoffman and Lauritzen [24] nucleation theory described below, crystal growth is favoured above nucleation at higher crystallisation temperatures. Therefore slower cooling rates give rise to lower nucleation density and larger spherulites. At faster cooling

rates total crystalline structure will be reduced due to less time available to crystallise.

The nucleation and growth rates of crystallisation during non-isothermal crystallisation are in a constant state of change due to dependence upon the degree of undercooling. Inaccuracy in results often occurs due to thermal lag and instrumental error when temperature does not remain constant [23]. All this, means kinetic analysis of non-isothermal crystallisation is increasingly difficult. Ozawa [25], developed one of the most popular models. By modifying the Avrami model, due to replacing the time function with a cooling function, the evolution of crystallinity with respect to time instead of temperature can be analysed. However like Avrami analysis, Ozawa analysis doesn't take into the account of secondary crystallisation. Cebe and Hong [26] showed that over a range of cooling rates, a large portion of the overall crystallinity in PEEK comes from secondary crystallisation, and that higher n values obtained for PEEK in non-isothermal conditions were due to changes in linear growth rates.

Cooling rate will effect the nucleation on fibre surfaces in carbon fibre PEEK composites [27]. By testing short beam shear stress of laminates it has been found that laminates cooled at or above 60^{o}C/min favour crystallisation in the polymer matrix over nucleation at the fibre surface. The critical rate for nucleation in the fibre surface lies between 30^{o}C/min and 60^{o}C/min.

1.2.3 Secondary Crystallisation and the HL Theory

A commonly adopted model for polymer crystallisation proposed by Hoffman and Lauritzen [4] is based on a secondary nucleation theory, describing crystallisation as a function of both nucleation and spreading events. The kinetics of secondary crystallisation are broken into two processes with associated rates, 1) nucleation of the polymer 2) the rate of which the polymer grows on the surface/lateral growth rate. Nucleation is described in three regimes (Figure 1-8 and Figure 1-9). Regime I, when growth rate (g) on the front laterally exceeds secondary nucleation (i) rate (g>>i). Regime II occurs when growth rate is comparable or smaller than nucleation rate, causing secondary layers to form before the initial layer has been covered (g≤i). In Regime III lateral growth is inconsequential to the overall growth rate, due to the nucleation of multiple sites (i>>g). In Regime III small cluster size and high nucleation rate causes a rough growth that is re-established every three or so stems [28] due to the high nucleation rate causing growth to only occur in small areas either side of the nucleus. The molecular mobility of the chains is also reduced due to the low temperatures associated with regime III. Crystals grown in regime III are spherulitic and exhibit chain folded lamellar habit [28-30] similarly to region II, however they are expected to have lower crystal perfection and melt at lower temperatures [31]. Current thinking links the concept of polymer chain motion via repetition to the nucleation theory of Hoffman and Lauritzen [24].

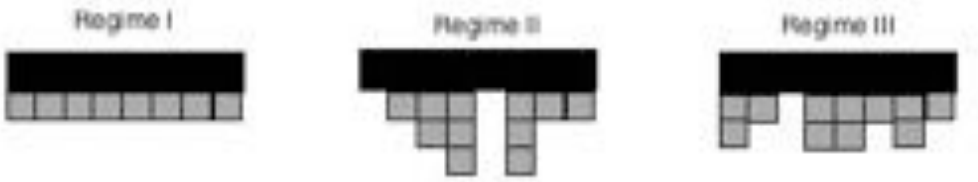

Figure 1-8: Schematic images of the Secondary Nucleation Theory. The differences between the growth rates in each regime change is shown.

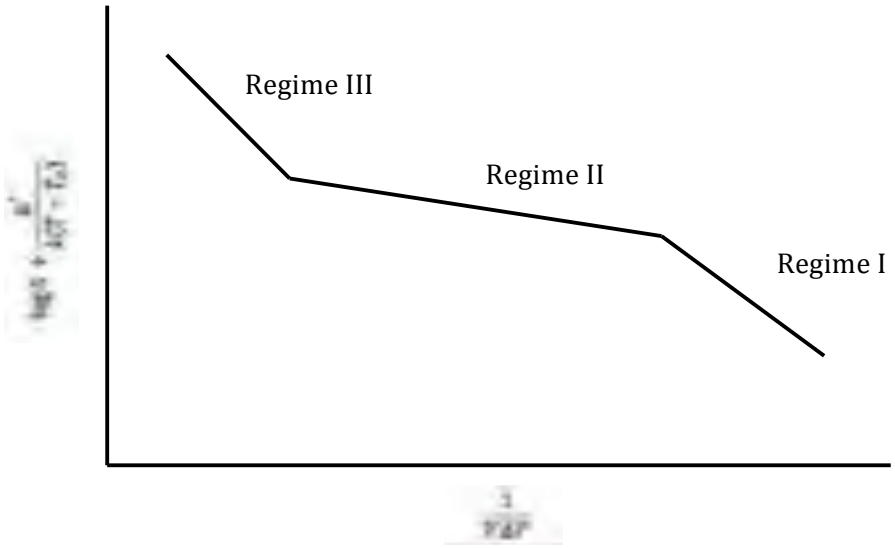

Figure 1-9: Secondary Nucleation Theory. Describing the formation of crystal growth (y-axis) as crystallisation temperature is increased (x-axis). (Adapted from Hoffman and Lauritzen, 1960).

The basis of secondary crystallisation is the formation of new crystals, however the nature and location of these crystals is widely debated. The Lamellar insertion model [32, 33] describes secondary crystals forming in the interlamellar amorphous layer as thinner lamellae. Hsiao et al. [33] used PEEK to determine this

formation of new lamellae due to a decrease of long spacing and lamellar thickness, however the amorphous layer thickness remained constant. However this theory was challenged by Verma et al., [12, 34] who argued the constant thickness of the amorphous layer is inconsistent, and secondary lamellae form between the lamellar stacks. This lead to the stack insertion model, [32, 35] in which the thinner secondary lamellae form in the interlamellar stacks. Work by Srinivas et al. [36] is consistent with this model of secondary crystallisation. A third model, Bundle-like secondary crystallisation model [37] describes crystals forming as bundle-like or fringed micelle type. These crystals then form in between the pre-existing crystals in the amorphous layer, either interlamellar or in stacks. These crystals are often found at lower temperatures and develop into mosaic blocks as temperature increases. A schematic of these three models can be found in Figure 1-10.

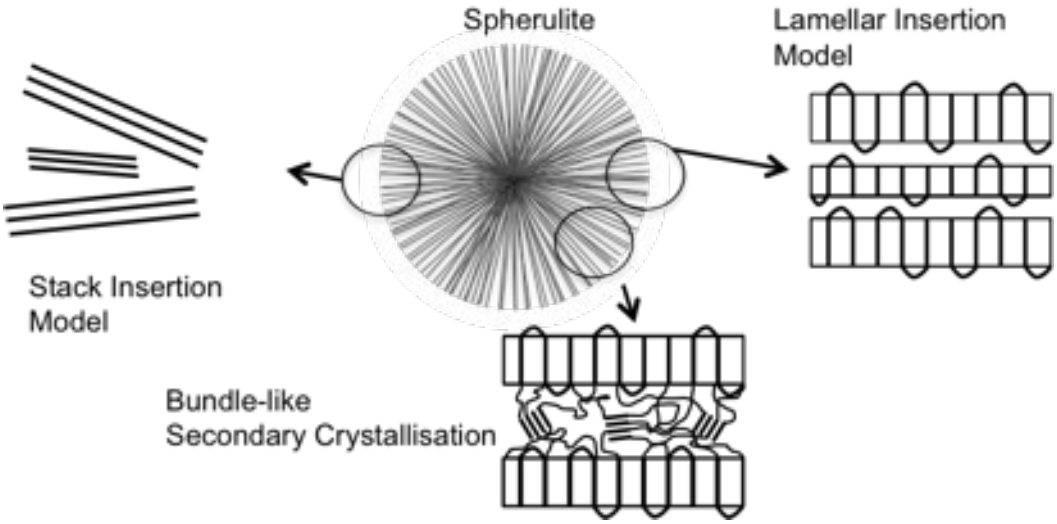

Figure 1-10: Schematic describing a number of Secondary Crystallisation Models.

1.3 Polyetheretherketone (PEEK)

Polyetheretherketone (PEEK) is a tough aromatic polymer with excellent mechanical and chemical properties such as very high thermal stability and good chemical resistance [38], with a high Tg of 143^{o}C [39], a high melting point around 343^{o}C [40], PEEK is therefore an attractive high-performance engineering thermoplastic. The high strength, melting point and dialectic properties make PEEK a perfect choice for use in aerospace applications. Its properties also make it a desirable matrix material in carbon/glass fibre reinforced composites as its high bond strength leads to decreased risk of delamination and moisture impregnation. These properties arise from its aromatic structure (Figure 1-11) and high nucleation density, which allows the polymer to crystalize readily. PEEK can be made amorphous or can be up to 43% crystalline depending on cooling rate from the melt [41]. PEEK is widely used in automotive and aerospace industries [42] due to service temperatures of up to 260^{o}C, and modulus of around 3.2GPa.

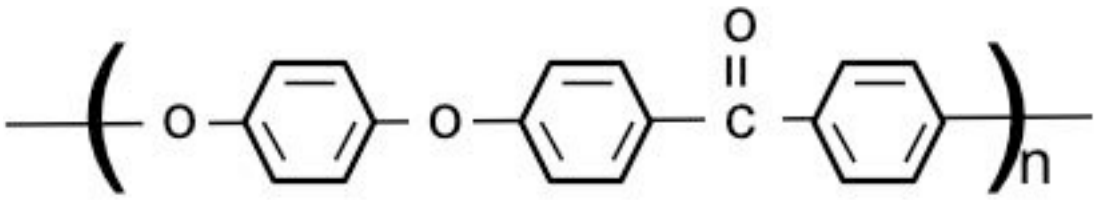

Figure 1-11: The chemical repeat unit of Polyetheretherketone (PEEK)[41]

The first reported synthesis of wholly aromatic poly(ether ketone ketone)s (PEKK) was in 1962 by Bonner [43]. Isophthaloyl chloride or terepthaloyl chloride was condensed with diphenyl ether using nitrobenzene as a solvent and aluminium

trichloride as a catalyst. Johnson et al. [44] attempted to synthesise PEEK by polycondensation of bisphenolate with activated dihalides using DMSO as a solvent and NaOH as a base. However due to crystallinity and resulting insolubility of polymers in DMSO, high molecular weight polymers were difficult to produce. Attwood [45] used diphenyl sulfone as a solvent to successfully produce high molecular weight PEEK (Figure 1-12). This technique was used to commercialise PEEK by ICI in 1982 [46].

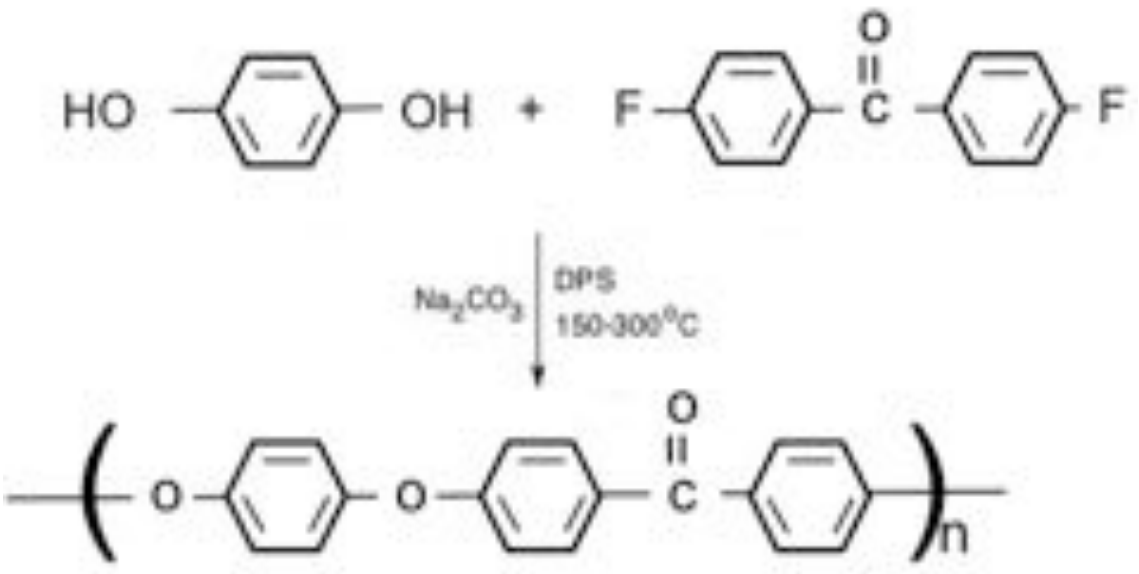

Figure 1-12: Schematic of the synthesis of PEEK.

PEEK's physical properties, just like all semi crystalline polymers are dependent on the microstructure, therefore they are sensitive to the process conditions such as heating and cooling rates.

In regards to the Hoffman and Lauritzen [24] theory on polymer crystallisation, regime I is not seen in PEEK [31]. The transition from regime II to III crystallisation

has been observed around 297°C for both isothermally cooled [29, 31] and non-isothermally cooled PEEK [30].

Blundell and Osborn reported [39] the peak for isothermal crystallisation of PEEK at 230°C. However literature varies in value for both peak crystallisation time and rate, often due to varied molecular weight of PEEK used in these studies. Crystallisation kinetics vary in respect to molecular weight due to its influence on molecular mobility caused by changes in chain length, the molecular mobility of the chains are also affected due to undercooling. Longer chain lengths are associated with high molecular weight, where there are more restrictions upon molecular movement due to a large number of chain entanglements. Day et al. [31] showed that the rate of crystallisation in PEEK was dependent upon molecular weight, with an increase resulting in a decrease in non-isothermal crystallisation temperature. Lu et al. [47] used wide angle X-ray scattering (WAXS) to show that lower molecular weight PEEK contained larger spherulites and a thicker lamellae thickness. Crystalline perfection was also high in low molecular weight PEEK. The melting temperature of low molecular weight PEEK is however lower than that of high molecular weight PEEK, due to the shorter chain lengths. As molecular weight increases, T_m will increase due to larger chain lengths, however this will be offset and T_m will then begin to decreases due to a lower perfection of crystals [47].

1.4 The Crystalline Morphology of PEEK

Various Microscopic investigations confirm that PEEK exhibits a spherulitic morphology. Methods used include, polarizing light microscopy [29], optical

microscopy [47], transmission electron microscopy (TEM) [48, 49] and scanning electron microscopy (SEM) [50, 51]. Due to the difficultly in observing the microstructure of PEEK, permanganic etching was used to allow the microstructure to be observed under SEM. When the nucleation density of PEEK is extremely high, a sheaf-like structure has been found, limiting the development of spherulites [12]. This sheaf-like growth in homogenously nucleated PEEK, has also been observed using TEM by Lovinger and Davis [49]. Blundell and Osborn [39] reported spherulitic radii of 12.7 and 21.9μm for crystallisation temperatures of 240°C and 287°C respectively, showing the radius of PEEK spherulites is affected by crystallisation temperature, linking back to the work of Hoffman and Lauritzen [24].

When crystallised at high temperatures, between 285°C and 300°C, thin films of PEEK have a tendency to form spherulites consisting of very thin, highly oriented lamella [49]. These lamellae are edge-on, meaning they are perpendicular to the radial growth direction, shown in Figure 1-13. Although this has been observed at all crystallisation temperatures, it is most common at high crystallisation temperatures, due to low nucleation density and high molecular mobility.

PEEK Thin Film Typical

Figure 1-13: Showing a Highly orientated, edge-on PEEK spherulite (left) compared to a spherulite of a typical polymer (right) (Adapted from Lovinger and Davis, 1985) [49].

Although specific details of their experiments varied, Cebe et.al [52], Lee et.al [53] and Talbott et.al [54] have all controlled crystallinity in PEEK by altering the cooling rates and analysing the effect on the mechanical properties of PEEK. Both Lee et.al [53] and Talbott et.al [54] tested dog bone specimens of PEEK under differing conditions, such as different strain rates. Cebe et.al [52] used thin films of PEEK. Due to the variability of these experiments an exact correlation between the test results cannot be expected however, the results for tensile yield stress and modulus with respect to degree of crystallinity are similar in all 3 experiments, with all showing the higher degree of crystallinity, brought upon by slower cooling rates, increased the tensile strength and modulus of the PEEK is obtained.

1.5 Double Melting of PEEK

Double melting behaviour is regularly observed in PEEK [39], where PEEK shows two endothermic phase transitions during melting. The double melting peaks has been attributed to two main hypotheses. Hypothesis one states that the two peaks are due to two different crystals or crystal morphologies [55] and a bimodal distribution of lamellar thicknesses, resulting in melting of the thinner and thicker

lamellae which are associated with the low and high endotherm, this is known as the dual lamellae population model [56, 57]. This model can be split into two. Dual lamellar stack insertion model describes thin and thicker lamellae in separate stacks. Lamellar insertion model descries thinner lamellae between thicker lamellae in the same stack [33, 58]. The second hypothesis states the two peaks are due to melting and recrystallization of the crystal morphology relating to the prior thermal history [59], any lamellae present melt and give rise to the lower endotherm, however continuous recrystallization (lamellar thickening) occurs resulting in lamellar which melt at higher temperatures, resulting in the higher endotherm. This is known as the melting-recrystallization model [39, 40].

1.5.1 Melt-Crystallisation Model

In the melt-crystallisation model the lower endotherm occurs after T_c, due to the melting of crystals that exist at room temperature prior to the heating scan; the higher temperature endotherm, results from the melting of crystals and thicker lamellar formed by simultaneous melting and recrystallisation during the DSC scan. The point of the higher endotherm represents the point where the on-going competition between melting and recrystallisation passes through maximum [39, 40].

Blundell [60] further supported this theory by partially melting PEEK at three separate temperatures between crystallisation and the higher melting endotherm, as an attempt to show that by interrupting the heating scan an increase in crystal perfection is created, therefore introducing crystals of greater stability. During reheating the melt and recrystallisation process would continue to reoccur and

another lower endotherm would be produced. His results strongly indicated that this process was occurring. As well as showing that the lower endotherm was moveable while the upper endotherm remained unchanged, Blundell also showed that as heating rate increased, the position of the lower peak also increased, while the upper peak decreased. This was collaborated by Lee et al. [53], who showed the same features when PEEK was cold crystallised (high super cooling), the reason for this being that as heating rate increased the time for recrystallisation and perfecting of the crystals decreased. However in melt-crystallised peak (low super cooling) the upper peak didn't change, as due to the slow crystallisation the chains are more perfect and therefore more independent of heating rate changes. Lee et al. adapted a model (Figure 1-14) from poly (**ε-**caprolactone) [53, 61] to show that dual melting was the sum of four contributions: melting of original crystals, their recrystallisation, re melting of crystallised polymer and melting of residual crystalline regions. They stated that there would be crystallisation exotherm, which is obscured by the melting endotherm, therefore obscuring the true melting peak. When heating rate is increased, recrystallisation time is decreased, therefore reducing the size of these peaks. If heating rate is increased to a high enough rate then recrystallisation is restricted resulting in a single melting peak signifying the melting of the original crystals.

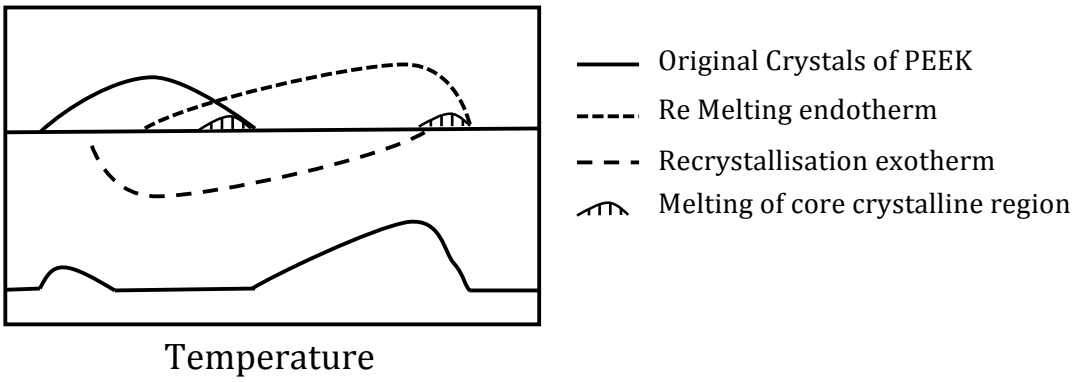

Figure 1-14: Schematic representing the double melting endotherm of PEEK. (Adapted from Lee et al., 1987)

1.5.2 Dual Lamellae Population Model

Cheng et al. and Bassett et al. [11, 50, 62] both helped develop the Dual Lamellae Population Model, which stated that two different populations of lamellar formed at different stages of crystallisation resulted in dual melting endotherms. Lattimer et al. [57] however suggested they form simultaneously. Basset et al. [50]observed by melt-crystallising samples for variety of times at 310^{o}C that crystals formed first have a higher melting than those formed secondary, therefore the higher melting peak cannot be formed by the lower peak and that the two separate peaks represent two different stages of morphology, primary and secondary.

Cebe and Hong [26] proposed that the lower melting point occurs due to secondary crystallisation, a population of smaller crystals, which are less stable, existing between the larger primary lamellae. This is in accordance with Tan et.al [13], which showed a crystallisable meta-stable melt to exist upon the reheating to Tc at slow DSC scans. This meta-stable melt matches the less stable inter lamellar crystals as described by Cebe and Hong [26]. Hsiao et al. [33] described that above

the lower endotherm the thinner lamellae will have melted away leaving only the thicker lamellae. Shown in Figure 1-15.

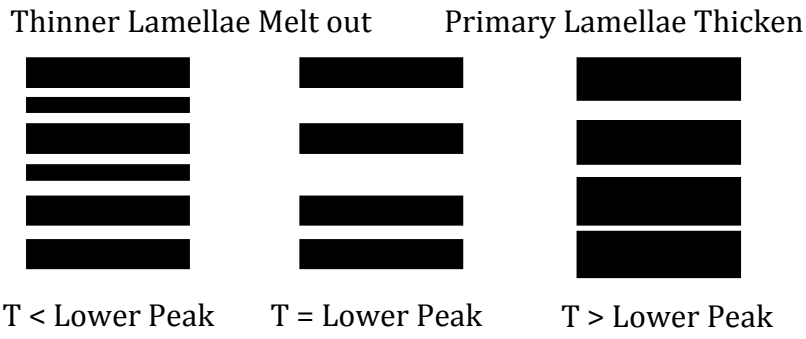

Figure 1-15: Dual Lamellar Population Model.

Verma et.al [12] used real time small angle X-ray scattering (SAXS) to show that secondary lamellar stacks that form later, between the primary lamellar stacks, melt first giving rise to a lower endotherm. These observations were supported by Lattimer et al. Wang et al. and Hsiao et al. [33, 57, 63] supported dual lamellar thickness models and showed an increase in lamellar thickness with increased crystallisation temperature.

Wei et al. [64] concluded that dual melting is a combination of both melt-recrystallisation theory and dual lamellae theory. If the crystallisation temperature is above 320^{o}C dual lamellae population is the mechanism of double melting due to the higher crystallisation temperature, however below 320^{o}C a combination of both theory's results in double melting. The lower endotherm is the result of melting of secondary crystals and instantaneous recrystallisation; the upper peak

then represents the melting of the perfected and primary crystals. This difference between single and multiple lamellae formation at low and high temperatures respectively was shown using SAXS and wide-angle x-ray scattering (WAXS) by Fougnies et al. [65, 66].

In both isothermal and non-isothermal crystallisations, the low melting endotherm appears just above T_c. The higher melting point will remain constant, at around 335^oC and will not be affected by T_c [26, 67]. Lee and Porter reported that as crystallisation time is increased, the low temperature endotherm shifts to a higher temperature; however the high temperature endotherm does not change. Lee and Porter [40] also reported that as the heating rate is increased, the time and amount of crystallisation decreases, resulting in a smaller heat of fusion for the high temperature melting endotherm and an increase in the heat of fusion of the low temperature endotherm.

Zhang and Zeng [68] discussed that when PEEK is held above its melting point both crystallisation and crosslinking can occur. Due to an increase in the higher melting endotherm and its ΔH_f it is considered that crystallisation is happening at the surface of the remaining lamellae with crosslinking occurring further away from the lamellae due to restrictions on the chains. An adapted model is shown in Figure 1-16.

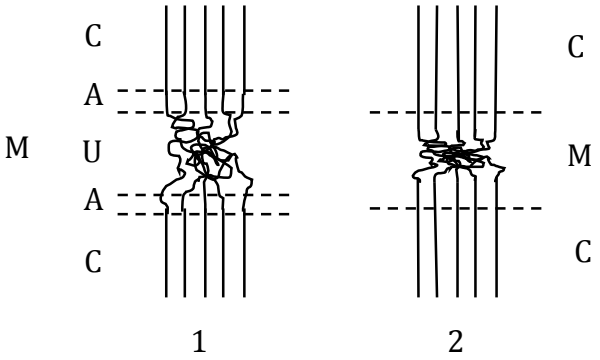

Figure 1-16: Adapted model showing crystallisation and crosslinking in PEEK held above its T_m (1) at beginning of annealing (2) sometime later. C – Crystalline Region, M – Melting Region, U – Region where crosslinking occurs, A – Region where crystallisation occurs.

Triple melting peaks have been observed in some polymers, specifically poly(ethylene terephthalate), PET. These three peaks have been attributed to the melting of the primary and secondary lamellae, which is formed on crystallisation, and the melting of the thickened lamellae, which was formed on heating to the melting point [69].

1.5.3 Isothermal Crystallisation and Avrami Analysis of PEEK

Isothermal crystallisation in PEEK has been shown to be at its most rapid at 230^{o}C [39]. Figure 1-17 shows when temperatures approaching Tg and T_m are used, the rate of crystallisation decreases. This intermediate temperature between Tg and T_m corresponds to the point at which nucleation and spreading events are interacting most favourably giving the fastest rate of crystallisation. Wang et al.

[63] showed that the fastest isothermal crystallisation kinetics where found around 230°C.

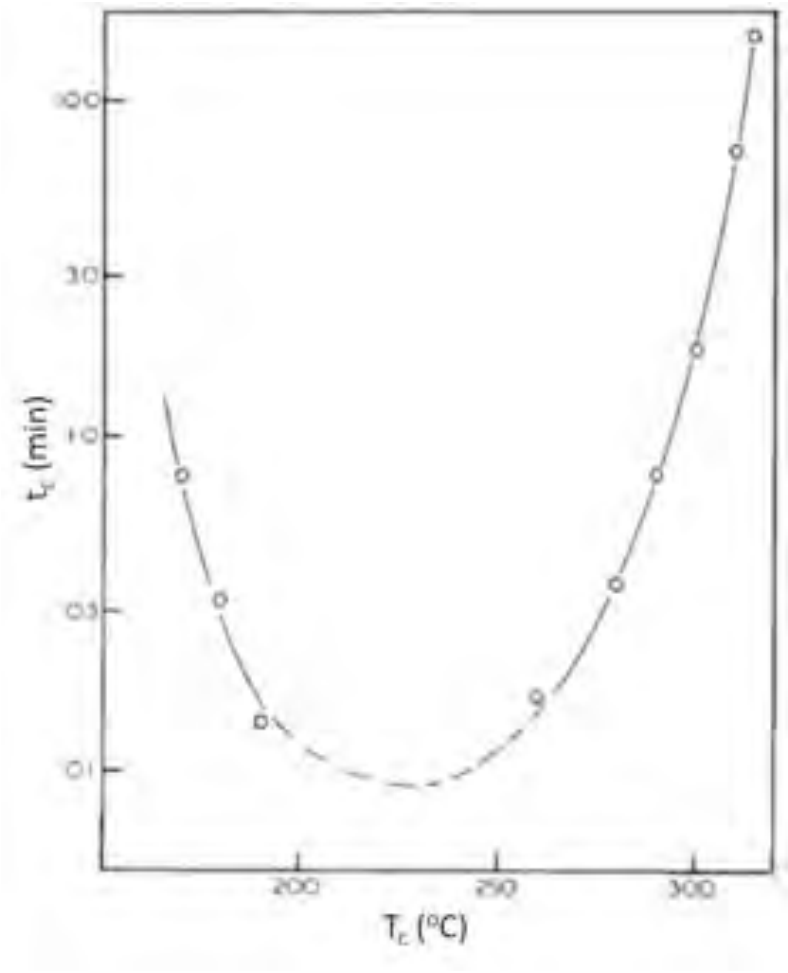

Figure 1-17: Crystallisation half life against isothermal crystallisation temperature for PEEK [39].

In Avrami analysis of commercially synthesised PEEK n values remain constant at 3 for a wide range of crystallisation temperatures (164°C to 315°C) [26, 70], which is consistent with heterogeneously nucleated spherulitic growth [71]. Lu and Hay [72] stated that a change in n value indicates a shift from primary to secondary

crystallisation. This slower process is described as 'filling in the holes of primary crystallisation' [22]. Hay and Kemmish [70] obtained an n value of 1 for secondary crystallisation, which indicates a one-dimensional rod like growth of crystals.

Crystallisation of PEEK has been investigated by Tardiff et al. [73] using Fast Scanning Calorimetry (Flash DSC). By investigating isothermal crystallisation at temperatures between 170°C and 310°C, an Avrami exponent of close to 3 was shown, which indicates an instantaneous nucleation (matching Cebe and Hong, [26]), followed by spherical growth and that crystallisation kinetics has a maximum of 230°C. After crystallisation at 250°C, a single melting endotherm was produced; temperatures below 300°C produced a broad peak, where a sharp peak was observed at crystallisation temperatures of 300°C and 310°C. Tardiff et al. [73] described the appearance of a single peak the result of stable crystal formation, which do not undergo reorganisation. However the subsequent melting endotherm at 250°C, was a broad peak which may represent the continued recrystallisation of the crystal structure.

Further investigation of isothermal crystallisation indicated the double melting peaks is a result of reorganisation during heating, a point also confirmed by Jin et al. [74]. Single melting peaks were obtained from isothermal holds above 260°C, which was related to crystals melted during the isothermal hold. With increased melting temperature, recrystallisation kinetics slow down, resulting in a shift in lower endotherm temperature and reduction in the upper endotherm. Continuation resulted in complete removal of the second melting endotherm. Both

Jin et al. and Tradif et al. [73, 74] used heating and cooling rates of 2000^{o}C s^{-1}, which provided acceptable crystallisation prevention.

1.6 Specific applications of PEEK

1.6.1 Aerospace

Fibrous composites have been used in the aerospace industry since the first flight of the Wright brothers in 1903. However aerospace design became dependent on metal alloys, specifically aluminium alloys. It took until the late 1960s before new composites were developed and applied. Firstly on a demonstration basis to military aircraft, however they were mostly brittle epoxy resins, which had poor tolerance to low-energy impact such as runway debris or impacts caused by manufacture or service. Although this tolerance was improved, damage-tolerance was still not as high as in thermoplastic materials. With the development of knowledge and processing techniques, improvements in fibre and matrix materials lead to the replacement of aluminium and titanium alloys on both military and civil aircrafts. Continuous development has led to the growing use of composites on more advanced applications such as unmanned aerial vehicles (UAVs) and satellites [75, 76].

The reason for the growing use of fibre filled composites such as PEEK composites, is due to their desirable key properties such as high specific strength and stiffness compared to metals, by reinforcing with glass or carbon fibre results in high strength to weight ratios that exceed those common in other aerospace materials. Another advantage of using composite and fabric in aerospace is their ability to be formed into specific shapes and needs. Maintaining these key properties at a

reduce weight is hugely important due to saving in fuel and therefore cost. By replacing metal alloys with PEEK composites a saving of up to 50% in weight can be made.

With the production of these composites an increase in cost of production occurs. Hand lay up techniques used to stack layers to create laminates; production costs can increase by 60%. The development of new technology is helping to reduce these manufacturing costs, such as the use of thermal oven processing instead of an autoclave can reduce processing time and energy by 90% resulting in a 50% cost saving. Other processes such as vacuum moulding and resin transfer moulding (RTM) are now also widely used [75, 76].

The market for PEEK in aerospace is growing due to the desire to produce lighter components and develop faster processing speeds. PEEK shows a high impact resistance over epoxy resins used in aerospace and posses at very high shelf-life at ambient temperatures, also high wear and fatigue resistance and high chemical resistance. [75, 76]. Manufacturers have developed PEEK composites for a wide range of aerospace technologies, however the development of PEEK films into aerospace is relatively new. Film based composites are often used in the automotive industry where a wide range of parts are produced from organosheet (a glass fibre reinforced semi-finished thermoplastic composite).

One of the largest problems for an aircraft is the build up of ice, for example, on the leading edge of the wing. Where potential dangers are substantial. It will essentially upset the lift of the wing and is most common at low altitudes, e.g. when landing or taking off. Another problem with ice build-up is ice shredding. Ice will

break off in large chunks and impact other components of the aircraft; this can cause damage to engine, a turbine blade or a fan compressor. The most common method of dealing with the ice build-up is 'bleed air'. In this process hot gas is diverted from the engine and pumped around the wing. This causes the following issues; it causes an efficiency penalty on the engine as you are removing energy from the airflow. It can also overheat composite wing structures, as it is not a controllable process. Other processes used include pneumatic systems, which have a rubber boot over the wing, which is inflated to crack off the ice, and electro thermal ice systems such as foils, wires and carbon nanotubes.

A wide body of research found in the literature discusses results of PEEK and carbon fiber. The aim of this thesis is to find a set of processing conditions for the production of PEEK and glass fiber laminates. The reasoning for this is an industrial one. Glass fiber improves the insulation behaviour in laminate production as it is non-conductive, furthermore glass fiber has been found to integrate easier and improve impregnation of laminates with the addition of further functional layers, whereas further compensations needs to be made for carbon.

Carbon fiber is lighter than glass which offers weight benefits, carbon also offers increase in strength however, there is an overall cost benefit and lower tensile modulus (improves flexibility for complex parts) which can be achieved in the use of glass fiber. Although final mechanical properties will be different due to the increases supplied by each form of fiber respectively the overall effect of processing conditions will be the same for both.

1.7 Project Aims

The aim of this thesis is to further investigate the processing and reproducibility of PEEK in both thermal analysis and composite production. Processing conditions for PEEK/fiber laminates are not clear; the objective of this thesis is to develop a clear set of processing conditions to increase the mechanical properties of PEEK/fiber laminates. Furthermore the effects taking results from multiple samples of PEEK against using one sample is not widely discussed in the literature. A further objective of this thesis is to show the reproducibility of PEEK at a number of temperatures and hold times above T_m.

The equilibrium melting temperature of PEEK has been widely quoted in the literature as 395^{o}C. Furthermore, although the detrimental effect of degradation has been investigated at temperatures of 380^{o}C and above, recommendations for the processing of PEEK recommends the need to heat above T_m^0. In Thermal Analysis, due to the effects of degradation it is recommended that a new sample of PEEK be used in each experiment. However, heat of fusion and crystallinity results are not consistent when a new sample is continuously changed.

- Chapter 2 will show the processing conditions and methods used in this work.
- Chapter 3 investigates the total number of runs available from one PEEK sample in DSC at a range of temperatures from melt to T_m^0, to obtain a range of consistent analysis before the onset of degradation.
- The effect of degradation has been highly investigated at temperatures of

380°C and above. Chapter 3 will investigate to what extent, degradation occurs below this temperature.

- Chapter 4 will give an insight into the effect and onset of degradation using the novel method of Flash DSC. Thermal cycling will be achievable while removing the effect of the heat cool cycle, thus isolating the hold time and temperature effects.
- The technique and processing conditions for the formation of PEEK/fibre laminates have been extensively investigated. However no clear, definitive set of conditions have been recommended. Instead, a multitude of temperatures and hold times have been given as satisfactory. Chapter 5 will conclude the best processing conditions for PEEK/Glass fibre laminates.
- Chapter 5 will also investigate the effect of pre drying both PEEK and glass fibre before processing.
- Chapter 6 will conclude the findings of this work.

2 Chapter 2: Materials, Experimental Techniques and Methods.

2.1 Materials

2.1.1 Polyetheretherketone (PEEK)

Victrex™ provided samples of PEEK 450PF. The powder was stored at ambient temperatures in airtight containers. GKN Aerospace supplied samples of PEEK film; films of 200, 75 and 50 microns were stored alongside PEEK powder. Table 2-1 shows the typical properties, supplied by Victrex™, of 450pf PEEK.

Property	450PF
Tensile Strength (23°C)/MPa	100
Tensile Modulus (23°C)/ GPa	3.7
Density/ g cm^{-3}	1.30
Glass Transition (T_g)/ °C	143
Melting Point/ °C	343

Table 2-1: Typical Values for selected properties of 450pf PEEK from Victrex™

2.2 Differential Scanning Calorimetry (DSC)

2.2.1 Experimental Technique

Differential scanning calorimetry (DSC) is a thermal analytical technique used to characterise thermal transitions measured from relative heat flow with time or temperature [77]. Thermal Transitions that can be obtained include glass transition temperature (Tg), crystallisation temperature, melting temperature, and heat of fusion (ΔH_f).

A power compensation DSC contains a sample and reference cell, each with an independent heater and a platinum resistance temperature sensor, shown in Figure 2-1 and Figure 2-2. Samples are placed inside an aluminium pan and crimped shut and an empty aluminium pan is used as a reference. Each individual heater ensures the sample and reference pan are heated uniformly at a pre-determined rate. The power required to keep the two cells at the same temperature is measured and converted to heat flow, as phase transitions occur the power is adjusted to maintain equilibrium between the reference and sample. When a sample absorbs energy as heat an endothermic relaxation is observed, i.e. Tg and melting. When a sample releases energy, an exothermic transition occurs, i.e. crystallisation. This change in heat flow is measured in milliwatts (mW), against temperature or time for non-isothermal or isothermal studies respectively.

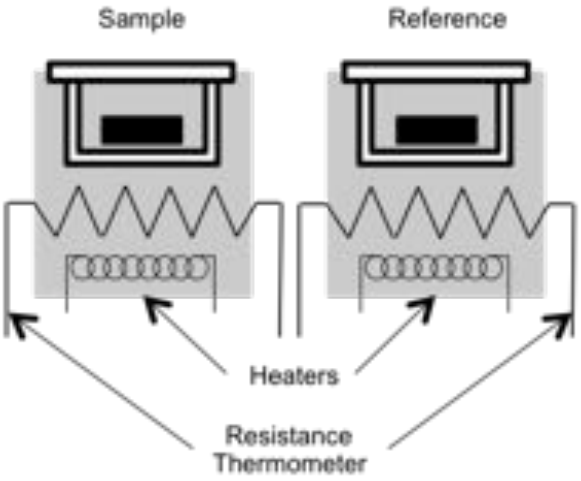

Figure 2-1: Schematic of a DSC unit.

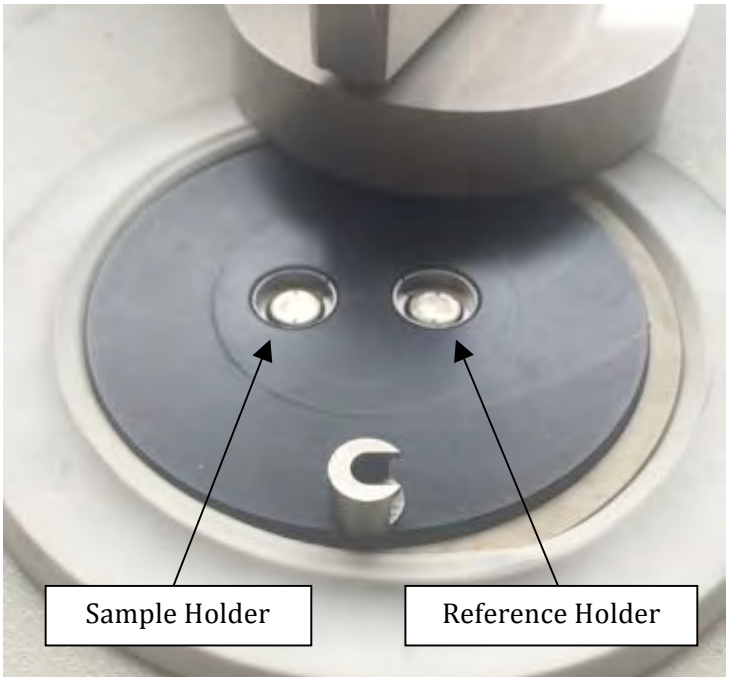

Figure 2-2: The sample and reference pans for Perkin Elmer DSC 7. Left pan indicates sample pan.

A Perkin-Elmer DSC-7 interfaced to a PC and controlled by Pyris Software, which, as described above is a power-compensating DSC. Other examples include heat-flux DSC, which uses a single heater for both cells, and temperature differences

are measured. The DSC was calibrated using two standards: indium and Zinc, using the melting onset temperature (In – 156.6^{o}C; Zn 419.5^{o}C) and heat of fusion values. The melting temperatures of these two materials were used to make corrections for thermal lag to allow extrapolation to zero heating rate.

2.2.2 Method

Each sample of PEEK was heated above equilibrium melting temperature (T_m^0) to 398^{o}C and held for 2 minutes to erase any thermal history. To create an amorphous sample of PEEK the samples were quenched cooled from the melt in liquid nitrogen.

Samples of 'as received' 450PF PEEK were prepared into an aluminium pan with a mass of 10 ± 0.5mg to record the thermal transitions of each sample. Samples were heated and cooled from 30^{o}C to temperatures between 350^{o}C – 420^{o}C at 20^{o}C per minute. Analysis was carried out on the first run to determine the effects of processing conditions on polymer morphology; subsequent scans were then analysed after the thermal history was erased.

Figure 2-3 shows the thermal response of an amorphous sample of PEEK 450PF. Three transitions/relaxations are apparent in fig 1.3; at 143^{o}C a clear glass to liquid transition is observable (a), in the range 175^{o}C to 210^{o}C the amorphous material transforms into a semi-crystalline solid as evidenced by the prominent crystallisation exotherm (b) and finally, a relatively broad melting endotherm is apparent in the range 275^{o}C to 350^{o}C (c).

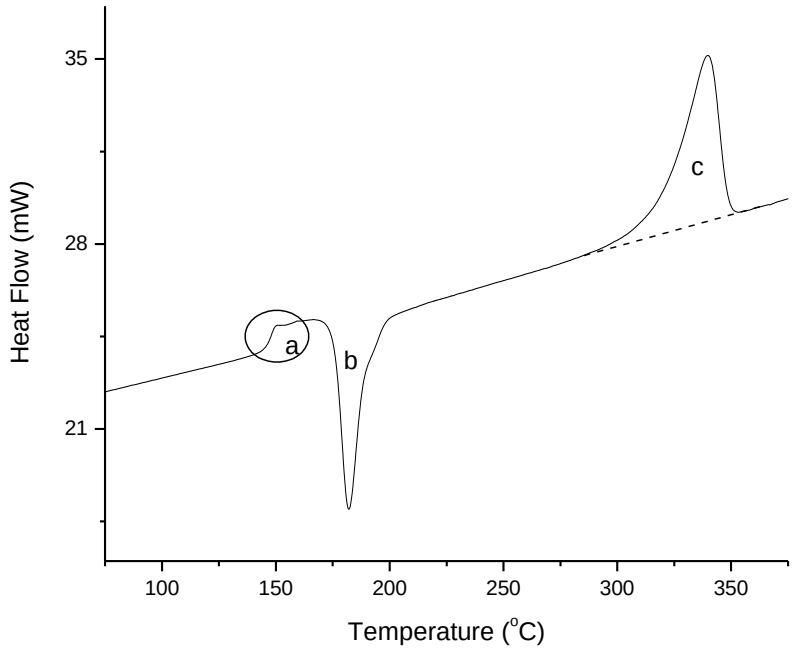

Figure 2-3: DSC scan for amorphous 450PF PEEK. A) Glass Transition, B) Crystallisation and C) Melting – Heat of Fusion.

The area in region (c) is defined as heat of fusion. Using the Equation 2-1 [78] the heat of fusion derived from the DSC experiment (ΔH_f) is divided by the heat of fusion for a fully crystalline PEEK at Tm ($\Delta H_{f100\%}$), defined as 130 J/G [39] giving the degree of crystallinity for the sample under investigation (X_c). Equation 2-2 takes into account the presence of reinforcing fibres, where X_{mr} is the fibre weight volume of the material [78, 79].

$$X_c = \frac{\Delta H_f}{\Delta H_{f100\%}} X\ 100$$ Equation 2-1

$$X_c = \frac{\Delta H_f}{(1 - X_{mr})\ \Delta H_{f100\%}} X\ 100$$ Equation 2-2

2.2.3 Characterisation

2.2.3.1 Definitions of Melting

The melting temperature (T_m) of PEEK is stated to be around 343°C [40], and refers to the point at which the last trace of crystallinity is erased and becomes amorphous and disordered. T_m is affected by the temperature of crystallisation, rising if a material is highly crystalline. PEEK exhibits a double melting peak and there has been debate on where the correct measurement of T_m is taken.

2.2.3.2 Onset, Peak, Endset.

Figure 2.3 presents the different points at which T_m can be taken from the endothermic melting peak of a DSC trace.

The onset of melting is obtained using two lines drawn at tangents to the baseline and low temperature side of the melting peak. The intercept of these lines indicate the onset of melting, in Figure 2-4 this is measured as 317°C. The intersect between the tangent to the baseline and high temperature side of the melting peak indicates the endset of melting. This has been measured as 348°C in

Figure 2-4. Both values can be used to determine errors in thermal lag. The final point of melting is the peak, on Figure 2-4 this is measured at 339°C.

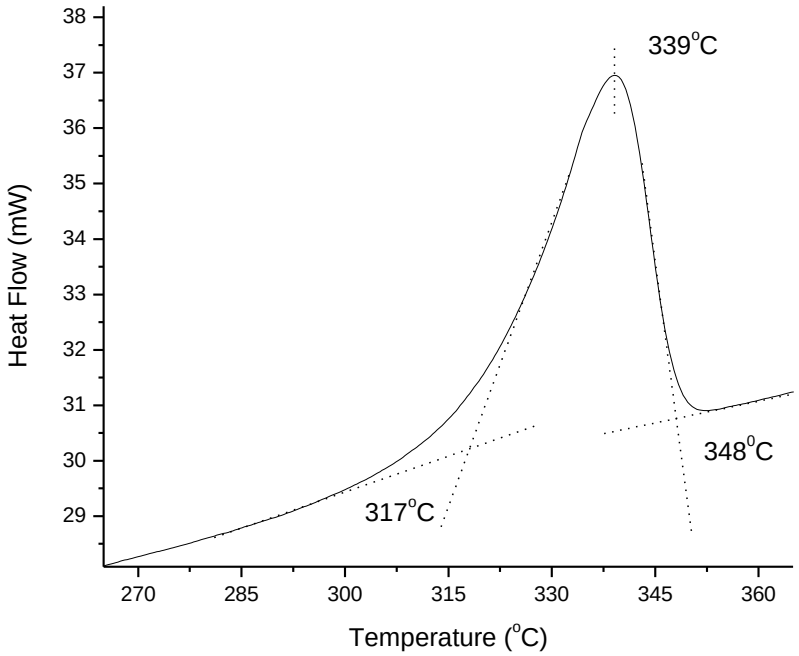

Figure 2-4: Showing the Onset, Endset and peak measurements of T_m of 450 PF PEEK.

2.2.3.3 Last Trace of Melting

The most common measurement of melting is taken at the end of the melting peak, known as the last trace of melting. This indicates complete melting of the sample. However there is an argument that the time taken to return to the baseline can be attributed to thermal lag in the DSC. This temperature is used as the upper limit to calculate the materials ΔH_f.

2.2.4 Variation of Integration Limits for the Determination of the Heat of Fusion

The melting endotherm can be used to calculate a value for the heat of fusion of the sample, which in turn can be used to determine the degree of crystallinity. However, unsystematic control of the integration limits leads to significant variability in the calculated values for heat of fusion (and therefore the degree of crystallinity). Figure 2-5 illustrates the definitions T_{upper} and T_{lower} (adopted in this study) that were used to systematically examine the effects of integration limits. The strategy was as follows; initial approximation for the values of T_{upper} and T_{lower} were made by visual inspection. This was taken from the point at which the melting endotherm started to increase from the baseline and on its return. T_{upper} was then fixed while T_{lower} was systematically varied (Figure 2-6). The effect on the heat of fusion was then assessed. Following this, T_{lower} was fixed at an intermediate value while T_{upper} was systematically varied (Figure 2-7). The effects on the heat of fusion are illustrated in Table 2-2 and in Figure 2-8.

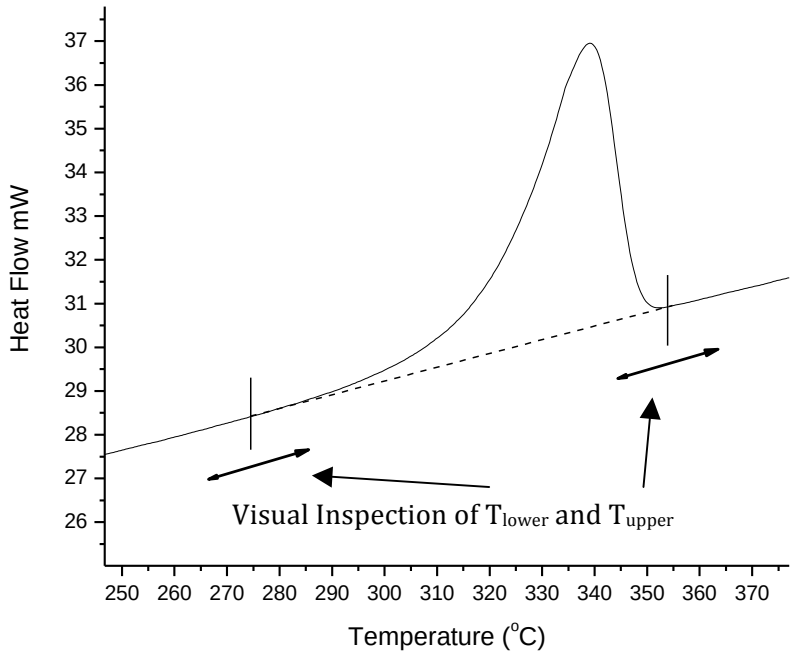

Figure 2-5: The systematic variation of T_{lower} and T_{upper} to determine heat of fusion.

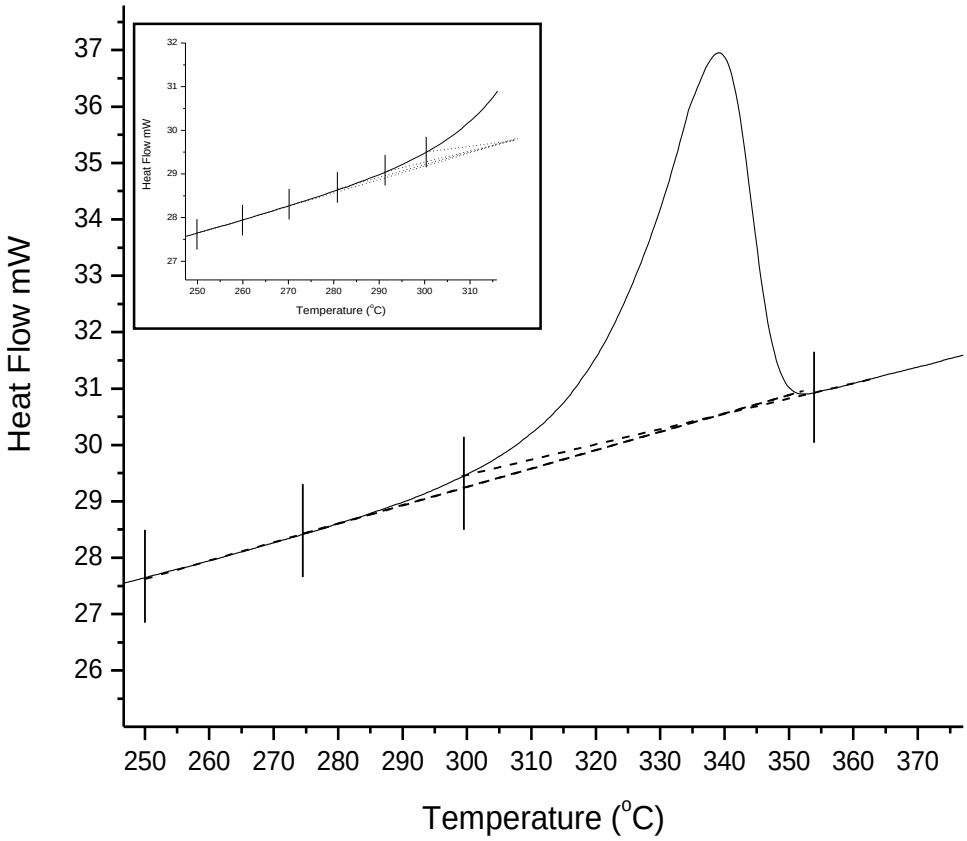

Figure 2-6: The integration limits of T_{lower} with a fixed T_{upper}.

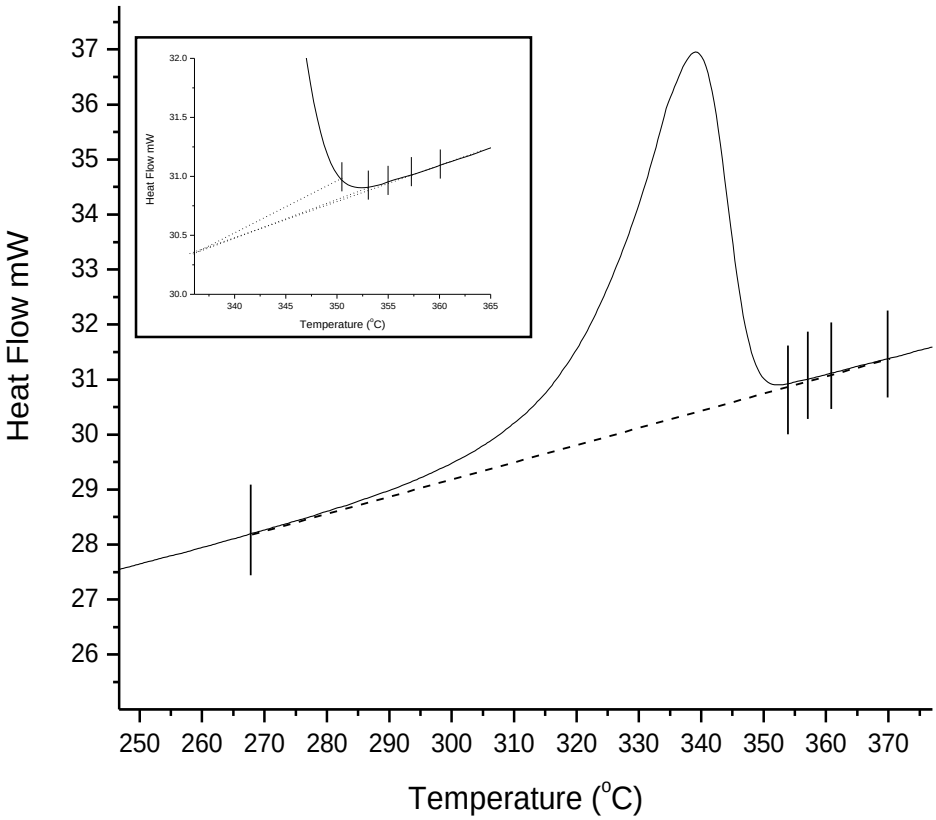

Figure 2-7: The integration limits of T_{upper} with a fixed T_{lower}.

T_{lower} (°C)	ΔH_f (J/g) (+/- 2 J/g)	T_{upper} (°C)	ΔH_f (J/g) (+/- 2 J/g)
301.7	35.8	350.0	36.0
295.0	37.2	351.0	38.0
290.1	37.8	352.0	39.0
285.1	38.1	353.0	39.0
280.1	38.4	354.0	40.0
275.0	38.5	355.0	40.0
270.1	38.5	356.0	40.0
265.0	38.4	357.0	40.0
260.0	38.3	360.0	40.0
255.0	38.1	370.0	40.0
250.0	37.9		

Table 2-2: The ΔH_f of 450PF PEEK with varied T_{upper} and T_{lower}.

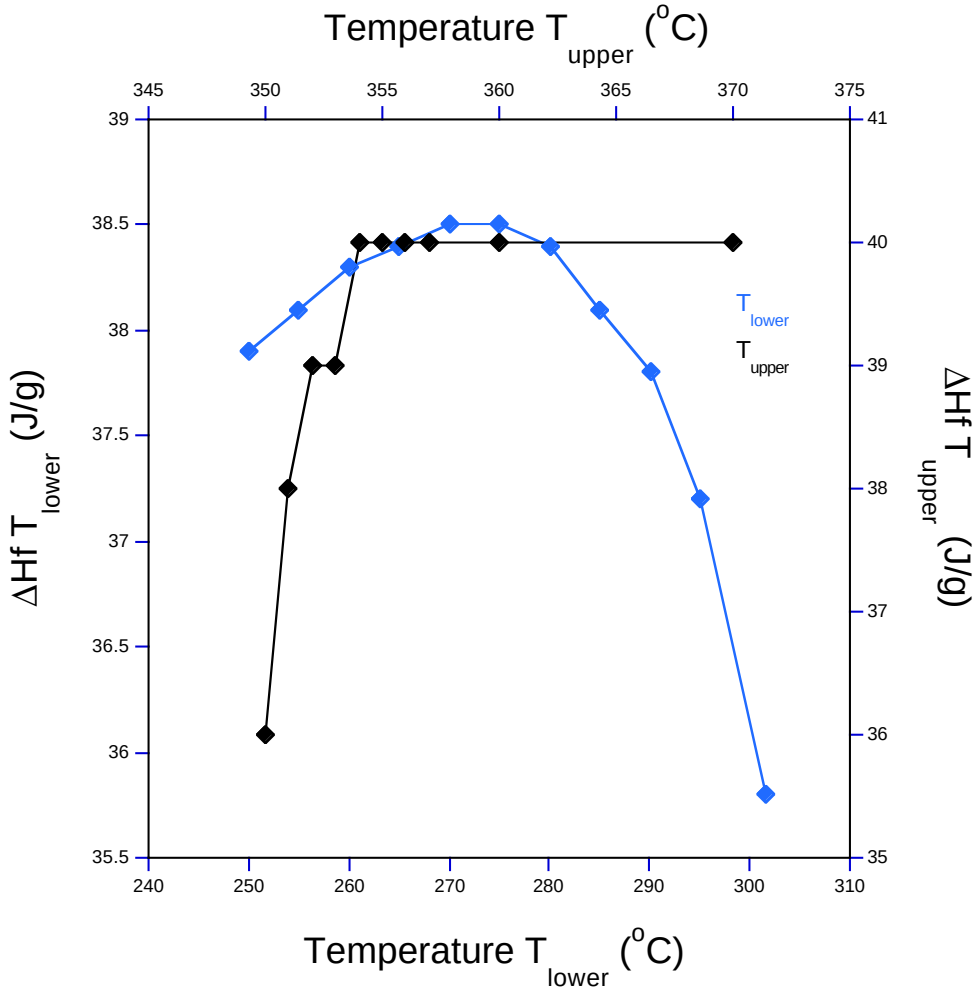

Figure 2-8: ΔH_f for 450PF PEEK with varied T_{upper} and T_{lower}. Point of consistency gives T values for future experiments.

The results shown in Table 2-2 and Figure 2-8 are representative of one sample from a multiple sample set. The measurement of ΔH_f and ΔH_c contains a variability of +/- 2 J/g, however this variability will cover each value in that run. For example, if sample 2 contains results of plus 2 % than those shown in Figure 2-8, then all results in that sample will be plus 2%. Therefore the values taken for T_{upper} and T_{lower} will not vary and are consistent over a range of samples tested.

It is clear that the heat of fusion is affected by the choice of integration limits, but there are values of T_{upper} and T_{lower} that are limiting values such that outside these limits, the heat of fusion reaches a plateau and is relatively unaffected by the choice of limits. The origin of this effect is most apparent, where it is clear that selecting a value of T_{lower} that approaches the onset of melting effectively reduces the measured peak area. A similar effect occurs with T_{upper}. From these results, for future experiments to maintain consistency, T_{upper} was taken from around 355^{o}C (+/- 2^{o}C). T_{lower} will be taken at 275^{o}C (+/- 2^{o}C).

2.3 Flash Differential Scanning Calorimetry

2.3.1 Experimental Procedure

Flash DSC is a form of rapid scanning DSC analysis, allowing ultra high heating an cooling rates over a large range of temperatures, allowing analysis of reorganisation processes conventional DSC is unable to measure. A Mettler Toledo Flash DSC 1 [80] is used connected to a T-100 intracooler allowing operation between -90^{o}C and 400^{o}C and analysed using software package STARe software V10. Argon gas is used to provide an inert atmosphere, to allow temperatures as low as -90^{o}C to be reached and assist in cooling the sample. Samples are typically between 100 ng to 10μg in size (conventional DSC uses around 10mg samples) and are placed directly onto a MultiSTAR chip sensor based on MEMS chip (micro-electro-mechanical systems). (Figure 2-9, Figure 2-10, Figure 2-11).

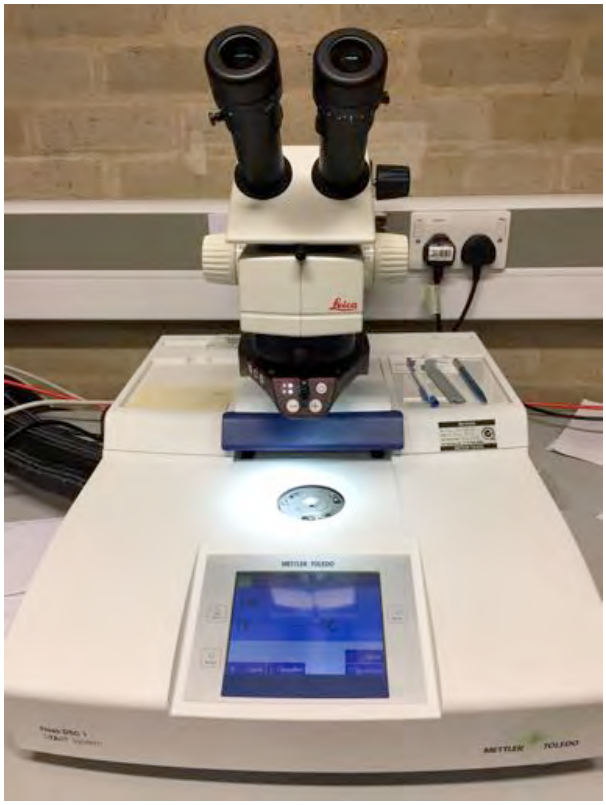

Figure 2-9: Mettler Toledo Flash DSC 1

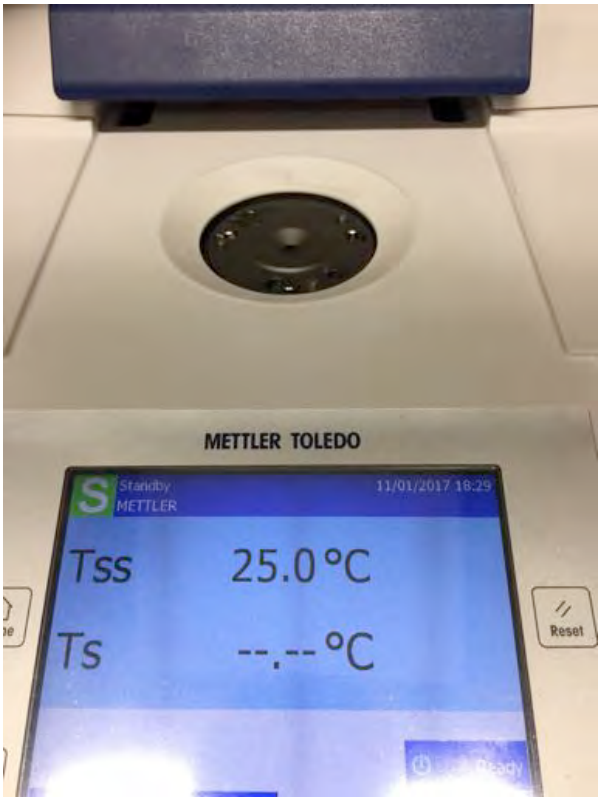

Figure 2-10: Mettler Toledo Flash DSC 1 sample bed and control system.

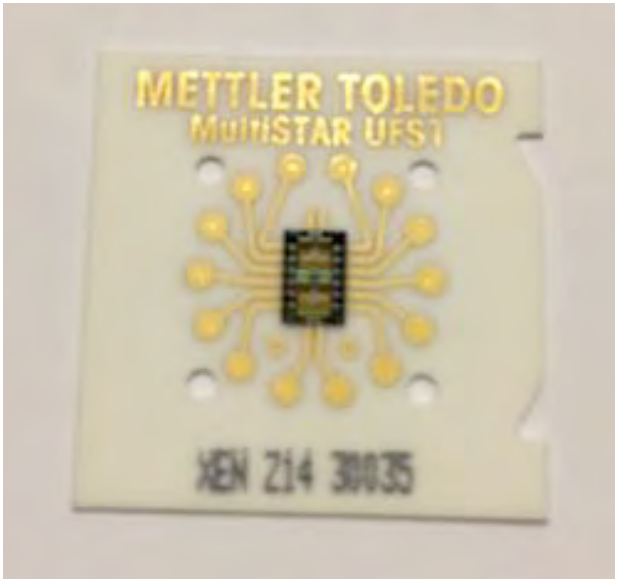

Figure 2-11: MultiSTAR chip sensor fro Flash DSC1.

Each Mettler Toledo FLASH DSC 1 chip sensor consists of 14 connection pads, 16 poly-silicon thermocouples, 8 for the sample and 8 for the reference sides of the chip [81, 82]. The sample area is a silcon nitride membrane, 2.1 μm thick, with an active zone 0.5 mm in diameter. To provide uniform temperature distribution the sample area is coated in 0.5 μm of aluminium. Chips are then placed inside the Flash DSC, with each connection pad touching a contact pin. Both the sample and reference sides of the sensor have two thermal resistance heaters, which generate the desired temperature profile. The main heater maintains the target temperature, while the compensation heater compensates for differences in temperature between the sample and reference cell (Figure 2-12).

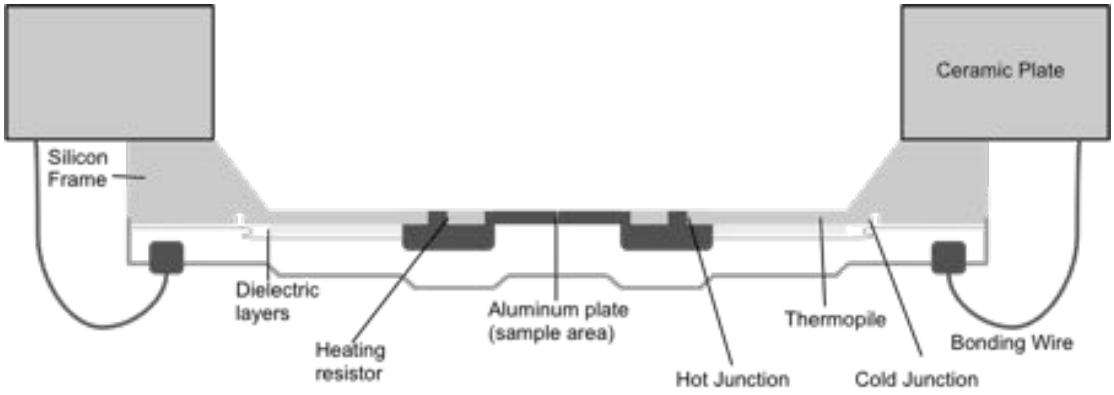

Figure 2-12:Schematic (not to scale) of the Flash DSC 1 chip sensor and ceramic base plate. [81, 82]

Heating rates of up to 40,000^{o}C s^{-1} and cooling rates of up to 4,000^{o}C s^{-1} can be achieved (conventional DSC has scanning rates of around 60^{o}C - 100 ^{o}C min^{-1}) [80]. These high rates can suppress reorganisation in polymers especially PEEK, which possesses fast crystallization kinetics. Allowing further analysis of reorganisation and crystallization kinetics of crystal structures.

2.3.2 Method

Each Flash chip sensor has a unique identification number eg. XEN Z14 30035. Electronic calibration of each chip is performed by the manufacturer (Xensor Integration [81]), which is imported onto the system. Each sensor goes through a number of pre set conditioning cycles (between 25°C and 450°C), to produce linear and reproducible baselines. Examples of an ideal chip conditioning runs are shown in Figure 2-13. Large spikes in the trace can reveal the presence of abnormalities or electrical malfunction in the chip. These faulty chips would be removed and not used. An ideal chip would show symmetrical traces with no spikes.

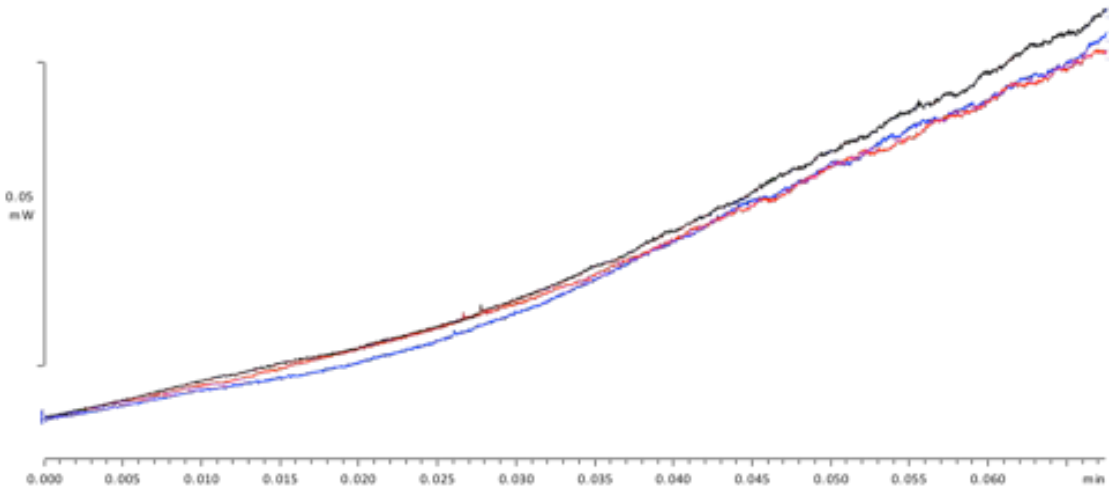

Figure 2-13: The heating and cooling cycle of an ideal chip sensor conditioning run. All lines represent the heat cycle of the same chip, any breaks or dips in the trace would represent a fault.

After a number of ideal conditioning runs have been achieved, a pre set correction run is applied to the sensor. Isothermal heating segments are applied

to calibrate the thermopile and the difference in temperature at the cold-junction. The sample support temperature used for this correction (-90°C) must be maintained for all subsequent experiments using corresponding chip.

2.3.3 Sample Preparation

Due to the size of the chip sensors, preparation of samples of extremely difficult. PEEK powder particles were smaller than the require sample size for Flash DSC. A particle of PEEK powder needs to be collected on a single human hair and applied to the centre of the sample side of the chip sensor while, the reference side is left blank. The Argon flow rate used was between 20 and 50mL min^{-1}. As well as being the cooling mechanism of the Flash DSC, the intracooler allows extremely fast quenching of the samples. Purging the instrument with Argon prevents internal ice formation.

When a particle of powder is in placed on the chip sensor, a slow heating rate is applied from 25°C to 400°C. A slow heating rate (1°C s^{-1}) is used to prevent the sample from jumping off the sensor. Two runs are applied to ensure that the sample is adhered to the surface of the membrane.

2.3.4 Effect of Thermal Lag

The delay in the conduction of heat (thermal lag) between the sensor and the sample will influence the onset of melting for samples tested. Thermal lag can originate from a combination of scanning rate and sample height. Results show that onset of melting occurs at a higher temperature, as the temperature of the sample is lower than that of the machine. Thermal lag is more pronounced in polymers, as they are thermal insulators. Thermal lag of the Flash DSC 1 was tested and a thermal lag of 0.86ms was found for samples using heating rates of

over 1000°C s^{-1}. Heating rates up to this point showed minimal thermal lag. Vanden Poel et al. [83, 84] described thermal lag up to 1000°C s^{-1} as low compared to other fast scanning techniques.

2.3.5 Estimation of Sample Mass

To be able to achieve accurate levels of crystallinity in samples analysed by Flash DSC 1 a known accurate value for the enthalpy of fusion (ΔH_f) must be obtained. Samples used on the Flash DSC are too small to be weighed by a balance; therefore an alternative method must be used. Using identical cooling rates, on both conventional and flash DSC will develop the same crystallinity within the sample. This is provided that the sample material is homogenous, isotropic and differences in sample masses do not introduce variations in crystallisation [83]. If crystallinity of both samples is same, the same can be assumed for the enthalpies of fusion for both samples.

The conventional DSC sample must be subjected to a heat/cool cycle, which can be replicated on the Flash DSC. Samples on both techniques must be cooled at 20°C per minute to create a shared thermal history. A slow cooling rate will allow PEEK to fully crystallise thus meaning there will be no crystallisation on heating. Heating rates typical to each technique were used, 20°C min^{-1} for flash DSC, and 100°C s^{-1} for conventional DSC. The enthalpy of melting is derived from the conventional DSC (ΔH_f (J/g)), and Flash DSC (Δh_{FDSC}) to calculate a sample mass. (Equation 2-3).

$$m = \frac{\Delta H_{FDSC}}{\Delta H_f}$$ Equation 2-3

2.4 Fourier Transform Infrared (FTIR) Spectroscopy

2.4.1 Method

A Nicolet 8700 FTIR using OMNIC operating system, with a Specac ATR golden gate attachment was used to analyse the samples. (Figure 2-14). Before each measurement, background scans were recorded, reducing the effect of water and CO_2 on the final FTIR spectrums. 100 scans were recorded on every sample, at a resolution of 4 cm^{-1}, with a zero filling of 2 gave final results at 0.5 cm^{-1} resolution. Any changes or movement of peak positioning and height were recorded. Figure 2-15 gives an example of a 450PF PEEK plaque FTIR spectrum.

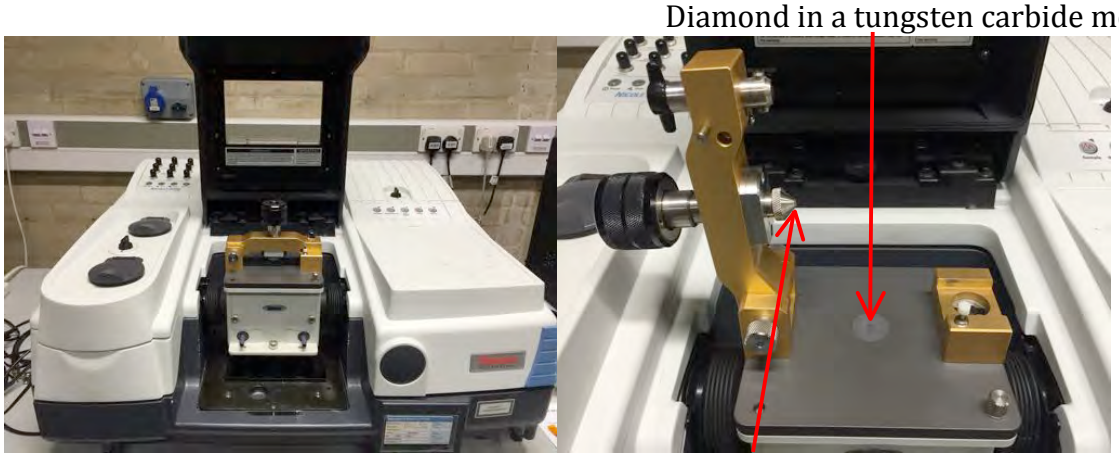

Figure 2-14: Nicolet 8700 FTIR with golden gate ATR attachment.

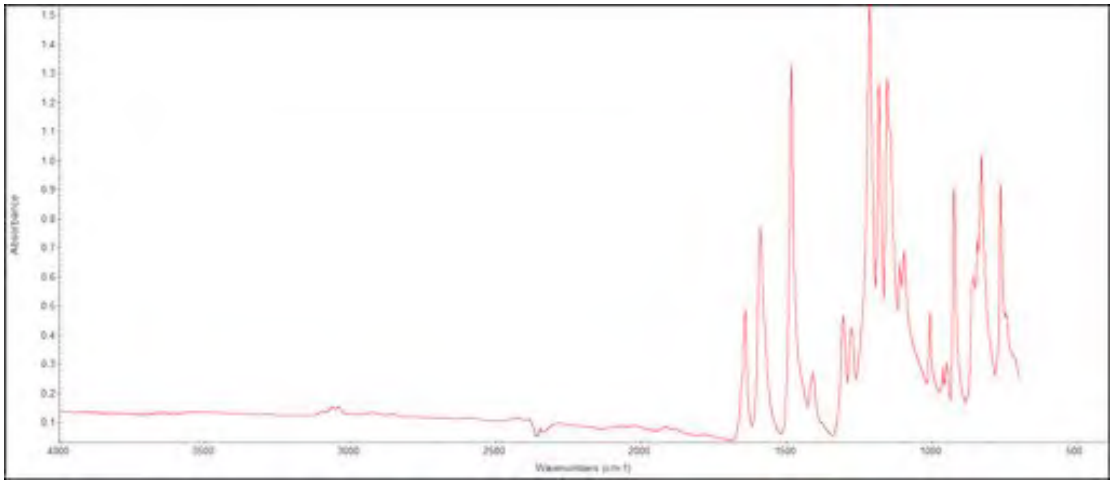

Figure 2-15: FTIR spectrum of 450PF PEEK plaque.

2.5 Thermogravimetric Analysis (TGA)

2.5.1 Experimental Technique

TGA involves the measurement of sample mass with temperature or time. The process is performed in a controlled atmosphere and is performed under the presence of gases e.g. oxygen, or in their absence using vacuum. Samples are placed in a sample pan, supported on a precision balance. Aluminium pans were used for experiments under 500^{o}C and platinum pans above 500^{o}C.

TGA experiments were completed on a Netzsch STA 449 C Jupiter attached to a PC for analysis. Each experiment is completed twice, to determine a buoyancy correction by running a mirror experiment with an empty sample pan. Every substance found in a gas atmosphere is subjected to a buoyant force, resulting in apparent mass changes, dependent on the volume of the sample and the density of the gas. Therefore corrections for buoyancy need to be made before each experiment.

TGA holds multiple benefits including, continuous recording of mass loss ensures no features of kinetics are overlooked, and the use of a single sample avoids any variations in kinetic parameter evaluations. The accuracy of the TGA can be affected by the arrangement of the furnace, and the surrounding atmosphere. These effects can be minimised by using smaller samples for temperature uniformity, consistent sample size and mass, and using a gas purge to create desired environment [85].

2.5.2 Method

In order to maintain consistence results sample weights were kept to 10mg ± 0.1mg, while also improving comparisons between TGA and DSC experiments. Temperature is increased at a pre-set rate inside a furnace; purge gas controls the sample environment. Typical temperature-time programs used can be seen in Figure 2-16. Any change in weight to the sample is presented on a XY axis. Loss of weight due to loss of water, oxidation and decomposition can be quantified.

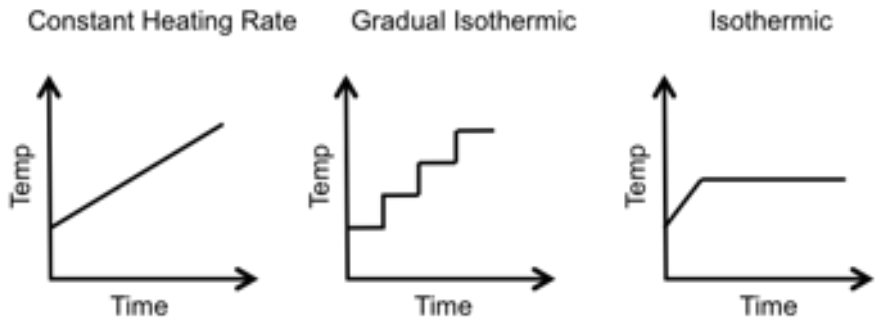

Figure 2-16: Typical temperature-time programs for TGA experiments.

2.6 Scanning Electron Microscopy (SEM)

2.6.1 Method

Samples were prepared using either cryogenic fracture, a hairline crack was placed in the sample before being submerged in liquid nitrogen, and after 60 seconds samples was removed and broken across the hairline crack. Alternatively, fracture under a known stress using tensile testing was used. Samples were mounted on an aluminium stub using carbon adhesive discs. Due to the thin nature of the samples, bostik adhesive was used to hold samples in place. To prevent charging of the sample inside the SEM AGAR silver dag was used at the base of each sample. Samples were then coated in platinum in a typical range of 2 – 20 nm using Polaron SC7640 sputter coater. Samples were imaged using a JOEL 6060 scanning electron microscope. A voltage of between 15 - 20 kV was used. A cross section of SEM samples can be seen in Figure 2-17.

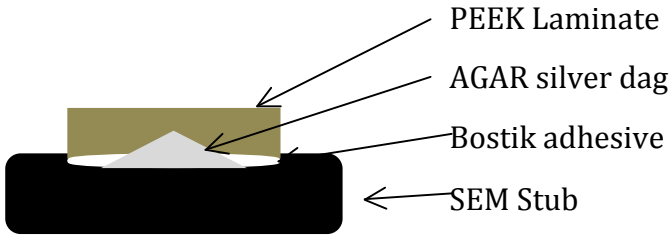

Figure 2-17: Cross Section of PEEK SEM sample.

2.7 Mechanical Testing

2.7.1 Tensile Testing

Tensile tests were completed on Instron 5566 test instrument interfaced with a PC using Bluehill 3 operating system. Samples were testing using grips of 5kN max load with a strain rate of 1mm/min. Load (N), extension (mm), tensile stress (MPa) and tensile strain (mm/mm) were analysed for each test.

Samples were cut to ASTM D3039 requirements with geometry's of, length of 220mm and widths of 20mm. Thickness of samples were taken from a three-point average. Young's modulus, elongation to break and ultimate tensile strength were determined from resulting stress strain curves. Five repeats were completed for each set of test parameters.

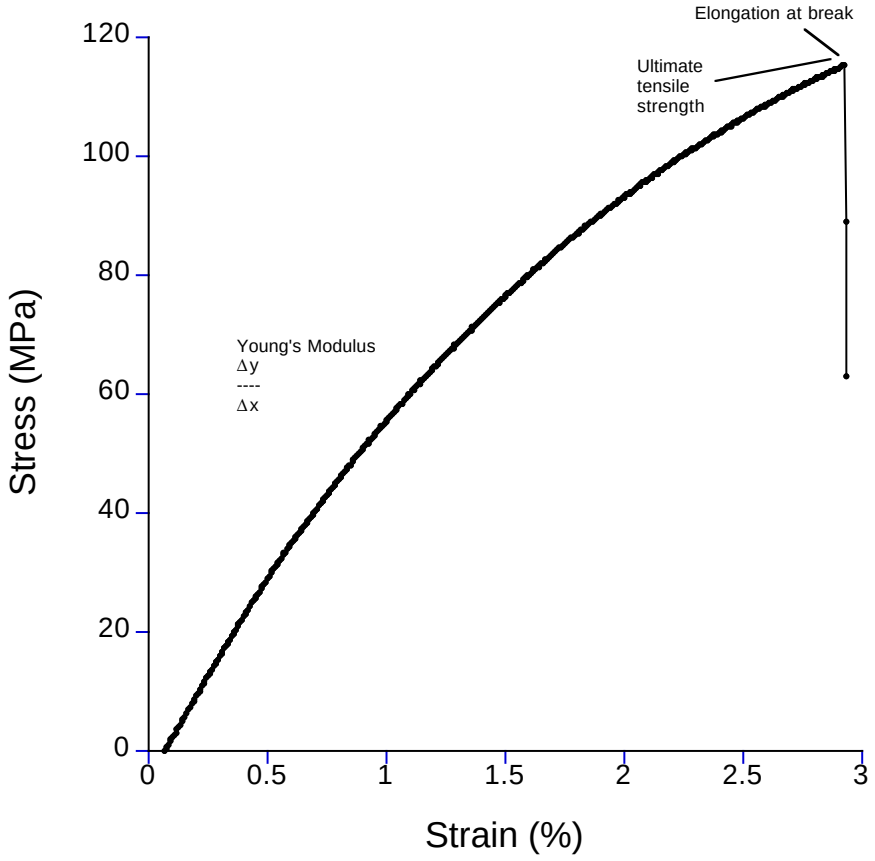

Figure 2-18: Stress-strain curve for PEEK laminate produced at 380°C. Indicating the determination for mechanical properties for each experiment.

Figure 2-18 indicates the determination of mechanical properties for varied samples. Young's modulus is taken from the initial linear portion of the stress-strain curve and determined from its gradient. Ultimate tensile strength is found at the maximum stress exhibited during the test, and elongation at break is determined from the maximum strain before failure. Figure 2-19 shows tensile test dog bone geometry cut to ASTM D3039 standards.

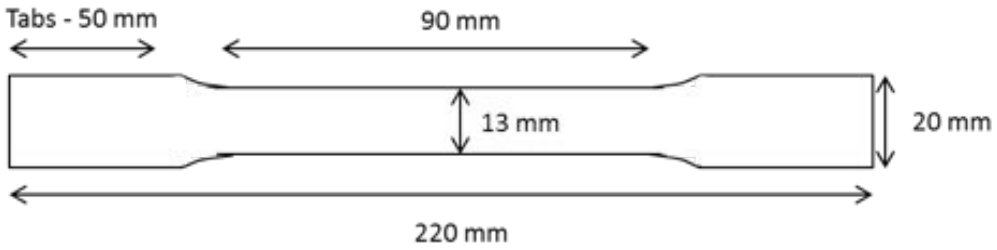

Figure 2-19: Geometry of dog bone samples of PEEK for use in Tensile. ASTM D3039 standard.

2.7.2 Hot Press Experimental Techniques

PEEK powder or films were kept overnight in an oven set at 140°C to remove any moisture. Samples were created using a Moore Hydraulic Press with JRD Bipel plates allowing for temperatures up to 400°C. Samples were created between two steel plates were covered in Kapton film. Kapton acted as a release agent for PEEK and can be used at temperatures above 400°C without degradation.

2.7.3 Method

To create plaques using PEEK powder a spacer was used to give a volume of 27.9cm^3. Using the density of PEEK (1.28-1.32g/cm^3) the mass of powder needed was found to be 36.3g. Samples were placed into the pre-heated press at 125°C and increased to minimal pressure to remove any potential air pockets. The press was then returned to contact pressure and temperature was increased to pre set target. Once sample reached temperature, a 5-minute hold at contact

pressure was conducted before pressure was increased to target. After pre set time at temperature and pressure, press was turned off and plaque/laminate was left to cool naturally to room temperature. The same process was used for PEEK film laminates without spacer.

3 Chapter 3 - Degradation in Thermal Cycling of PEEK

3.1 Introduction.

This chapter aims to complete a more detailed investigation into the onset and cause of degradation in PEEK. Degradation has been widely studied at temperatures above 380°C. Authors such as Day et al. and Jonas and Legras [86-89] stated that degradation of PEEK is initiated at temperatures of 380°C and is increased at higher processing temperatures. The current extent of research into the onset, cause and effect of degradation in both polymers including PEEK will be described.

This chapter will extend this work to analyse the effect of degradation at temperatures below 380°C. Furthermore, this chapter will investigate the effect of temperature on PEEK degradation to determine the repeatability of one sample of PEEK to be used in thermal analysis in an effort to increase consistency of results.

3.1.1 Equilibrium Melting temperature of PEEK

With high glass transition, melting point, and thermal stability, PEEK is both a widely used and analysed high-end thermoplastic; consequently due to its stability at high temperatures it is difficult and expensive to process in industry. It is widely recommended that PEEK be heated above its equilibrium melting temperature (T_m^0) to remove any residual nuclei, deleting any previous thermal history and enabling consistent results to be obtained [89].

The point, at which melting (T_m) is observed, is dependent on crystallisation temperature (Tc), this relationship between T_c and T_m was shown by Hoffman and Weeks [90]. T_m^0 is the equilibrium melting temperature relating to the melting temperature of the ideal crystal. It is defined as the melting temperature of an infinite stack of extended chain crystals [91]. It is not possible to directly measure T_m^0 from an experiment due to chain-folded lamellar growing to a finite thickness during crystallisation. It is therefore extrapolated from experimentally observed melting temperatures. By determining T_m^0 and establishing the degree of super cooling ($\Delta T = T_m^0 - T_c$), a better understanding of temperature dependence on crystallisation rates can be gained. One of the most commonly used methods of determining T_m^0 is Hoffman and Weeks [90], gained by using the relationship between T_m, and T_c, shown in Equation 3-1.

$$T_m = T_m^0\left(1 - \frac{1}{2\beta}\right) + \frac{T_c}{2\beta}$$

Equation 3-1

Where $\beta = (\sigma_e l/\sigma l_e)$ and σ is the fold surface free energy, l is the lamellae thickness and e refers to equilibrium conditions. In the absence of re-crystallisation or annealing during melting, β is equal to 1 and a plot of T_m against T_c, which is linear, will give a slope of 1/2 β. This line intersects the equilibrium condition of $T_m = T_c$ at T_m^0. The slope must be 0.5. Herrod-Taylor [92] used an extrapolation of Hoffman Weeks plot to $T_m = T_c$ to obtain a value of 397.3°C. This relates closely to the most common literature value of T_m^0 at 395°C given by Blundell and Osborn [39].

Blundell and Osborn related the melting point of lamellar crystals directly to the crystal thickness (l_c) using the Thomson-Gibbs equation. (Equation 3-2) [40].

$$T_m = T_m^0\left(1 - \frac{2\sigma_e}{\Delta H_F l_c}\right)$$ Equation 3-2

Where T_m^0 relates to the thermodynamic melting point of infinite perfect crystals, ΔH_f the heat of fusion, and σ_2 relates to the surface energy of planar surface lamellae. By using the Thomson-Gibbs relationship it is assumed that no lamellar thickening occurred on heating. Herrod-Taylor concluded that although molecular reorganisation is known to occur due to a Hoffman and Weeks β value in slight excess of 1 being obtained, close agreement with Blundell and Osborn's T_m^0 value suggested any lamellar thickening occurring was not significant [92].

Literature values for a definitive value for T_m^0 however, vary. Although 395°C is widely used [39, 93], Lee and porter [40] quoted a T_m^0 at 389°C ± 4°C. Medellin-Rodriguez et al. [94] reported a variation in T_m^0 for PEEK dependent on morphology regime changes with values given at 359°C, 362°C and 395°C. Ko and Woo [67] derived an equilibrium melting temperature at 384°C, whereas both Yang and Carvalho and Bretas [95, 96] found T_m^0 to be as low as 359.6°C and 357.3°C respectively. Each value was derived using the Gibbs Thompson methods and analysis of lamella thickening. However the experimental procedure varied with hold temperatures ranging from 400°C (40) to 420°C (93) and hold times of

30 minutes (67) to 1 to 42 hours (40). However, it is widely discussed that the process of heating PEEK to high temperatures results in thermal degradation.

3.1.2 Degradation of Polymers

Polymer degradation will result in impaired physical properties and changes to polymer crystallinity, where the extent of deterioration relates to the extent of degradation [85].

Forms of degradation such as, thermal, oxidative, and chemical have been examined. At temperatures beyond a polymer's melting point (T_m), thermal degradation can occur, affecting the chemical bonds of the polymer, limiting their ability to reform on cooling. Due to oxygen diffusion into a material, oxidative degradation occurs most commonly at the polymer surface, as extra time is needed for oxygen to diffuse into the bulk of the sample [97]. Jonas and Legras [89] found degradation increased in the presence of oxygen when the surface area to the experimental pan was increased. Chemical degradation involves a change in polymer properties due to a chemical reaction. A common thermolytic degradation process is known as pyrolysis. Pyrolysis is a chemical reaction necessary for the gasification and combustion of natural and synthetic macromolecules, and occurs in the absence of oxygen [98].

Degradation is caused by a process of chain scission, with random scission along the chain backbone, known as random chain scission (Figure 3-1), or chain end scission occurring at the polymer chain ends (Figure 3-2). Both processes result in formation of free radicals. The occurrence of degradation in these forms can result in weight loss and crosslinking. Kodera [98] stated a major contribution in weight

decrease is the volatilisation of low molecular weight products by chain end scission, which are considered to volatise instantaneously. Low molecular weight products are formed of random chain scission.

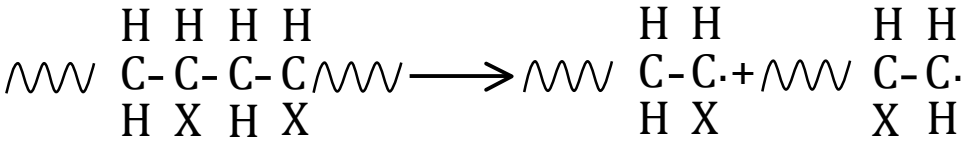

Figure 3-1: Example of Random Chain Scission

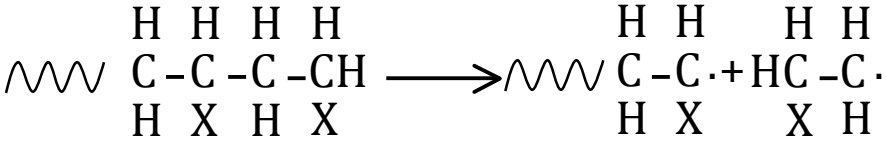

Figure 3-2: Example of Chain End Scission

3.2 Degradation of PEEK

3.2.1 Thermogravimetric Analysis of Degradation

Thermogravimetric analysis (TGA) is a common form of analysis used to measure degradation in polymers. Changes in mass of a sample are measured to analyse production of volatiles and decomposition of the sample. Analysis of a polymer can be conducted over long isothermal holds, giving the service life of a material at specific temperatures.

Hay and Kemmish [99] stated PEEK degradation is initiated by random homolytic scission of either the ether or carbonyl bonds. The radicals produced abstract hydrogen from the adjacent phenylene units or terminate by combination producing crosslinks. If products of the scission are sufficiently mobile they will volatise. Crosslinking will occur at an early stage of decomposition. Day et al. [87] discussed primary random chain scission occurring at the ether linkages of PEEK; only under extreme pyrolysis does scission also occur at the ketone linkages. (Figure 3-3)

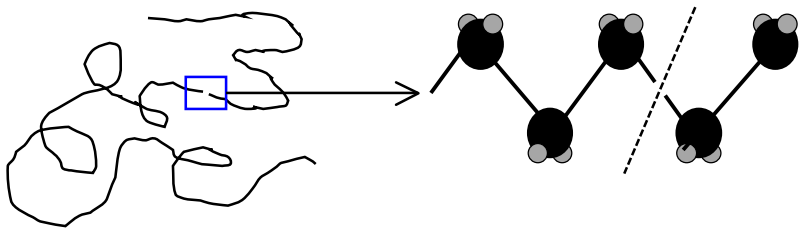

Figure 3-3: Schematic of Random Chain Scission in Polymers

Patel et al. [100] analysed PEEK degradation using Thermogravimetric analysis (TGA), showing a two-stage process. Stage one being the decomposition of the ether and ketone bonds caused by random chain scission, occurring around 555^{o}C and centred at 585^{o}C. Stage two occurs above 600^{o}C and is formed of the decomposition of cross-linked bonds, formed at stage one. These results were taken in a nitrogen environment, thus reducing the effects of degradation [29, 79]. In oxygen environments the first stage of decomposition occurs sooner at around 520^{o}C. Vasconcelos et al. [101] further evidenced this two-step process, describing phenol as the main degradation product of the step one and oxidation as step two. This in turn reduces activation energy as oxidation adds to random chain scission, reducing the amount of energy needed. Naffakh et al. showed the process of degradation to start at 470^{o}C in oxygen, whereas Jonas and Legras stated that degradation is noticeable at temperatures as low as 385^{o}C [89, 102]. Chen et al. [29, 79] also showed that PEEK was fully decomposed at 570^{o}C. Furthermore, Chen et al. used rheological analysis to show an increase in molecular weight in PEEK due to a branching mechanism leading to crosslinking. Liu et al., Cole and Casella, and Jonas and Legras [89, 97, 103] have all shown a large increase in onset, speed and overall degradation in oxygen. At an increased heating rate onset of degradation occurs at a higher temperature. This is expected, as energy must first be absorbed before decomposition initiates [101].

Fourier transform infrared spectroscopy was used on PEEK films [97] to expand further knowledge on the two-stage degradation of PEEK. In an inert atmosphere stage one produces a new carbonyl species, which absorbed at a much faster rate

in oxygen. The second mechanism of degradation produced a second species, described possibly as ester groups.

As previously discussed, use of dynamic runs in TGA to measure the thermal stability of PEEK is widely reported. However, definitive values for onset of degradation vary. Figure 3-4 shows a weight loss degradation curve for 450PF PEEK heated to 750°C at 20°C per minute in an oxidative environment. The curve shows that PEEK 450PF is stable until 540°C. 50% decomposition has occurred by 628°C and full decomposition by 706°C.

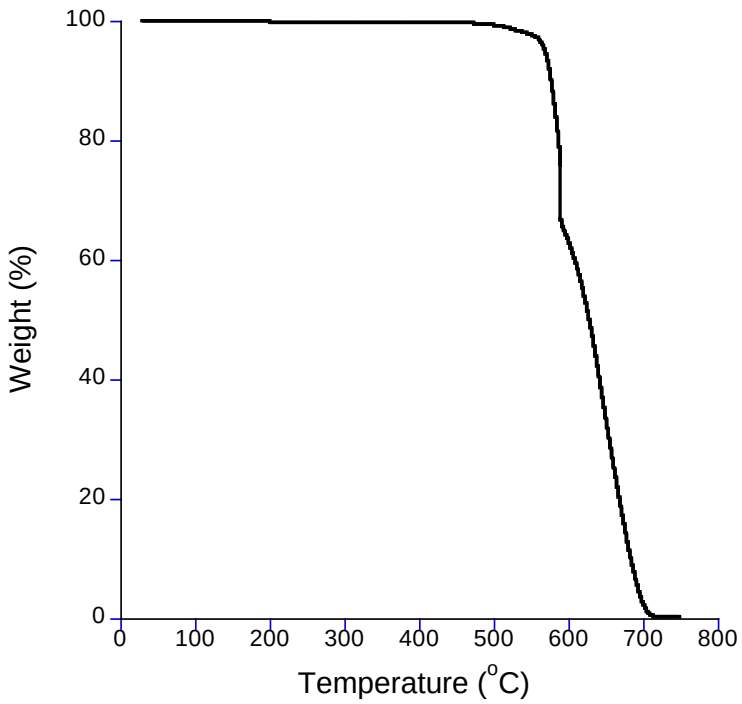

Figure 3-4: TGA analysis of PEEK 450PF heated to 750°C at 20°C per minute.

Activation energy of PEEK degradation kinetics has been analysed by Nam and Seferis [104] using the following equations. Reaction rate can be defined as the derivative of conversion with respect to time. Conversion can be shown (Equation 3-3) as the ratio of actual weight loss to weight loss at a given stage of the degradation process;

$$\propto = \frac{M_0 - M}{M_0 - M_f} \quad \text{Equation 3-3}$$

Where M, M_o, and M_f are the actual, initial and final weight of the sample, respectively. The rate of conversion can then be expressed as Equation 3-4;

$$\frac{d\propto}{dt} = k(T)f(\propto) \quad \text{Equation 3-4}$$

Where t is the time, k(T) is the rate constant, and f(α) is the conversion-dependence function. After integration, Equation 3-5;

$$g(\propto) = \int_0^{\propto} \frac{d\propto}{f(\propto)} = k(T)t \quad \text{Equation 3-5}$$

Where g(α) is the integrated form of the conversion-dependence function. The temperature dependence of the rate constant, k(T), may be described by the Arrhenius expression, Equation 3-6;

$$k(T) = A \exp\left(-\frac{E}{RT}\right)$$ Equation 3-6

Where A is the pre-exponential factor, E is the activation energy, and R is the gas constant. By combining and re arranging Equations 3-5 and 3-6, activation energy can be obtained, Equation 3-7;

$$\ln t = \left[\frac{g(\alpha)}{A}\right] + \frac{E}{RT}$$ Equation 3-7

Activation energy can be obtained from the slope ln t versus T^{-1} at a constant conversion level. In dynamic heating experiments, the integral form of the rate equation is expressed as;

$$g(\alpha) = \frac{AE}{qR} p(x)$$ Equation 3-8

Where

$$p(x) = \int_{\infty}^{x} \frac{\exp(-x)}{x^2} dx$$ Equation 3-9

X = E/RT, f(α) and g(α) are the conversion-dependence functions defined in equations c and a, respectively, and q is the heating rate. Nam and Seferis found activation energy to be 242.5 ± 4.0 and 241.4 ± 4.0 kJ/mol for isothermal and dynamic heating experiments, respectively.

3.2.2 Differential Scanning Calorimetry analysis of PEEK Degradation

Day et al. [86-88] has extensively analysed PEEK degradation at temperatures above its T_m (380°C – 420°C) using Differential Scanning Calorimetry (DSC). Day et al. [88] studied PEEK in oxygen and nitrogen environments for hold times up to 120 minutes. At increasing hold temperatures (380°C – 420°C) the amount of re-crystallisable material decreased and an increase in glass transition temperature was reported, a similar trend was observed for increased hold time. At temperatures above 400°C crosslinking was evident. Day emphasised PEEK should be processed in a non-oxidative environment to decrease the speed of degradation. These observations were extended [86] using methods such as solution viscometry and FT-IR. PEEK was found to be stable in nitrogen for up to six hours whereas chain scission and crosslinking occurred in oxygen, with spectroscopic evidence suggesting chain cleavage occurs at adjacent carbonyl functional groups, subsequent hydrogen abstraction from the aromatic rings then leads to crosslinking between adjacent aryl rings. Day [87] went on to state that random chain scission occurred at ether linkages (Figure 3-5).

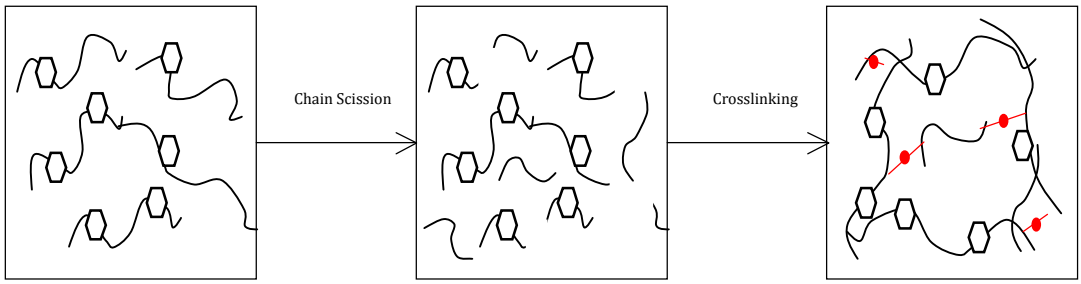

Figure 3-5: Schematic of chain scission and crosslinking in polymers.

Day's research was expanded by Jonas and Legras [89]. PEEK was repeatedly recycled, heated and cooled between hold periods totalling over 100 minutes at the following temperatures; 385°C, 400°C, 410°C, 440°C. Signs of degradation through a decrease in heat of crystallisation (ΔH_c) were present at all temperatures although minimal at 385°C even in air. With increased time and temperature the decrease in ΔHc became substantial. Reasons given for the depression of ΔHc included reduction in molecular mobility due to increase in molecular viscosity, resulting in lower crystallisation. Jonas and Legras stated that seed destruction is only initiated by heating above 385°C, above this temperature self-nucleation is depressed and therefore any decrease in crystallisation can only be considered due to degradation. Optical microscopy showed no significant change in spherulite size between 385°C and 400°C, therefore any difference in crystallinity was due to the decrease in nucleation density. A recommendation of heating to 400°C was given for PEEK processing, to both avoid self-nucleation and reduce degradation. Crosslinking is formed of progressive branching, causing degradation. Crosslinking

was found to occur at processing conditions over 415°C, increasing in volume with increased hold times [105], and leading to an increase in viscosity.

Deslandes and Boudreau [106] used micro indentation to study degradation at temperatures 370°C – 415°C. At temperatures below 385°C a marginal decrease was observed whereas a much larger decrease was observed at 415°C. At the surface of PEEK a minor decrease in mechanical properties was observed as low as 370°C, however, variations were much more significant above 400°C.

Phillips et al. [107] studied the effect of exposure to air on PEEK/carbon fibre composites at varied temperatures. Results showed that at temperatures below 400°C, ΔH_f and melting temperature remained consistent over the times tested, a decrease was seen immediately at 420°C. At 400°C ΔH_f was stable for hold times of over 20 minutes; a decrease in melting temperature was seen after holds of 15 minutes. TGA analysis indicated a weight loss of less than 2% for temperatures up to 440°C for times of up to 180 minutes. Salek [108] analysed resin flow for carbon/PEKK composites and found after reheating a poly(ether ketone ketone) (PEKK) sample held for over 2 hours at 360°C, no recrystallisation or melting peak was observed. Reasoning was given that according to research by Day; this would be caused by crosslinking, due to the inability of cross-linked material to re-crystallise. Cole and Casella [97] completed further work on PEEK/carbon fibre, where no significant difference in the degradation of PEEK composites and neat PEEK were found.

Lee and Porter [109, 110] also discussed degradation in composites; repeated melting of PEEK composites resulted in a decreased number of nuclei available for

crystallisation. The number of matrix spherulites formed on cooling decreases with increased holding time in the melt, leading to an enhanced transcrystalline region. At increased hold times increased matrix adhesion occurred due to destroyed nuclei leading to increased crystallisation on the carbon fibre.

Mclauchin et al. [111] studied degradation effects on injection moulding cycles. Three moulding/regrinding cycles at die temperatures of 380^{o}C could be performed without an appreciable drop in tensile strength. Reduction after three cycles was due to the deleterious effects of chain scission becoming dominant over the strengthening effect of crosslinking. Increases in the crystallinity of PEEK can increase strength and modulus; therefore any increase in chain scission resulting in a reduction in crystallinity can reduce such properties.

The main volatile of PEEK decomposition has been shown to be phenol, at extremely high temperatures other volatiles such as benzene and hydroquinane are also produced [87]. Patel et al. [100] stated that the scission of ether and ketone bonds makes up to 21% of weight loss; any extra weight loss would be due to release of such volatiles. Random chain scission has been described as occurring at the ether linkages. Only under extreme pyrolysis does chain scission also involve the ketone linkages [87]. Kashiwagi [112] stated that thermal stability in polymers increases in direct response to the number of aromatic groups in the main chain per repeat unit of the polymer chain, splitting these chains can reduce thermal stability of a polymer. In some polymers such as SPEEK [113], water evaporation has been suggested as a main reason for weight loss, however in

PEEK, Xin Lu et al. [114] showed there was negligible weight loss in the area around 100°C, where weight loss due to water evaporation would be expected.

3.2.3 Double Crystallisation Peaks in PEEK

Dual crystallisation peaks is a phenomenon not widely reported in literature. Cold crystallisation occurs upon heating of an amorphous or partially crystallised polymer above its Tg, whereas Melt-crystallisation occurs on cooling. However, single crystallisation peaks are often observed. Double cold crystallisation peaks have been reported by Zhu et al. [115-117] in PET films and fibres, initiated by the extent of nucleation and diffusion in the crystallisation of the interlamellar and interspherulitic amorphous regions. Amorphous interlamellar regions will crystallise at lower temperatures due to the presence of some order, whereas the fully amorphous interspherulitic regions hold no order. When nucleation is dominant increased number of interlamellar regions are formed, occurring with high super cooling, and crystallisation occurs from the glassy state. With low super cooling and crystallisation from the melt, diffusion is dominant, leading to an increased number of interspherulitic regions. Furthermore, due to the presence of two peaks due to two different forms of amorphous region, any changes in position, height and shape of the peaks may reflect changes in the structure of the respective amorphous region.

Lu et al. [114, 118] linked their theory of double melting to the double crystallisation process. Where double melting was due to separate crystal growth dimensions (Avarmi index 1 and 2) at lower and higher temperatures.

Sandler et al. [119] discussed the presence of a double crystallisation peak in PEEK composites as resulting from the interaction between the matrix and carbon fibre filler during processing. PEEK composites were formed using carbon nanofillers; with increased loading of nanofillers a second crystallisation peak occurred, increasing in size in correlation with number of nanofillers. Molecules in the vicinity of the dispersed nanofibres are hindered in their mobility and their ability to participate in the formation of spherulites. Eventually as spherulite growth increased the hindered molecules will be integrated into crystallisation leading to the formation of two crystallisation peaks. Thus no double melting peak on reheating is witnessed, only an increase in broadness of the melting peak indicating distribution in spherulite size.

3.3 Results

3.3.1 Thermogravimetric Analysis of PEEK

Dynamic heating runs of PEEK have been widely investigated at temperatures in excess of T_m, measuring degradation and mass loss. Figure 3-6 shows a Dynamic heating run of PEEK in an oxidative environment. It is clear decomposition begins at 540^{o}C, 50% decomposition has occurred by 628^{o}C and full decomposition by 706^{o}C.

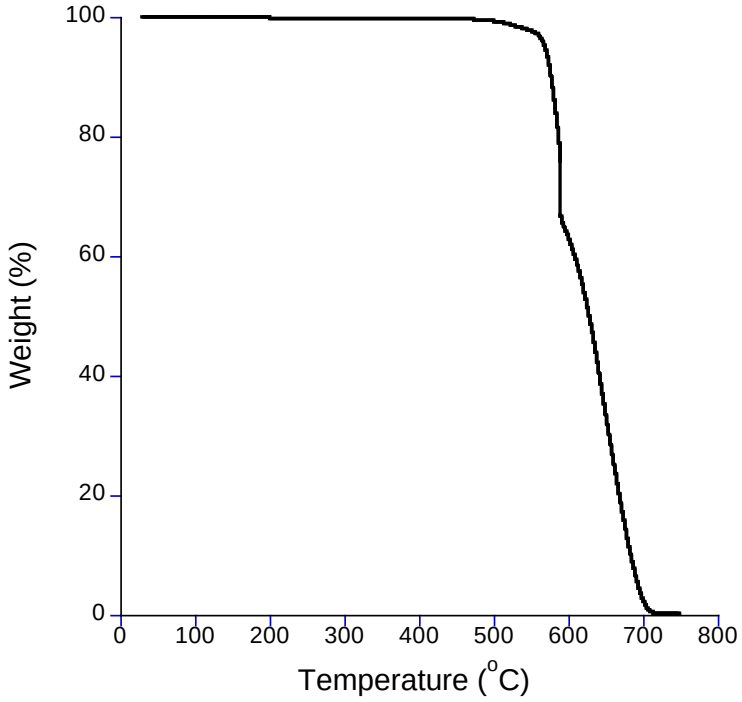

Figure 3-6: TGA heating run of 450PF PEEK heated to 750°C.

Further analysis was completed on the effects of isothermally holding PEEK at temperatures near its T_m for a range of hold times. This area of research is not significantly covered in literature however, is important in allowing comparisons of thermal degradation in TGA and Differential Scanning Calorimetry (DSC) data.

The variation of sample mass with time at three storage temperatures in the melt is shown in Figure 3-7 in comparison to a hold temperature at 500°C showing high levels of mass loss. It is apparent that thermal degradation is beginning to occur however, the mass loss is very limited in comparison to that observed on storage at 500°C. At 398°C (a temperature that is generally referred to as equal to or just above the equilibrium melting temperature), mass loss and therefore degradation

(at least according to TGA) is insignificant. This is supported by Jonas and Legras [89] who showed mass loss of less than 2% at holds of 60 minutes.

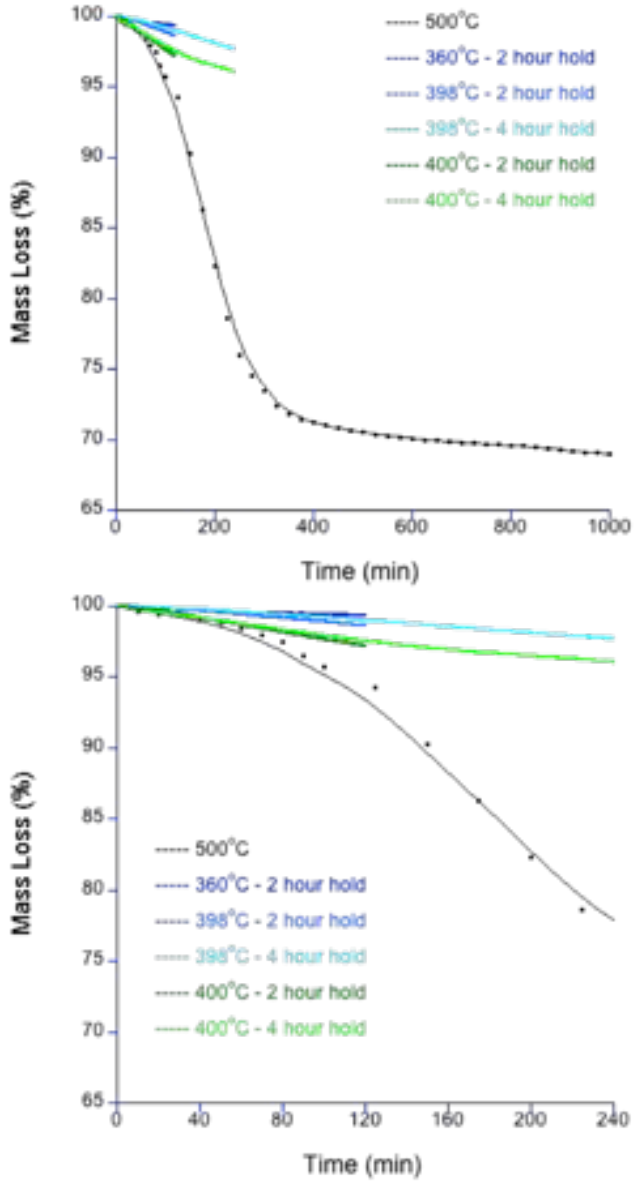

Figure 3-7: TGA of PEEK held for a varied hold time over a range of temperatures. Please note that TGA analysis at 500°C is used as a comparison and was conducted in Nitrogen atmosphere therefore, degradation is decreased.

Figure 3-8 shows the melting region of two samples of PEEK. Both samples were heated to 398°C and held at that temperature prior to cooling to 50°C. The samples were then reheated and the heats of fusion recorded. Samples were held at 398°C (temperature is between literature values for T_m^0 (395°C) and literature values for increase in degradation (400°C)). Hold times of 2 and 150 minutes (2 minutes represents a comely used thermal analysis hold time to confirm full melting, 150 minutes represents and accumulation of 12 runs with hold times of 10 minutes). It is clear that storage for 150 minutes resulted in a depression of the heat of fusion i.e. prolonged storage at 398°C resulted in a change to the material such that the non-isothermal crystallisation on cooling was hindered and the subsequent heat of fusion reduced. The use of TGA indicates that storage at 398°C does not cause significant chemical change to PEEK; however, the use of DSC reveals thermal instability, which manifests itself as a change in the crystallisation behaviour of PEEK.

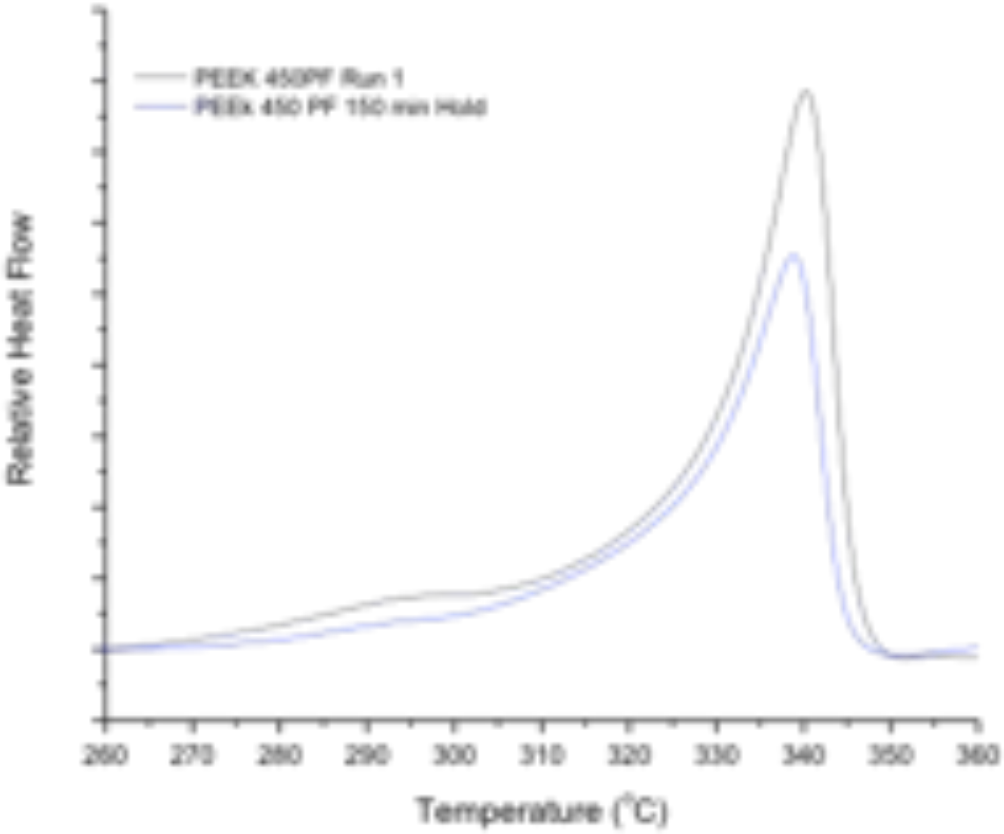

Figure 3-8: DSC trace of PEEK 450 PF after run 1 and 150 minute hold at 398°C.

3.3.2 Thermal Cycling and Degradation of PEEK.

3.3.2.1 Isothermal Holds

TGA analysis showed minimal weight loss in PEEK over prolonged hold times however, further analysis completed using DSC to record any changes to X_c as a consequence of changes in both hold temperature and isothermal hold time have shown a depression in X_c, believed to be brought upon by degradation.

When processed at temperatures above T_m^0, a reduction in X_c has been widely reported in PEEK. Depression in X_c has been observed at temperatures as low as 375°C (although minimal). In order to achieve consistent results in DSC analysis, PEEK is heated to above its T_m^0 (395°C) to remove any prior thermal history however, the extent of which degradation inhibits this must be further investigated.

The change in ΔH_f and ΔH_c for a number of isothermal holds at 398°C are shown in Figure 3-9. It is apparent that a reduction in X_c is observed as hold time is increased. It is clear that a substantial increase in degradation occurs as isothermal hold time increases to over 30 minutes. This increase in degradation corresponds to the appearance of a second crystallisation peak on cooling. This second peak is seen at hold times of up to 60 minutes. This will be discussed further later in this chapter.

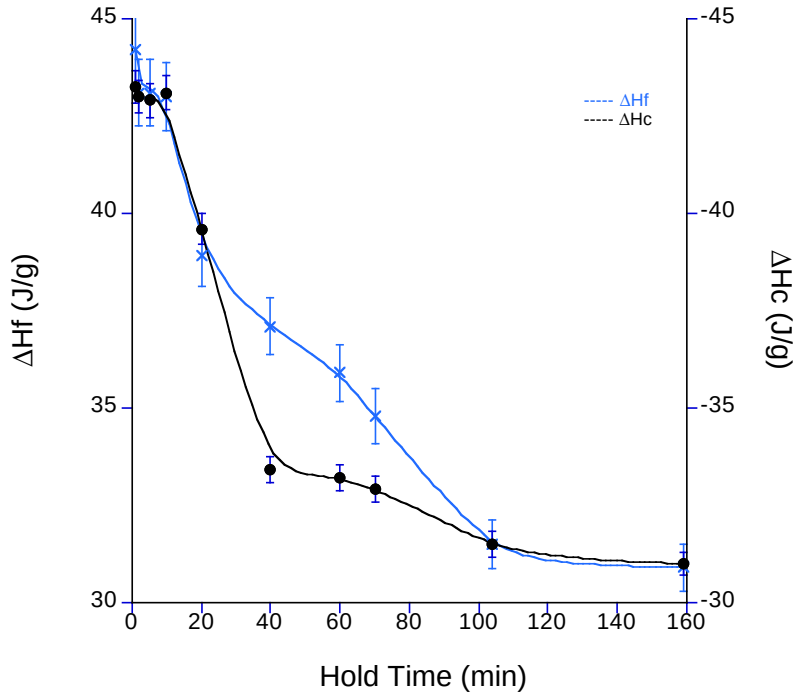

Figure 3-9: Comparison of ΔH_f and ΔH_c for 450 PF PEEK held for varied times at 398°C.

Figure 3-10 shows the decrease in ΔH_f and ΔH_c after an isothermal hold of 70 minutes at varied final hold temperatures above T_m. It is clear that the degradation is linked directly to an increase in temperature as well as isothermal hold time. A reduction in X_c is consistent with crosslinking and it is apparent that significant containment of the polymer chains is occurring. When PEEK is held at high temperatures, polymer chains will begin to degrade, a process called random chain scission, as described in the literature [87, 97, 99]. This process will create free radicals, which will proceed in two steps. Firstly, a propagation step, where a free radical takes an electron from another molecule, thus creating another free radical;

this continues the process of chain scission. A termination step is where two free radicals join together, once this happens they can no longer interact, this continues the process of crosslinking. As crosslinking is more pronounced, there will be a decrease in the number of PEEK chains available for crystallisation on cooling.

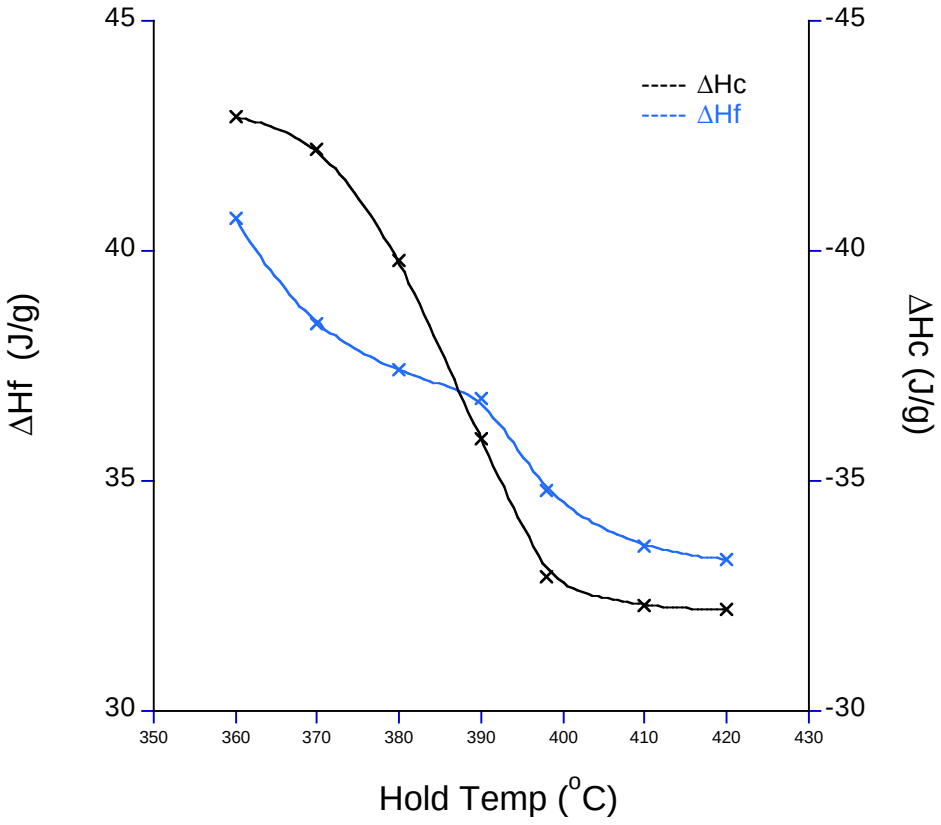

Figure 3-10: Comparison of ΔH_f and ΔH_c for 450PF PEEK held for 70 minutes at varied T_c.

Using the method of isothermal holds to measure degradation shows the decrease in X_c over prolonged hold times. However, to further analyse the effect of degradation between runs, a method of non-isothermal testing must be used, known as thermal recycling. Overall hold times can be calculated by combining

hold time at final hold temperature with heating and cooling rate to allow comparisons with isothermal holds.

Time vs. temperature programs for both isothermal and non-isothermal holds in DSC are shown in Figure 3-11. Separate samples of 450PF PEEK were heated to 398°C and held for 2 minutes. This cycle was repeated and subsequent ΔH_f and ΔH_c were recorded. This process was repeated with various final hold temperatures.

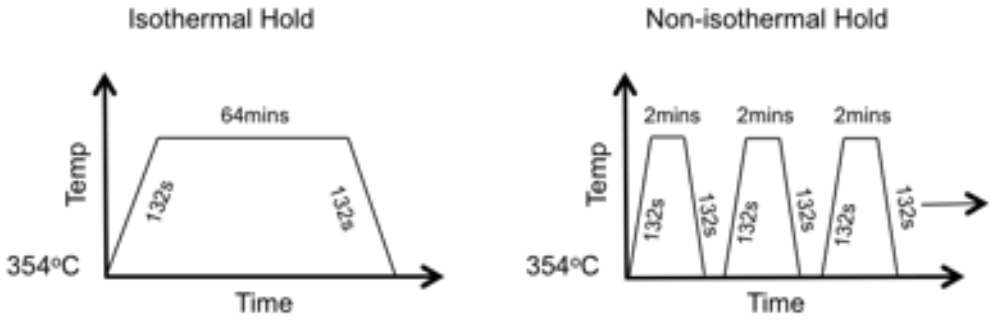

Figure 3-11: Time vs. temperature program for DSC runs of isothermal and non-isothermal analysis heated to 398°C. 64 minute hold time represents the complete total of hold time plus heat/cool cycle represented in non-isothermal holds.

3.3.2.2 Effect of Run rate in Non-isothermal holds.

In DSC analysis the number of runs obtained from one sample to gain consistent results is not conclusively agreed upon in the literature, and is commonly not disclosed. Changes to the sample's morphology due to degradation will result in varied results. To combat this, samples are often changed after each run; this however, leads to further variations in results due to differences in sample weight, size, position etc. It is not made clear in the literature the number of consistent results, which can be obtained from one sample before degradation becomes a factor.

Figure 3-12 shows the exothermic crystallisation peaks on cooling of a sample of PEEK heated to a final hold temperature of 360, 390, 398 and 420^{o}C respectively. Each sample was held at its final temperature for 2 minutes before cooling, this process was repeated through 12 cycles. Each thermal recycling experiment was completed at 10^{o}C intervals from 360^{o}C to 420^{o}C. The results shown were selected as they showed the clearest changes to crystallisation peak. Table 3-1 shows the T_c onset; T_c peak and ΔH_c for each hold temperature. It is clear that ΔH_c is depressed as run number increases. It is also clear that this process is accelerated at increased temperature. At a hold temperature of 360^{o}C, after 12 runs there was no change in ΔH_c, indicating that no significant degradation has occurred. This allows multiple runs of the same PEEK sample to be obtained. Values for ΔH_c at 398^{o}C indicate no change in ΔH_c until run 5, which is matched with a significant second

crystallisation peak (T_{c2}). It is apparent that when heating to 398^{o}C, 3 runs of the same sample will give consistent results.

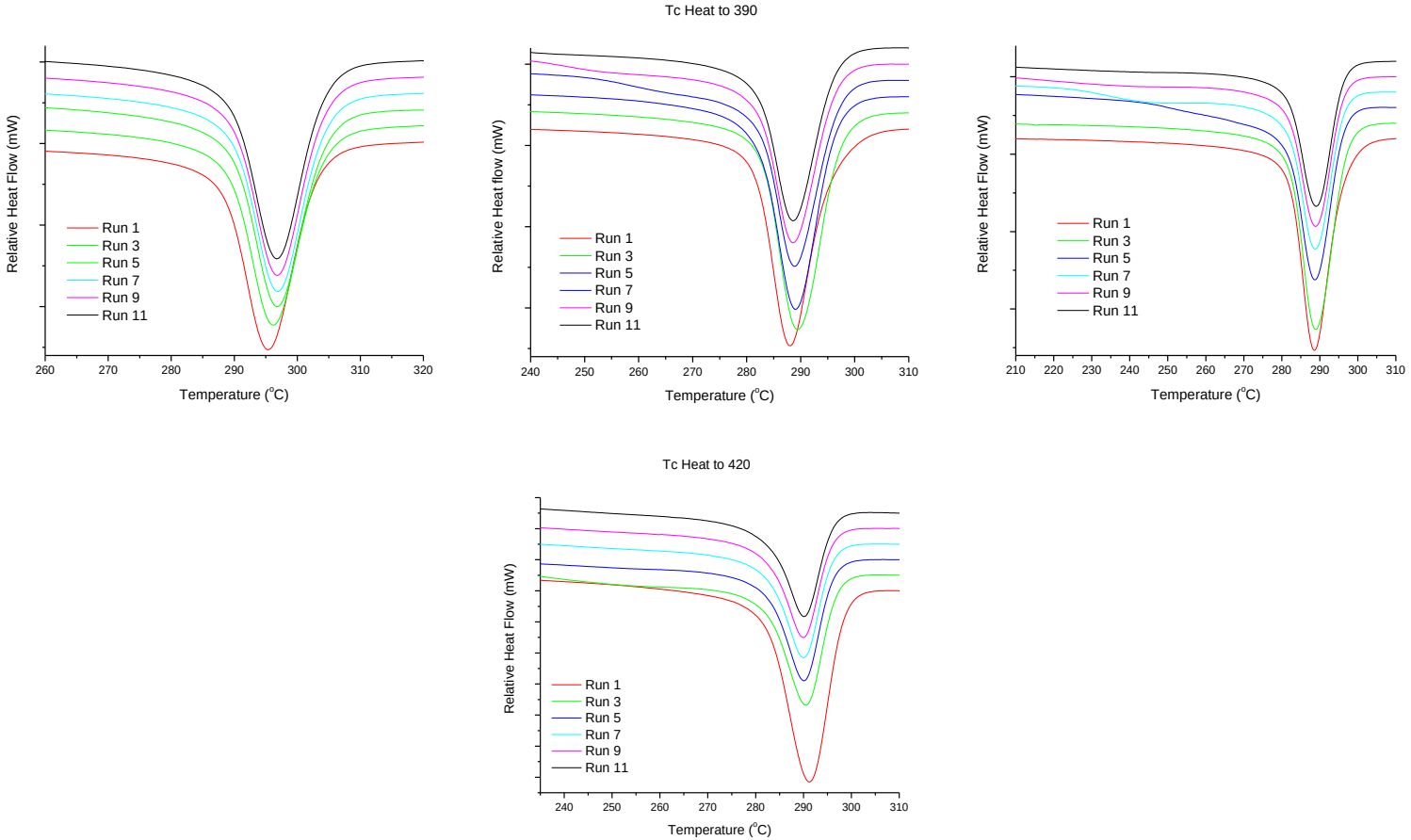

Figure 3-12: Non-isothermal crystallisation following storage time of 2 minutes where $T_{s\,is}$ (Top L-R) 360°C, 390°C and 398°C, (Bottom L-R) 420°C

		Run 1	Run 2	Run 3	Run 4	Run 5	Run 6	Run 7	Run 8	Run 9	Run 10	Run 11
360°C	**T_c Onset**	303.6	304.4	304.6	305.0	305.0	305.0	305.0	305.0	305.0	305.0	305.0
	T_c Peak	295.0	295.0	296.0	296.7	296.7	296.9	296.9	296.9	296.7	296.0	297
	ΔHc (J/g)	-46.5	-45.0	-44.5	-44.7	-44.6	-44.6	-45.0	-45.0	-45.0	-45.0	-45.0
390°C	**T_c Onset**	296.8	297.6	298.0	297.1	297.1	297.0	297.7	297.2	297.1	297.2	297.0
	T_c Peak	287.9	288.9	289.5	289.1	289.1	288.9	288.9	288.5	288.5	288.5	288.5
	ΔHc (J/g)	-46.0	-45.8	-45.6	-45.9	-45.6	-45.3	-45.0	-44.6	-43.8	-42.8	-39.9
398°C	**T_c Onset**	297.0	298.0	297.5	297.0	296.0	296.0	296.0	296.0	296.0	296.0	296.0
	T_c Peak	288.5	289.3	288.0	288.0	288.0	288.0	288.0	288.0	289.0	289.0	289.0
	ΔHc (J/g)	-46.0	-46.0	-46.0	-45.7	-45.0	-44.0	-39.0	-35.0	-34.0	-33.0	-32.9
420°C	**T_c Onset**	299.0	298.3	297.3	297.1	296.6	296.4	296.6	296.5	296.6	296.6	296.5
	T_c Peak	291.1	290.9	290.5	290.1	290.1	298.9	289.9	289.9	289.9	290.1	290.1
	ΔHc (J/g)	-45.7	-44.3	-35.7	-31.2	-29.4	-28.6	-27.8	-27	-26.6	-26.1	-25.7

Table 3-1: Values for T_c and ΔH_c for non-isothermal crystallisation of 450PF PEEK at varied hold temperatures.

Please note errors – T_c Onset - +/- 2°C, T_c Peak - +/- 0.5°C, ΔH_c - +/- 2 J/g.

Crystallisation (T_c peak) occurs at a higher temperature at hold temperatures of 360-370°C. Once hold temperature increases to 380°C and above, T_c peak is consistent. It is clear that heating to 370°C does not remove residual nuclei present in PEEK, thus allowing these nuclei to act as nucleation sites for crystallisation on cooling. No change in T_c peak is observed between hold temperatures at 380°C and 420°C. This indicates that any residual nuclei have been removed once hold temperatures of 380°C are achieved. This is in disagreement with common thought of T_m^0 [39].

Figure 3-13 shows the subsequent melting peaks (T_m) of each PEEK sample shown above, resulting T_m onset, T_m last trace, T_m peak and ΔH_f are shown in Table 3-2. It is clear a significant decrease in ΔHf is observed, which directly result from the depression of ΔHc reported already. Therefore a steady decrease in ΔH_f is seen with increasing run number, occurring earlier at increased hold temperature. No systematic variation is observed in hold temperatures of 360-380°C over the number of runs tested. The decrease of ΔH_f coincides with a depression and broadening of the T_m endotherm. T_m onset is shown to decrease to between 315-320°C before a gradually increasing to plateau around 322°C. This is due to a continued depression of ΔH_f creating a steeper curve. No change in T_m last trace or T_m peak is observed.

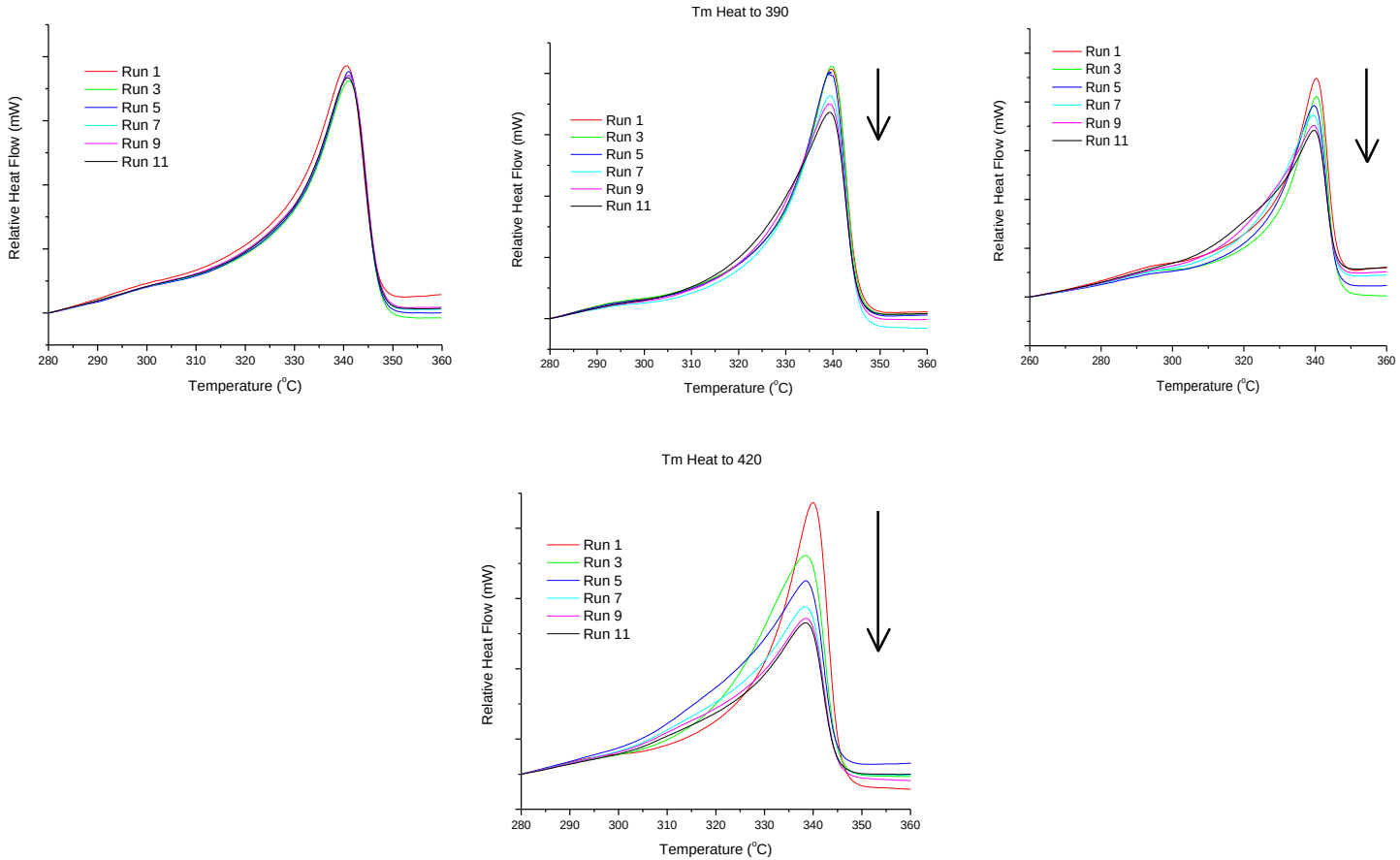

Figure 3-13: Melting of 450PF PEEK following multiple runs with storage time of 2 minutes with hold temperature of (Top L-R) 360°C, 390°C and 398°C, (Bottom L-R) 420°C. Arrow represents a decrease in ΔH_f with increased run and temperature.

		Run 1	Run 2	Run 3	Run 4	Run 5	Run 6	Run 7	Run 8	Run 9	Run 10	Run 11
360°C	**T_m Onset**	329.0	328.5	329.0	329.0	329.0	329.0	329.0	328.7	328.0	328.0	329.0
	T_m LT	351.0	352.0	353.0	352.0	352.0	352.0	352.0	352.0	352.0	352.0	352.0
	T_m Peak	340.0	340.5	341.0	341.0	341.0	341.0	340.8	340.8	341.0	340.8	341.0
	ΔHf (J/g)	44.0	44.5	45.0	45.0	44.8	44.8	44.4	43.5	43.5	44.0	44.0
390°C	**T_m Onset**	328.5	328.0	328.0	327.7	327.4	326.9	325.4	324.4	323.4	322.4	322.0
	T_m LT	350.0	350.0	350.0	350.5	350.0	351.0	352.0	351.5	351.0	350.0	349.7
	T_m Peak	339.7	339.7	339.8	339.7	339.5	339.5	339.5	339.2	339.2	339.2	339.2
	ΔHf (J/g)	42.0	42.4	42.6	42.3	42.4	42.9	42.2	42.0	41.9	41.3	40.7
398°C	**T_m Onset**	328.0	328.0	328.5	328.0	325.0	323.0	321.0	320.0	320.0	322.0	322.0
	T_m LT	350.0	350.0	351.0	351.0	350.0	350.0	350.0	350.0	350.0	349.0	350.0
	T_m Peak	340.0	340.0	340.0	339.8	339.0	339.0	339.0	339.0	339.0	339.0	339.0
	ΔHf (J/g)	42.6	42.0	42.5	42.0	41.0	40.8	40.6	40.0	40.0	39.0	39.0
420°C	**T_m Onset**	328.8	324.6	319.2	315.4	318.8	320.6	320.5	321.1	320.7	321.5	321.7
	T_m LT	352.0	352.0	351.0	350.0	349.0	350.0	350.0	350.0	350.0	350.0	350.0
	T_m Peak	339.9	338.8	338.5	338.5	338.5	338.5	338.2	338.5	338.5	338.5	338.5
	ΔHf (J/g)	43.8	42.2	40.9	39.7	38.4	37.3	35.5	33.9	33.4	32.0	31.1

Table 3-2: Values for T_m and ΔHf for non-isothermal crystallisation of 450PF PEEK at hold temperatures 360°C - 420°C. **Please note errors –**

T_m Onset - +/- 3°C, T_m LT - +/- 1°C, T_m Peak - +/- 0.5°C, ΔH_f - +/- 3 J/g.

Figure 3-14 shows the cooling and subsequent heating curves for a range of run numbers of PEEK thermally cycled to varied final hold temperatures. Runs 5 and 9 are shown to give the clearest indication of any changes occurring. It is clear both the depression of ΔH_c and ΔH_f alongside the broadening of T_c and T_m occur at an earlier run number when hold temperature is increased. This shows the increase in degradation brought upon by increased processing temperature. Furthermore, the formation of T_{c2} is clear on cooling, for hold temperature of 398°C, T_{c2} appears at run 5. At hold temperatures in excess of 398°C, T_{c2} peak has already been observed by an earlier run. A broadening of the T_m endotherm may relate to varied sizes of spherulite formation. This proposes one theory about the production of T_{c2} to be explored further later in this chapter.

It is clear that an increase in both hold temperature and run number substantially increases degradation in PEEK, resulting in a decrease in X_c.

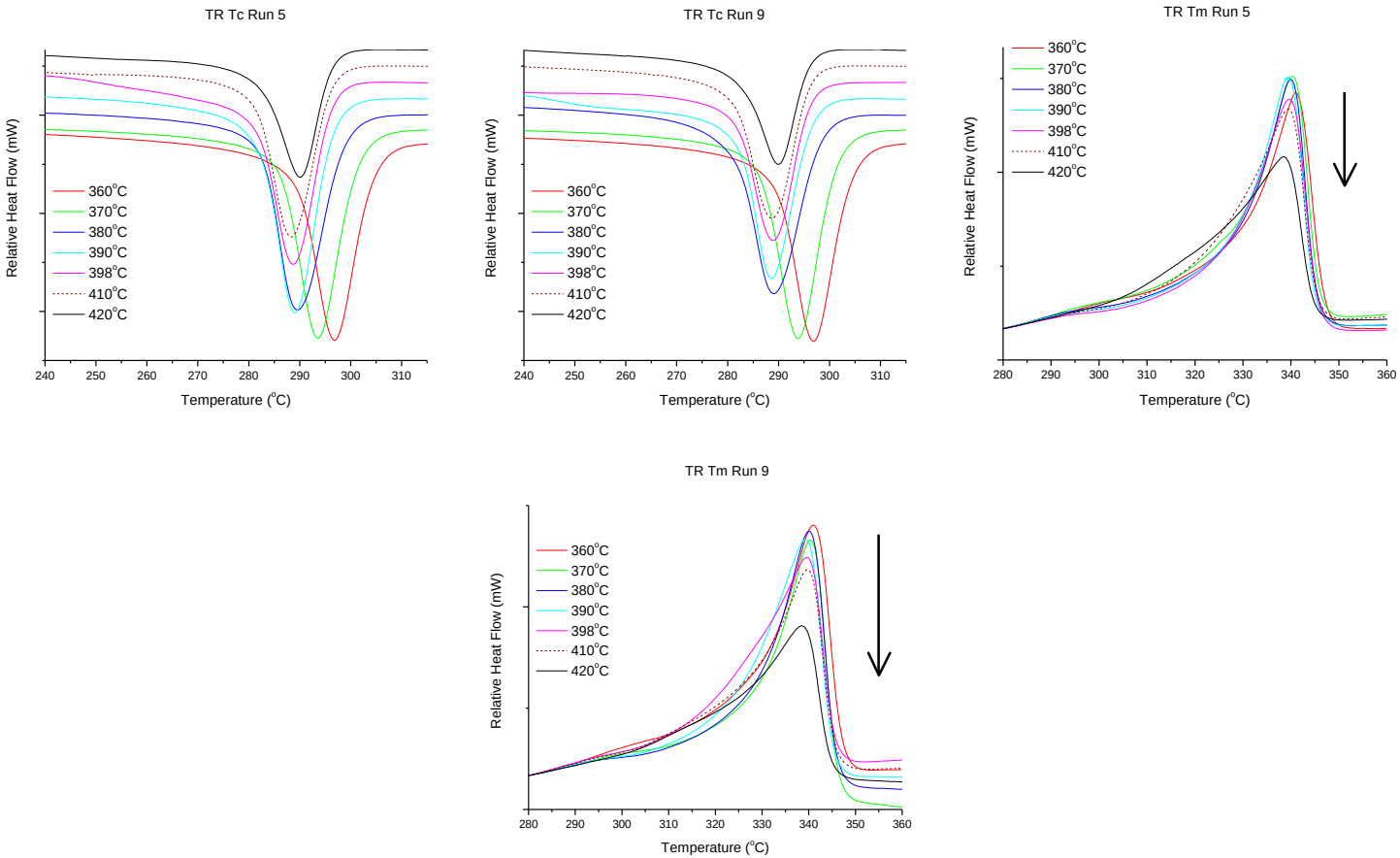

Figure 3-14: Non-isothermal crystallisation and subsequent melting following storage time of 2 minutes with varied T_s. (Top L-R) Run 5, Run 9 and (Bottom L-R) Run 5, Run 9. Arrow indicates a decrease in ΔH_f with an increase in temperature.

The decrease in ΔH_f and ΔH_c of PEEK thermally cycled to varied final hold temperatures are shown in Figure 3-15. It is clear that ΔH_c is depressed as run number is increased, brought upon by an increase in degradation. This depression of X_c is seen further on the subsequent ΔH_f, as the melting of crystals on reheating comes as a direct result of the crystals formed on cooling. Furthermore, a clear trend can be observed, in that an increase in hold temperature increases the development of degradation. It is apparent that a sudden substantial decrease in ΔHc is observed, occurring dependent on final hold temperature. This decrease coincides with the disappearance of T_{c2}, consistent with results found in isothermal holds. It is clear from figure 3-15, repeatable results can be obtained for up to 3-4 runs with a final hold temperature of 398^{o}C however, values of ΔH_f and ΔH_c are consistent and therefore reproducible at temperatures below 390^{o}C for up to 12 runs.

This proves samples do not need to be heated to above T_m^0 to obtain repeatable results. As temperatures approach above 390^{o}C, any results obtained will be inconsistent due to the effects of degradation; therefore a fresh sample of PEEK must be used. However, multiple runs can be generated from one sample if heated to lower temperatures.

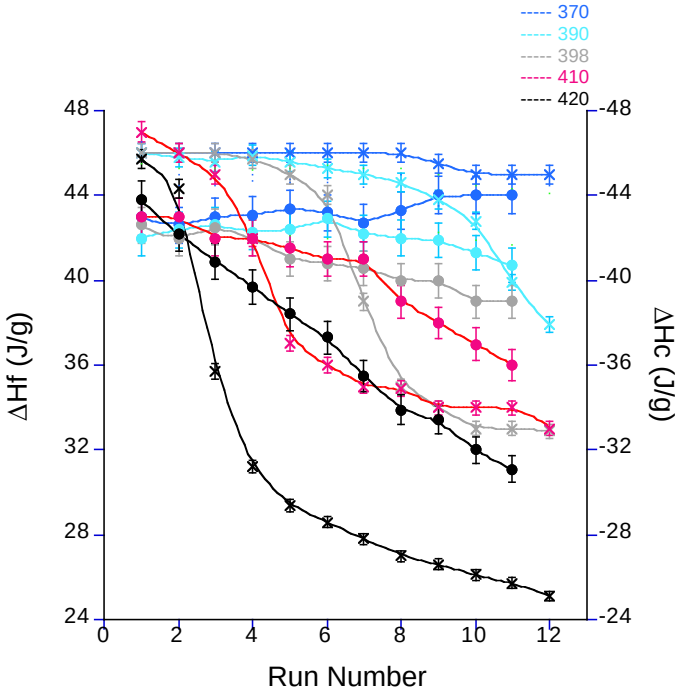

Figure 3-15: Comparison of ΔH_f and ΔH_c for 450PF PEEK thermally recycled varied temperatures. x – ΔH_c, • - ΔH_f.

Figure 3-16 shows the increase in Tg with run number for samples of PEEK thermally cycled to varied hold temperature. It is clear that with increased run number an increase in Tg is observed, which is more pronounced at higher hold temperatures. There is a negligible effect on Tg at temperatures of 390°C and below. An increase in Tg is further evidence of crosslinking as a combination of two reasons. Firstly crosslinking limits the mobility of the PEEK chains, therefore demobilising them, meaning more energy is needed to allow the chains to move. Secondly crosslinking increases the density of the structure meaning there is a

reduction in free volume, there is therefore less room to accommodate these motions.

Further measurements of glass transition, ΔCp and breadth are shown in Figure 3-17; results are shown in Table 3-3. It is clear that these show a similar trend and again negligible increase is seen at 390°C and below. Above 390°C a substantial increase in observed. A significant increase in ΔCp is observed which relates closely to the disappearance of T_{c2}. This is expected as both breadth and ΔCp will increase with increased energy needed for transition, this is brought upon by crosslinking.

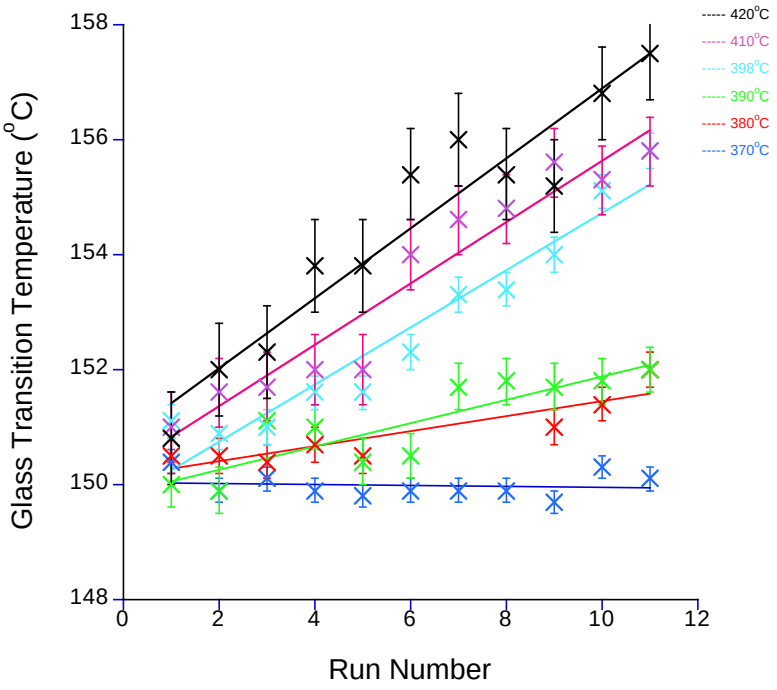

Figure 3-16: Graph showing the increase of Tg with increasing number of runs to final hold temperature of 450PF PEEK.

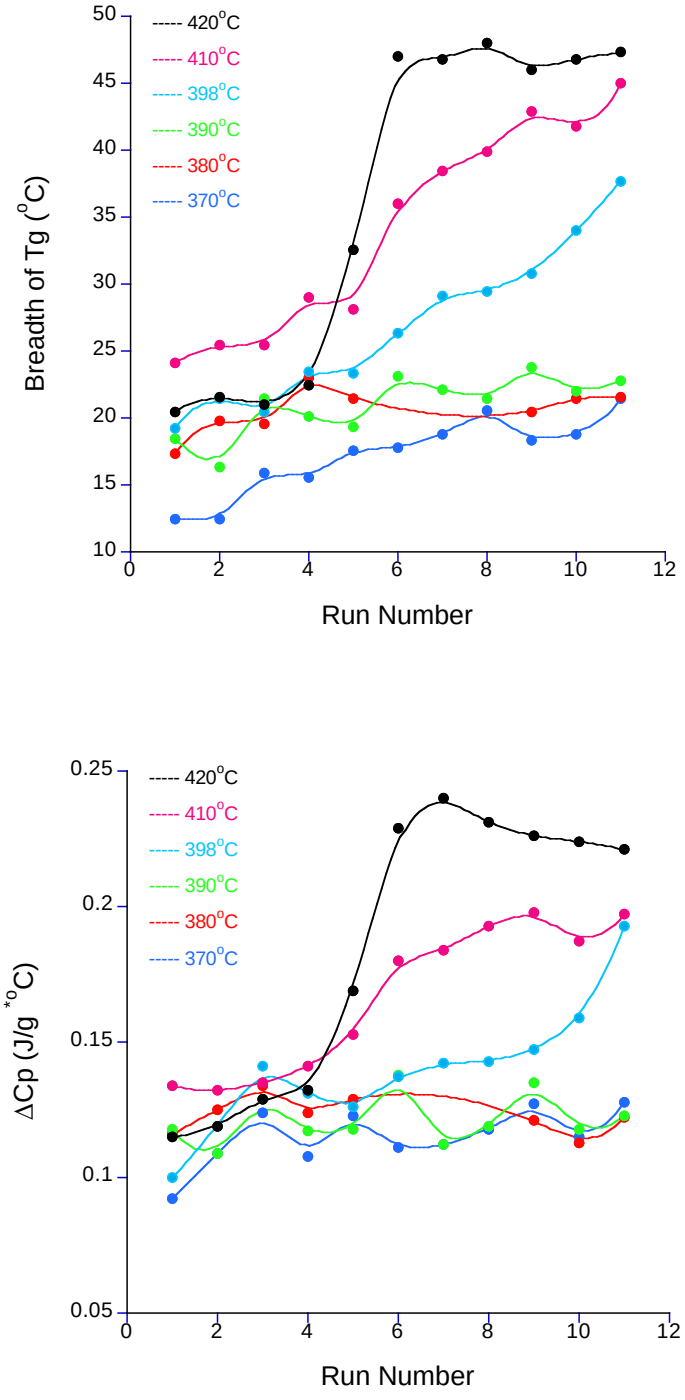

Figure 3-17: Graph showing the increase in Breadth and ΔCp of Tg with increasing number of runs to final hold temperature of 450PF PEEK.

		Run 1	Run 2	Run 3	Run 4	Run 5	Run 6	Run 7	Run 8	Run 9	Run 10	Run 11
370^{0}C	**Tg (^{o}C)**	150.4	149.9	150.1	149.9	149.8	149.9	149.9	149.7	150.8	150.1	150.7
	Breadth (^{o}C)	12.5	12.4	15.9	15.6	17.6	17.8	18.8	20.6	18.3	18.8	21.4
	ΔCp (J/g $^*{}^o$C)	0.092	0.109	0.124	0.108	0.123	0.111	0.112	0.118	0.127	0.115	0.128
390^{0}C	**Tg (^{o}C)**	150.0	149.9	151.8	151.0	150.4	150.5	152.2	151.8	151.7	151.8	151.7
	Breadth (^{o}C)	18.5	16.3	21.4	20.1	19.3	23.1	22.1	21.5	23.8	22.0	22.8
	ΔCp (J/g $^*{}^o$C)	0.118	0.109	0.129	0.117	0.118	0.138	0.112	0.119	0.135	0.118	0.123
398^{0}C	**Tg (^{o}C)**	151.1	150.9	151.0	151.6	151.6	152.3	153.3	153.4	154.0	155.1	156.0
	Breadth (^{o}C)	19.2	21.5	20.5	23.5	23.3	26.3	29.1	29.5	30.8	34.0	37.7
	ΔCp (J/g $^*{}^o$C)	0.100	0.119	0.141	0.131	0.126	0.137	0.142	0.143	0.147	0.159	0.193
420^{0}C	**Tg (^{o}C)**	150.8	152.0	152.3	153.8	153.8	155.4	157.2	155.4	154.1	156.8	157.5
	Breadth (^{o}C)	20.5	21.6	21.0	22.4	32.6	47.0	46.8	48.0	42.0	46.8	47.3
	ΔCp (J/g $^*{}^o$C)	0.115	0.119	0.129	0.132	0.169	0.229	0.240	0.231	0.226	0.224	0.221

Table 3-3: Tg, Breadth and ΔCp of Non-isothermal recycled PEEK following storage time of 2 minutes at varied hold temperatures. **Please note errors - Tg - +/- 2^{o}C, Breadth - +/- 2^{o}C, ΔCp - +/- 0.10.**

Results indicate that T_m^0 is the tipping point at which conditions for crosslinking and degradation overcome recrystallisation, and changes to the morphology of PEEK are even more pronounced. Reproducible results are obtained at hold temperatures below 390°C, and changes to T_c temperature show that pre-existing nuclei in the melt have been removed.

Once above T_m, PEEK begins to degrade, through the process of chain scission. The splitting of the polymer chains produces free radicals and decreases the size of chain length, a process confirmed by Day [86]. A reduction in chain length results in a depression of T_m, and formation of a varied size of spherulites results in a broadening of T_m endotherm, seen through the decrease in T_m onset. When two free radicals join together (termination step) they cease the ability to join in crystallisation. This cross-linked or web like structure impairs selected amorphous regions ability to crystallise, decreasing the X_c of PEEK. Results indicate that the process of crosslinking continues at a slower rate once a bulk of the amorphous region has already cross-linked, results showing a smaller depression in ΔH_f and ΔH_c between each run.

3.3.2.3 Effect of Hold time in Non-isothermal Holds.

The extent of degradation in PEEK is shown to be directly related to processing temperature. Furthermore, the duration of hold time at elevated temperatures will further effect degradation and processing results. To investigate the effect of hold time on degradation, further tests were conducted. Figure 3-18 shows the T_m endotherms for samples of PEEK thermally recycled to 398^{o}C with varied hold times. Hold times of 10 seconds to 10 minutes were investigated. It is apparent that degradation is increased with increased hold time, and it is clear that the extent of degradation is directly related to the hold time.

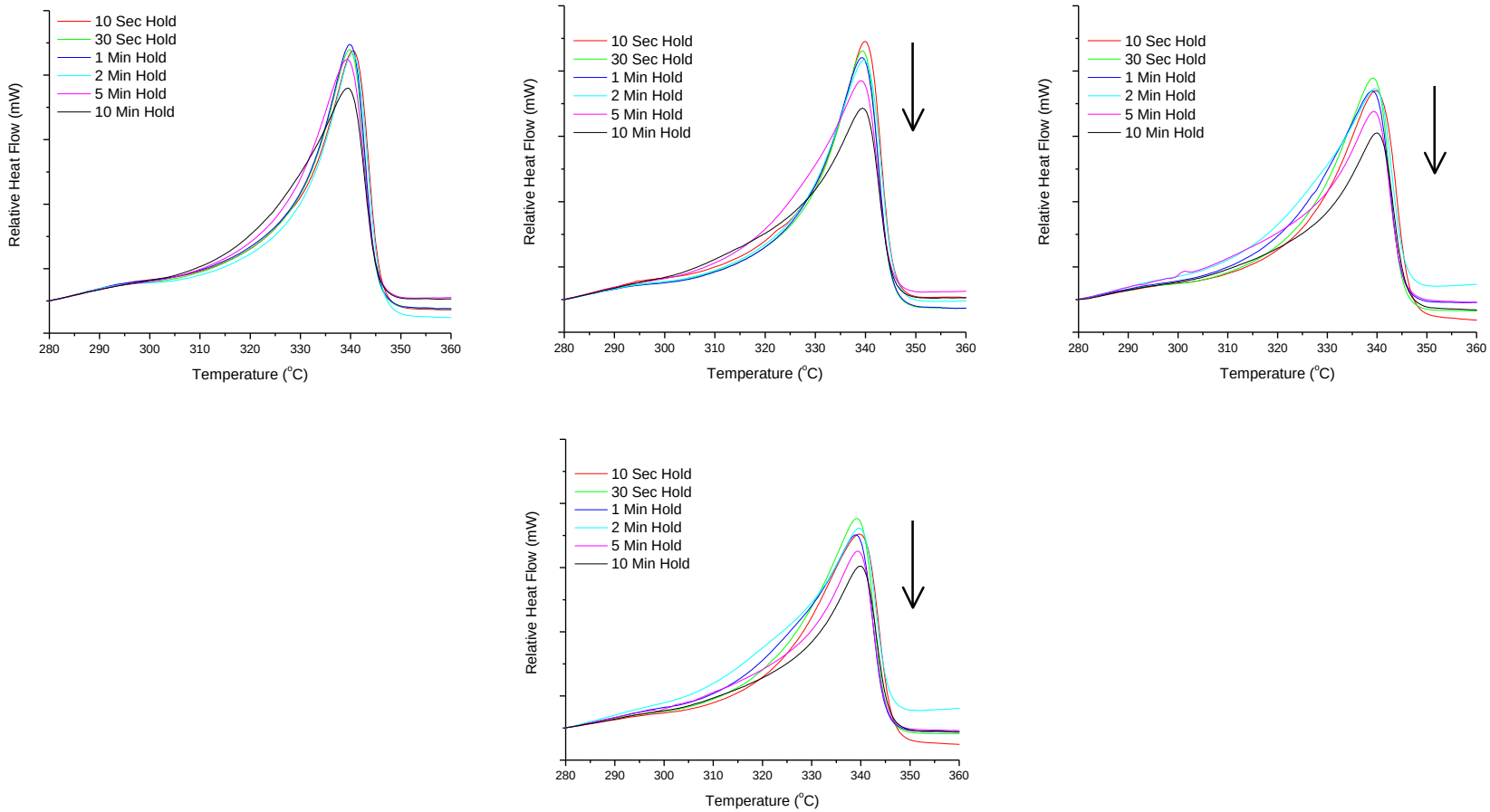

Figure 3-18: Melting of 450PF PEEK, with a Ts of 398°C, following varied storage times. (Top L-R) Run 3, Run 5 and (Bottom L-R) Run 9, Run 11. Arrow indicates a decrease in ΔH_f with an increase in hold time and run number.

Figure 3-19 shows the decrease in ΔH_c and ΔH_f for PEEK thermally cycled to 398°C for varied hold times. It is clear that degradation occurs at an earlier run number as hold time is increased. Using smaller hold times repeatable results can be obtained at higher temperatures. Hold times of less than 1 minute gave consistent levels of X_c for up to 6 runs. This indicates that residual nuclei are being removed allowing consistent values of ΔH_f to be obtained, and that degradation is not having a depressing effect on the X_c of PEEK. As hold time is increased the number of consistent runs obtainable from one sample of PEEK is greatly decreased.

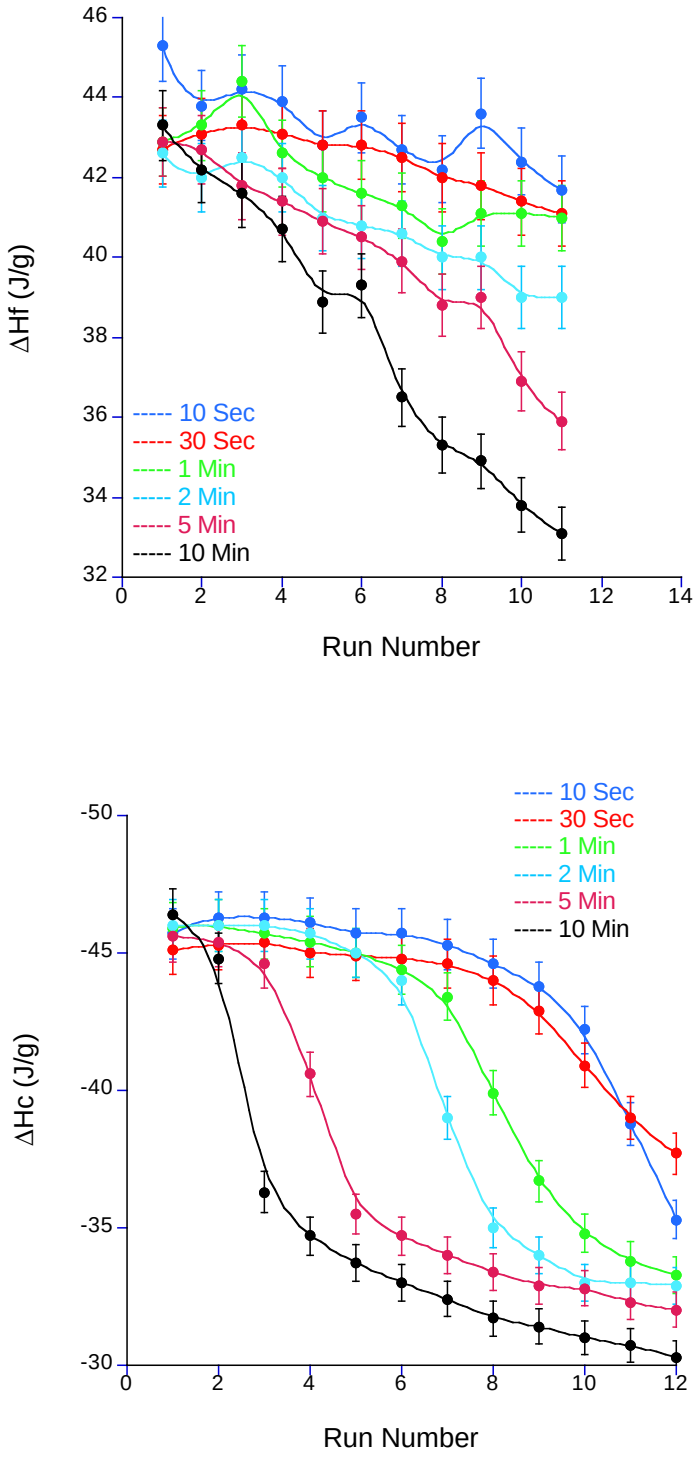

Figure 3-19: Comparison of the decrease in ΔH_f and ΔH_c for 450PF PEEK thermally recycled to 398°C and held for varied amounts of time.

It is clear the depression of X_c is consistent at all hold times, only appearing at an earlier run with increased time. This indicates crosslinking occurs over a distinct pathway, with both time and temperature affecting the speed of this reaction.

To confirm these results, Table 3-4 and Table 3-5 show data for ΔH_f and ΔH_c for samples of PEEK recycled at hold temperatures of 360, 398 and 420°C for varied holds of 10 seconds and 2 minutes. It is clear that at lower hold temperatures consistent values can be obtained for hold times of up to 5 minutes per run over the total number of runs tested. As hold times are increased to 10 minutes, consistent results are still obtained for up to 7 runs. This indicates that although chain scission and crosslinking are occurring once PEEK is in the melt, the reaction occurs at a depressed rate. Runs at to 420°C showed an immediate decrease in X_c, with hold times longer than 10 seconds showing an immediate depression in X_c.

Run Number	360°C		398°C		420°C	
	ΔH_c (J/g) (+/- 2 J/g)	ΔH_f (J/g) (+/- 3 J/g)	ΔH_c (J/g) (+/- 2 J/g)	ΔH_f (J/g) (+/- 3 J/g)	ΔH_c (J/g) (+/- 2 J/g)	ΔH_f (J/g) (+/- 3 J/g)
1	-46.5	44.0	-46.0	42.6	-45.7	43.8
2	-45.0	44.5	-46.0	42.0	-44.3	42.2
3	-44.5	45.7	-46.0	42.5	-35.7	40.9
4	-44.7	45.0	-45.7	42.0	-31.2	39.7
5	-44.6	44.8	-45.0	41.0	-29.4	38.4
6	-44.6	44.8	-44.0	40.8	-28.6	37.3
7	-45.0	44.4	-39.0	40.6	-27.8	35.5
8	-45.0	43.5	-35.0	40.0	-27.0	33.9
9	-45.0	43.5	-34.0	40.0	-26.6	33.4
10	-45.0	44.0	-33.0	39.0	-26.1	32.0
11	-45.0	44.0	-33.0	39.0	-25.7	31.1

Table 3-4: Comparison of ΔH_f and ΔH_c for 450PF PEEK thermally recycled to 360°C, 398°C and 420°C, with a holding time of 2 minutes.

Run Number	398°C		420°C	
	ΔH_c (J/g) (+/- 2 J/g)	ΔH_f (J/g) (+/- 3 J/g)	ΔH_c (J/g) (+/- 2 J/g)	ΔH_f (J/g) (+/- 3 J/g)
1	-45.7	45.3	-45.7	42.7
2	-46.3	43.8	-45.7	42.6
3	-46.3	44.2	-45.2	42.4
4	-46.1	43.9	-44.6	41.7
5	-45.7	42.8	-40.8	41.5
6	-45.7	43.5	-38.3	42.0
7	-45.3	42.7	-37.2	41.4
8	-44.6	42.2	-36.4	40.8
9	-43.8	43.6	-35.7	40.2
10	-42.2	42.4	-35.0	39.5
11	-38.8	41.7	-34.7	38.7

Table 3-5: Comparison of ΔH_f and ΔH_c for 450PF PEEK thermally recycled to 398°C and 420°C, with a holding time of 10 seconds.

Figure 3-20 shows a percentage loss of ΔH_f and ΔH_c due to degradation between the first and final run of PEEK thermally cycled to varied hold temperatures (2 minute holds) and for varied hold times (at 398^{o}C). It is clear that a substantial increase in degradation is observed above 380^{o}C. Results have indicated that at temperatures below 380^{o}C residual nuclei in the melt will not be fully removed, therefore for repeatable results in thermal analysis if PEEK a hold temperature of 380^{o}C should be used. It is also clear that increased hold time, steadily increases the level of degradation through crosslinking occurring in PEEK, therefore hold times should be kept to below 2 minutes at processing temperatures above 380^{o}C.

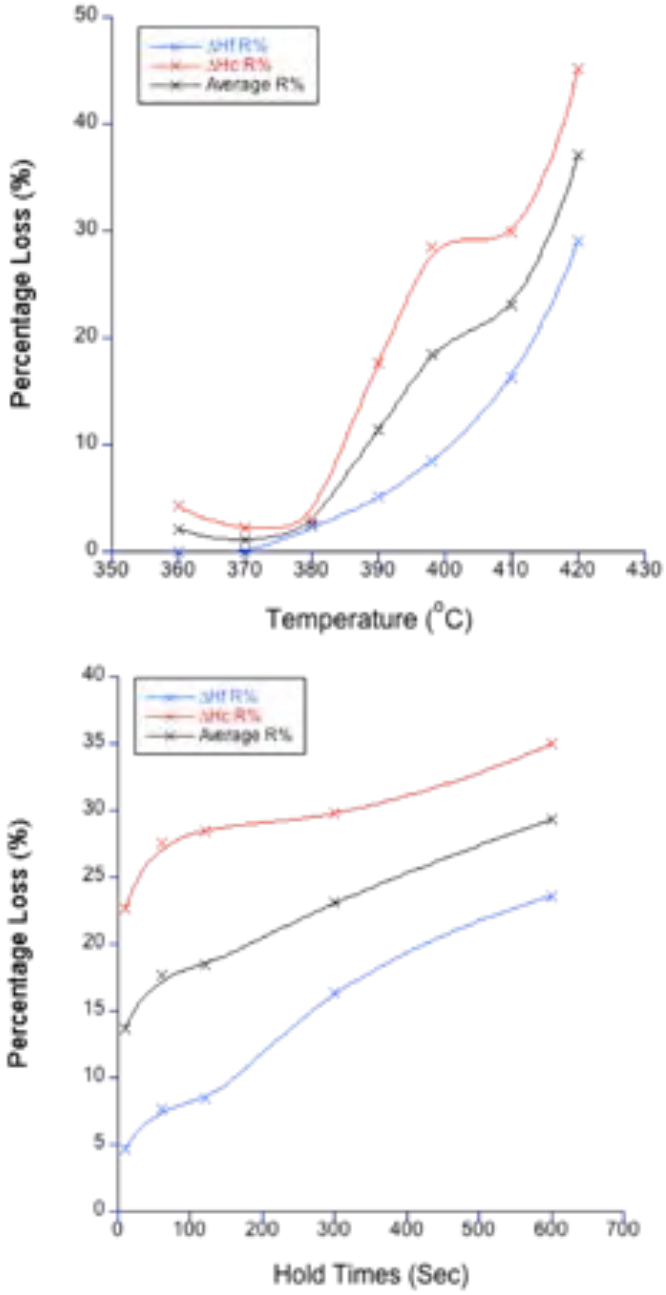

Figure 3-20: Average percentage Loss in ΔH_f and ΔH_c vs. temperature and vs. time at 398°C.

Figure 3-21 shows a schematic representation of the crosslinking reaction, which causes the depression of X_c at high temperatures in PEEK. TGA results indicated there is minimal weight loss over 4 hours in an oxygen environment; therefore it is believed that oxidative degradation would not cause such large decreases in X_c at these temperatures. Therefore this supports the notion that degradation is occurring due to a chain scission process. As random chain scission increases a cross-linked reaction occurs, creating a web like structure, which limits PEEKs ability to re-crystallise.

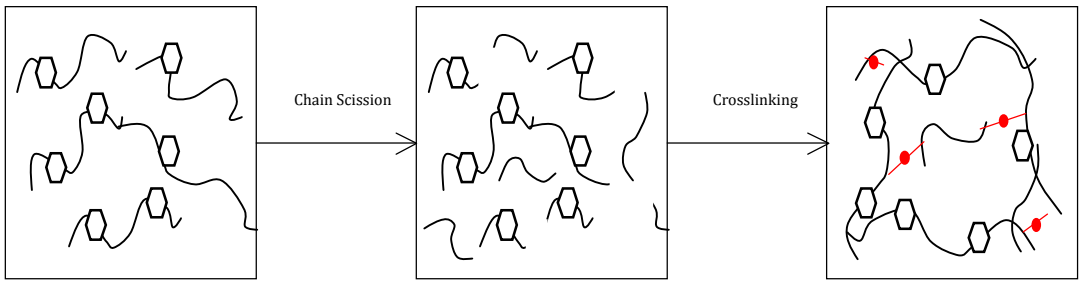

Figure 3-21: Schematic of chain scission and crosslinking in polymers.

Figure 3-22 shows the decrease in ΔH_f and ΔH_c in both isothermal and non-isothermal holds of PEEK at 398^{o}C. It is clear that both methods show similar patterns of degradation and depression of X_c. However, degradation occurs quicker in isothermal holds. This also shows that multiple runs of one sample allow consistent values to be obtained before the effects of degradation occur in non-isothermal holds.

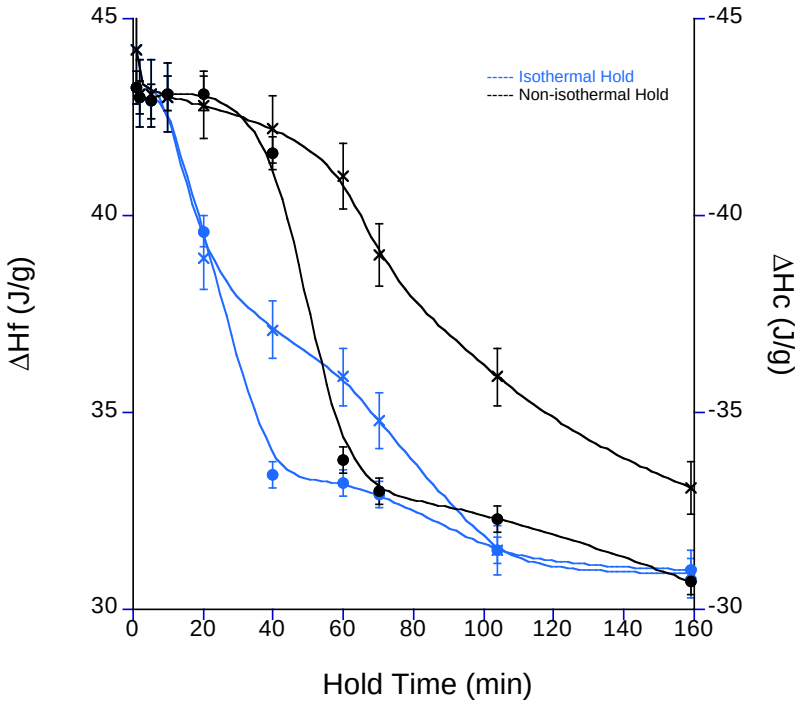

Figure 3-22: Comparison of decrease in X_c in Isothermal and Non-isothermal holds of 450 PF PEEK at varied holding times at 398°C. x $-\Delta H_f$, • - ΔH_c.

This is consistent with previous work such as Day, and Jonas and Legras [86-89] who showed the decrease in X_c due to degradation. However, results of this study have shown that at hold temperatures of 370°C - 380°C, repeatable results can be obtained from one sample of PEEK, if hold time is closely monitored, therefore removing any inconsistency obtained through changes in PEEK sample. This questions previous work, which has suggested that PEEK must be heated to above T_m^0 to obtain consistent results.

Figure 3-23 shows the variation in ΔH_f between run 1 and run 2 of PEEK in DSC heated to 390°C when a new sample is used for each experiment. This is compared to a single sample of PEEK thermally cycled to 390°C (the figure shows results for one sample of PEEK thermally cycled). It is clear that using the same sample of PEEK before degradation occurs gives a more consistent level of result than if a new sample is used after each run. This will allow a more conclusive level of analysis.

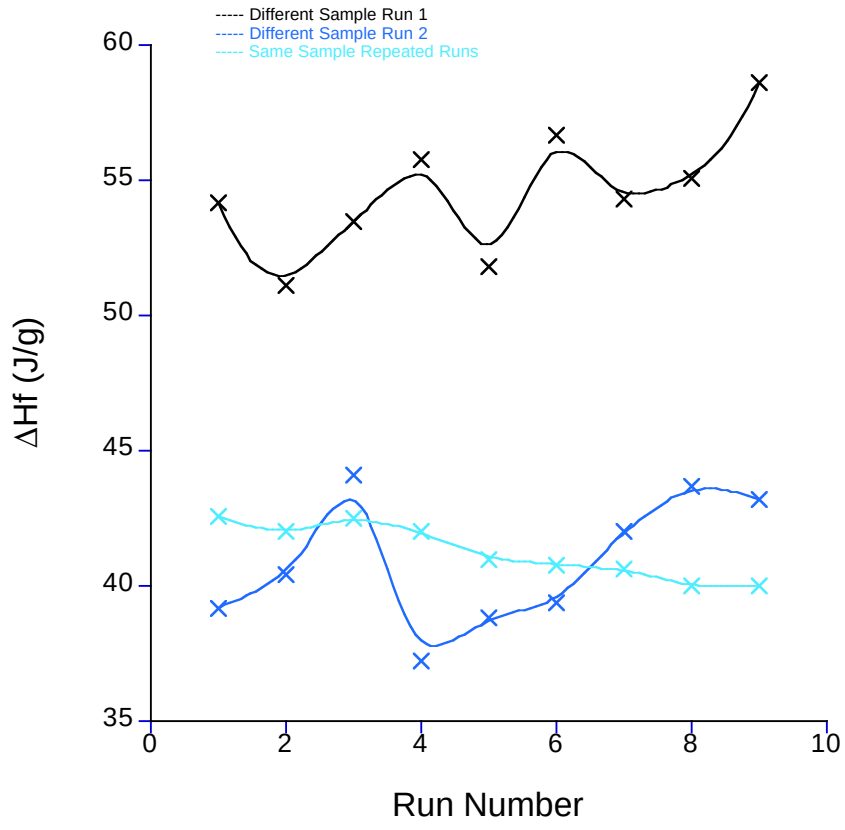

Figure 3-23: Variation in ΔH_f, between the same sample of PEEK thermally cycled and a new sample of PEEK used before each run.

Previous work has indicated minimal to no degradation occurring below 370°C however, further work has showed that if processed at 360°C for a sustained period of time, evidence is given that crosslinking is active at temperatures lower than previously reported. Further work was completed to analyse the effect of degradation at lower temperatures later in this chapter.

3.3.3 Avrami Analysis

Figure 3-24 shows the combined crystallisation exotherm for thermally cycled PEEK held at 398°C for 5 minutes per run. It is clear as run number increases a depression in ΔH_c is observed. Furthermore crystallisation time decreases with an increase in run number. This is consistent with crosslinking. As crosslinking increases, the remaining nuclei available for crystallisation decrease. As this continues with each run, crystallization time will continue to fall.

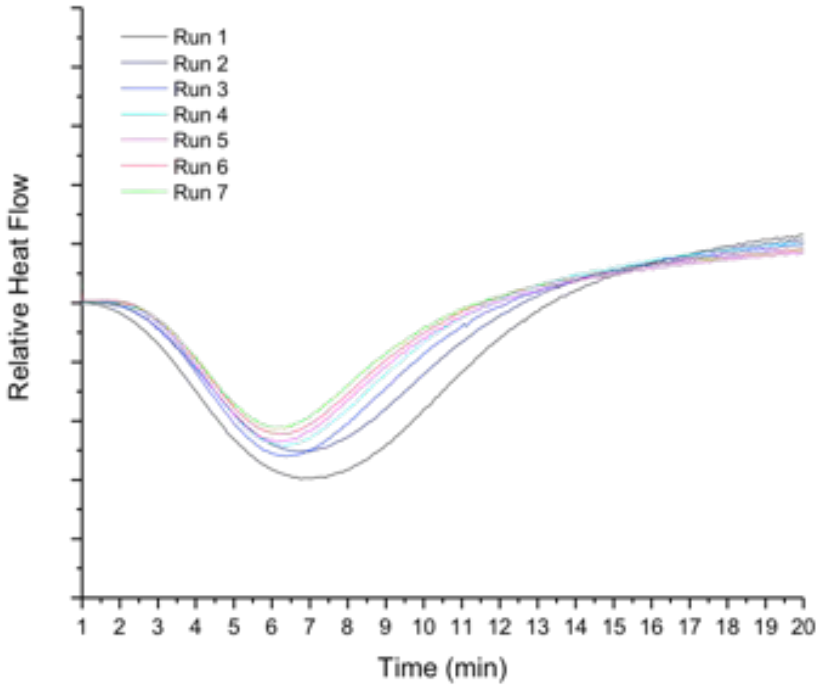

Figure 3-24: Crystallisation exotherms of 450PF PEEK thermally cycled for 5 minutes at 398°C.

Figure 3-25 shows the Avrami analysis of relative crystallinity against time. It is clear that the time need for PEEK to complete crystallisation decreases with each run number. Further confirming the process of crosslinking.

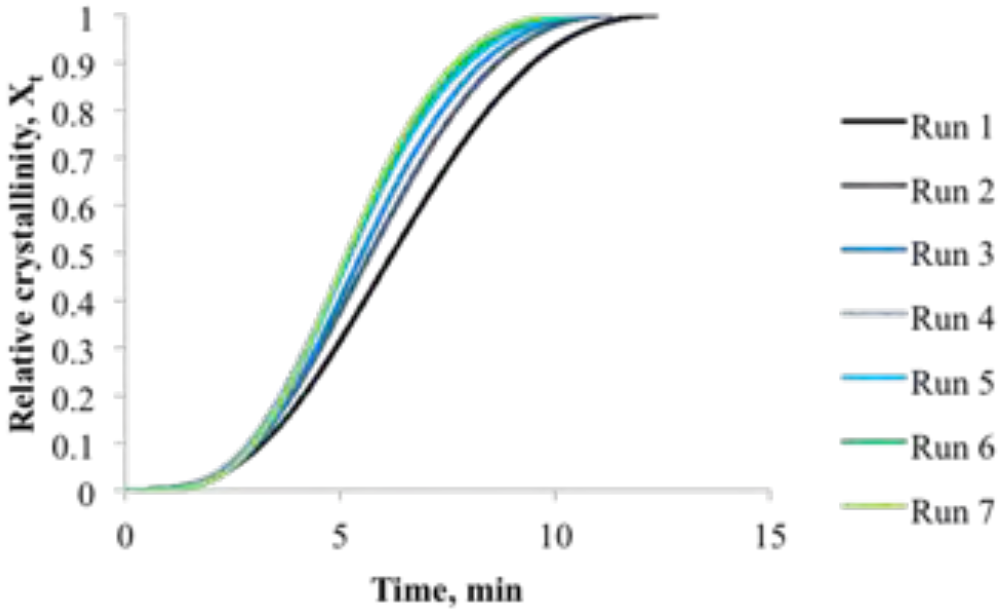

Figure 3-25: Avrami analysis of 450PF PEEK thermally cycled for 5 minutes at 398°C.

3.3.4 Degradation of PEEK at 360°C and below

Previous work has shown degradation to occur above temperatures of 370°C. Degradation at temperatures below this has been described as minimal and has not been significantly investigated. However results above show a definite decrease in X_c at temperatures lower than 370°C if hold times are long enough. Thermal cycling experiments were extended to look at temperatures just above the melting endotherm (360°C), at the T_{upper} of the melting endotherm (355°C) and during the process of melting (350°C). Runs were extended to gain a greater knowledge of the extent of degradation at these temperatures. Hold times of 10 minutes were used.

Figure 3-26 and Figure 3-27 shows the cooling exotherms for 360°C and 355°C respectively. It is clear that with increasing run number a decrease in X_c is apparent. The pattern of X_c depression follows the same route as holds of higher temperatures. Although the number of runs needed before degradation takes a measurable effect on the depression of X_c is increased at these temperatures, it proves crosslinking is occurring.

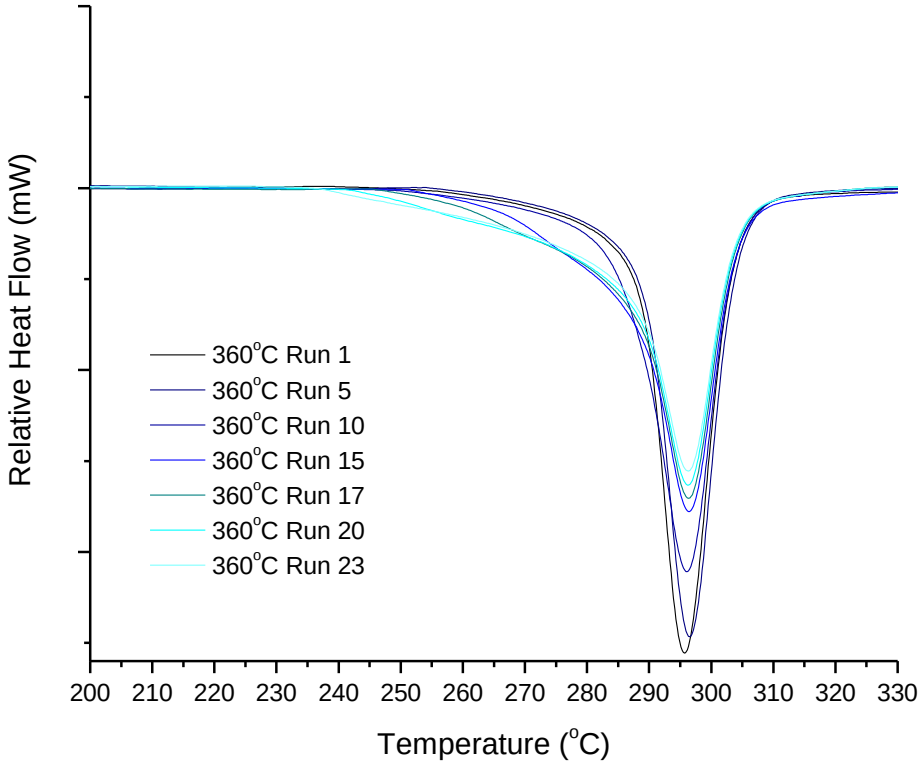

Figure 3-26: Cooling exotherms for PEEK thermally recycled to 360°C.

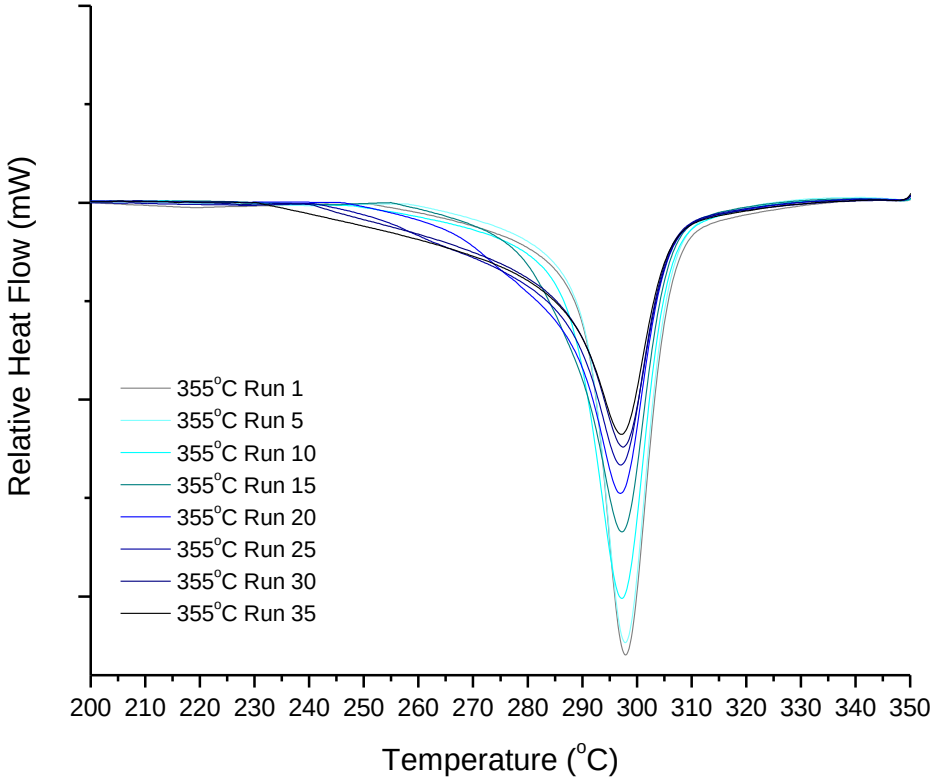

Figure 3-27: Cooling exotherms for PEEK thermally recycled to 355°C.

Figure 3-28 and Figure 3-29 show the cooling exotherm and resulting melting endotherm of hold temperature 350°C.

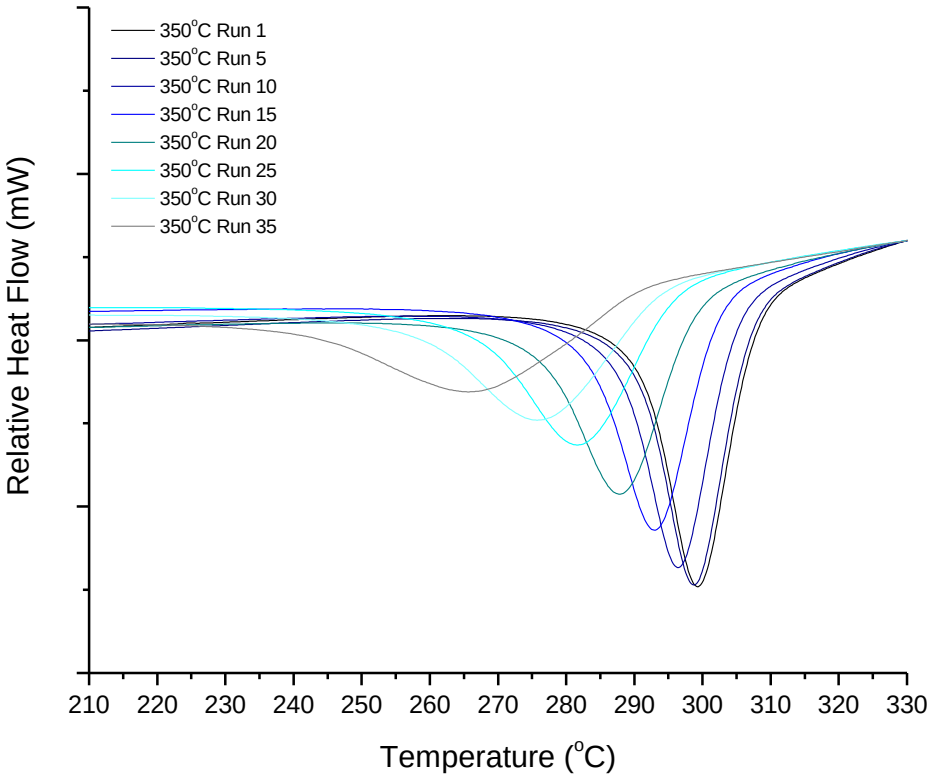

Figure 3-28: Cooling exotherms for PEEK thermally recycled to 350°C.

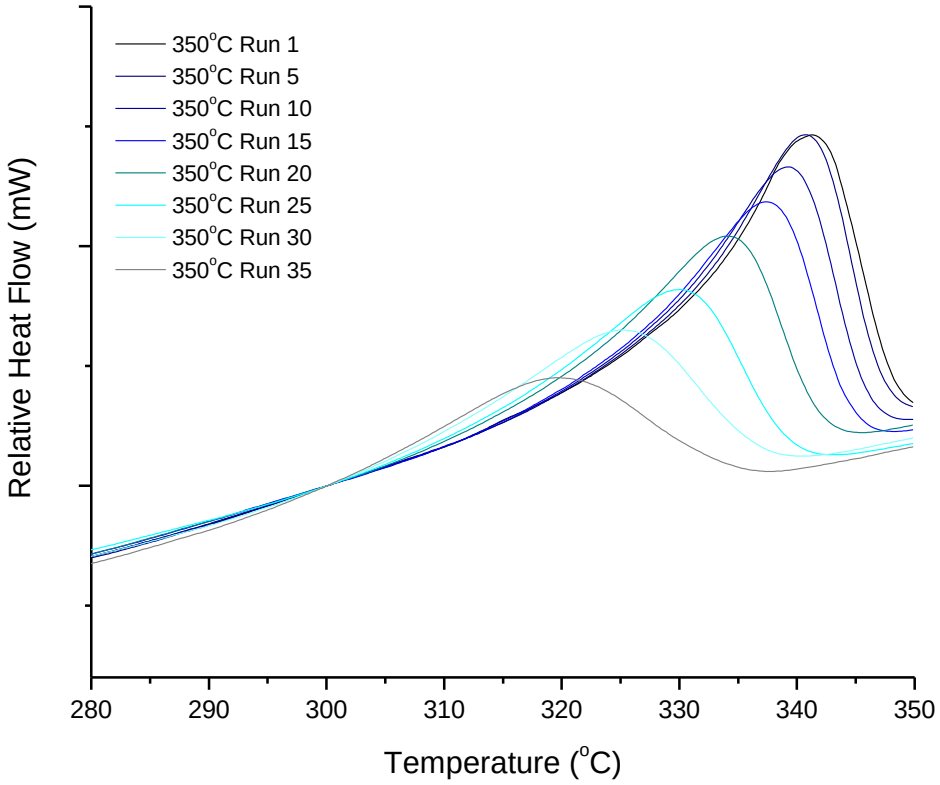

Figure 3-29: Melting endotherms for PEEK thermally recycled to 350°C.

A clear variation in the DSC traces of the 350°C hold time is seen. A decrease in overall X_c is still observed along with a broadening on T_m. However at this hold temperature there is a clear decrease in temperature of both T_m and T_c. This result varies from holds above this temperature, where stable values were obtained.

Figure 3-30 and Figure 3-31 show the variation in ΔH_f, ΔH_c and Tg respectively. The clear decrease in value shows that degradation is occurring at lower temperatures in the melt. Furthermore the systematic increase in Tg at all three temperatures gives further evidence to the process of crosslinking occurring. The

continued recycling of 350°C holds showed a continued decrease in X_c until an almost fully cross-linked material is formed.

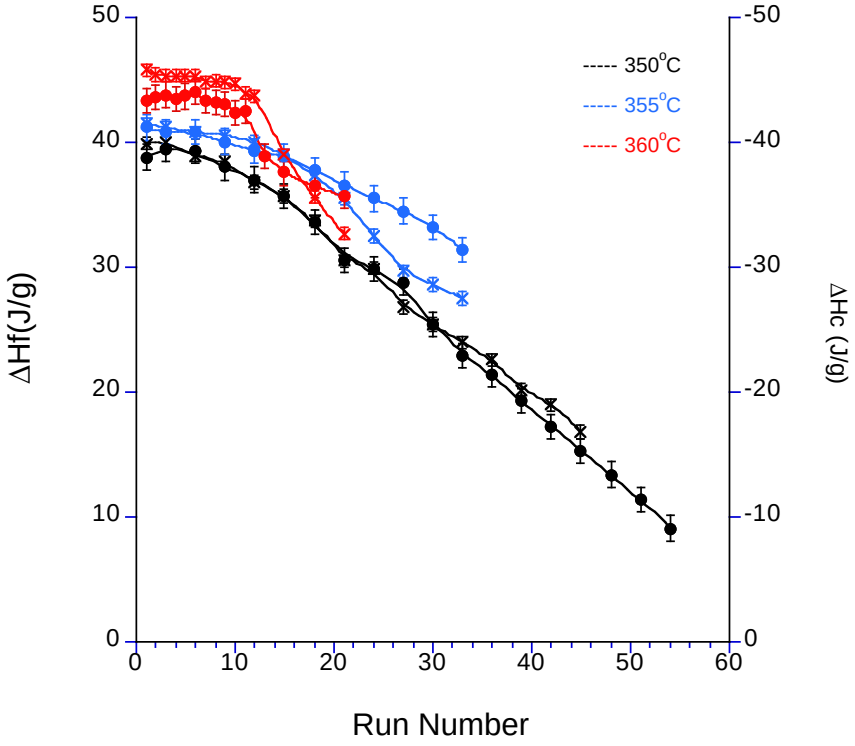

Figure 3-30: Decrease in ΔH_f and ΔH_c values for increasing run number at hold temperatures of 350°C, 355°C, 360°C. x $-\Delta H_c$, • - ΔH_f.

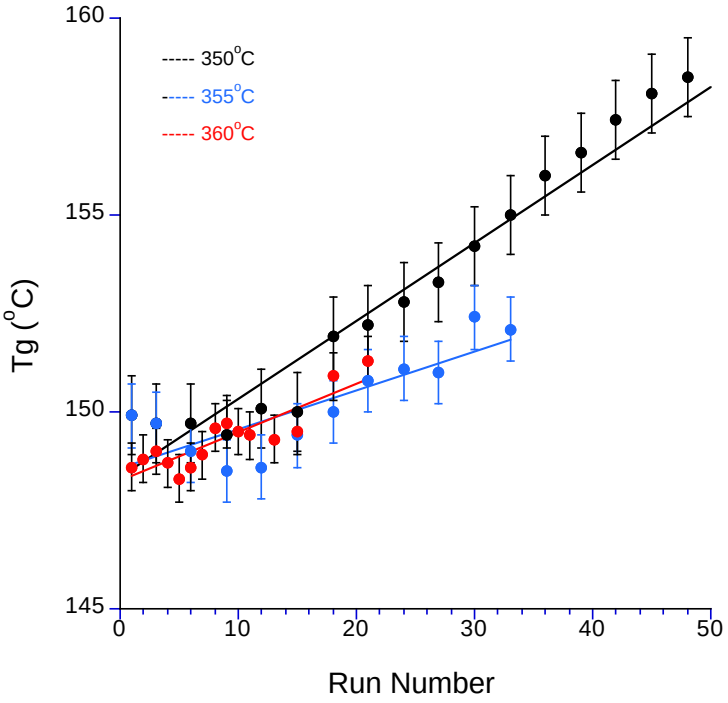

Figure 3-31: Increase in Tg for increasing run number at hold temperatures of 350°C, 355°C, 360°C.

It is clear that at temperatures below what has previously been stated in the literature degradation is active in PEEK; giving rise to the theory that crosslinking is an active process as soon as PEEK begins to melt. For temperatures above the last trace of melting a clear trend is seen, as hold time is increased, less hold time is needed to introduce degradations. Figure 3-32 shows a trace of hold temperature vs. log time above 354°C. Results from holds at 350°C indicate that the process of crosslinking and degradation is occurring during the process of melting. Results actually indicate that degradation is increased when PEEK is held before it has fully melted.

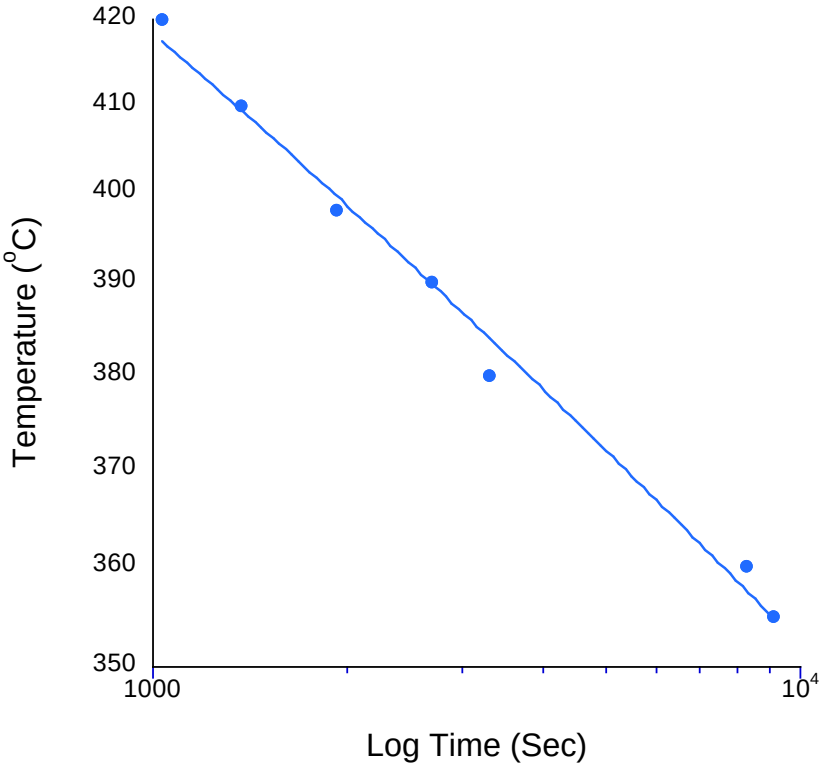

Figure 3-32: Plot of hold temperature vs. Log time at point of first signs of degradation.

The longer PEEK spends at temperatures around T_m degradation increases. This process is further increased at higher temperatures. Figure 3-33 shows that by increasing time held at lower temperatures, degradation rates of higher temperatures can be replicated. ΔH_f values are shown vs run number for holds at 350°C, and 355°C with holds of 10 minutes and, 398°C, 410°C and 420°C with holds

of 2 minutes. It is clear that by increasing hold time at lower temperatures, the 350°C and 410°C curves overlap, as do 355°C and 398°C.

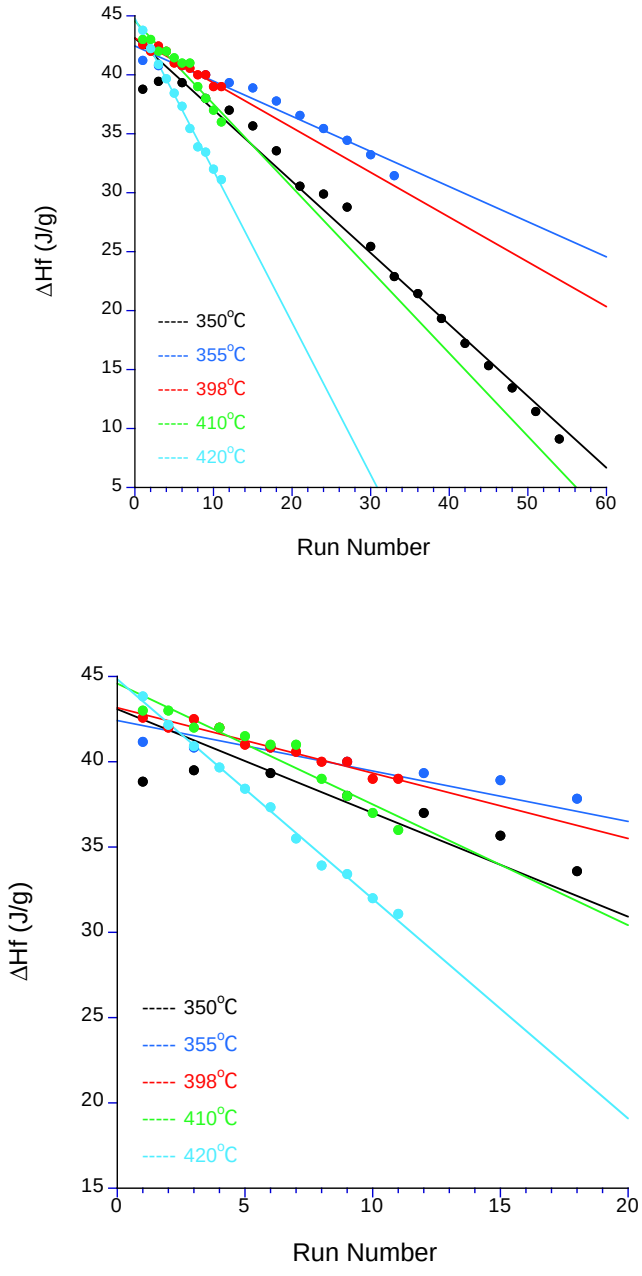

Figure 3-33: Values of ΔH_f against run number for varied hold temperatures. 350-355°C 10-minute holds, 398-420°C 2 minute holds. Top figure to run 60. Bottom figure to run 20.

3.3.5 Double Crystallisation Exotherms in PEEK.

Analysis of the cooling exotherms shows an anomaly in the form of a second crystallisation peak (T_{c2}). Dependent on final hold temperature, a varied number of runs are needed for T_{c2} to appear. Initially a broadening of T_c occurs, before the appearance of a second peak. This peak moves to a lower temperature as run number continues before disappearing. At higher hold temperatures this phenomenon occurs at an early run number. This movement of T_{c2} corresponds directly to the large decrease in ΔH_c seen in results above. Furthermore T_{c2} relates directly to a broadening of T_m.

Figure 3-34 and Figure 3-35 show three cooling exotherms of PEEK thermally cycled to 390°C and 398°C respectively, clearly showing the movement to a lower temperature of T_{c2}. The main crystallisation peak can be observed at 288°C in both figures, T_{c2} can be observed moving from peak at 270°C to 250°C before disappearing. Figure 3-36 shows the resulting heating endotherms showing a broadening of T_m.

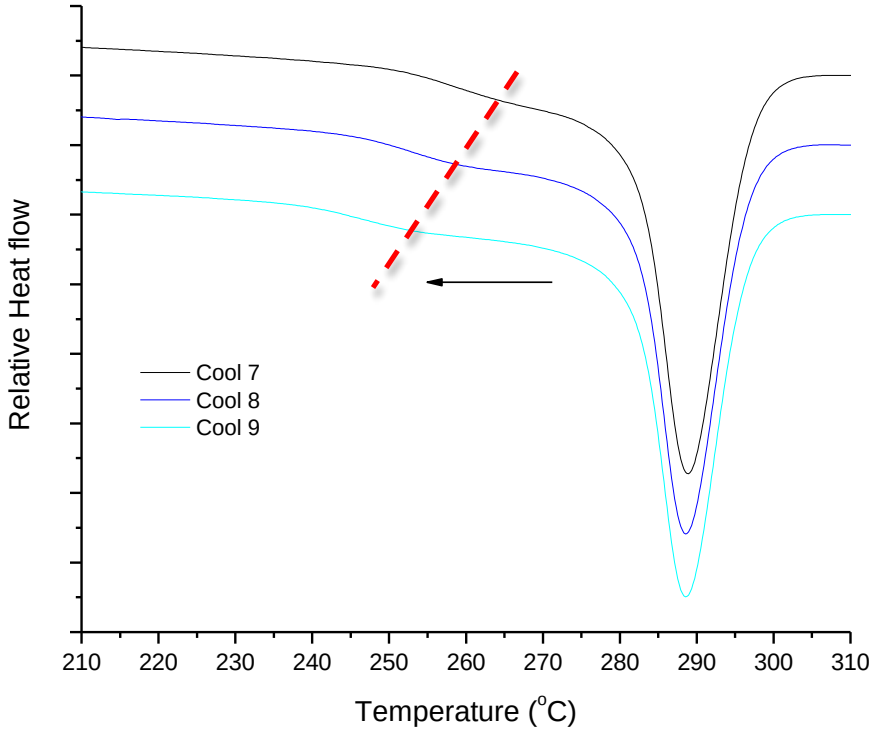

Figure 3-34: Cooling endotherms of PEEK thermally cycled to 390°C. Main crystallisation peak can be observed at 288°C, T_{c2} can be observed moving from peak at 270°C to 250°C

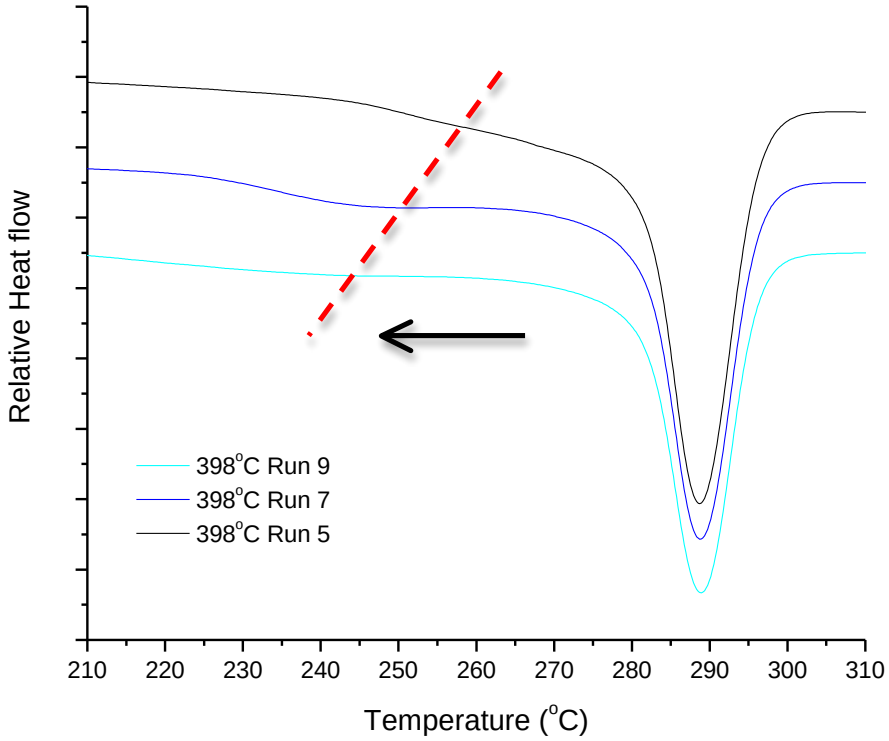

Figure 3-35: Cooling endotherms of PEEK thermally cycled to 398°C. Main crystallisation peak can be observed at 288°C, T_{c2} can be observed moving from peak at 270°C to 250°C

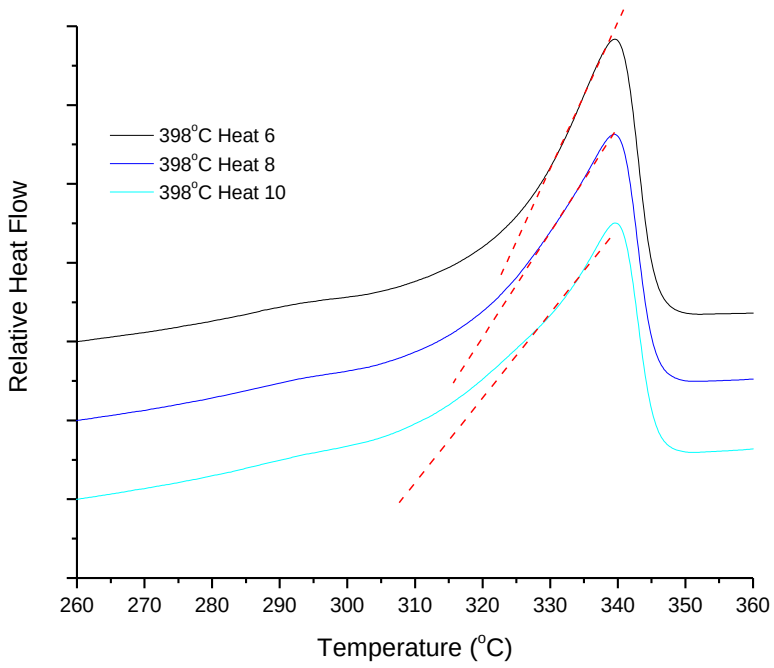

Figure 3-36: The broadening of the melting endotherms of PEEK thermally cycled to 398°C due to crosslinking.

Sandler et al. [119] reasoned that the presence of double crystallisation peaks in PEEK composites was due to the interaction between the matrix and carbon fibre filler, with increased filler resulting in a second crystallisation peak. The same theory can be applied to this work by replacing the presence of carbon fibre with the presence of cross-linked chains. If the presence of crosslinking hinders the mobility of other molecules, inhibiting their ability to participate in crystallisation, T_{c2} appears. With increased crosslinking this delay in the hindered molecules ability to crystallise is increased, moving T_{c2} to a lower temperate. However as with PEEK composites, eventually spherulite growth increases and hindered molecules are integrated into crystallisation, therefore there is no significant

double melting peak on re heating. However the varied size of spherulites formed results in a broadening of T_m. Crosslinking grows to a point where hindered molecules are no longer able to join in with crystallisation, resulting in a loss of T_{c2} and a reduction in variation in spherulite size. This results in a decrease in the breadth of the T_m endotherm.

A second theory can relate T_{c2} to crosslinking directly. As shown in results above the appearance in T_{c2} relates closely to a large reduction in ΔH_c values as well as an increase in Tg. Both are indicators of crosslinking. Crosslinking is an exothermic reaction, which would result in an exothermic peak on a DSc curve if the reaction were strong enough. It has been shown that crosslinking is an on-going form of degradation occurring as soon as PEEK is in the melt however, it is a slow process, quickening at higher temperatures. The large decreases in ΔHc observed show an increase in crosslinking over a period of 2-3 runs. This increase in the crosslinking reaction may result in a much stronger change in heat flow observed by DSc, resulting in the appearance of T_{c2}.

Table 3-6 shows the values for the first sign of decrease in T_m onset and ΔH_f as well as the first sign of increase in Tg. It is clear that the appearance of T_{c2} directly relates to the changes in these measured values, which all can be used as evidence of both degradation and crosslinking. This supports the theory that the appearance of T_{c2} is an observable exotherm on the DSC trace.

Hold Temp (°C)	T_m Onset Decrease (Run Number)	Tg Increase (Run Number) (+/- 1)	ΔHc Decrease (Run Number) (+/- 1)	T_{c2} occurrence (+/- 1)
360 (10 min hold)	6	15	10	13
370	>12	>12	>12	>12
380	10	12	10	11
390	7	7	8	7
398	5	6	5	5
410	3	3	4	3
420	2	1	2	2

Table 3-6: The run number of first signs of change for different indicators of crosslinking. All Hold times are 2 minutes unless stated.

3.3.6 FTIR Analysis of PEEK

3.3.6.1 Theory and Application to PEEK

Figure 3-37 shows Fourier-transform infrared spectroscopy (FTIR) spectra of semi crystalline PEEK 450 PF, which are comparable to previous results gained by authors such as Chalmers et al [120]. Distinct spectral features are shown in the finger print region of the spectrum (1700cm^{-1} – 650cm^{-1}) (Figure 3-38 to Figure 3-40).

A carbonyl stretching vibration is observed at 1653cm^{-1} with an associated shoulder at 1252cm^{-1}, alongside an intense sharp band at 1227cm^{-1}. At 1490cm^{-1} another intense sharp band is observed which is associated with aromatic ring

absorption, identifying the sample as a thermoplastic. Absorption bands can become sharper and more intense with changing morphology, while other bands can decrease in intensity.

With semi crystallised PEEK, a shift in the carbonyl stretching frequency from 1653cm^{-1} to 1648cm^{-1} is observed.

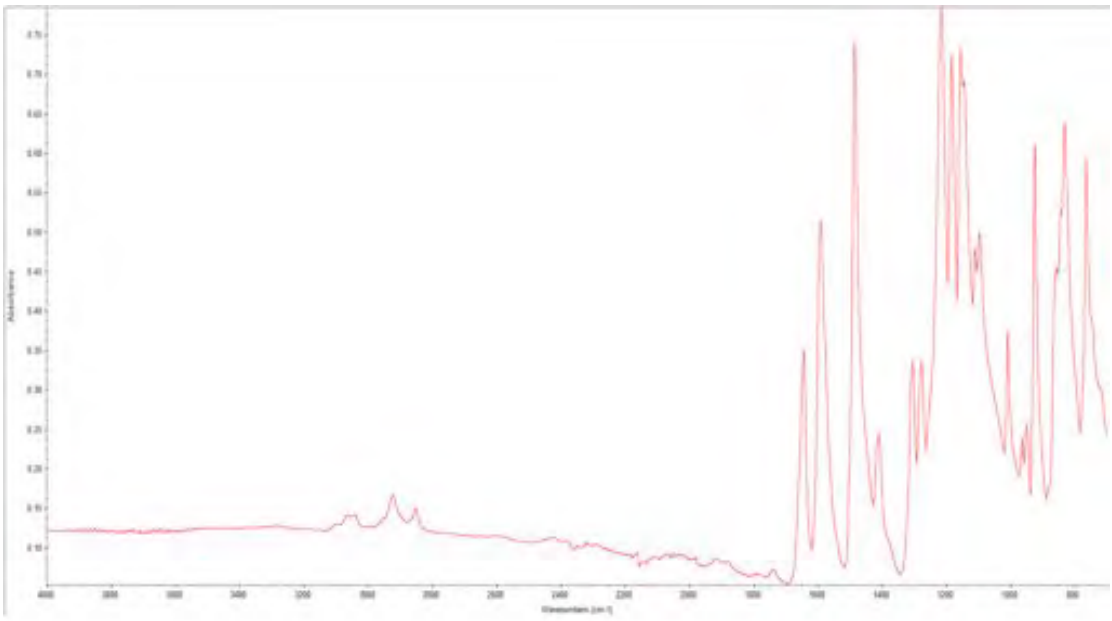

Figure 3-37: FTIR Spectrum of PEEK 450PF

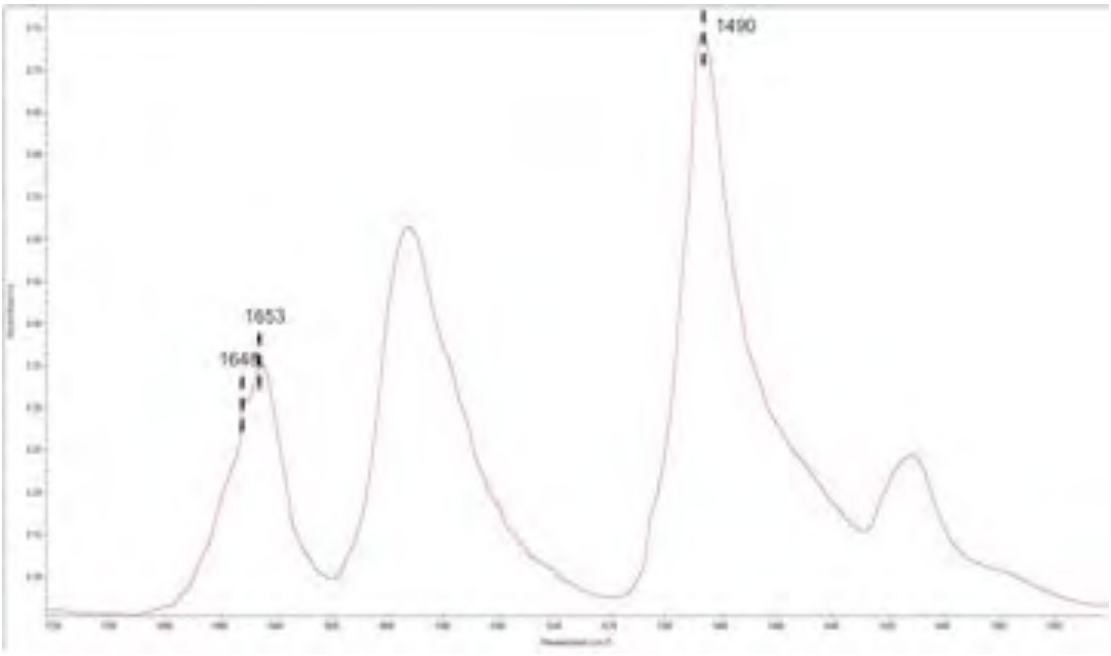

Figure 3-38: FTIR Spectrum of PEEK 450PF (1720cm^{-1} – 1360cm^{-1})

Figure 3-38 shows peaks at 1653cm^{-1} (P_1) and 1648 cm^{-1} (P_2), which is associated with a carbonyl stretching frequency common to PEEK. P_1 relates to the crystalline phase, where P_2 relates to the amorphous phase. Peak 1490cm^{-1} helps identify the sample as an aromatic thermoplastic, due to its presence in all aromatic thermoplastic spectrums.

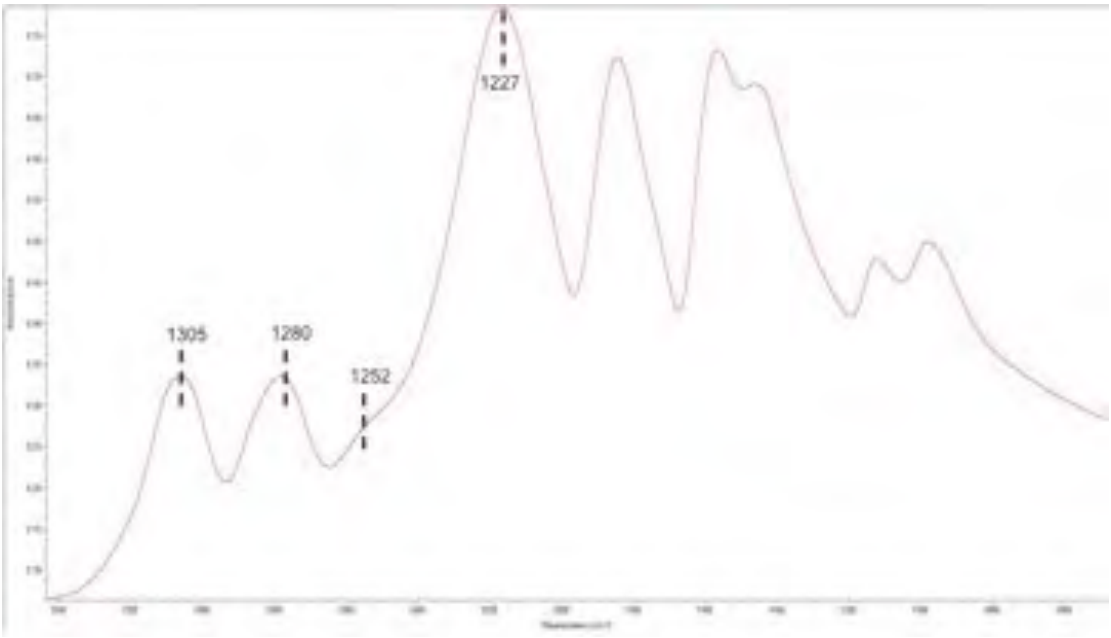

Figure 3-39: FTIR Spectrum of PEEK 450PF (1340cm^{-1} – 1060cm^{-1})

Figure 3-39 shows peaks at 1305cm^{-1} and 1280cm^{-1}, which can vary in intensity with sample crystallinity. These peaks were used by Chalmers et al. [120] to calculate an area ratio, which could be correlated to polymer crystallinity, and are exclusive to PEEK. Peaks at 1252cm^{-1} relate to carbonyl stretching, whereas peaks at 1227cm^{-1} relate to stretching of the carbon-oxygen-carbon bond. Both are common to PEEK.

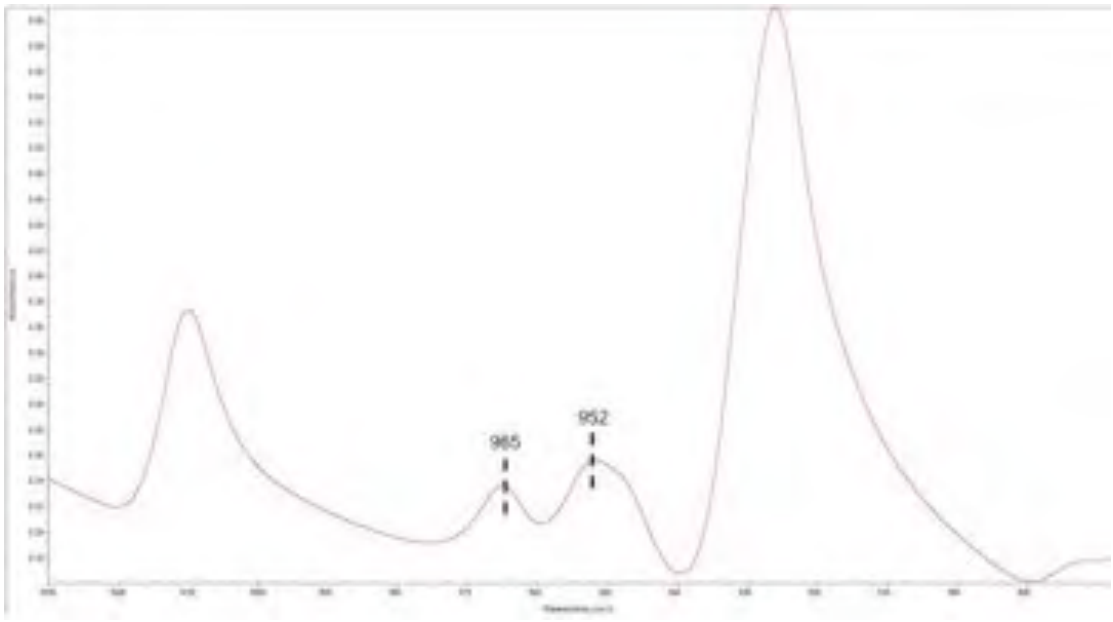

Figure 3-40: FTIR Spectrum of PEEK 450PF (1030cm^{-1} – 890cm^{-1})

Figure 3-40 shows peaks at 965cm^{-1} and 952cm^{-1} which were used by Jonas et al. [121] to calculate the factor of sample crystallinity due to their variation in intensity. Analysis of crystalline sensitive peaks to gain quantitative information on the degree of crystallinity, requires a reference peak which is unaffected by crystallisation changes. Both Jonas et al. and Chalmers [120, 121] used the peak at 952cm^{-1} as such a reference peak. Its occurrence is as a result of out of plane vibrations of the aromatic rings. A linear relationship was found between area ratios of peaks at 970cm^{-1} and 952cm^{-1}, and the degree of crystallinity measured by WAXS, suggesting that peaks at 970cm^{-1} are sensitive to crystallinity [120].

3.3.6.2 Results

A sample of PEEK was held at 398°C in DSC prior to cooling to 50°C. Before samples were reheated and heats of fusion recorded, the sample was then removed from its DSC pan and analysed on FTIR to observe any changes to the PEEK molecular chain brought on by degradation.

Figure 3-41 shows the FTIR spectra of PEEK after a number of holds at 398°C. It is clear, a decrease in peak heights at wavelengths 965cm^{-1} and 950cm^{-1} is observed at increased stages of thermal degradation. As discussed above both Jonas et al. and Chalmers [120, 121] used the peak at 952cm^{-1} as a reference peak in their analysis of PEEK crystallinity. It is apparent that thermal degradation limits the use of peak 952cm^{-1} as it is no longer unaffected by PEEK crystallinity.

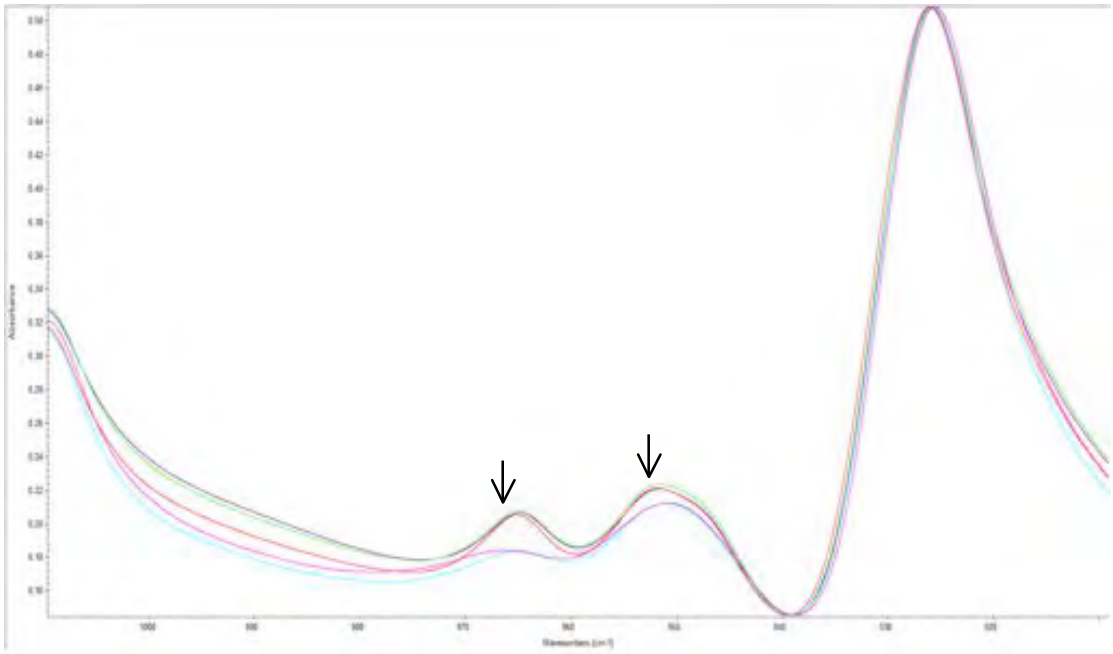

Figure 3-41: Decrease in peak size at 952cm^{-1}. As degradation increases, a decrease in peak size is observed.

Figure 3-42 to Figure 3-44 show the variation in FTIR spectra for the same sample of PEEK at three storage times. The sample was held at 370°C and analysed on FTIR before reheating. It is clear that an increase in thermal degradation (significantly between storage times of 5 – 10 hours) alters the size and/or position of a range of peaks.

Figure 3-42 shows a clear change in peak height at P_1 and P_2, which are related to the crystalline and amorphous regions of PEEK structure respectively. It is apparent that thermal degradation results in a decrease in the crystalline peak coinciding with an increase in amorphous peak intensity. This can be correlated to significant change in the crystallisation behaviour of PEEK as shown by DSC analysis: crystallinity values were obtained through DSC at each stage of degradation. Initial X_c was measured at 30%, after 5 hours X_c was 21%. After 10 hours X_c had fallen to 6%.

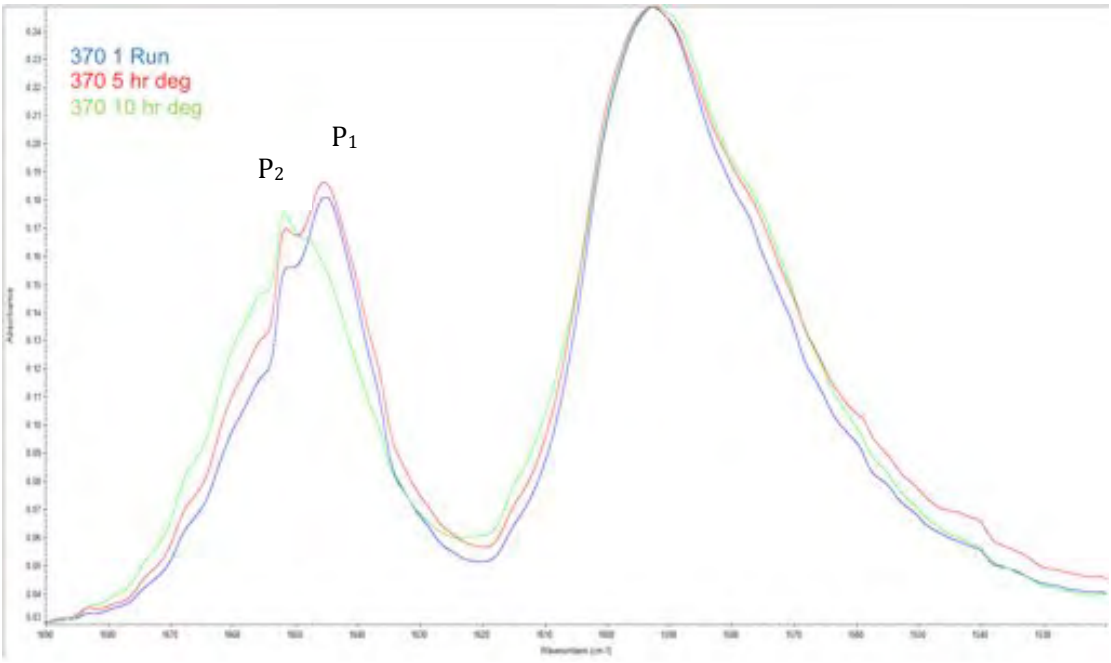

Figure 3-42: FTIR Spectrum of PEEK 450PF degraded over varied hold times. (1690cm^{-1} – 1530cm^{-1})

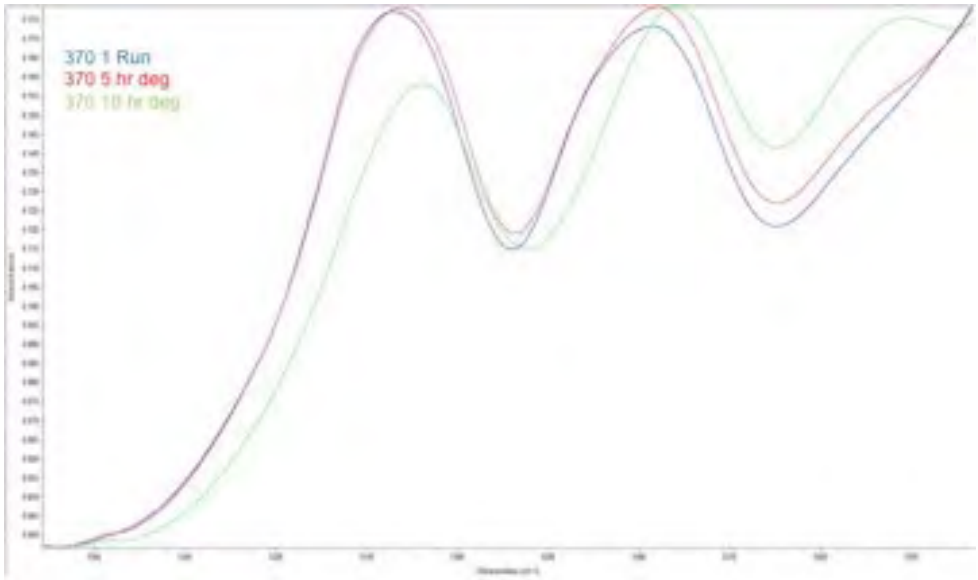

Figure 3-43: FTIR Spectrum of PEEK 450PF degraded over varied hold times. (1340cm^{-1} – 1250cm^{-1})

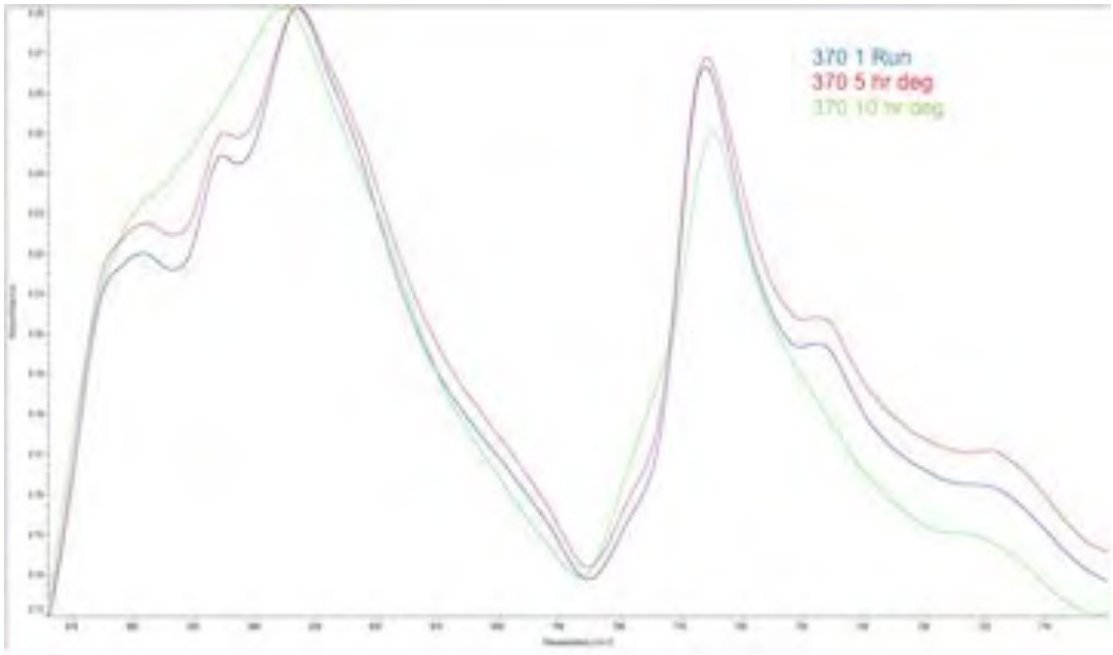

Figure 3-44: FTIR Spectrum of PEEK 450PF degraded over varied hold times. (870cm^{-1} – 710cm^{-1})

Figure 3-43 shows clear movement in peak 1305 cm^{-1} and 1280 cm^{-1}, as used by Chambers et al. [120] to indicate changes in crystallinity. However, the most significant movement is seen when X_c has been substantially diminished. Variation at P_1 and P_2 show a more systematic measurement to the depression in X_c.

The variation of peak height at P_1 and P_2 are shown in more detail in Figure 3-45. A sample of PEEK was held at 398^{o}C for hold times of 5 minutes before cooling to 50^{o}C. Samples were removed from the DSC and analysed on FTIR. An FTIR spectrum was recorded after every DSC run. It is clear that thermal degradation resulted in a decrease in P_1 coinciding with an increase in P_2. This change in peak

height links directly to reduction in heat of fusion shown in Table 3-7. It is apparent that a change in peak ratio can be seen before a depression in heat of fusion is observed. This indicates peak ratio can be used as a precursor for thermal degradation.

FTIR indicates a significant chemical change in PEEK, and a high level of thermal instability at temperatures around T_m^0.

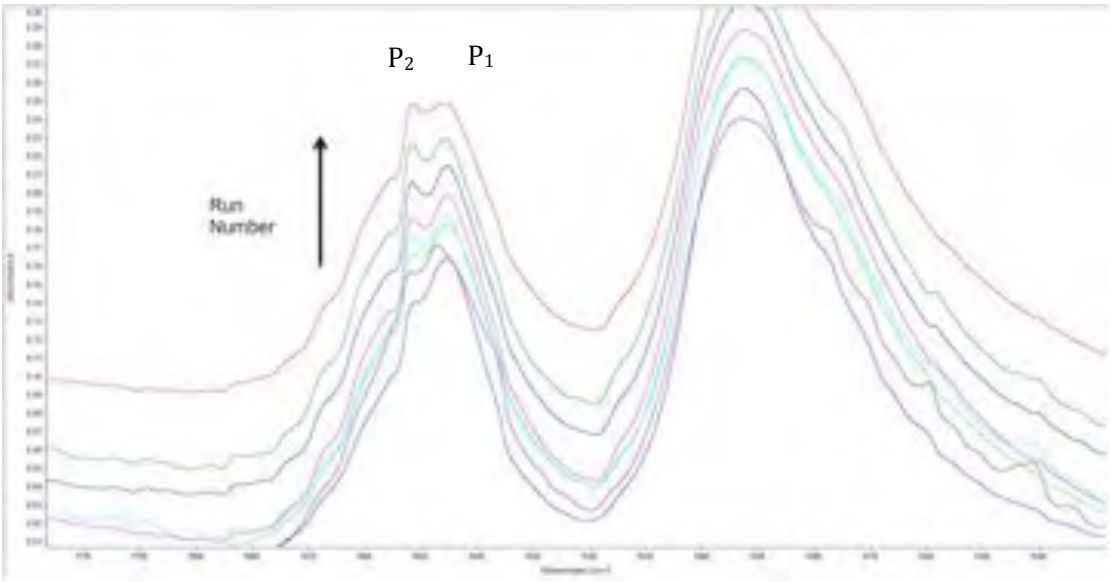

Figure 3-45: FTIR Spectrum of PEEK 450PF showing the changes in P_1 and P_2 tested over 8 DSC runs. ($1690cm^{-1}$ – $1530cm^{-1}$)

Run Number	ΔHf (J/g)
1	37.6
2	37.3
3	37.2
4	36.0
5	32.0
6	32.0
7	28.2
8	26.0

Table 3-7: ΔH_f for 450PF PEEK after 5 minute holds at 398°C.

Figure 3-46 shows the variance in heat of fusion compared to variance in peak height ratio between P_1 and P_2. It is apparent that a decrease in X_c due to degradation corresponds to an increase in peak ratio between P_1 and P_2. This indicates that peak P_1 and P_2 can be used as a measurement of PEEK crystallinity even when high levels of thermal degradation is evident. An increase in the size of the amorphous peak (P_2) is a clear sign of the decrease in regions available for crystallisation in PEEK. Previous measurements of PEEK crystallinity have been shown to be susceptible to the influence of degradation.

To confirm these conclusions, further runs of thermally degraded PEEK were completed using holds of 10 minutes (Figure 3-47). It is clear that the same pattern of peak height ratio is observed.

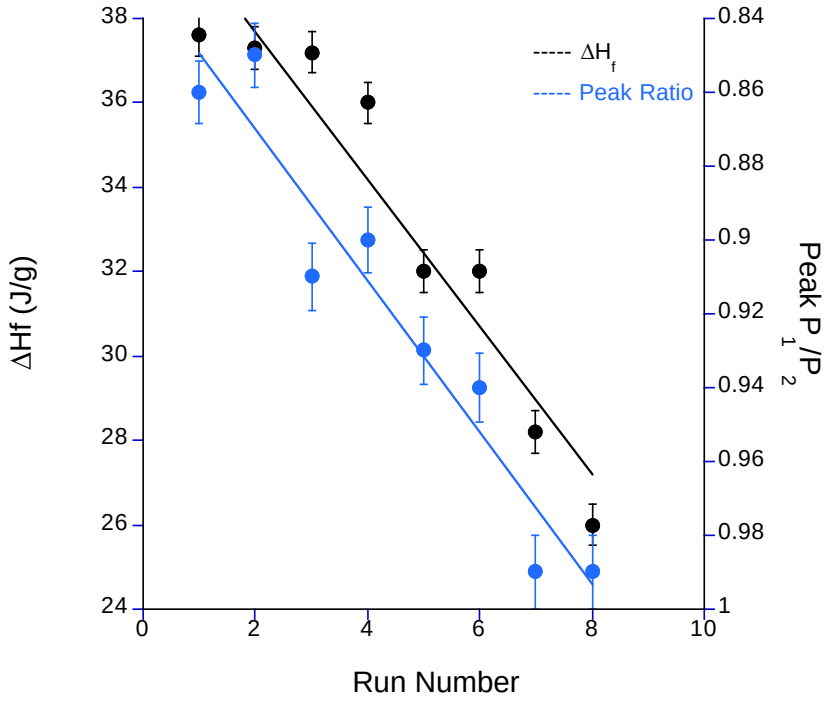

Figure 3-46: Changes in both ΔH_f and variance in peak heights at 1651cm^{-1} and 1645cm^{-1} with increasing 5 minute hold run number and degradation.

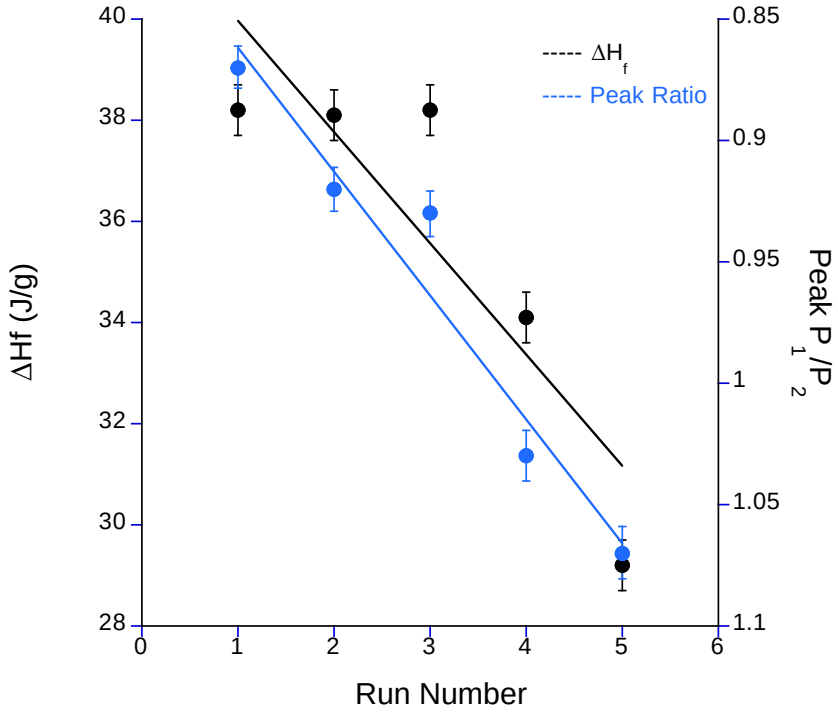

Figure 3-47: Changes in both ΔH_f and variance in peak heights at 1651cm^{-1} and 1645cm^{-1} with increasing 10 minute hold run number and degradation.

The use of FTIR further indicates the thermal instability of PEEK at temperatures near T_m^0, apparent from the change in crystallisation behaviour. The variation of peak height susceptible to changes in the amorphous region (P_2) of PEEK indicates a process of crosslinking resulting in a depression in the crystalline region (P_1).

3.4 Conclusions

Results clearly indicate that T_m^0 is more than just the equilibrium melting point. Once T_m^0 is reached degradation of the PEEK increases significantly.

- At temperatures ranging from 360°C – 380°C multiple runs of the same sample can be used to gain consistent and repeatable results as long as hold time at these temperatures do not exceed 2 minutes.
- Temperatures of 380°C would be recommended as up to 12 runs can be gained from a single sample and values of T_c are consistent with those of a higher temperature. This indicates that all prior thermal history is erased at this temperature.
- For samples taken above these temperatures the amount of runs that can be obtained without degradation of the sample drops significantly. However, if time spent in the melt at lower temperatures is increased, degradation is active and will begin to reduce X_c of PEEK.
- Degradation occurs due to a chain scission process, shortened chain lengths result in a depression of T_m peak and an increase in free radicals. This leads to crosslinking, a combining of chains, which cannot then be reprocessed.
- As well as leading to a depression in X_c, this also constrains some nuclei slowing and eventually preventing their involvement in recrystallisation. This is shown as a production and then disappearance of T_{c2} on cooling.
- Increasing temperature and hold time greatly increases the development of cross-linked chains resulting in a large drop in overall crystallinity in PEEK.
- Analysis has shown that using a single sample of PEEK for multiple runs gives more consistent and repeatable results in DSC.
- When the number of runs available at a chosen temperature and hold time is known this method is more reliable than using a new sample of PEEK for each run.

- From analysis on the FTIR it is clear that the variation of peak height at P_1 and P_2, can be used as an indicator of degradation in PEEK. As thermal degradation increases a coinciding decrease in peak height at P_1 and increase in height at P_2 occurs.
- These changes in peak height indicate a decrease in the crystalline region of PEEK (P_1), this gives further evidence to crosslinking reducing the number of nuclei available for crystallisation on cooling.
- It is known that increasing crystallinity in PEEK will increase desirable mechanical properties such as strength and stiffness. Therefore a decrease in X_c due to degradation will greatly reduce these properties, affecting the performance of PEEK.
- However, Lee and Porter [40] discussed how decreasing crystallinity in PEEK could improve the production of laminates. They found that by destroying nuclei in PEEK encourage nuclei to nucleate heterogeneously on the surface of the fibres, improving impregnation. Therefore if a perfect compromise can be found where PEEK can be degraded enough to not see a significant drop in mechanical properties while still encouraging nucleation on the fibre surface, laminate production could be improved.

4 Chapter 4 - Fast Scanning Calorimetry of PEEK 450PF

4.1 Introduction

Using thermogravimetric analysis the degradation of PEEK was found to be minimal over a prolonged period of time at 400°C. However, a detailed DSC analysis was conducted to study the effect that both hold temperature and hold time have on the degradation of PEEK. A systematic decrease in crystallinity was observed with increased hold temperature and hold time, an effect that begins as soon as PEEK enters the melt. Furthermore FTIR analysis has shown a clear change in the chemical structure of PEEK when crystallinity is depressed as a result of degradation.

Due to the slow heating and cooling rates using conventional DSC, it is difficult to separate degradation caused at hold temperature from degradation caused by the heat and cool cycle.

Flash DSC, due to its extremely fast processing rates will enable any degradation caused in the heat/cool cycle to be minimalised, allowing a clear view of the degradation effects of hold temperature and hold time. Poel et al. [83] demonstrated that successful experiments could be conducted with heating rates up to 20,000°C/s and with cooling rates of up to 5000°C/s. To maintain these high rates sample size is kept to between 0.01 and 2 μg, to minimise any thermal lag. Due to the high crystallisation rate of PEEK, fast cooling rates are required to prevent crystallisation. Although in previous work, PEEK has been cooled to

acceptable rates for an amorphous sample by liquid nitrogen, a small level of crystallisation is still present [122].

Both Tardif et al. and Jin et al. [73, 74] both used heating and cooling rates of 2000°C/s to obtain acceptable levels of crystallisation prevention. However, neither completely describes their rates for testing. Current work using Flash DSC on PEEK, has focused on isothermal crystallisation, an investigation in the thermal cycling and degradation of PEEK has not been completed using this technique before.

4.2 Results

4.2.1 Obtaining Cooling Rate Required to Prevent Crystallisation

Due to the high cooling rates of the Flash DSC 1, investigation into which cooling rates allow complete crystallisation of PEEK must be obtained. **Error! Reference source not found.** show the heating endotherms from a sample of PEEK heated to 398°C at 1000°C s^{-1}, and cooled at varied cooling rates from 0.1°C/sec to 5000°C/sec. It is clear that if cooling rates are too high to allow complete crystallisation of PEEK, a diminished melting endotherm is observed. At cooling rates of 1000°C/s and below, X_c is stable, indicating that PEEK has fully crystallised on cooling. Cooling rates above this show depression in X_c, indicating that PEEK has not fully crystallised. Therefore a cooling rate of 1000°C/s will be used for the subsequent experiments to confirm any changes in X_c are due to degradation.

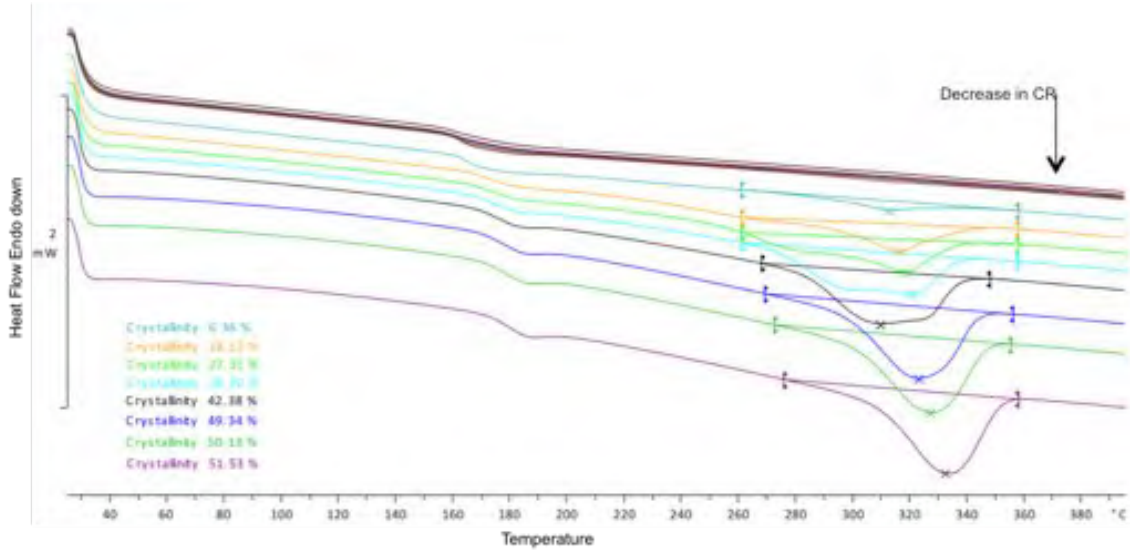

Figure 4-1: Flash DSC 1 melting endotherm for PEEK 450PF with varied cooling rate. Traces show that cooling rates of 1000°C/s and above allow PEEK to fully crystallise.

4.2.2 Obtaining Hold Time Required to Remove Prior Thermal History.

The Flash DSC 1 allows multiple runs of one sample to be completed at a substantially higher rate than conventional DSC; to do this a hold time of 0.1 seconds is used at the melt. It is important to confirm that this hold time is sufficient enough to allow complete melting of PEEK. Figure 4-2 shows the melting endotherm of three samples of PEEK heated to 398°C and held for 0.1, 1 and 60 seconds. It is clear that X_c for all three samples is equal, clearly indicating that 0.1s is long enough to allow full melt of PEEK, thus removing any prior thermal history.

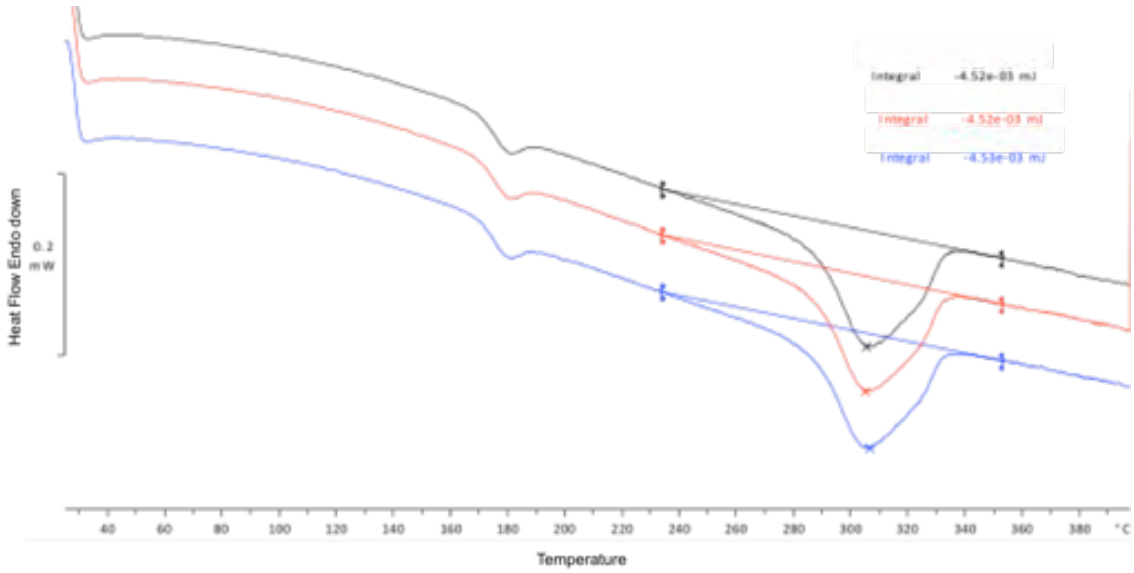

Figure 4-2: Flash DSC 1 melting endotherm of three samples of PEEK 450PF held at varied hold times.

4.2.3 Flash DSC 1 Method for Thermal Cycling

Using the high heating and cooling rate of flash DSC 1 thermal cycling was conducted while removing the effect of degradation on the heat and cool cycle. Therefore degradation could only occur during pre set hold times. The fast heat/cool rates allow any degradation outside of hold time to be removed. However, this fast cooling would not allow crystallisation on cooling, thus a heating endotherm could not be observed, therefore to obtain a heating endotherm to allow X_c to be measured a cooling rate 0.33^{o}C/s is used after a pre-determined number of runs. Slower cooling rates were used at a similar total cold time across experiments e.g. 10 and 30 minutes. This would allow comparison on degradation at similar time points.

4.2.4 The Effect of Hold Time on PEEK degradation.

Experiments, which were completed on conventional DSC, were replicated on Flash DSC 1 to analyse varied hold times at 398°C. Samples of PEEK 450PF were heated to 398°C and held for hold times of 2 – 20 minutes. The processing rates eliminated any degradation caused by the heat/cool cycle, which is apparent in conventional DSC. Therefore, degradation will only occur during the hold period. Comparisons can then be made with conventional DSC analysis and conclusions can be drawn on the extant of degradation caused by continuous heat/cool cycle and overall hold time in the melt.

Figure 4-3 and Figure 4-4 show the depression of T_m and X_c respectively in the heating endotherms of thermal cycled PEEK for hold times of 10 minutes. The depression of X_c is clearly observed. Figure 4-5 – Figure 4-7 show the heating endotherms of thermally recycled PEEK, with hold times of 2, 5 and 20 minutes respectively. It is clear a decrease in X_c is observed with increasing run number. This gives further evidence of the increase in crosslinking caused by degradation in PEEK.

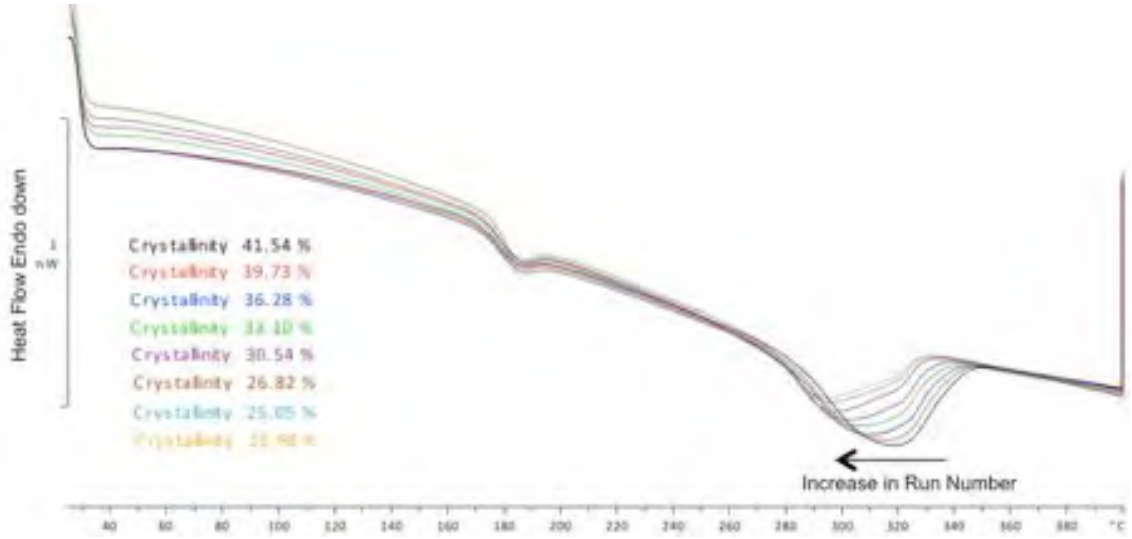

Figure 4-3: Decrease in T_m with increase run number for 450PF PEEK held at 398°C for 10 minutes. Heating Endotherms taken after 10, 30, 60, 90, 120, 180, 240, and 300 minutes of total hold time.

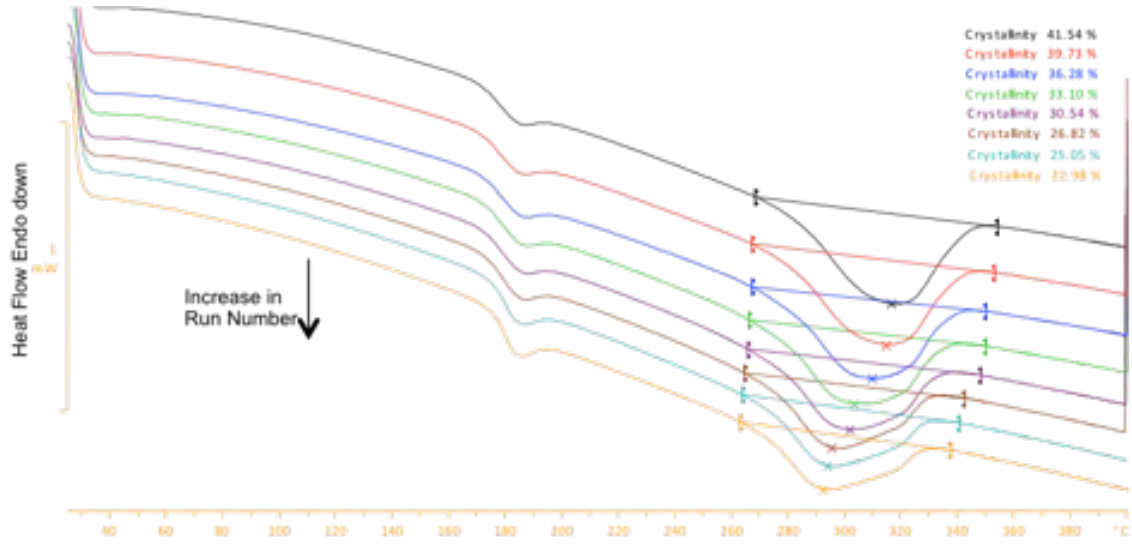

Figure 4-4: Decrease in X_c with increase run number for 450PF PEEK held at 398°C for 10 minutes. Heating Endotherms taken after 10, 30, 60, 90, 120, 180, 240, and 300 minutes of total hold time.

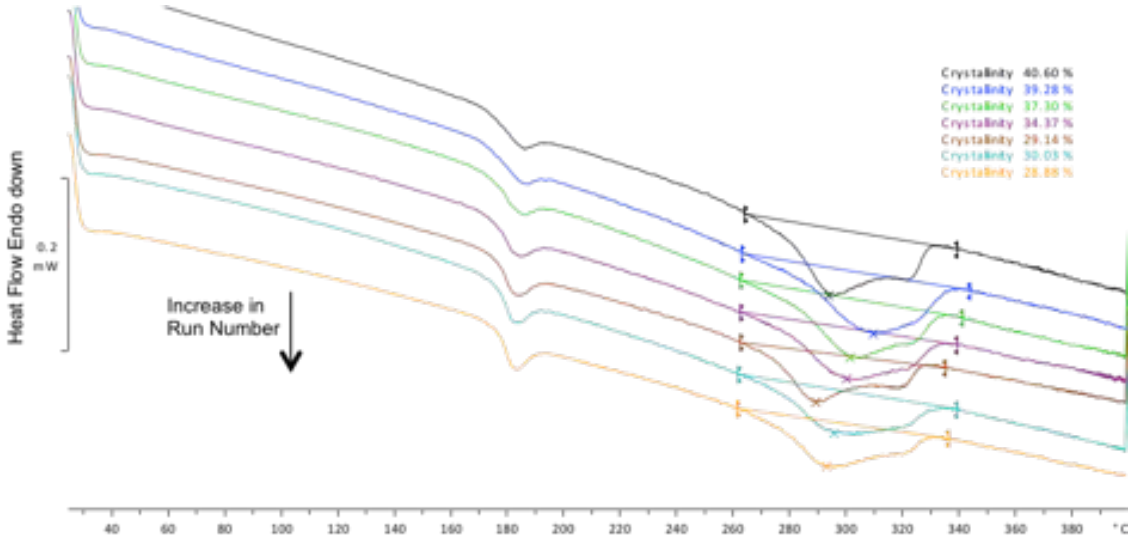

Figure 4-5: Decrease in X_c with increase run number for 450PF PEEK held at 398°C for 2 minutes. Heating Endotherms taken after 2, 10, 30, 60, 90, 120, and 180 minutes of total hold time.

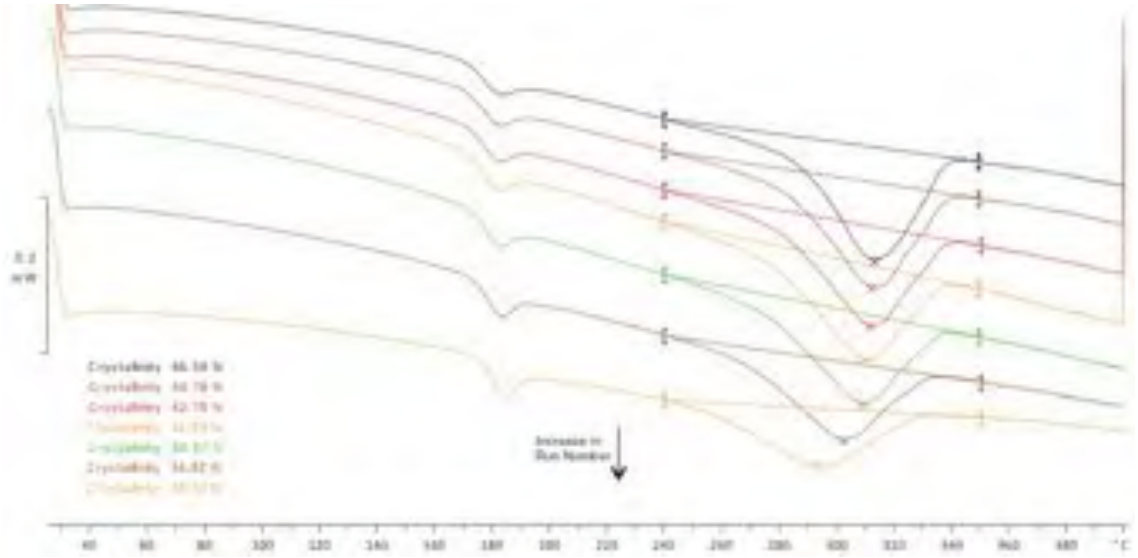

Figure 4-6: Decrease in X_c with increase run number for 450PF PEEK held at 398°C for 5 minutes. Heating Endotherms taken after 5, 30, 60, 90, 120, 180, and 240 minutes of total hold time.

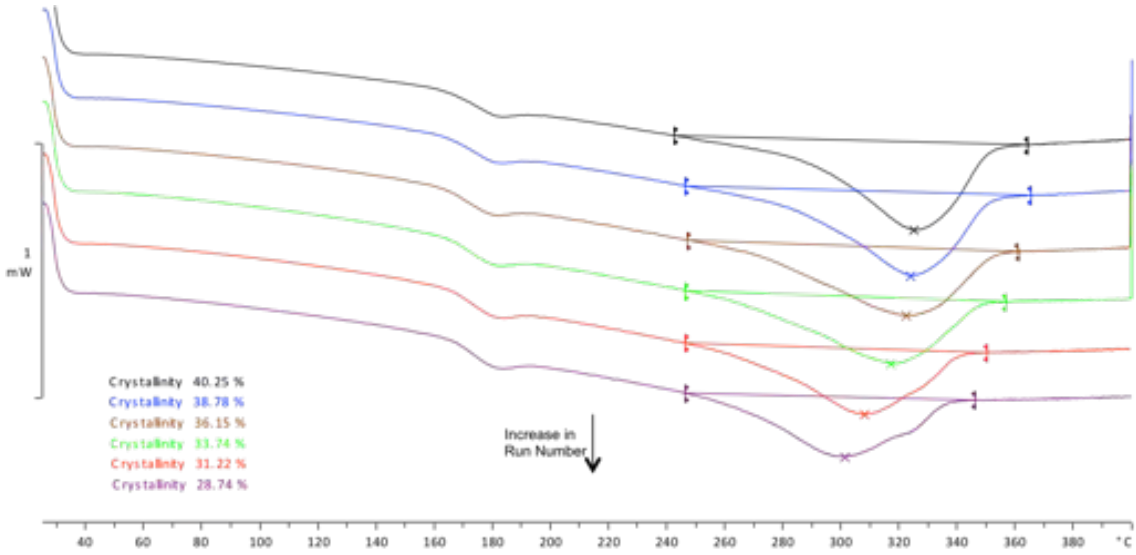

Figure 4-7: Decrease in X_c with increase run number for 450PF PEEK held at 398°C for 20 minutes. Heating Endotherms taken after 20, 60, 120, 180, 240, and 300 minutes of total hold time.

Due to the small size of the flash DSC samples (e.g. 0.00024mg) in comparison to standard DSC (10mg), an increase in sample size variation will occur. Therefore initial ΔH_f values will vary. To counter this variation Figure 4-8 shows a percentage change in X_c of PEEK against total hold time. It is clear that X_c decreases as hold time increases. It is apparent that all hold times show significant degradation over a similar time frame, showing for example that multiple holds of 2 minutes will result in similar pattern of degradation occurred during fewer 10 minute holds.

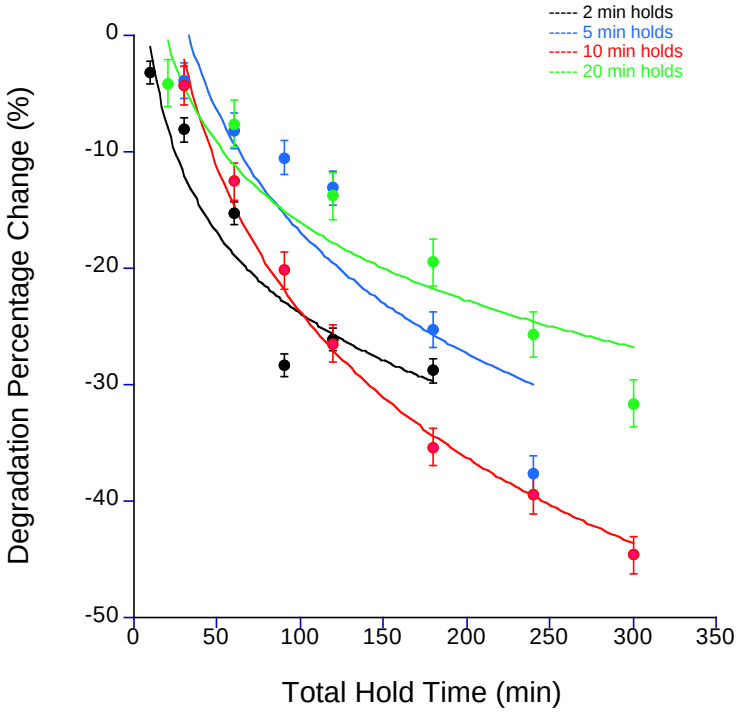

Figure 4-8: Comparison of Flash DSC X_c after a varied total hold time at 398°C.

Figure 4-9 shows the total run time before observed degradation against hold time. It is clear that conventional DSC shows a decrease in run time before degradation as hold time is increased. However, in Flash DSC total run time before degradation remains the same, no matter what hold time is used. It is indicated that using flash DSC 1, PEEK can be held at 398°C for 30 minutes before degradation will be observed, therefore if heat and cool cycles are eliminated, a total of 30 minutes at 398°C can be achieved without degradation. If heat and cool cycles cannot be eliminated (conventional DSC/Industry), the rate of heating and cooling must be included in the 30-minute total in melt time. If hold times are of 10 minutes or more than degradation will occur after 30 minutes at 398°C (T_m^0). If hold times are

held below 10 minutes then total time spend at 398°C can be increased up to 50 minutes.

Literature widely quotes the need to achieve T_m^0 (395°C) to achieve complete processing. These results show that if process time is increased past 30 minutes then degradation will occur, resulting in changes to PEEK properties. However, if processing time is controlled, then this available process time will increase without the effects of degradation.

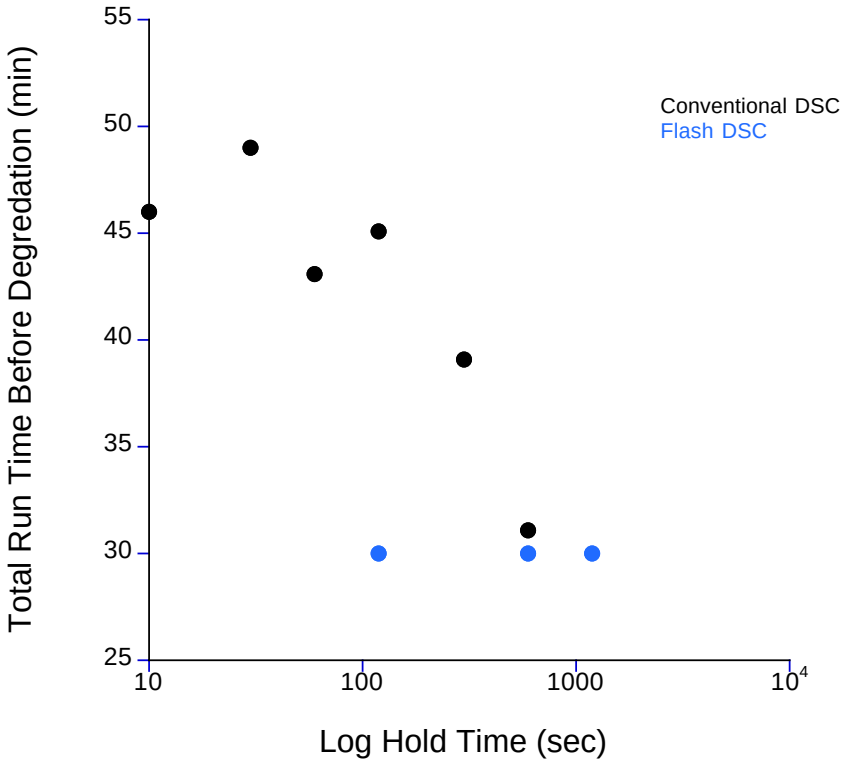

Figure 4-9: A comparison of run time before first sign of degradation in 450PF PEEK thermally recycled to 398°C using conventional DSC and FLASH DSC 1.

4.2.5 The Effect of Hold Temperature on PEEK degradation.

Figure 4-10 and Figure 4-11 show the heating endotherms of PEEK held for multiple runs of 10-minute holds at final hold temperatures of 360°C. It is clear that there is a movement in melting peak to lower temperatures as total hold time increases. However, crystallinity does not decrease for up to a total of 300 minutes hold time. When compared to conventional DSC analysis, a decrease in X_c is observed after a high number of runs. This indicates the process of the heat cool cycle has an increased effect on PEEK degradation.

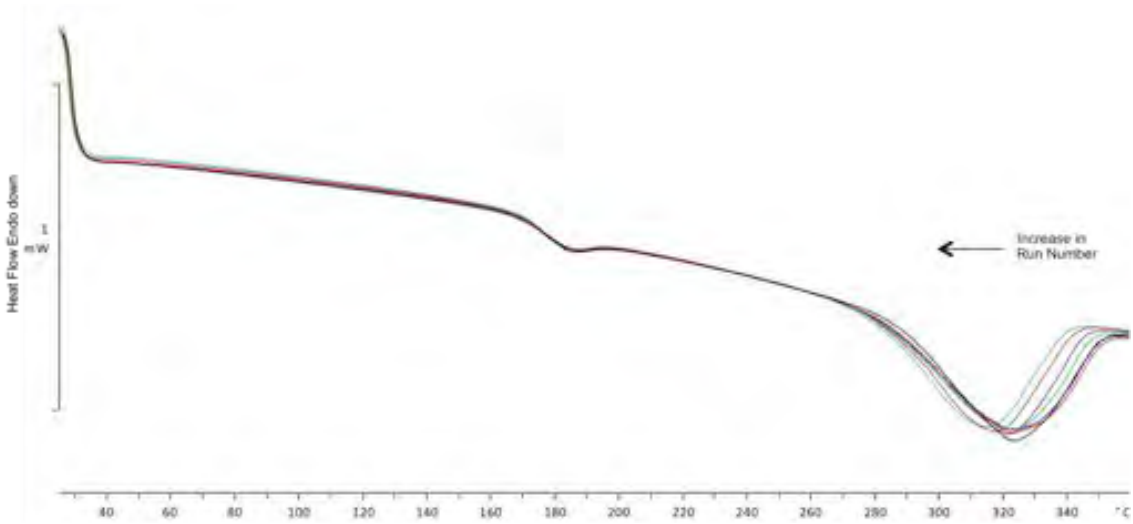

Figure 4-10: Movement of the melting endotherm for 405PF PEEK thermally recycled to 360°C for 10 minute holds.

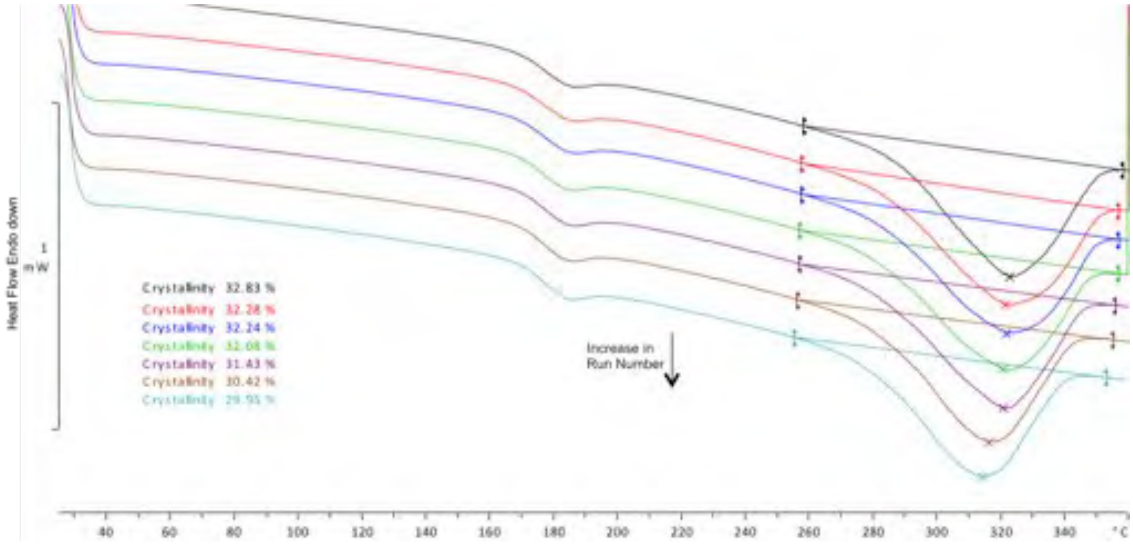

Figure 4-11: Variation on X_c for 405PF PEEK thermally recycled to 360°C for 10 minute holds. Heating Endotherms taken after 10, 30, 60, 90, 120, 180, and 300 minutes of total hold time.

Figure 4-12 and Figure 4-13 show the melting endotherms of 10 minute thermally cycled PEEK at final hold temperatures of 380 and 398°C. It is clear that at final hold temperature of 380°C degradation occurs at a similar rate as hold times of 360°C. Once hold temperature is increased to 398°C, degradation occurs at a highly increased rate. This indicates that a significant increase in degradation rate is observed comparable to the increase seen in conventional DSC where degradation increased after 380°C.

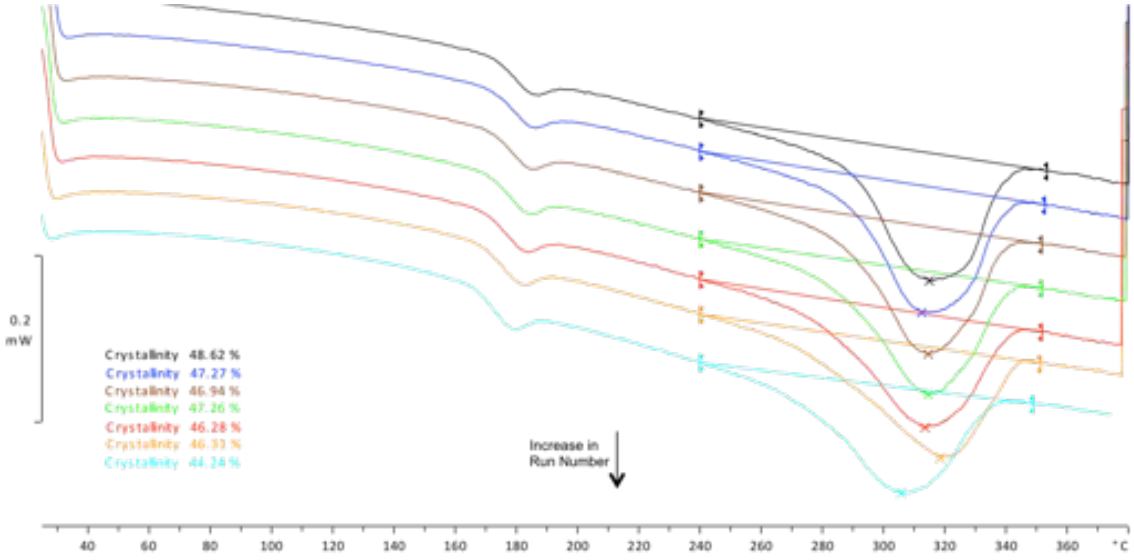

Figure 4-12: Variation on X_c for 405PF PEEK thermally recycled to 380°C for 10 minute holds. Heating Endotherms taken after 10, 30, 60, 90, 120, 180, and 300 minutes of total hold time.

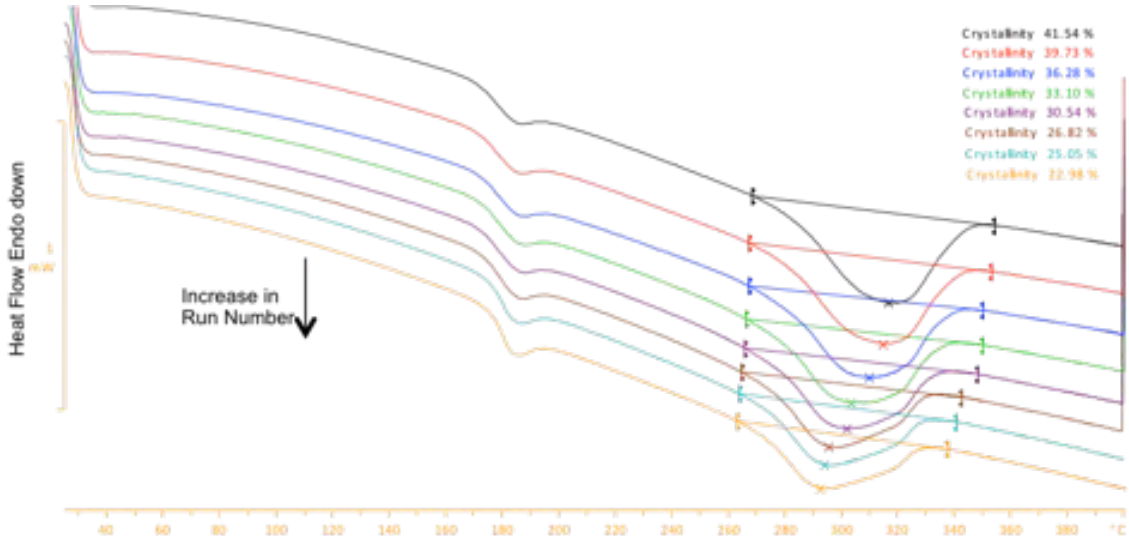

Figure 4-13: Variation on X_c for 405PF PEEK thermally recycled to 398°C for 10 minute holds. Heating Endotherms taken after 10, 30, 60, 90, 120, 180, and 300 minutes of total hold time.

Figure 4-14 shows degradation percentage over total hold time for hold temperatures of 360, 380 and 398°C. It is clear how degradation is greatly increased over 380°C. This is conclusive with results from conventional DSC.

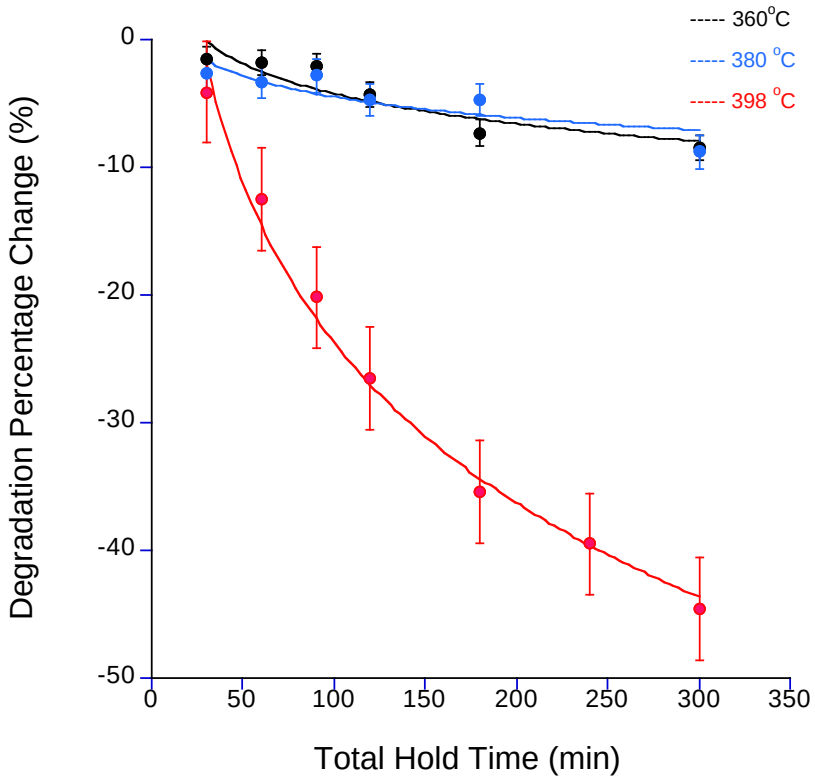

Figure 4-14: Comparison of Flash DSC X_c after hold times of 10 minutes at hold temperatures of 360°C, 380°C, and 398°C.

4.3 Conclusions

- At temperatures above 380°C it is clear that degradation is increased, giving further evidence to conclusions drawn from thermal cycling on conventional DSC.
- The clear increase in degradation above 380°C gives further supports evidence from Chapter 3 that the removal of self-nucleation and self-seeding occurs at this temperature. This will allow consistent values of X_c to be obtained from one sample of PEEK.
- In contrast to conventional DSC work, at temperatures below 380°C, minimal to no degradation is observed. This indicates that the process of heating and cooling the sample increases the onset of degradation in conventional DSC.
- When processing or analysing PEEK at 395°C, a total of 30 minutes of process time can be used before degradation has a significant effect on the crystallinity of PEEK.

5 Chapter 5 PEEK laminates

5.1 Introduction and Literature Review

The processing conditions for the formation of PEEK/fibre laminates have been widely investigated. However, no clear definitive sets of conditions have been concluded. Varied literatures recommend a range of processing temperatures, hold times and hold pressures. The aims of this chapter are to investigate varied processing conditions and their effects on the mechanical properties of PEEK/Glass fibre laminates, and in conclusion recommend a conclusive set of processing conditions. Furthermore the processes of pre-drying both PEEK and glass fibre has not been widely covered in the literature. This chapter will investigate the process of pre-drying and its effect on laminate properties.

5.1.1 Processing Parameters in the Production of PEEK/GF composites

5.1.1.1 Composites in the Crystallisation of PEEK

Fibre-reinforced PEEK composites can be formed using PEEK as a matrix; this can have a profound increase on mechanical properties. A large quantity of research has focused on the benefits of carbon PEEK composites. Lee and Porter [109] state that increasing the carbon fibre content decreases the amount of undercooling necessary for crystallisation, due to the added fibres, in this case carbon, acting as heterogeneous nucleation sites. A transcrystalline layer is formed around the carbon fibres, improving properties such as tensile strength and toughness [123] and gives higher deflection and strength at failure [124]. This transcrystalline layer

is formed by high nucleation density on the fibres, combining with epitaxial growth of crystallisation [123, 125, 126]. Medellin Rodriguez and Phillips [127] state that to form epitaxial growth perpendicular to the carbon fibres, a lattice match between PEEK and graphite is needed. Zhang et.al [123] showed that the transcrystalline layer formed when PEEK was melted at 395°C ($T_m^{0)}$ but not when melted at 375°C. This indicates that PEEK needs to be heated to T_m^0 for effective fibre nucleation and transcrystalline growth to occur, due to any residual nuclei that may cause nucleation in the PEEK matrix being removed.

The presence of fibres in a composite can limit the growth of spherulites; due to the fibres limiting the space available for spherulite growth, causing early impingement, as shown by Gao and Kim [78] using carbon fibre reinforced PEEK composites. They found due to the densely packed fibres offsetting the effects of abundant nucleation at the fibre surfaces, there were much lower levels of crystallinity than in neat PEEK.

Although specific details of their experiments varied, Cebe et.al, Lee et.al and Talbott et.al [52-54] have all controlled crystallinity in PEEK by altering the cooling rates and have assessed these effects on the mechanical properties of PEEK. Although exact correlation between the test results cannot be expected, all three experiments show a higher degree of crystallinity, brought upon by slower cooling rates; increased the tensile strength and modulus of the PEEK.

Vu-Khanh and Frika, [128] stated that in a carbon PEEK composite a large transcrystalline layer can improve stiffness and strength through improved stress transfer from the matrix to the fibres. However Gao and Kim [129] found that this

transcrystalline layer and high matrix crystallinity has a negative effect on PEEK carbon composites interlaminar fracture toughness. Jar et.al [130] also found improvements in tensile strength and delamination energies (mode I and II), when forming temperature was increased to 400^{o}C. This increase in temperature helped eliminate more crystalline elements of the polymer, making the nucleation on the fibres more favourable. For the PEEK composite to improve and maximize its fracture toughness, the fibre-matrix interface must be of sufficient strength to avoid premature delamination, as well as the matrix being able to undergo deformation in the amorphous regions to absorb energy. Gao and Kim [129, 131] proved, when taking into account cooling rate these two properties vary in an opposite manner. When subjected to a fast cool there will be a relatively low degree of crystallinity, favouring energy absorption through plastic deformation in the matrix however, the interfacial strength will be low, massively increasing the chances of premature delamination. Although a slow cool will give a strong interfacial strength to avoid premature delamination, it will also increase the crystallinity of the matrix, reducing deformation; therefore the material will be brittle. Diez-Pascual et al. [132] described how fillers have a nucleating effect in composites increasing crystallisation temperature however, the same fillers result in the more dominant effect of hindering diffusion, decreasing crystallinity, and also decreasing crystallisation temperature. The presence of glass fibre was found to delay the onset degradation in the matrix, while also increasing tensile modulus and strength.

Impact damage performance in carbon fibre PEEK composites were studied by both Uralil et.al, and Gao and Kim [131, 133], both studies looked at the

delaminated area and residual compressive strength of the composites. By using ultrasonic C-scan it was found that the greatest delaminated area was found in highly crystalline PEEK, which also showed the greatest reduction in compressive strength, indicating poor impact damage performance. However, it was noted that the damage tolerance of highly crystalline PEEK composites was higher than in carbon/epoxy composites. It has been shown that samples with smaller spherulites show greater fracture toughness and impact damage tolerance, even when the degree of crystallinity of the sample is similar [134]. Lustiger and Newaz [135] prepared samples of 42% crystallinity, one set prepared by fast cooling, forming small spherulites due to the reduced crystallisation time. Set two were formed by slow cooling, forming large spherulites. After etching, the samples with large spherulites showed direct evidence of preferential crack growth down the center of the spherulites. Samples with smaller spherulites showed a more tortuous fracture path, allowing the absorption of more energy, resulting in an observed higher fracture toughness and impact damage resistance.

An important measurement of PEEK infusion is macro and micro impregnation. Macro-impregnation describes the matrix flow between the fibre bundles and yarns, whereas micro-impregnation describes the matrix flow inside each bundle, around individual fibers. Wang et al. [136] described the time required to impregnate the fibres is governed by transversal micro flow into the fibre bundles rather than macro infiltration of the polymer into the fibre structure.

In this study PEEK has been infused with glass fiber. This is due to the increase in strength provided by the fiber's into the laminate stack. The introduction of glass

fiber is also essential for the support of extra layers introduced into the laminate for use in aerospace applications.

5.1.1.2 Infusion of PEEK

The infusion of multiple polymers to produce semi-crystalline thermoplastics including PEEK has been investigated using different techniques, such as hot press, compression molding, resin transfer molding (RTM) and double belt press [136-138]. Thermoplastics such as PEEK, show an indefinite shelf life, high thermal stability (operating temperature up to 250^{o}C) and strength (100 MPa), while also having shorter processing cycles, double belt processing of a PEEK laminate can take less than 5 minutes, which results in lower processing costs. Drawbacks include high viscosity (up to 100 Pa s in the melt) and high processing temperatures (370 - 400^{o}C) [137].

A number of processing methods for the creation of a polymer composite are shown in Figure 5-1. Powder impregnation, uses strands of reinforcement pulled through a powdered resin, with pins or rollers pulling the fibres, allowing space for polymer particles. However difficulties arise in controlling the fibre volume fraction. Further methods include the combination of commingled fibres of; reinforcement and polymer. This is an alternative to the use of the matrix in powder form. Film stacking involves the processes of heating the polymer film to above its T_m and applying pressure to force the melted polymer into the fibres [139]. Automated tape placement processing uses a polymer and composite tape compressed under a processing roller of which the tip is heated, often with a gas

torch resulting in melting and consolidation [140]. Double belt press systems use a form of film stacking, which is passed through 2 sets of rollers on a conveyor. Between the two rollers is a heating and cooling plate, which separates the process into zones. The temperatures at different stages of the belt press can be adjusted [141] (Figure 5-2). In Resin Transfer molding [138] fibre mat is placed inside a clamped mold, before resin at low viscosity is pumped into the mold under pressure.

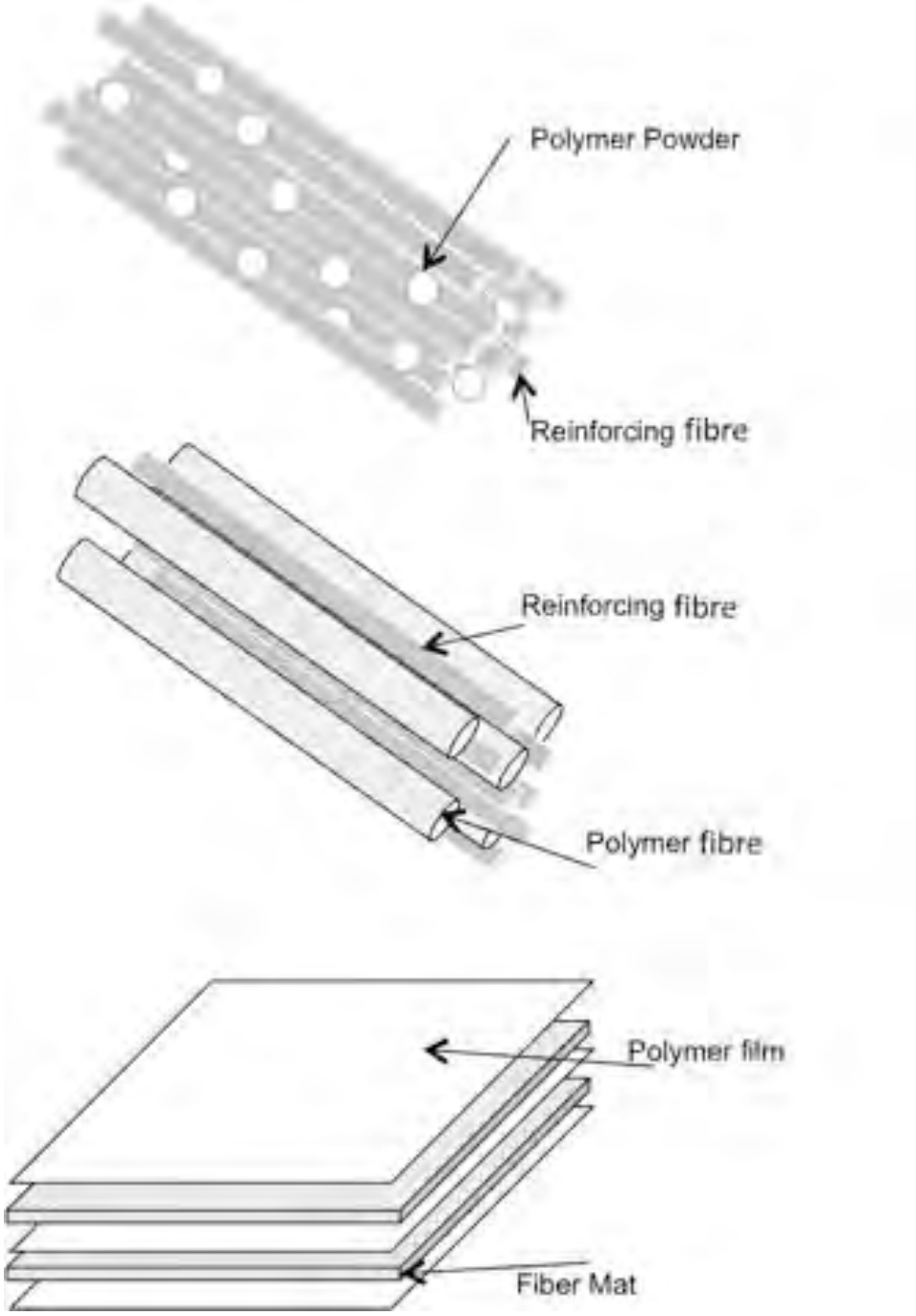

Figure 5-1: Forms of mixing prior to melting. Powder impregnation, commingled fibres and film stacking.

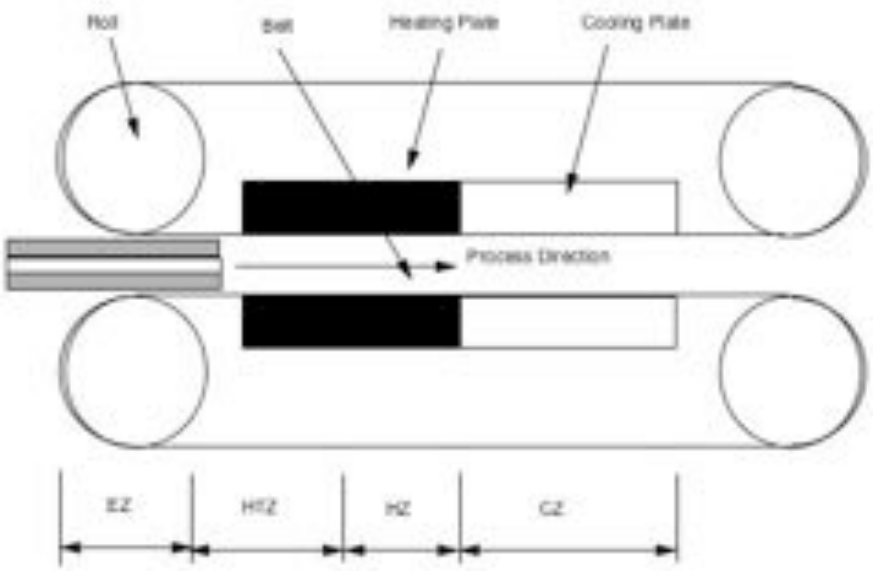

Figure **5-2**: Schematic of double belt press. EZ – entrance zone (70 – 340°C), HTZ – high temperature zone (200 – 410°C), HZ – heating zone (150 – 250°C), CZ – cooling zone (70-220°C).

The process of fibre wetting has been analysed to observe the flow of liquid polymer over fibre surfaces. Mullins et al. [142] described three distinct cases that occur when a droplet contacts a fibre. 1) Film flow along a fibre with no droplets present. 2) Axisymmetric barrel shaped droplets connected by film. 3) Clamshell shaped droplets of various sizes with no connecting film. The formation of these droplets can be affected by both viscosity and fibre orientation.

Composite production using a hot press consists of the compression of polymers and fillers at high temperatures. Figure 5-3 shows a schematic of PEEK and glass fibre lay up during a hot press cycle. A release agent is required to allow removal of the composite from the steel backing plates, in the case of PEEK; Kapton is used due to its ability to reach high temperatures. From the literature, it is clear that the major factors that influence the infusion of PEEK are processing temperature,

processing time and processing pressure. Other factors include viscosity, and direction of fibres.

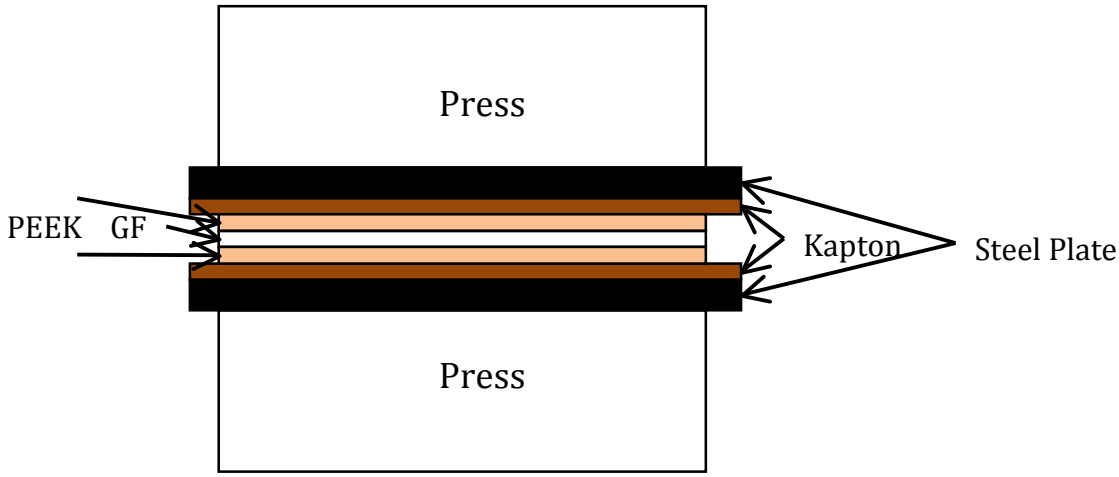

Figure **5-3**: Schematic of PEEK/GF hot press.

5.1.2 Hot Press

5.1.2.1 Importance of Temperature and Viscosity

Processing temperature has an important impact on both the impregnation and mechanical properties of composites. Process temperature is directly related to material viscosity, effecting the composite consolidation. Furthermore, when polymers are held for a sustained period of time above T_m, degradation can occur. Beehag and Ye [105] used hot press cycles to test processing conditions of PEEK/carbon fibre composites. It was indicated that infusion quality was unmistakably improved at 400^{o}C. They also observed that processing at 415^{o}C material degradation occurred, a process, which increased in longer hold times.

This is due to a process of chain scission and cross-linking, resulting in an increase in PEEK viscosity [99]. Increased viscosity impedes the ability of molten PEEK to flow into the fibre bundles resulting in a loss of impregnation. As temperature is further increased past 400°C, this effect is increased and a PEEK processing window from 5 minutes at 420°C to 33 minutes at 380°C was given [143]. Figure 5-4 shows the relationship of viscosity with temperatures approaching the T_m^0 of PEEK.

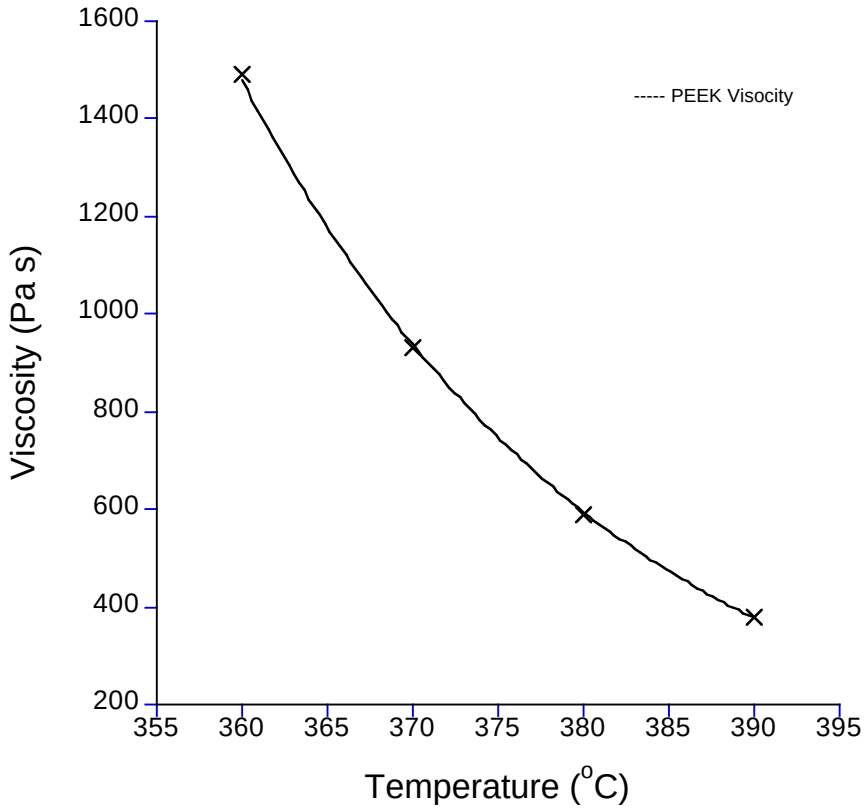

Figure **5-4**: PEEK viscosity against temperature. [99][143].

Jar et al. [144] used SEM imagery to show how hold temperature can affect the spherulite structure of PEEK composites. Composites produced at 350°C show a fine spherulite structure, with highly ordered crystals, which results in a sharp DSC melting endotherm. At 370°C a reduced density of fine crystals were observed, whereas at 390°C a less ordered structure was observed with large spherulites and a quasi-transcrystalline structure.

Literature shows a wide range of recommend processing temperatures for PEEK composites. The requirement to heat to 400°C due to decrease in viscosity and production of a transcrystalline layer is widely stated [105, 145]. However, lower temperatures have also been recommended for processing, due to the increase in degradation when heating above T_m^0. Therefore processing times are reduced at higher temperatures, thus not allowing sufficient time for impregnation of the fibre mat. Furthermore, due to a lowering of viscosity at high temperatures, overflow out of the hot press can occur [146]. The extensively used ICI recommended processing of PEEK composites, including the use of APC-2 PEEK composite, uses a processing temperature of 380°C [134, 147, 148]. Temperatures as high as 420°C and as low as 370°C [89, 149] have also been used in the literature. Manson and Seferis [149] stated that as long as pressure above 0.2 MPa and a hold time of 15 minutes were used then a processing temperature of 375°C produced satisfactory laminate quality, with pressure and hold time having a secondary influence on laminate production. Manson and Seferis also stated that two PEEK films are still easily detectable when processed at 400°C, describing the importance of a homogenous pre-peg for preparation of homogenous laminates. Fujihara et al. [150] tested hold temperatures from 380-440°C and stated that degradation was

observed at each hold time. Therefore low hold temperature with short hold times are recommended.

Zalaznik et al. [151] compared neat PEEK to PEEK formed by compression molding at temperatures below (300°C), around (350°C) and above (400°C) the T_m of PEEK. Hardness values of PEEK were significantly higher at temperatures at and above PEEKs T_m, leading to an increase in brittle failure.

5.1.2.2 Importance of Holding Time

Due to factors such as degradation, hold time must be closely monitored. Allowing sufficient time for viscous PEEK to flow into the fibre mat however, prolonged periods at high temperatures will increase degradation, increasing viscosity and reducing mechanical properties. Studies by Beehang and Ye, Nazem and Salek et al. [105, 108, 152] showed increased processing time improves overall quality and removes the presence of any voids. Both Beehang and Ye and Nazem [105, 152] showed that a processing time of 60 to 120 minutes helps overall impregnation of the fibre mat. However, even at low temperatures such as 380°C, recommended hold times are substantially longer than that shown for the onset of degradation [143]. Salek et al. [108] reported that in PEKK, viscosity will increase after 30 minutes, and the closer the temperature is to the materials T_m^0 the faster this increase will be; however, within a stable temperature range there is no effect. Literature values for processing times vary dramatically. From 7 minutes, 20 minutes, 30 minutes to over 60 minutes [149, 153-155]. Beehag and Ye [105]

showed consolidation quality was improved at 400°C when hold time was increased from 10 to 60 minutes.

De Almedia et al. [143] analysed how viscosity increased over time at different temperatures. Viscosity increases dramatically at 420°C and 410°C after around 10 minutes, 400°C showed an increase after 15 minutes. Viscosity rose after 25 and 30 minutes for 390°C and 380°C respectively.

5.1.2.3 Importance of Hold Pressure

Both Peltonen et al. and Nygard et al. [156, 157] suggested that if processing pressure is too high, or applied to early, it will flatten and compress the reinforcing fibres. This prevents infusion due to a decrease in flow space between the fibre yawns, which decreases overall tensile strength. The room between fibres relates directly to the permeability of the fibre bundle, effecting fibre flow [158]. Mallick and Ragone [159] confirmed this using SEM images, showing the difference between a polyamide-6 and glass fibre composite at high and low pressure. It was reported that at high pressures a much lower level of impregnation was observed.

Kuo et al. [146] suggested that loading pressure could be varied in accordance with the pressing temperature. A high pressing load (higher than 2 MPa) at high temperatures may force the molten polymer out of the laminate; therefore a lower temperature with a higher pressure could prevent this. This was also confirmed by Peltonen and Tormala [160], who described a decrease in impregnation with an increase in isotropic pressure. Beehag and Ye [145] tested a variety of pressures

and stated that any pressure of 0.2 MPa or above produced good quality laminates, any produced at ambient pressure showed poor infusion.

Again this has led to a variance in recommend processing pressures in the literature. The ICI recommended pressure is 1.4 MPa [46] However, Ye et al. recommended pressure of 1.2 MPa, whereas Ye et al. [154, 155] described poor consolidation at 380^{o}C using pressure of up to 3MPa. Manson and Seferis [149] stated that as long as pressure is over 0.2 MPa holding pressure is a secondary influence, yet further experiments on PEEK composites have been completed at 1 MPa [153]. Talbott et al. and Mason et al. [54, 161] indicated that a low pressure combined with fast cooling could induce voids and fibre buckling in PEEK composites.

Lin ye et al. [155] describes an increase in spherulite size (from 5 to 15 μ m) as pressure was increased from 0.1 to 200 MPa. Modulus, critical stress and strain at crack initiation all fell with increasing pressure. Increased pressure suppressed the smaller crystal section of the DSC melting endotherm, showing a suppression of smaller crystals with less perfection.

5.1.2.4 Cooling of PEEK

Cooling rate can have further effects on the mechanical properties and overall quality of polymer composites. Manson et al. [161] stated that an increase in cooling rate resulted in an increase in void content and surface buckling in PEEK

composites. Diez-Pascual et al. [132] stated that a cooling rate of less than 3°C/min helped minimize the formation of internal pores and improve fibre impregnation.

Lustiger et al. [134] tested three variations of cooling methods. 1) Fast cooling resulted in a mix of isolated and fibre nucleated spherulites. 2) Under slow cooling larger fibre nucleated spherulites were seen exclusively, resulting in reduced matrix toughness. Implications of this were low fracture toughness and impact delamination, alongside an increase in compressive strength. 3) Annealing conditions resulted in properties found between fast and slow cooling. Recommendations were given to avoid slow cooling due to increase crystallinity and spherulite size resulting in increased brittleness. Jar and Kausch [147] described the decrease in delamination resistance with increased cooling rate as only occurring in specimens formed at 400°C. Crystallinity was found to be higher in the centre of composites due to a slower overall cooling rate. Vu- Khanh and Frika [128] showed that increasing cooling rate resulted in large decreases in the size of the transcrystalline layer formed in composites. An increase in cooling rate from 1°C/min to 80°C/min can decrease the size of the transcrystalline layer from around 40 μ m to 5 μ m. It was also shown that the optimal time for production of transcrystalline layer was around 7 to 20 minutes before decreasing in size.

Unger and Hansen [148] tested a combination of cooling rates and annealing temperatures. To form an amorphous composite a cooling rate of 5000°C/min or greater was needed, which showed a dramatic loss of modulus around Tg. Increasing cooling rate decreased crystallisation temperature. A method of quench

cooling followed by an anneal cycle was recommended to reduce residual stress. Chen [79] also found that increasing cooling rate decreased melting temperature.

5.1.2.5 Processing of PEEK

For PEEK composite processing, Mayer et al. [141] stated the importance of 1) melting of the polymer without thermal degradation. 2) Impregnation of the reinforcing structure. 3) Consolidation and cooling of the laminate. The importance of a quality impregnation is further described by Beehag and Ye [105]. A decrease in void content results in a decrease in mode II fracture toughness. Mode I interlamellar fracture growth resistance showed little correlation with consolidation quality.

The literature shows a wide variance in the recommended processing conditions for PEEK composites. Although research into processing conditions is substantial, an indisputable step-by-step method of temperature, pressure, time and cooling rate has not yet been agreed upon. ICI recommended processing temperature is 380^{o}C and multiple papers describe satisfactory composites produced at this temperature however, other papers describe PEEK viscosity at 400^{o}C as minimal level needed for fibre impregnation, alongside the formation of a transcrystalline layer needed for improved mechanical properties. Recommended hold times vary from 20 to 120 minutes. Pressure must be applied to improve impregnation of the matrix into the reinforcing fibres however, too substantial a pressure will compact the fiber mat resulting in poor infusion. Figure 5-5 shows a processing graph for the production of a PEEK laminate. If pressure is applied too early then the fibres

can be damaged or flattened, reducing levels of infusion, therefore the polymer is pre heated to obtain temperature. Once the polymer passes into the melt, pressure is increased, this is then held until impregnation of the fibres is complete. Often pressure is kept during cooling before being released.

Data for the processing of PEEK/fibre composites is clearly available in the literature. However, there is no clear case of research finding the exact parameters needed for specific applications. Processing parameters need to be explored to determine the exact requirements for your application.

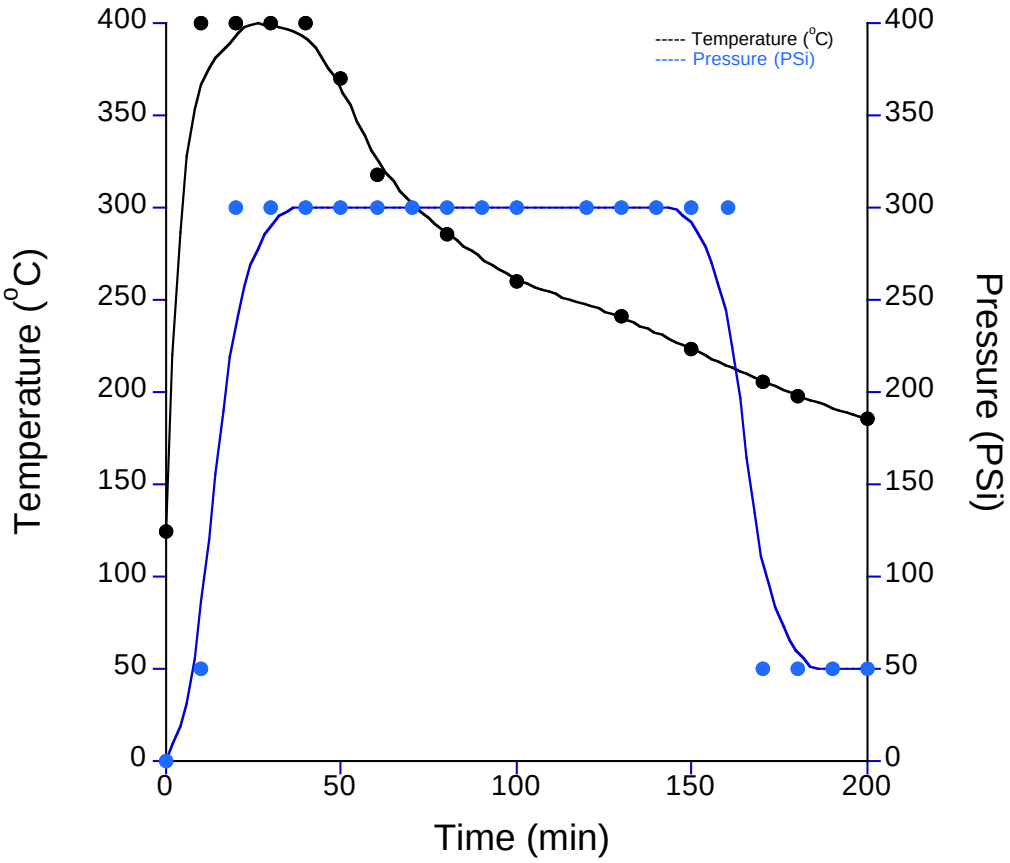

Figure **5-5**: A processing graph for PEEK film heated to 400°C for 30 minutes at 300 psi pressure.

The PEEK films used in this study include the addition of talc additives. This is due to improvement in dielectric properties supplied by the talc additives to the PEEK matrix, including improvement in temperature dispersion to the surface of these laminates for use in industrial applications. The addition of talc filler will delay the onset of degradation, which has been widely discussed in the previous chapters of this study. However, although talc will be delay onset of degradation, the pattern of degradation caused by increasing temperature and hold time will still be apparent.

The effect this has on the impregnation and mechanical properties of these laminates will be discussed in this chapter.

5.1.3 Pre-Drying of PEEK

One aspect of PEEK composite production, not extensively covered in the literature, is the pre-drying of PEEK and/or glass fibre before production. Pre-drying is useful to remove both moisture and any volatiles present, which may hinder impregnation. The majority of literature on PEEK composites does not mention pre-drying; however Cogswell [162] does mention its importance if water molecules are present, as polymers can be prone to degradation if they contain water. In glass fibre reinforced plastics, water may react with the surface of the fibre and therefore pre-drying is recommended. One possible reason for the lack of pre drying in the literature may be due to the high water resistance of PEEK. Diez-Pascual et al. [132] oven dried for 24 hours at 140^{o}C to remove any absorbed moisture.

The technique and processing conditions for the formation of PEEK/fibre laminates have been extensively investigated. However, no clear, definitive set of conditions has been found. Instead, a multitude of temperatures and hold times have been recommended and given as satisfactory. The aim of this chapter is to conclude the best processing conditions for PEEK/GF laminates, as well as to investigate the importance of pre-drying.

5.2 Results

Production of PEEK laminate was completed using 200-micron thick, 30% talc filled PEEK films either side of a glass fibre mat. Samples of PEEK and glass fibre were pre dried in an oven at 140°C for 2 hours before production (results of tests on pre drying are shown later in this chapter). Stage one of testing analysed the production of PEEK-to-PEEK films. Stage two introduced a glass fibre mat. Analysis of laminate impregnation was completed using optical microscopy, SEM and tensile testing.

Table 5-1 shows the varied processing conditions used for PEEK film impregnation. Pressure was maintained until press temperature had dropped below 200°C, due to maximum X_c being achieved due to slow cooling rate.

Method Number	Hold Temperature (°C)	Pressure (psi)	Dwell Time (min)
1	370,380,390,400	100	5
2	370,380,390,400	100	30
3	370,380,390,400	300	5
4	370,380,390,400	300	30

Table 5-1: Experimental matrix for stage 1 PEEK laminates production.

Figure 5-6 and Figure 5-7 show optical microscopy images taken of films produced at two extremes of 370°C and 400°C. Production of PEEK-to-PEEK films showed good infusion at all test procedures. There is a clear infusion between the two PEEK films with no clear break between; this indicates a high level of infusion between PEEK and PEEK. This is expected, as there are no foreign agents in between e.g. fibers. Therefore all tests conditions were taken through to stage 2.

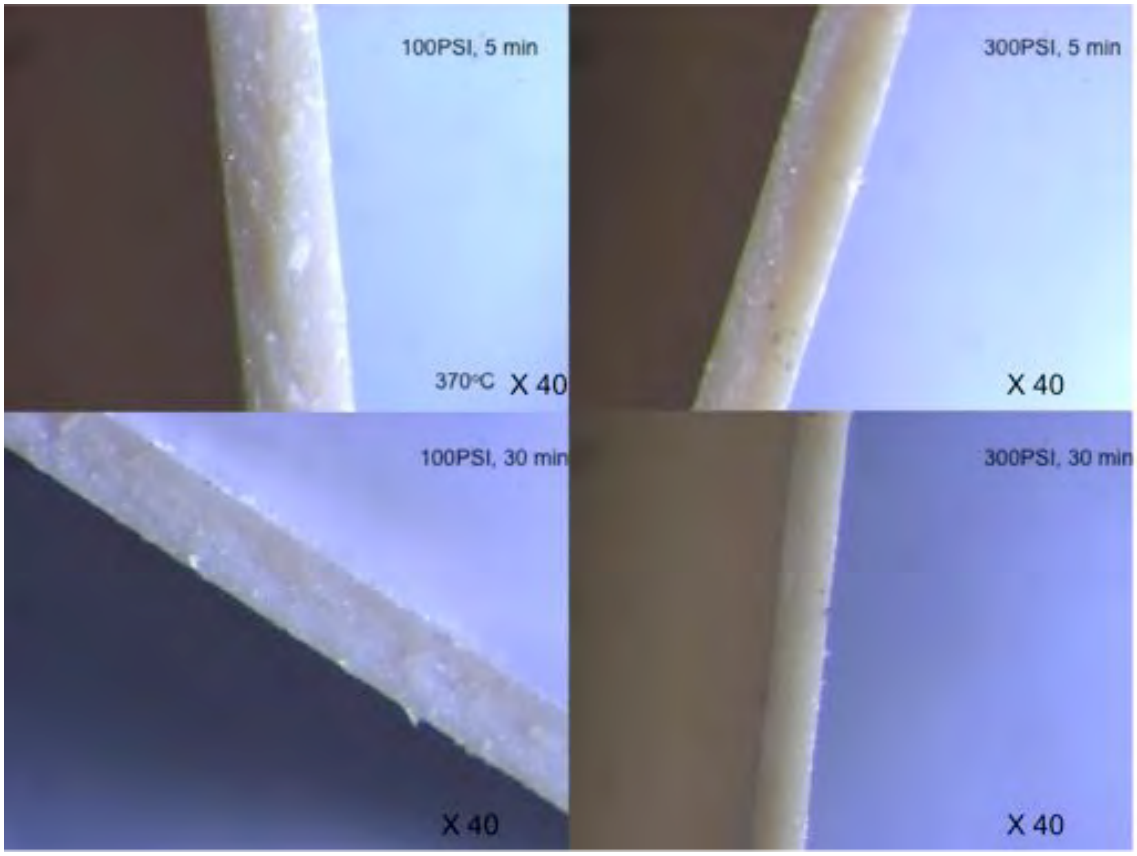

Figure **5-6**: PEEK-to-PEEK films produced at 370°C. High level of consolidation is seen.

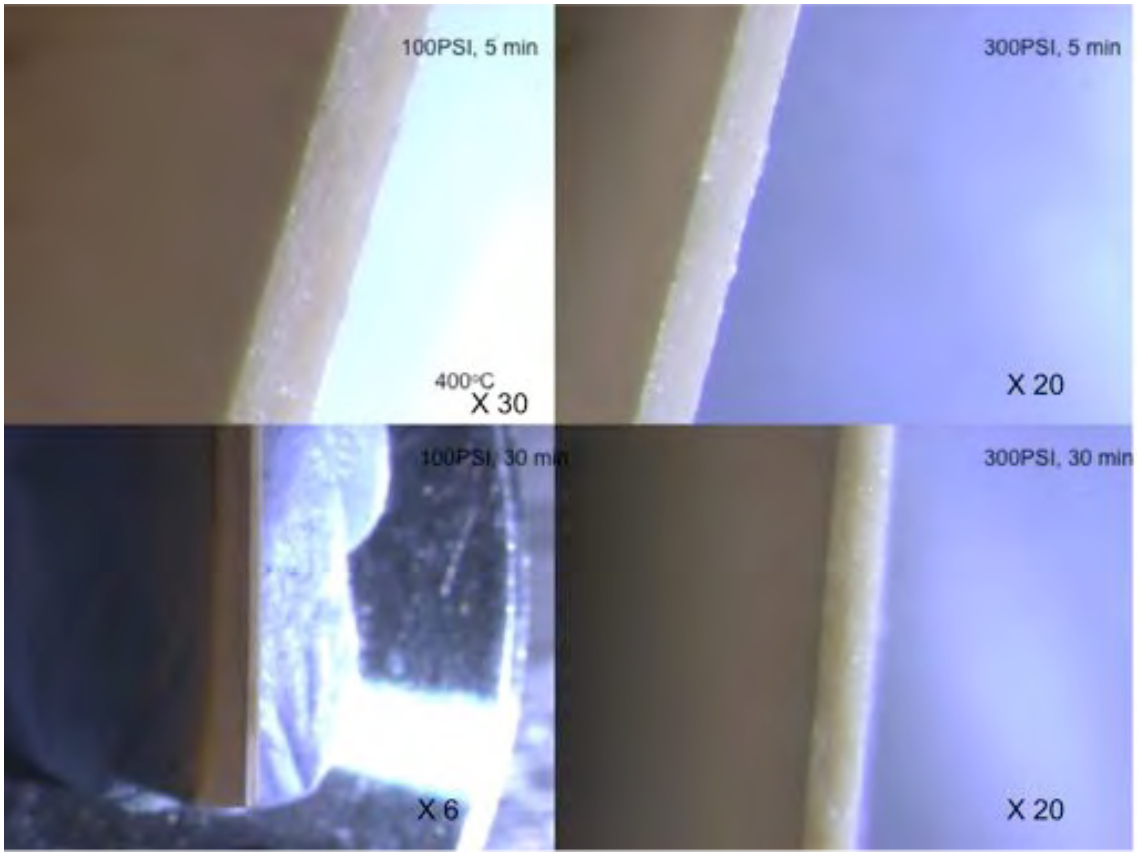

Figure **5-7**: PEEK-to-PEEK films produced at 400°C. High level of consolidation is seen.

Figure 5-8 shows DSC results for a sample of PEEK formed at each processing condition shown in Table 5.1. Samples were heated to 400°C, and results were taken from the first heating run, allowing the results of each processing conditions to be analysed. It is clear that at higher processing pressures, X_c was decreased when temperature was increased however, low processing pressure showed no systematic variation in crystallinity. It is believed that at high processing pressures, compression of the talc filler in the PEEK film results in early impingement of spherulite formation.

It is clear that PEEK-to-PEEK lamination can be completed at temperatures as low as 370°C, with hold times of 5 minutes. However, the presence of glass fibre in stage two will need further development of processing conditions.

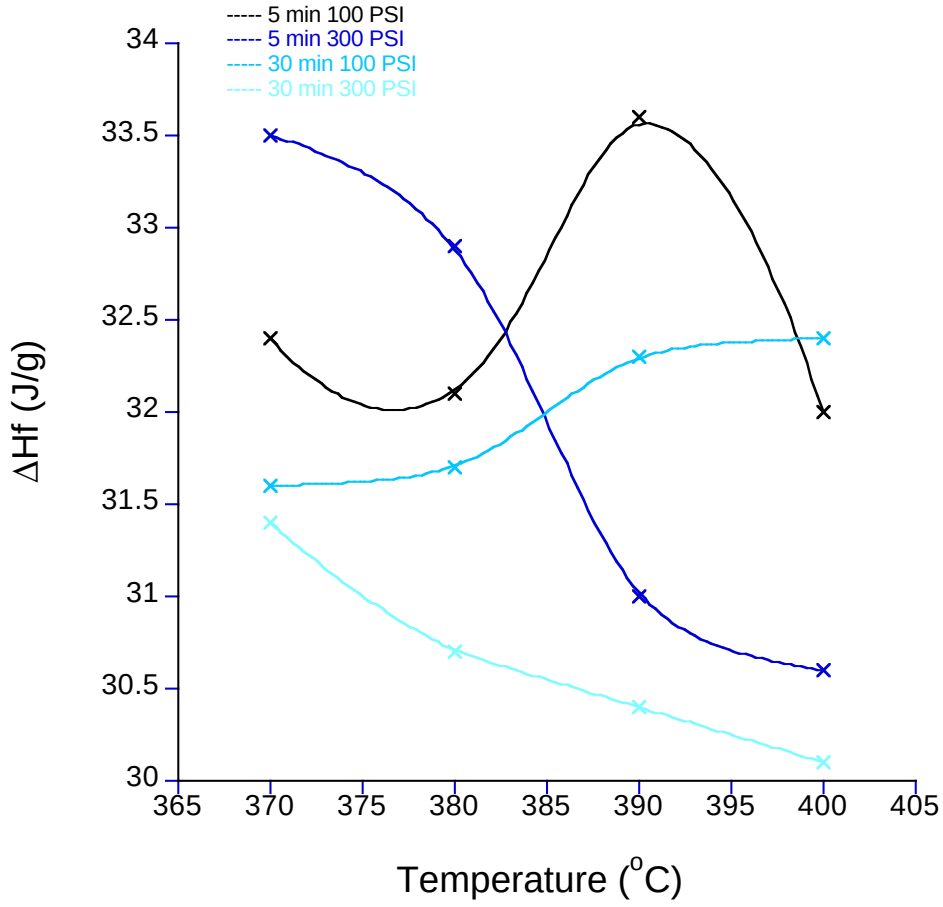

Figure **5-8**: Variance in ΔH_f for PEEK-to-PEEK films produced using different test parameters.

5.2.1 PEEK Glass fibre laminate production.

Successful processing conditions from stage one were replicated for the production of PEEK/Glass fibre laminates. Figure 5-9 shows SEM images of

PEEK/GF laminates produced at 370°C with varied hold time and pressure. It is clear that at all processing conditions, voids were present, both at contact points with GF bundles and in between bundles. This indicates that viscosity at 370°C is too high for PEEK flow around the fibre mat.

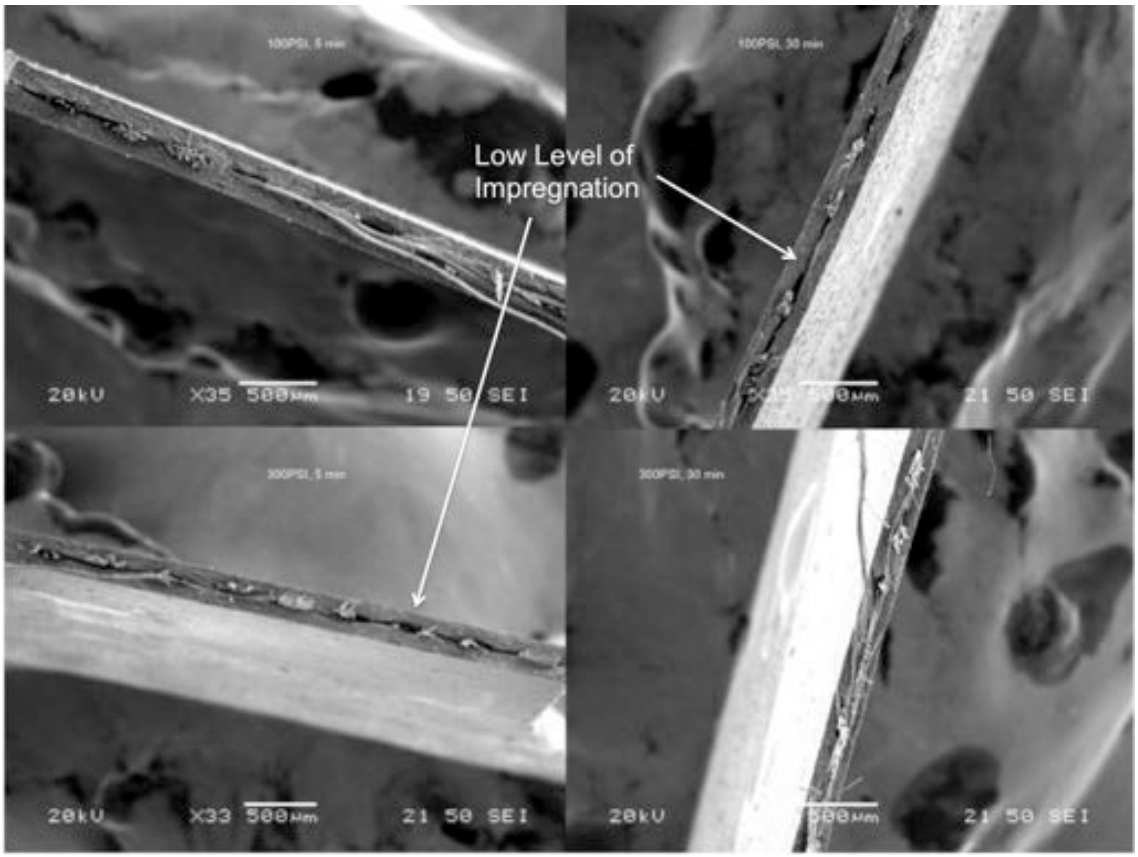

Figure **5-9**: SEM images of stage two laminates produced at 370°C.

Figure 5-10 shows SEM images of the same processing conditions, at hold temperature of 380°C. Similar voids present at 370°C are clear in these laminates; however, at processing conditions of 100 psi for 30 minutes voids were only

present at the glass fibre bundles. Macro impregnation present between fibre bundles was increased. Figure 5-11 and Figure 5-12 show laminates produced at 390°C and 400°C respectively. Similar results of macro impregnation are seen, therefore, it is clear an increase of either hold pressure or hold temperature results in an increase in impregnation. This is apparent at processing conditions of 390°C, 30 minutes, and 100 psi, which shows a major improvement in impregnation. This indicates that the combination of a longer hold times with a lower pressure can increase impregnation.

Results clearly indicate that at processing temperatures of 370°C viscosity is too high for PEEK laminate production. Furthermore, processing temperatures of 390°C shows comparable if not better impregnation than at 400°C, indicating that an increase in polymer degradation at higher temperatures is hindering laminate production. It is apparent that hold pressure of 300 psi results in compression of the glass fibre mat, resulting in a decrease in visible impregnation. Hold times of five-minutes do not allow enough time for full impregnation.

However, errors in the production of SEM samples can occur. Due to the thin nature of the samples cryogenic fracture can prove difficult. Therefore, some areas of the samples may have been subjected to a pulling force, resulting in an increase in visible voids or GF strands seen in the SEM images. Therefore further analysis of mechanical test data of each laminate has been completed.

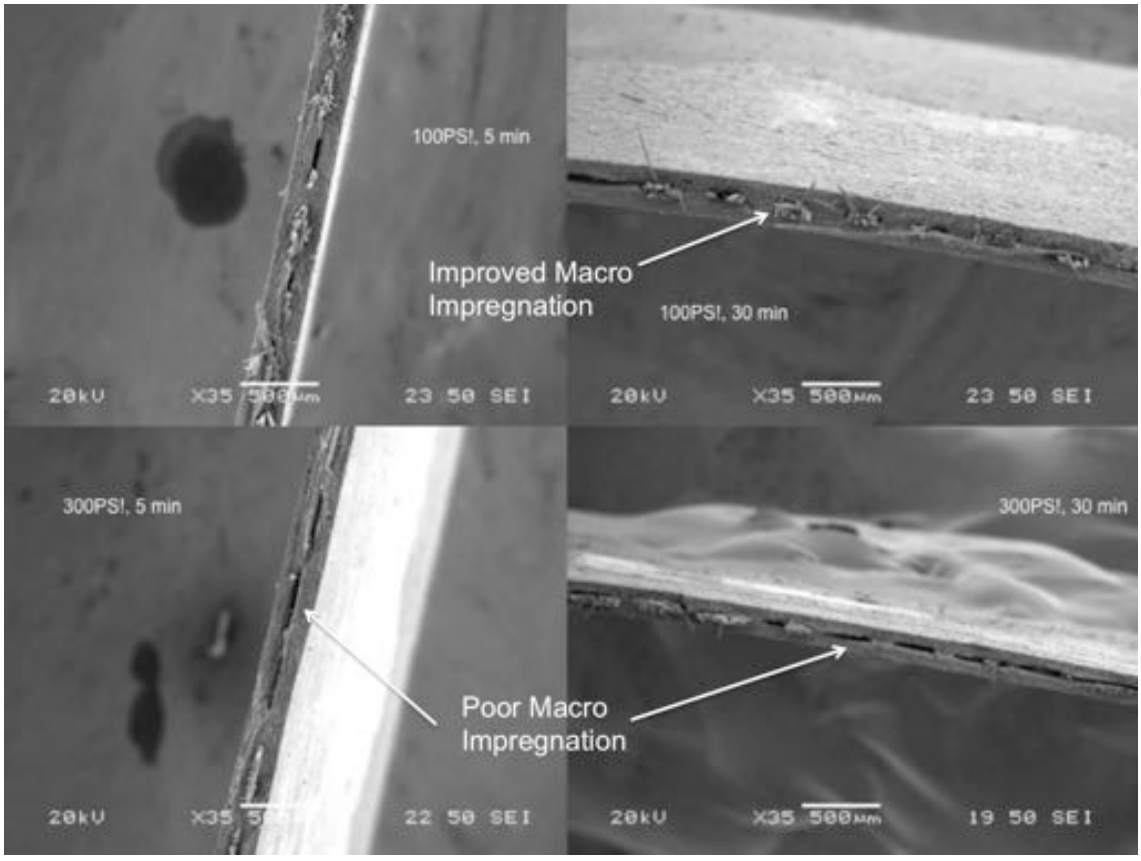

Figure **5-10**: SEM images of stage two laminates produced at 380°C.

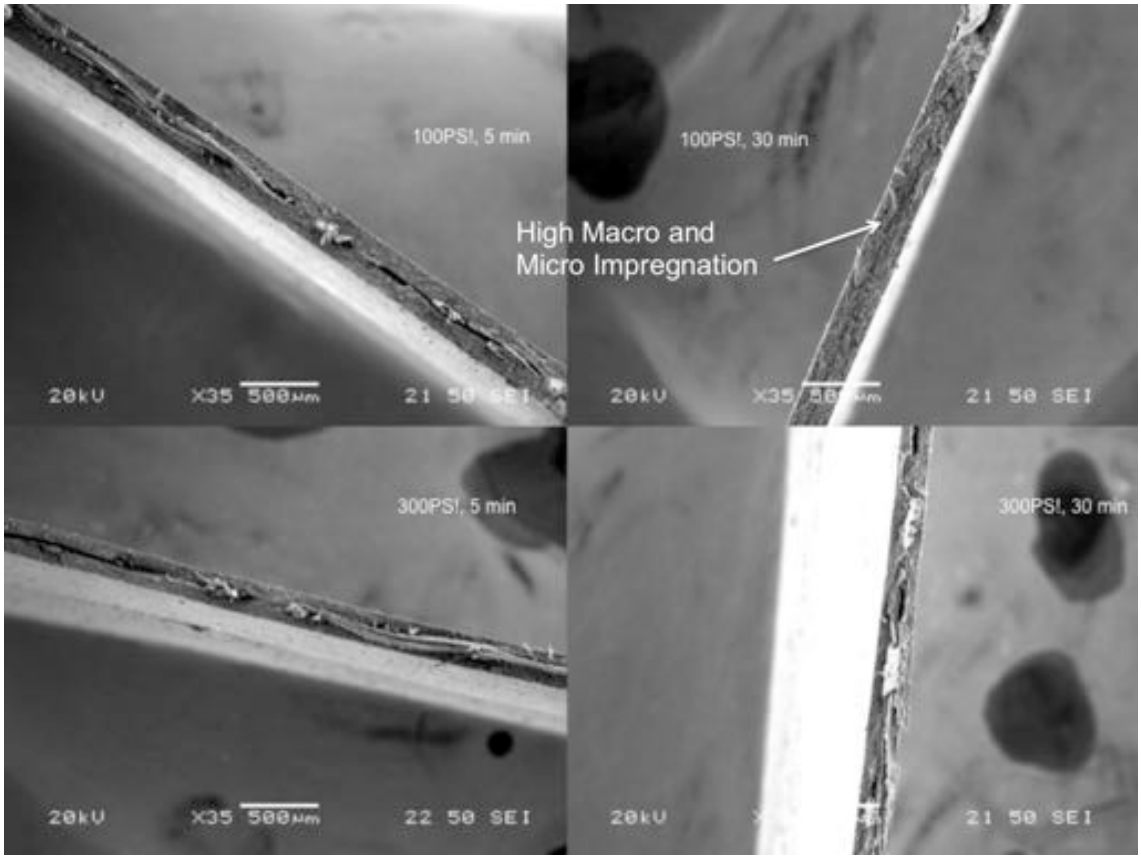

Figure **5-11**: SEM images of stage two laminates produced at 390°C.

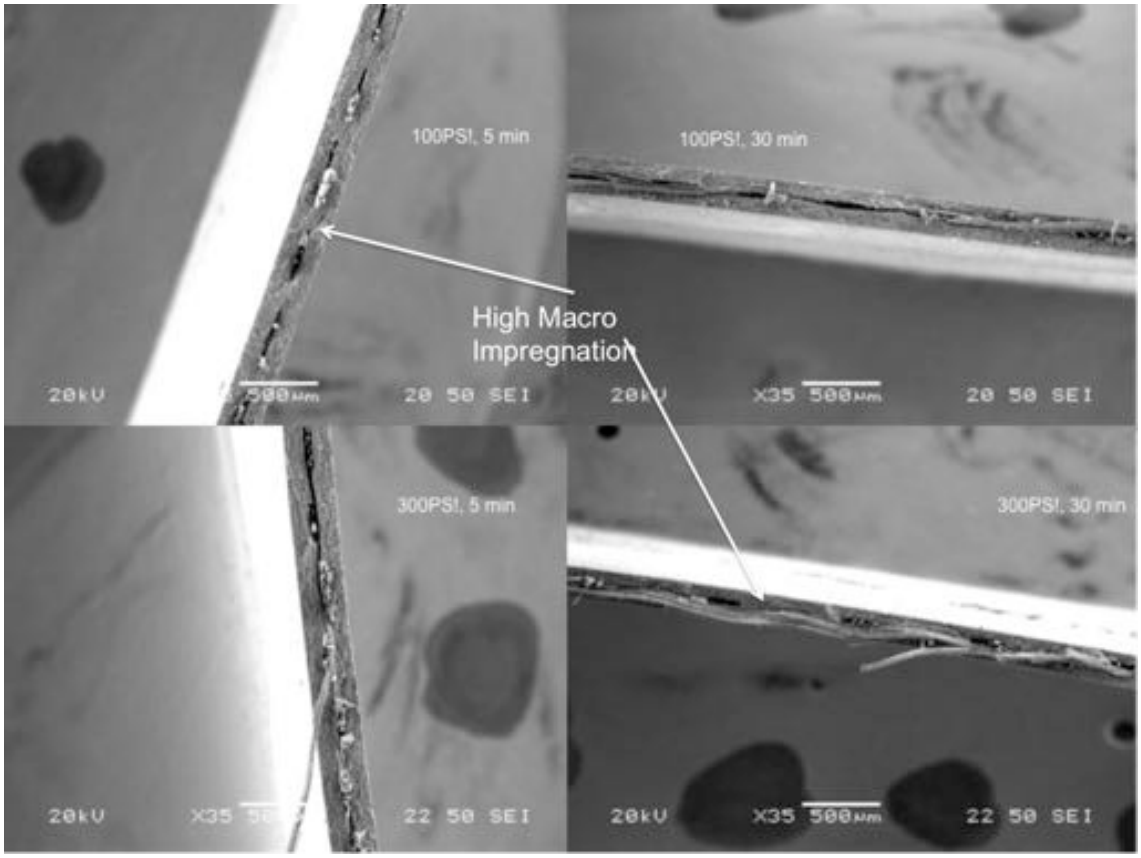

Figure **5-12**: SEM images of stage two laminates produced at 400°C.

Figure 5-13 and Figure 5-14 show the Ultimate Tensile Strength (UTS) and Elongation to break (EtB) for samples of PEEK/GF laminate produced at a variety of processing conditions. Mechanical testing in the form of dog bone tensile tests was completed on five samples cut from each laminate. Any samples, which failed at the neck, were discarded and re-tested. Reasoning for this, was due to potential weakening of the sample at the neck due to the process of cutting, pulling the glass fibre. It is clear that increases in processing pressure increases both EtB and UTS of PEEK/GF laminates, a small increase is also observed with increasing

temperature. Furthermore, increases in hold time clearly show further increase in both EtB and UTS, which is backed up by SEM imagery, which shows improved impregnation with longer holds. It is clear that as temperature is increased to 400°C the formation of a transcrystalline layer results in an increase in mechanical properties.

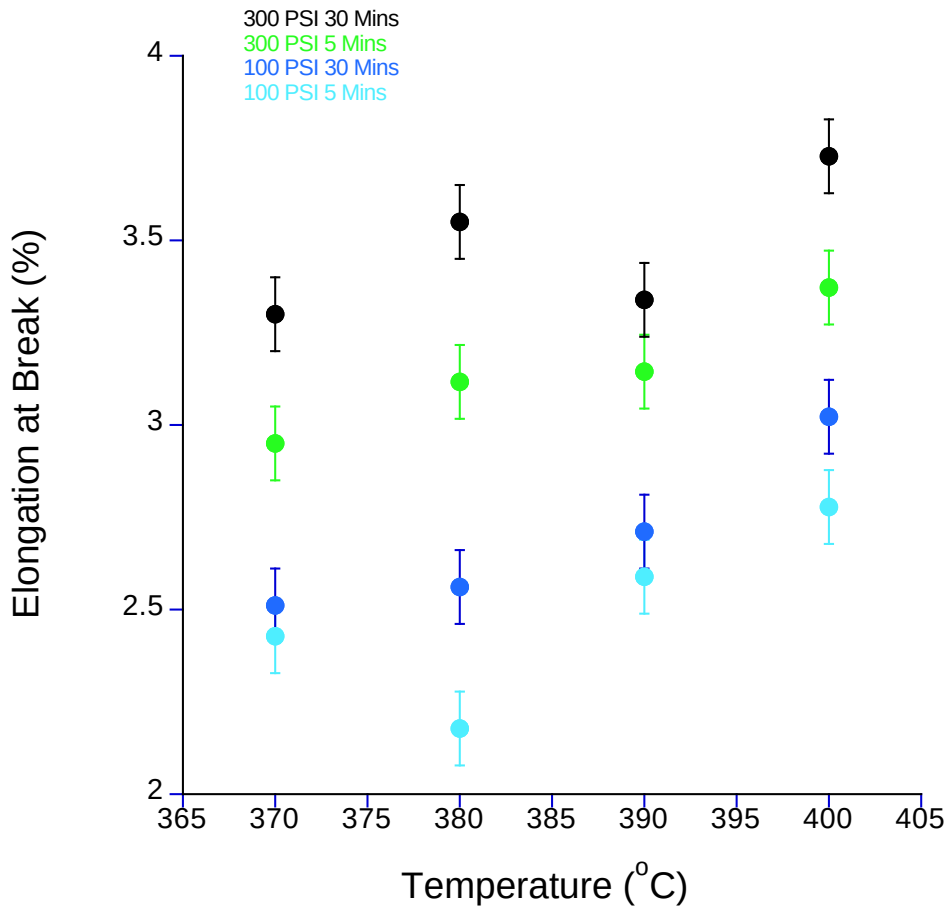

Figure **5-13**: Elongation at break for laminates produced at varied temperature, pressure and hold times.

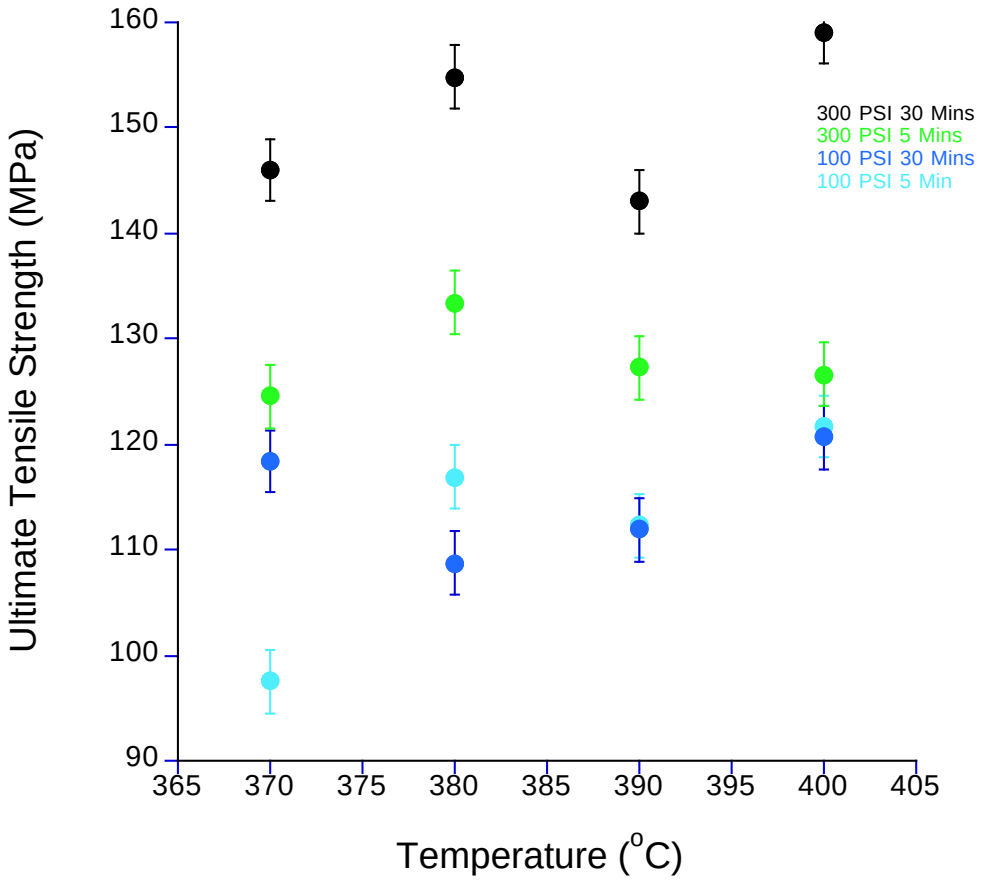

Figure **5-14**: Ultimate tensile strength for laminates produced at varied temperature, pressure and hold times.

Mechanical tests clearly indicate an increase in material properties are observed with an increase in processing pressure and hold time however, SEM images showed no clear improvement in impregnation when pressure and hold time conditions were increased. It is apparent that a hold pressure of 100 psi and a hold

time of 5 minutes produce a low level of impregnation. However, SEM imagery indicated, the effect of fibre compression at high pressures can also result in poor impregnation. Figure 5-15 show SEM images of laminates produced at 20-minute hold time and 200 psi pressure (matches more closely to 1.4 MPa pressure recommended in literature). It is clear that the use of 200 psi has increased the level of macro impregnation, a similar increase in micro impregnation is also observed. A small void line is present between the two layers of PEEK film indicating that full impregnation hasn't yet been achieved; however, an increase in dwell time may lead to full impregnation. At 400^{o}C the void between layers has been removed and better quality impregnation has been achieved. This indicates that the use of 200 psi pressure offers a compromise of improved impregnation levels, with increased mechanical properties. Furthermore a hold time of 30 minutes is a minimum requirement at temperatures of less than 400^{o}C.

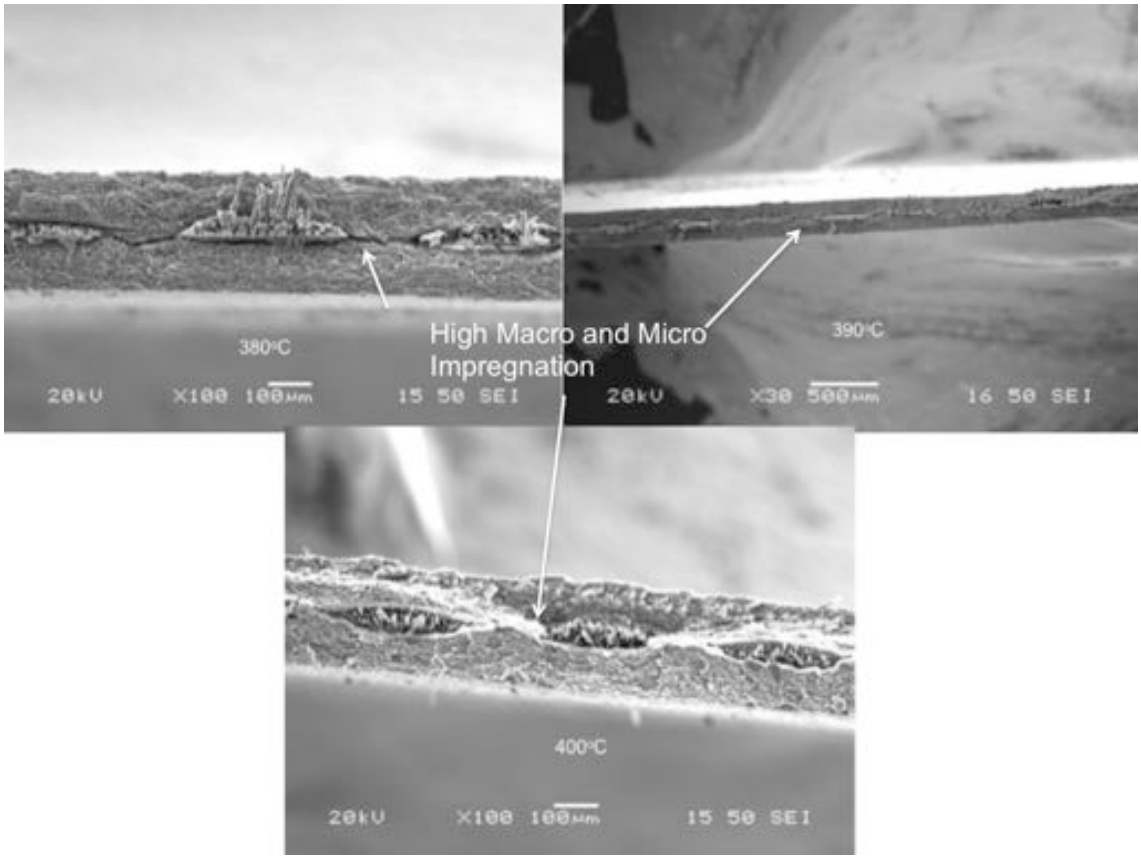

Figure **5-15**: SEM images of laminates produced using 200 psi for dwell time of 30 minutes.

5.2.2 Further testing PEEK Glass fibre laminates

Table 5-2 shows a second matrix of experiments, produced to help narrow down the best set of processing conditions for PEEK/GF laminate production. Previous results indicated that hold times of shorter than 30 minutes results in reduced impregnation of the fibre mat, therefore hold times of 30 and 60-minute were used. Pressure was maintained at 200psi.

Hold Temperature (°C)	Hold Pressure (psi)	Dwell Time (min)
360	200	60
380	200	30
380	200	60
400	200	30
400	200	60

Table 5-2: Second test matrix for further analysis of PEEK/GF laminates.

Figure 5-16 shows SEM images of PEEK/GF laminate produced at 360°C. It is clear that overall impregnation was poor. Increasing hold time to 60 minutes resulted in an increase in impregnation over previously produced samples at 370°C, however; overall it is clear that increase viscosity of PEEK at temperatures of 370°C and below results in laminates of both poor impregnation and mechanical properties.

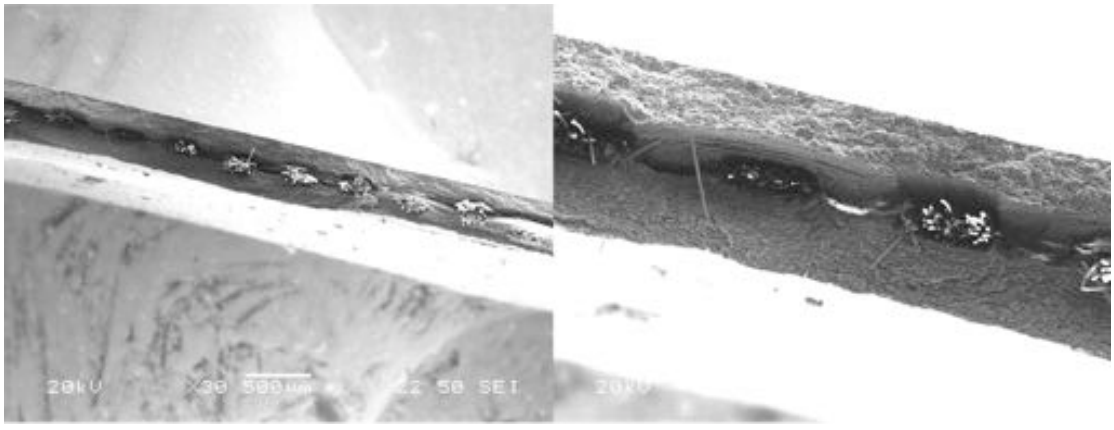

Figure **5-16**: PEEK laminate produced at 360°C, 60 minutes, and 200 psi.

Figure 5-17 and Figure 5-18 show SEM images of laminates produced at 380°C with hold times of 30 and 60 minutes respectively. At 30 minute hold times, a clear void between the PEEK film and the fibre bundles can be seen, indicating that hold time was not of sufficient enough for PEEK impregnation. As hold time is increased to 60 minutes, impregnation was clearly improved. Although an opening is still present between the two sheets of PEEK film, voids around the fibre bundle are decreased. This indicates for laminates produced at 380°C, hold times of greater than 30 minutes are required.

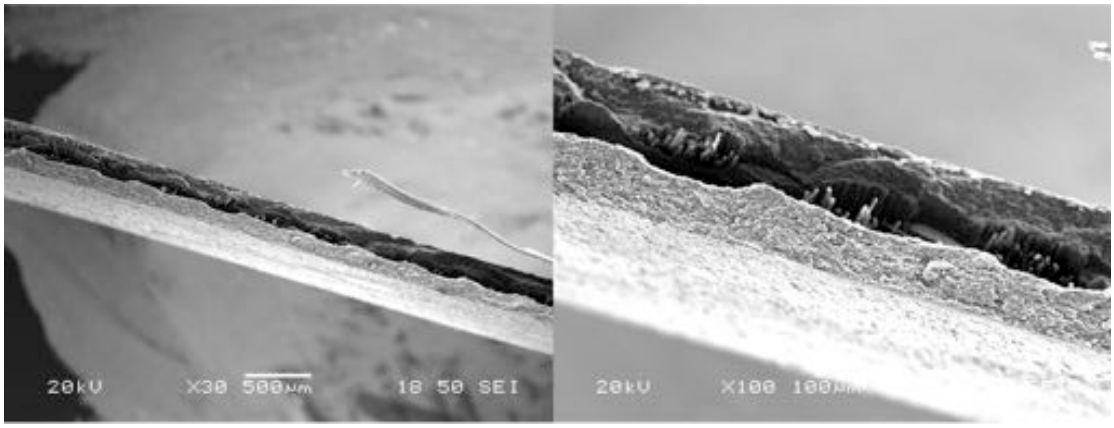

Figure **5-17**: PEEK laminate produced at 380°C, 30 minutes, and 200 psi.

Figure **5-18**: PEEK laminate produced at 380°C, 60 minutes, and 200 psi.

Figure 5-19 and Figure 5-20 show SEM images of laminates produced at 400°C with hold times of 30 and 60 minutes respectively. Further visible improvement in impregnation was seen as processing temperature was increased. Similar levels of impregnation are observed between laminates produced at 380°C for 60 minutes, and 400°C for 30 minutes. Void content in both laminates is low, indicating good levels of impregnation. It is clear that by varying processing temperatures in relation to dwell time similar results can be achieved. Further improvements in levels of impregnation were observed when hold time was increased to 60-minutes. Due to the reduced viscosity of PEEK at 400°C, PEEK will flow more freely into the glass fibre mat. An increase in hold time will reduce the need for high hold pressures, reducing the risk of fibre compression.

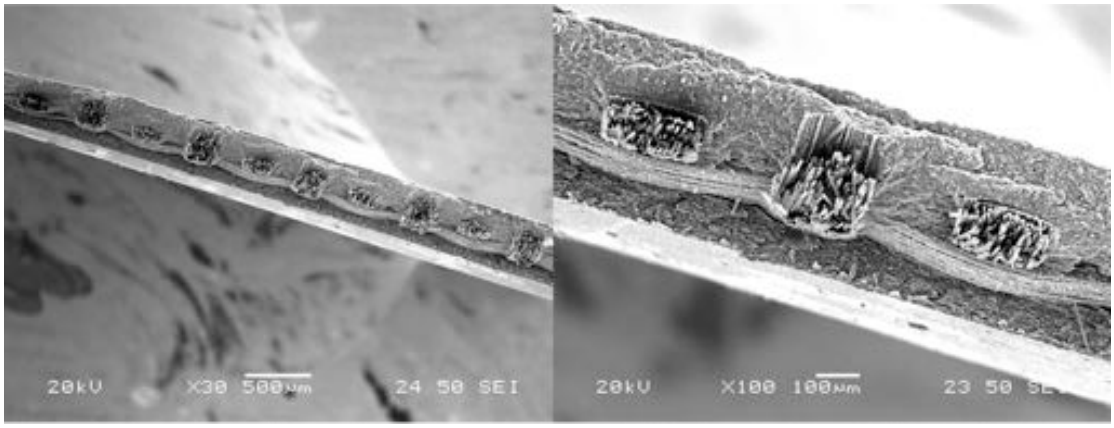

Figure **5-19**: PEEK laminate produced at 400°C, 30 minutes, and 200 psi.

Figure **5-20**: PEEK laminate produced at 400°C, 60 minutes, and 200 psi.

Table 5-3 shows the levels of crystallinity of the PEEK/GF laminates. It is clear there is no conclusive variation in X_c due to changes in processing conditions. It is widely acknowledged that at high temperatures degradation will reduce crystallinity. Crystallinity is depressed further in PEEK/GF laminates due to the glass fibres acting as barriers to crystallisation, however crystallisation will occur earlier due to increases in heterogeneous crystallisation on the fibre, increasing the level of

bonding between the PEEK/GF. As no variation is seen in X_c as processing temperature increases, this indicates that the presence of glass fibre is delaying the onset of degradation.

Laminate	**X_c (%)**
360/60min/200 psi	24
380/30min/200 psi	26
380/60min/200 psi	26
400/30min/200 psi	24
400/60min/200 psi	25

Table 5-3: X_c results for PEEK laminates under different processing conditions.

Figure 5-21 to Figure 5-25 and Table 5-4 to Table 5-8 show the stress vs. strain curves and mechanical test results for laminates produced at processing conditions shown above. Results obtained for Young's Modulus cannot be taken as absolute values due to the inaccuracy of testing the dog bone samples. However, it is widely known that the introduction of GF can greatly increase the Young's modulus of PEEK laminates [128]. Values obtained can however be used as direct comparisons of the processing conditions used in this study. Tests completed using strain gauges on PEEK/GF samples showed an increase in Young's Modulus to around 17 GPa.

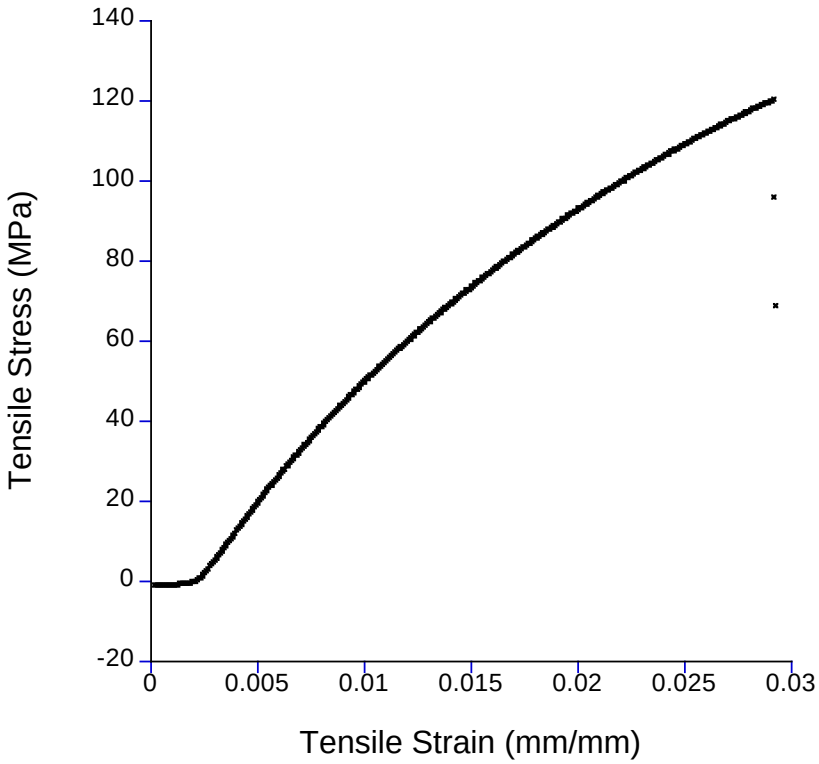

Figure **5-21**: Stress vs Strain curve for 360°C/60min/200 psi laminate.

Sample Number	UTS (MPa)	% Elongation	Young's Modulus (GPa)	Energy to Break (KJ/m^2)
1	108.4	2.6	6.4	0.089
2	107.2	2.6	6.5	0.087
3	120.3	2.9	6.7	0.105
Average	**112.0**	**2.7**	**6.5**	**0.095**
SD	5.9	0.1	0.12	0.003

Table 5-4: Results, averages and standard deviation results for ultimate tensile strength, percentage elongation, Young's modulus, and energy to break. For laminate produced at 360°C, 60 minutes, 200 psi.

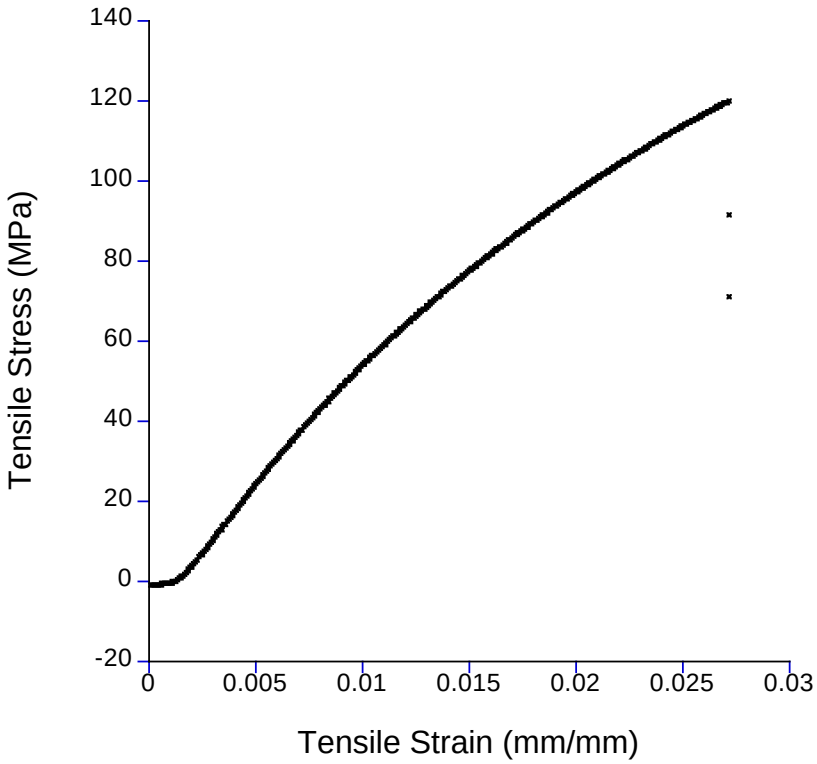

Figure **5-22**: Stress vs Strain curve for 380°C/30min/200 psi laminate.

Sample Number	UTS (MPa)	% Elongation	Young's Modulus (GPa)	Energy to Break (KJ/m^2)
1	124.8	2.7	7.0	0.094
2	119.9	2.7	6.8	0.096
3	120.6	2.7	6.9	0.094
Average	**121.8**	**2.7**	**6.9**	**0.095**
SD	2.16	0.00	0.08	0.001

Table 5-5: Results, averages and standard deviation results for ultimate tensile strength, percentage elongation, Young's modulus, and energy to break. For laminate produced at 380°C, 30 minutes, 200 psi.

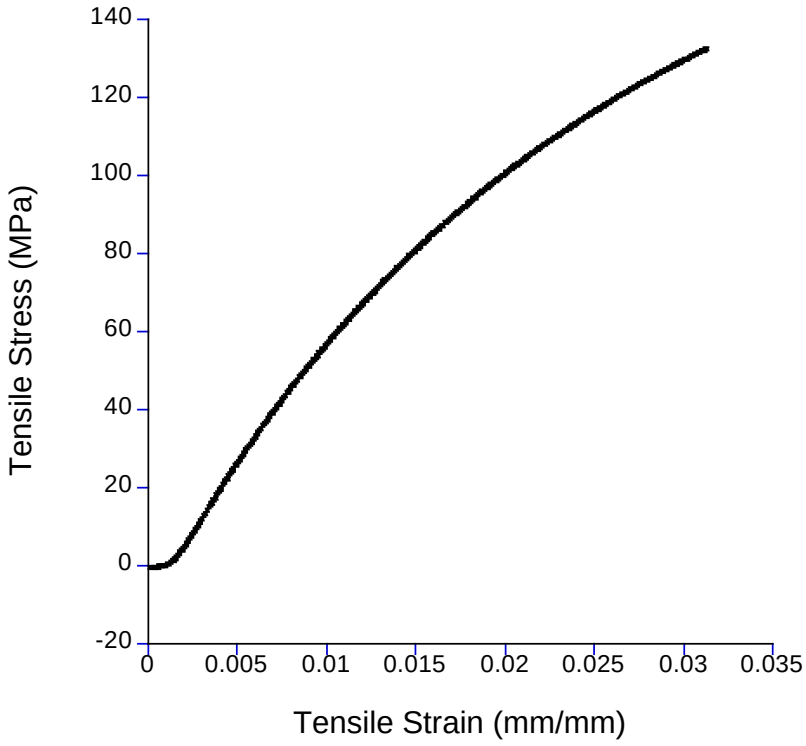

Figure **5-23**: Stress vs Strain curve for 380°C/60min/200 psi laminate.

Sample Number	UTS (MPa)	% Elongation	Young's Modulus (GPa)	Energy to Break (KJ/m²)
1	132.4	3.1	7.1	0.129
2	127.1	2.9	7.0	0.126
3	130.3	3.2	6.9	0.116
Average	**129.9**	**3.1**	**7.0**	**0.123**
SD	2.18	0.12	0.08	0.005

Table 5-6: Results, averages and standard deviation results for ultimate tensile strength, percentage elongation, Young's modulus, and energy to break. For laminate produced at 380°C, 60 minutes, 200 psi.

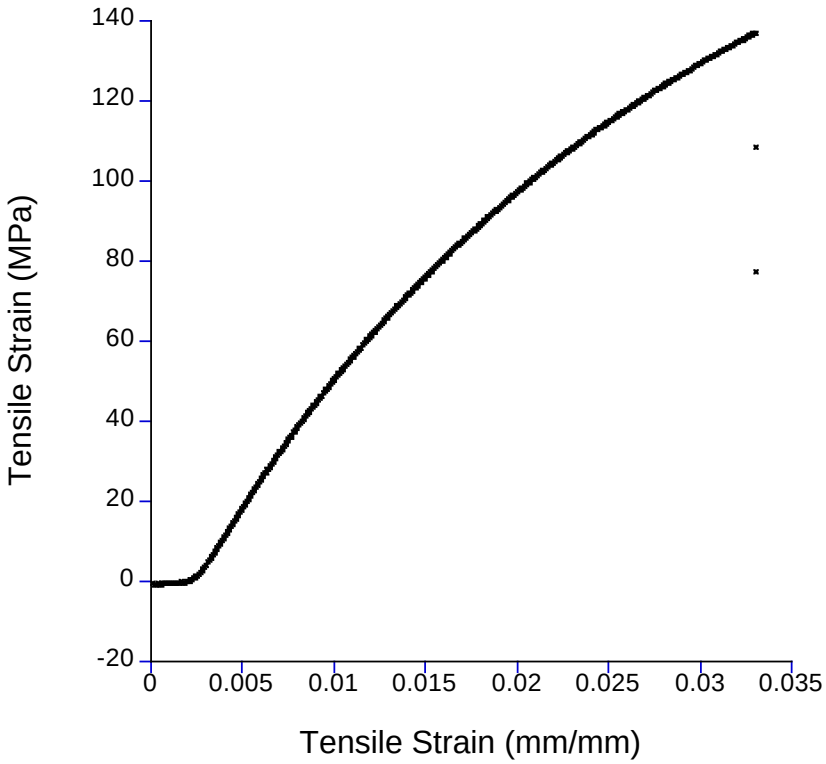

Figure **5-24**: Stress vs Strain curve for 400°C/30min/200 psi laminate.

Sample Number	UTS (MPa)	% Elongation	Young's Modulus (GPa)	Energy to Break (KJ/m^2)
1	136.9	3.3	7.0	0.120
2	132.0	3.2	7.0	0.111
3	141.6	3.3	6.8	0.111
Average	**136.8**	**3.3**	**6.9**	**0.114**
SD	3.91	0.05	0.09	0.004

Table 5-7: Results, averages and standard deviation results for ultimate tensile strength, percentage elongation, Young's modulus, and energy to break. For laminate produced at 400°C, 30 minutes, 200 psi.

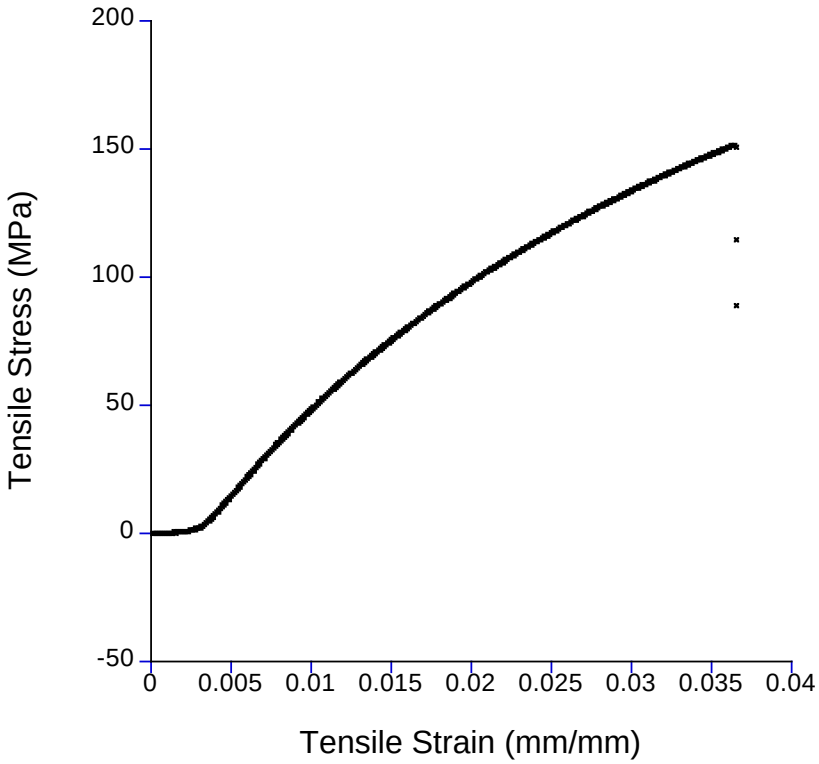

Figure **5-25**: Stress vs Strain curve for 400°C/60min/200 psi laminate.

Sample Number	UTS (MPa)	% Elongation	Young's Modulus (GPa)	Energy to Break (KJ/m^2)
1	140.7	3.3	7.1	0.116
2	151.0	3.6	7.1	0.131
3	142.3	3.3	7.2	0.115
Average	**144.7**	**3.4**	**7.1**	**0.121**
SD	4.52	0.14	0.05	0.007

Table 5-8: Results, averages and standard deviation results for ultimate tensile strength, percentage elongation, Young's modulus, and energy to break. For laminate produced at 400°C, 60 minutes, 200 psi.

Figure 5-26 shows the UTS and EtB for PEEK/GF laminates produced using varied conditions. It is clear that the mechanical properties of PEEK laminates are increased with increased hold temperatures. Furthermore, at longer hold times a further increase is observed. This is due to the reduced number of nuclei available for crystallisation in the polymer matrix, resulting in the development of a transcrystalline layer produced at forming temperatures above T_m^0, this was also described by [105, 108, 141]. The formation of spherulites off the fibre surface increases the bond strength of laminates produced at high temperatures. Figure 5-27 shows the Young's modulus and Energy to break for the same PEEK/GF laminates. It is clear that Young's modulus is increased with processing temperatures of 380°C and above. An increase in hold time shows a further increase in Young's modulus. Energy to break is increased at hold temperatures of 380°C and above however, at 380°C, hold time must be greater than 30 minutes.

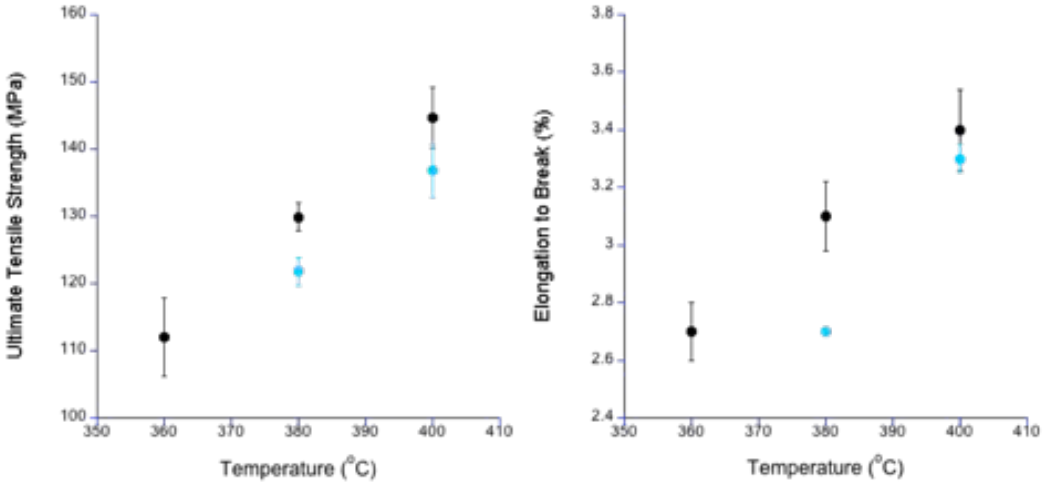

Figure **5-26**: Ultimate tensile strength and Elongation to break for PEEK/GF laminates produced with varied processing conditions. Black dots represent 60-minute holds, blue 30 minute holds.

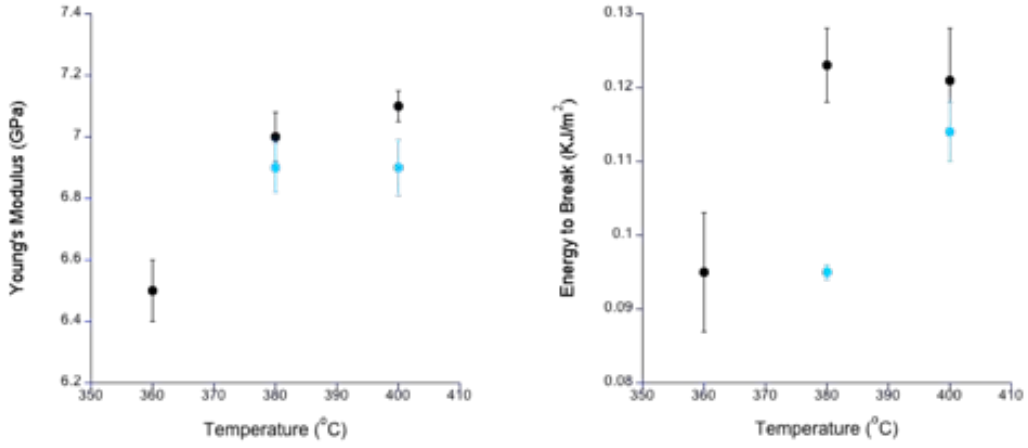

Figure **5-27**: Young's modulus and Energy to break for PEEK/GF laminates produced with varied processing conditions. Black dots represent 60 minute holds, blue 30 minute holds.

It is clear that laminates produced at 370°C and below show poor impregnation and mechanical properties. Laminates produced at hold temperatures of 380°C show the largest variation between hold times, with a substantial increase in mechanical properties found when hold time was increased to 60 minutes. Highest levels of impregnation and mechanical properties were found in laminates produced at hold temperatures of 400°C. Increased hold time of 60 minutes showed the best results.

Figure 5-28 shows SEM images of a PEEK/GF laminate of increased thickness produced at 400°C, for 60 minutes at 200 psi. These laminates were produced to show the effect of these processing conditions on laminates of greater thickness. Each laminate was produced with 150 micron PEEK either side of two GF mats separated by a 50 micron PEEK film. It is clear that a high level of impregnation has been achieved, with high macro impregnation and an increased amount of micro impregnation of the fibre bundles.

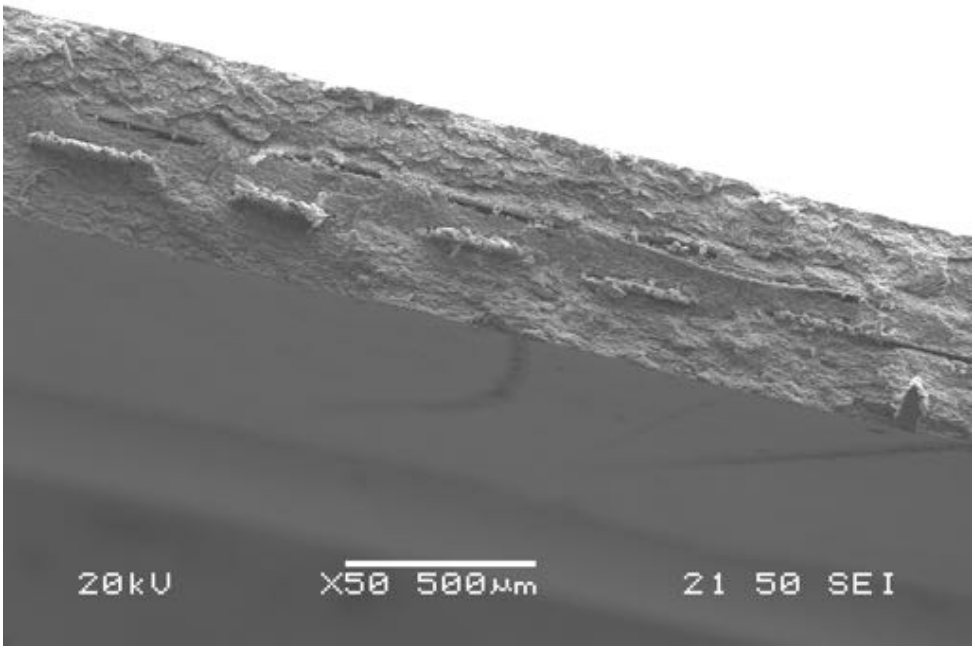

Figure **5-28**: 400 micron Laminate produced at 400°C, 60 minutes, 200 psi.

5.2.3 Effect of Pre-Drying

As previously discussed the process of pre-drying in PEEK/GF production is not widely covered in the literature. Figure 5-29 shows SEM images of three PEEK/GF laminates produced with matching processing conditions, with three varied methods of pre-drying. Laminates were produced with no pre-drying cycle, PEEK only pre-drying cycle, and PEEK and GF pre-drying cycle. Each pre-drying consisted of a 24-hour hold in an oven at 140°C. Laminates were processed at hold temperature of 400°C, for 60 minutes, at 200 psi. It is clear that fibre impregnation is improved with pre-drying. Laminates produced with no pre-dry cycle show large void content and clear split between layers, a clear decrease in void content is shown with pre-drying of PEEK. Laminates produced after a PEEK/GF pre-

drying cycle shows a very high level of impregnation. This indicates that pre-drying of PEEK/GF is essential for high levels of impregnation. This is due to the removal of any moisture and foreign particles in the sample, which can cause air pockets and nucleation; removal of these further encourages nucleation with the fibre surface.

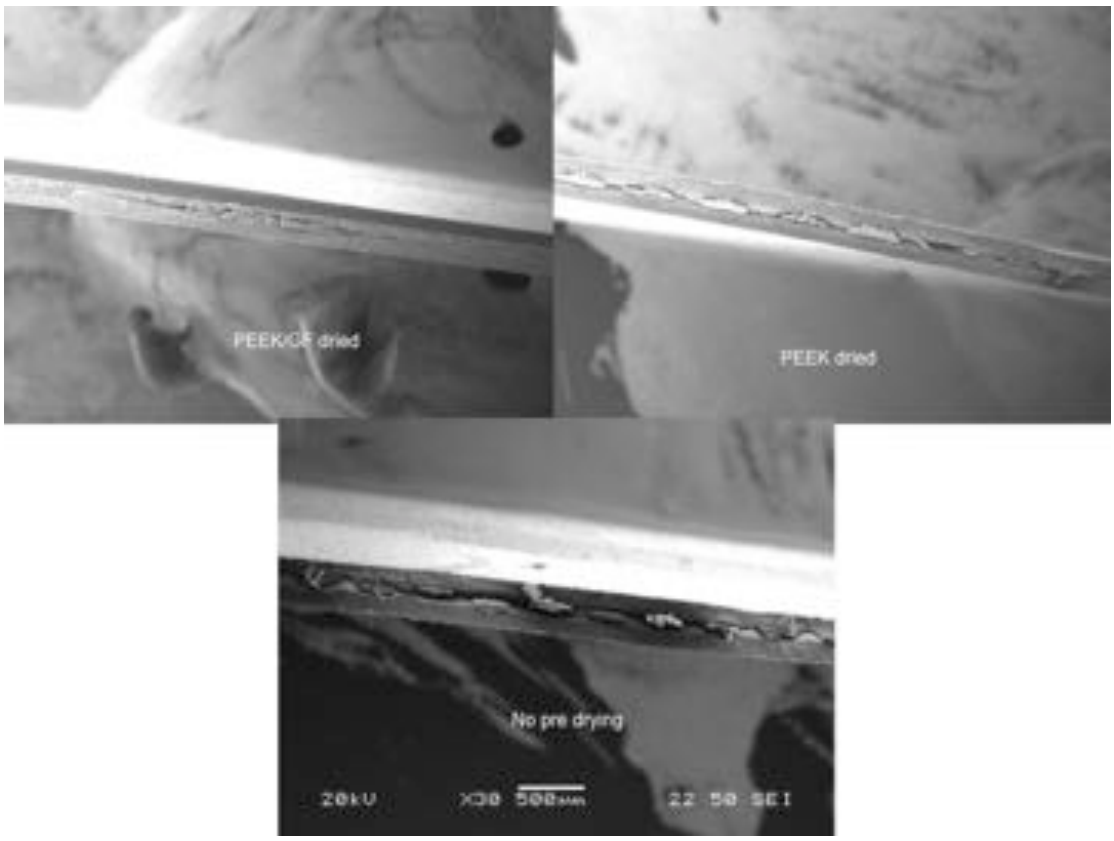

Figure **5-29**: Laminates produced with different pre-drying sequence.

Table 5-9 and Figure 5-30 shows the mechanical properties of laminates produced with a 24 hour pre drying cycle vs laminates with no pre dry cycle. PEEK/GF laminates were produced at 400^{o}C, 60 minutes, and 200 psi. It is clear that pre-

dried laminates show a clear increase in mechanical properties. This indicates a much higher level of impregnation and bond strength.

Before the laminate production, both the PEEK film and GF mat must be pre-dried in an oven at 140°C, preferably for 24hrs. Further tests have shown the importance of completing this process in an oven and not in the press itself. As press drying show lower levels of impregnation. This indicates that removable of any particles in the press can get caught in the PEEK or Kapton layer.

Sample Number	UTS (MPa)	% Elongation	Young's Modulus (GPa)	Energy to Break (KJ/m^2)
1	104.5	2.7	5.6	0.069
2	113.8	3.1	5.8	0.076
3	119.0	3.8	5.4	0.098
Average	**112.4**	**3.2**	**5.6**	**0.081**
SD	6.10	0.45	0.16	0.01

Table 5-9: Results, averages and standard deviation results for ultimate tensile strength, percentage elongation, Young's modulus, and energy to break. For laminate produced with no pre-drying, at 400°C, 60 minutes, 200 psi.

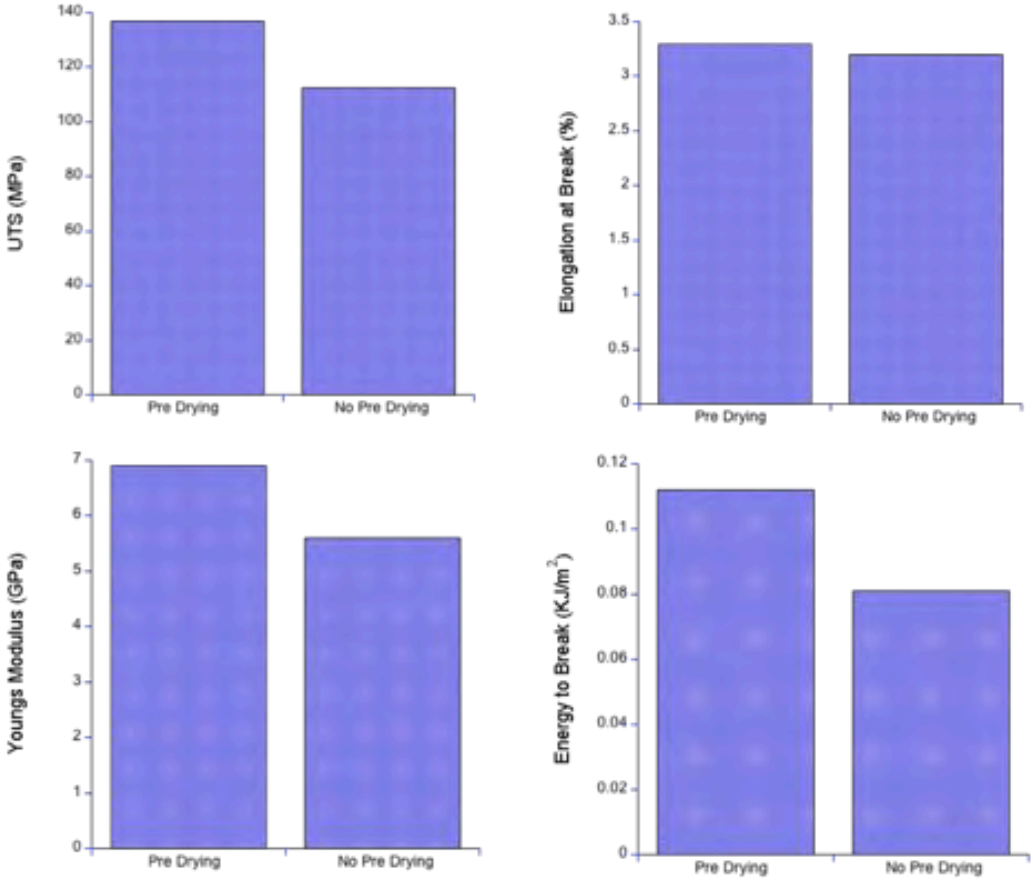

Figure **5-30**: Mechanical properties for pre-dried and non pre-dried PEEK laminates produced at 400°C/30 mins/200 psi.

5.3 Conclusion

Literature showed varied processing methods for the production of PEEK/GF laminates. Various recommendations for temperature, pressure and dwell times are given which differ from experiment to experiment. Papers that haven't conducted reviews of processing conditions have used ICI recommended conditions of 380^{o}C, and 1.4MPa, pressure.

- Results have shown that the best processing conditions for PEEK/GF laminates were 400^{o}C, 60 minutes hold time, 200 psi.
- Impregnation and mechanical properties for the processed laminates were clearly improved as temperature was increased. This was due to the decrease in viscosity of PEEK allowing better flow between the fibre bundles.
- Furthermore, the effect of crosslinking decreased the number of nuclei in PEEK; this therefore increased the nucleation on the fibre bundles. This increased the laminates mechanical properties.
- When dwell time was increased 30 to 60 minutes, again impregnation and mechanical properties increased. This was due to the increased time allowed for the PEEK to impregnate the fibre bundles.
- Pressures of 100, 200, and 300 psi were all used. SEM images showed poorly formed laminates at both 100 and 300 psi. Low pressures didn't execute enough force to push viscous PEEK into the fibre bundles. Indicates

are that 300 psi depressed the fibre bundles, diminishing the ability viscous PEEK to impregnate the fibre matt.

- Results have proven that pre-drying both the PEEK and Glass fibre is vitally important to the production process. Impregnation and mechanical properties are increased if materials are dried in an oven for 24 hours before production.

6 Chapter 6 – Conclusions and Further Work

6.1 Conclusions

The aim of this thesis was to further investigate the processing and reproducibility of PEEK in both thermal analysis and composite production. A clear set of processing conditions was to be developed to increase the mechanical properties of PEEK/fiber laminates. Hold temperatures 380^{o}C, with hold time and hold pressure of 60 minutes and 200 psi respectively have shown to give the best combination of impregnation and mechanical properties. The effects of taking results from multiple samples of PEEK against using one sample has been investigated and recommendations given for the analysis of PEEK by showing the reproducibility of PEEK at a number of temperatures and hold times above T_m. It has been shown that at hold temperature of 380^{o}C multiple runs PEEK can be obtained without the effect of degradation, while removing self-nucleation.

Values for ΔH_f of PEEK and therefore X_c can vary due to the placement of integration limits on the DSC software. It is therefore important to obtain a set of limits, which will give a consistent level of determining a materials X_c. By varying the T_{lower} and T_{upper}, values of 270^{o}C and 356^{o}C were obtained as integration limits respectively.

Previous literature has widely reported high levels of degradation of PEEK at T_m^0, decreasing in intensity as temperature decreases to below 380^{o}C. Significant variations in results are found when a different sample of PEEK is used for each experiment in thermal analysis. Samples of PEEK were thermally cycled to varied

temperatures, with varied hold times in DSC. It was clear that degradation occurs significantly lower than previously reported, at temperatures as low as 350°C. Degradation rate increases linearly with increases in hold temperature. It was shown that at hold times of 380°C prior thermal history was removed and up to 12 consistent runs could be obtained from one PEEK sample. As temperature was increased to T_m^0, the number of runs available reduced to 3. This indicates that T_m^0 can be found at 380°C, with 395°C being a point where degradation increases significantly.

Through the analysis of the cooling cycle, a double crystallisation exotherm was observed on crystallisation, coinciding with a significant drop in ΔH_c. This gives further evidence to crosslinking causing the decrease in PEEK X_c. As crosslinking increases the nuclei available for crystallisation is constrained. This results in a second crystallisation peak, moving to a lower temperature as containment increases. Once crosslinking reaches a point where these nuclei can no longer crystallise, the second crystallisation exotherm is removed and ΔH_c significantly decreases.

FTIR analysis has shown that the height of peaks 1653cm^{-1} (crystalline phase) and 1648cm^{-1} (amorphous phase) can be used to analysis the extent of degradation. As crosslinking increases the amorphous peak increases in size in ratio to the crystalline peak.

Flash DSC, a novel thermal analysis technique was used to analyse PEEK through thermal cycling in ways unachievable in conventional DSC. The fast heating and cooling rates available allowed the removal of any degradation caused in the

heat/cool cycle, allowing only degradation caused by hold time at final temperature. There was a clear increase in degradation above 380°C, giving further evidence that T_m^0 is significantly lower than previously reported. Furthermore, no degradation below 380°C was seen over the times tested. This indicates that depression of X_c in conventional DSC is due to the slow heating/cooling rates over hold time. For thermal analysis at 395°C, results show that a total of 30 minutes process time can be used before degradation causes a depression in X_c.

Hot press manufacturing was used to produce a number of PEEK/Glass fibre laminates. Varied processing conditions were analysed to give the best levels of impregnation and mechanical properties. Literature had showed a large number of recommendations but no definitive set of process conditions for laminate production. It was found that hold temperature of 380°C, combined with 200 psi pressure and 60-minute hold times produced laminates with the high levels of fibre impregnation and the best mechanical properties. This indicated that using controlled thermal degradation of PEEK in laminate production could increase mechanical properties, through the encouragement of fibre nucleation. Furthermore, the importance of pre drying both the fibre mat and PEEK was shown. Laminates produced after a 24-hour pre drying cycle showed an increase in mechanical properties.

6.2 Further Work

FTIR analysis has shown the peaks relating to both the crystalline and amorphous region (1653cm^{-1} and 1648cm^{-1}) of PEEK vary in height at varied stages of degradation. The amorphous peak increases in size as a result of crosslinking. Further work is needed to develop a direct measurement of peak height to the level of PEEK degradation. This would allow a FTIR spectrum to show the extent of degradation in a PEEK part and give an accurate prediction of crystallinity.

The investigation into the reproducibility of PEEK in DSC has been successful, however further investigation into the variability on grades of PEEK needs to be completed. Initial work has been completed to further investigate the process of degradation through thermal cycling on the Flash DSC. This work allows analysis of degradation that occurs only when PEEK is in the melt, removing the heat/cool cycle. Further work will replicate all experiments from conventional DSC to Flash DSC so direct comparisons to the onset and extent of degradation could be completed over a range of temperatures and hold times. If the move to replicate these experiments on Flash DSC was completed earlier this could of added further support to this research.

The grade of PEEK used in chapter 5 incudes introduction of Talc filler due to the needs of industry. This effect of this filler will reduce the effect of degradation. Therefore the results, which were provided in chapters 3 and 4, would need to be repeated with the introduction of talc filler. This will give a more accurate prediction of degradation rates with these particular PEEK films.

Prior literature has given multiple recommendations for the processing conditions of PEEK/glass fibre laminates. No consistent set of conditions has been given however. Chapter 5 resulted in a set of processing conditions resulting in the best mechanical properties. However, the same lack of conclusive conditions is shown in other processing techniques for example, autoclave cycles. Further work will look to develop a set of processing conditions resulting in the best mechanical properties for varied processing techniques as well as the introduction of further layers into the initial PEEK build. Furthermore time constraints prevent the use of strain gauges on tensile tests, this would allow a more accurate comparison of PEEK/Glass fiber laminates industrial values.

Further work for the production of PEEK/Glass fibre laminates by hot press can be investigated with the use of PEEK powder. PEEK powder can be dispersed into the dry fibre mate. When lamination takes place the PEEK powder will encourage nucleation with the PEEK film, improving infusion.

6.1 References

1. Young, R.J. and Lovell.P. A., *Introduction to Polymers.* 2011. **3rd Edition**.
2. Sperling, L.H., *Introduction to the Physical Science.* 1992(2 Edition): p. 198.
3. Kong, Y. and J.N. Hay, *The measurement of the crystallinity of polymers by DSC.* Polymer, 2002. **43**(14): p. 3873-3878.
4. Price, F.P., *The structure of high polymer spherulites.* Journal of Polymer Science, 1959. **37**(131): p. 71-89.
5. Long, Y., R.A. Shanks, and Z.H. Stachurski, *Kinetics of polymer crystallisation.* Progress in Polymer Science, 1995. **20**(4): p. 651-701.
6. Keith, H.D. and Padden Jr, F.J., *Spherulitic Crystallization from the Melt. II. Influence of Fractionation and Impurity Segregation on the Kinetics of Crystallization.* Journal of Applied Physics, 1964. **35**(4): p. 1286-1296.
7. Padden Jr, F.J. and H.D. Keith, *Spherulitic Crystallization in Polypropylene.* Journal of Applied Physics, 1959. **30**(10): p. 1479-1484.
8. Magill, J.H., *Formation of spherulites in polyamide melts: Part III. Even-even polyamides.* Journal of Polymer Science Part A-2: Polymer Physics, 1966. **4**(2): p. 243-265.
9. Magill, J.H., *Morphogenesis of Solid Polymer Microstructures*, in *Treatise on Materials Science & Technology*, J.M. Schultz, Editor. 1977, Elsevier. p. 1-368.
10. Bassett, D.C. and B. Turner, *On chain-extended and chainfolded crystallization of polyethylene.* The Philosophical Magazine: A Journal of Theoretical Experimental and Applied Physics, 1974. **29**(2): p. 285-307.

11. Cheng, S.Z.D., M.Y. Cao, and B. Wunderlich, *Glass transition and melting behavior of poly(oxy-1,4-phenyleneoxy-1,4-phenylenecarbonyl-1,4-phenylene) (PEEK).* Macromolecules, 1986. **19**(7): p. 1868-1876.

12. Verma, R., H. Marand, and B. Hsiao, *Morphological Changes during Secondary Crystallization and Subsequent Melting in Poly(ether ether ketone) as Studied by Real Time Small Angle X-ray Scattering.* Macromolecules, 1996. **29**(24): p. 7767-7775.

13. Tan, S., et al., *Crystallization kinetics of poly(ether ether ketone) (PEEK) from its metastable melt.* Polymer, 1999. **40**(5): p. 1223-1231.

14. Mandelkern, L., *The Crystalline State* Physical Properties of Polymers, 1984.

15. Grebowicz, J., S.F. Lau, and B. Wunderlich, *The thermal properties of polypropylene.* Journal of Polymer Science: Polymer Symposia, 1984. **71**(1): p. 19-37.

16. Suzuki, H., J. Grebowicz, and B. Wunderlich, *Glass transition of poly(oxymethylene).* British Polymer Journal, 1985. **17**(1): p. 1-3.

17. Huo, P. and P. Cebe, *Effects of thermal history on the rigid amorphous phase in poly(phenylene sulfide).* Colloid and Polymer Science, 1992. **270**(9): p. 840-852.

18. Bonnet, M., K.-D. Rogausch, and J. Petermann, *The endothermic "annealing peak" of poly(phenylene sulphide) and poly(ethylene terephthalate).* Colloid and Polymer Science, 1999. **277**(6): p. 513-518.

19. Wunderlich, B., *Macromolecular physics, vol. 2 crystal nucleation, growth, annealing. Academic Press New York 1976, .* Kristall und Technik, 1977. **12**(1): p. K11-K12.

20. Huang, J., A. Prasad, and H. Marand, *Study of the temperature dependence of isothermal spherulitic growth rate data for poly(pivalolactone) in blends with poly(vinylidene fluoride): a link between coherent secondary nucleation theory and mixing thermodynamics.* Polymer, 1994. **35**(9): p. 1896-1908.

21. Avrami, M., *Kinetics of Phase Change. I General Theory.* The Journal of Chemical Physics, 1939. **7**(12): p. 1103-1112.

22. Banks, W., et al., *The crystallization of polyethylene I.* Polymer, 1963. **4**: p. 61-74.

23. Di Lorenzo, M.L. and C. Silvestre, *Non-isothermal crystallization of polymers.* Progress in Polymer Science, 1999. **24**(6): p. 917-950.

24. Lauritzen, J.I. and J.D. Hoffman, *Formation of Polymer Crystals with Folded Chains form Dilute Solution.* Journal of Research National Bureau of Standards, 1960. **64**(A): p. 73.

25. Ozawa, T., *Kinetics of non-isothermal crystallization.* Polymer, 1971. **12**(3): p. 150-158.

26. Cebe, P. and S.-D. Hong, *Crystallization behaviour of poly(ether-ether-ketone).* Polymer, 1986. **27**(8): p. 1183-1192.

27. Vu-Khanh, T. and J. Denault, *Effect of Molding Parameters on the Interfacial Strength in PEEK/Carbon Composites.* Journal of Reinforced Plastics and Composites, 1993. **12**(8): p. 916-931.

28. Hoffman, J.D., *Regime III crystallization in melt-crystallized polymers: The variable cluster model of chain folding.* Polymer, 1983. **24**(1): p. 3-26.

29. Chen, J.Y., M. Chen, and S.-C. Chao, *Thermal Stability and crystallisation kinetics of poly(ether ether ketone).* Macromolecular Chemistry and Physics, 1998. **199**(8): p. 1623-1629.

30. Chen, M. and C.-T. Chung, *Analysis of crystallization kinetics of poly(ether ether ketone) by a nonisothermal method.* Journal of Polymer Science Part B: Polymer Physics, 1998. **36**(13): p. 2393-2399.

31. Day, M., et al., *Effect of molecular weight on the crystallization behaviour of poly(aryl ether ether ketone): a differential scanning calorimetry study.* Polymer, 1991. **32**(7): p. 1258-1266.

32. Hsiao, B., et al., *Time-resolved X-ray studies of structure development in poly(butylene terephthalate) during isothermal crystallization.* Polymer, 1999. **40**(12): p. 3515-3523.

33. Hsiao, B.S., et al., *Time-resolved X-ray study of poly(aryl ether ether ketone) crystallization and melting behaviour: 1. Crystallization.* Polymer, 1993. **34**(19): p. 3986-3995.

34. Verma, R.K., et al., *SAXS studies of lamellar level morphological changes during crystallization and melting in PEEK.* Polymer, 1996. **37**(24): p. 5357-5365.

35. Wang, Z.G., et al., *The nature of secondary crystallization in poly(ethylene terephthalate).* Polymer, 1999. **40**(16): p. 4615-4627.

36. Srinivas, S. and G.L. Wilkes, *Structural and relaxation studies during crystallization of New TPI polyimide.* Polymer, 1998. **39**(23): p. 5839-5851.

37. Marand, H., et al., *Influence of Structural and Topological Constraints on the Crystallization and Melting Behavior of Polymers. 2. Poly(arylene ether ether ketone).* Macromolecules, 2000. **33**(9): p. 3392-3403.

38. Jones, D.P., D.C. Leach, and D.R. Moore, *Mechanical properties of poly(ether-ether-ketone) for engineering applications.* Polymer, 1985. **26**(9): p. 1385-1393.

39. Blundell, D.J. and B.N. Osborn, *The morphology of poly(aryl-ether-ether-ketone).* Polymer, 1983. **24**(8): p. 953-958.

40. Lee, Y. and R.S. Porter, *Double-melting behavior of poly(ether ether ketone).* Macromolecules, 1987. **20**(6): p. 1336-1341.

41. Nguyen, H.X. and H. Ishida, *Poly(aryl-ether-ether-ketone) and its advanced composites: A review.* Polymer Composites, 1987. **8**(2): p. 57-73.

42. Platt, D.K., *Engineering and High Performance Plastics.* Rapra technology Ltd, 2003. p. 52-54.

43. Bonner, W.H., *US Patent 3,065,205.* 1962.

44. Johnson, R.N., et al., *Poly(aryl ethers) by nucleophilic aromatic substitution. I. Synthesis and properties.* Journal of Polymer Science Part A-1: Polymer Chemistry, 1967. **5**(9): p. 2375-2398.

45. Attwood, T.E., et al., *Synthesis and properties of polyaryletherketones.* Polymer, 1981. **22**(8): p. 1096-1103.

46. Imperial Chemcial Industries PLC., *Aeromatic Polymer Composites Data Sheets.* Fiberite Corp., Wilmington, Delware, 1986.

47. Lu, Q., et al., *Synthesis, morphology, and melting behavior of poly(ether ether ketone) of different molecular weights.* Journal of Applied Polymer Science, 2009. **114**(4): p. 2060-2070.

48. Kumar, S., D.P. Anderson, and W.W. Adams, *Crystallization and morphology of poly(aryl-ether-ether-ketone).* Polymer, 1986. **27**(3): p. 329-336.

49. Lovinger, A.J. and D.D. Davis, *Electron-microscopic investigation of the morphology of a melt-crystallized polyaryletherketone.* Journal of Applied Physics, 1985. **58**(8): p. 2843-2853.

50. Bassett, D.C., R.H. Olley, and I.A.M. Al Raheil, *On crystallization phenomena in PEEK.* Polymer, 1988. **29**(10): p. 1745-1754.

51. Blundell, D.J., et al., *Spherulitic morphology of the matrix of thermoplastic PEEK/carbon fibre aromatic polymer composites.* Journal of Materials Science, 1989. **24**(6): p. 2057-2064.

52. Cebe, P., S.Y. Chung, and S.-D. Hong, *Effect of thermal history on mechanical properties of polyetheretherketone below the glass transition temperature.* Journal of Applied Polymer Science, 1987. **33**(2): p. 487-503.

53. Lee, W.I., et al., *Effects of Cooling Rate on the Crystallinity and Mechanical Properties of Thermoplastic Composites.* Journal of Reinforced Plastics and Composites, 1987. **6**(1): p. 2-12.

54. F. Talbott, M., G. Springer, and L. A. Berglund, *The Effects of Crystallinity on the Mechanical Properties of PEEK Polymer and Graphite Fiber Reinforced PEEK*. Vol. 21. 1987. 1056-1081.

55. Bell, J.P. and T. Murayama, *Relations between dynamic mechanical properties and melting behavior of nylon 66 and poly(ethylene terephthalate).* Journal of Polymer Science Part A-2: Polymer Physics, 1969. **7**(6): p. 1059-1073.

56. Cebe, P., *Annealing study of poly(etheretherketone).* Journal of Materials Science, 1988. **23**(10): p. 3721-3731.

57. Lattimer, M.P., et al., *On the origin of the multiple endotherms in PEEK.* Polymer, 1992. **33**(18): p. 3971-3973.

58. Jonas, A.M., T.P. Russell, and D.Y. Yoon, *Synchrotron X-ray Scattering Studies of Crystallization of Poly(ether-ether-ketone) from the Glass and Structural Changes during Subsequent Heating-Cooling Processes.* Macromolecules, 1995. **28**(25): p. 8491-8503.

59. Holdsworth, P.J. and A. Turner-Jones, *The melting behaviour of heat crystallized poly(ethylene terephthalate).* Polymer, 1971. **12**(3): p. 195-208.

60. Blundell, D.J., *On the interpretation of multiple melting peaks in poly(ether ether ketone).* Polymer, 1987. **28**(13): p. 2248-2251.

61. Lee, W.I. and G.S. Springer, *A model of the manufacturing process of thermoplastic matrix composites.* Journal of composite materials, 1987. **21**(11): p. 1017-1055.

62. Cheng, S.Z.D., et al., *Size effect of metastable states on semicrystalline polymer structures and morphologies.* Thermochimica Acta, 1999. **332**(2): p. 105-113.

63. Wang, J., et al., *Synchrotron small-angle x-ray scattering study of crystalline structures and isothermal crystallization kinetics of poly(aryl ether ether ketones).* Macromolecules, 1992. **25**(25): p. 6943-6951.

64. Wei, C.-L., M. Chen, and F.-E. Yu, *Temperature modulated DSC and DSC studies on the origin of double melting peaks in poly(ether ether ketone).* Polymer, 2003. **44**(26): p. 8185-8193.

65. Fougnies, C., et al., *Time-Resolved SAXS, WAXS, and DSC Study of Melting of Poly(aryl ether ether ketone) (PEEK) Annealed from the Amorphous State.* Macromolecules, 1997. **30**(5): p. 1392-1399.

66. Fougnies, C., et al., *Time-Resolved SAXS, WAXS, and DSC Study of the Annealing of Poly(aryl ether ether ketone) (PEEK) from the Glassy State.* Macromolecules, 1997. **30**(5): p. 1385-1391.

67. Ko, T.Y. and E.M. Woo, *Changes and distribution of lamellae in the spherulites of poly(ether ether ketone) upon stepwise crystallization.* Polymer, 1996. **37**(7): p. 1167-1175.

68. Zhang, Z. and H. Zeng, *Effects of thermal treatment on poly(ether ether ketone).* Polymer, 1993. **34**(17): p. 3648-3652.

69. Kong, Y. and J.N. Hay, *Multiple melting behaviour of poly(ethylene terephthalate).* Polymer, 2003. **44**(3): p. 623-633.

70. Hay, J. and D.J. Kemmish, *Crystallization of PEEK, a polyaryl ether ketone: molecular weight effects*. Vol. 11. 1989. 29-35.

71. Morgan, L.B., *Crystallization phenomena in fibre-forming polymers.* Journal of Applied Chemistry, 1954. **4**(4): p. 160-172.

72. Lu, X.F. and J.N. Hay, *Isothermal crystallization kinetics and melting behaviour of poly(ethylene terephthalate).* Polymer, 2001. **42**(23): p. 9423-9431.

73. Tardif, X., et al., *Experimental study of crystallization of PolyEtherEtherKetone (PEEK) over a large temperature range using a nano-calorimeter.* Polymer Testing, 2014. **36**: p. 10-19.

74. Jin, L., et al., *Crystallization behavior and morphological characterization of poly(ether ether ketone).* Polymer, 2014. **55**(20): p. 5255-5265.

75. Soutis, C., *Fibre reinforced composites in aircraft construction.* Progress in Aerospace Sciences, 2005. **41**(2): p. 143-151.

76. Soutis, C., *Carbon fiber reinforced plastics in aircraft construction.* Materials Science and Engineering: A, 2005. **412**(1–2): p. 171-176.

77. Groenewoud, W.M., *CHAPTER 1 - DIFFERENTIAL SCANNING CALORIMETRY*, in *Characterisation of Polymers by Thermal Analysis*. 2001, Elsevier Science B.V.: Amsterdam. p. 10-60.

78. Gao, S.-L. and J.-K. Kim, *Cooling rate influences in carbon fibre/PEEK composites. Part 1. Crystallinity and interface adhesion.* Composites Part A: Applied Science and Manufacturing, 2000. **31**(6): p. 517-530.

79. Chen, M. and S.-C. Chao, *Thermal stability and nonisothermal crystallization of short fiber-reinforced poly(ether ether ketone) composites.* Journal of Polymer Science Part B: Polymer Physics, 1998. **36**(12): p. 2225-2235.

80. Toledo., M. *Flash Differential Scanning Calorimeter*. Available from: http://us.mt.com/gb/en/home/products/Laboratory_Analytics_Browse/TA_Family_Browse/Flash_DSC.html.

81. Iervolino, E., et al., *Temperature calibration and electrical characterization of the differential scanning calorimeter chip UFS1 for the Mettler-Toledo Flash DSC 1.* Thermochimica Acta, 2011. **522**(1): p. 53-59.

82. van Herwaarden, S., et al., *Design, performance and analysis of thermal lag of the UFS1 twin-calorimeter chip for fast scanning calorimetry using the Mettler-Toledo Flash DSC 1.* Thermochimica Acta, 2011. **522**(1): p. 46-52.

83. Poel, G.V., et al., *Performance and calibration of the Flash DSC 1, a new, MEMS-based fast scanning calorimeter.* Journal of Thermal Analysis and Calorimetry, 2012. **110**(3): p. 1533-1546.

84. Vanden Poel, G. and V.B.F. Mathot, *High performance differential scanning calorimetry (HPer DSC): A powerful analytical tool for the study of the metastability of polymers.* Thermochimica Acta, 2007. **461**(1): p. 107-121.

85. Morris, J.N., *Elements of Polymer Degradation, Leo Reich and Salvatore S. Stivala, McGraw-Hill Book Company, New York (1971).* AIChE Journal, 1972. **18**(2): p. 82-114.

86. Day, M., J.D. Cooney, and D.M. Wiles, *A kinetic study of the thermal decomposition of poly(aryl-ether-ether-ketone) (PEEK) in nitrogen.* Polymer Engineering & Science, 1989. **29**(1): p. 19-22.

87. Day, M., J.D. Cooney, and D.M. Wiles, *The thermal degradation of poly(aryl—ether—ether—ketone) (PEEK) as monitored by pyrolysis—GC/MS and TG/MS.* Journal of Analytical and Applied Pyrolysis, 1990. **18**(2): p. 163-173.

88. Day, M., et al., *Thermal degradation of poly(aryl-ether–ether-ketone) (PEEK): A differential scanning calorimetry study.* Journal of Applied Polymer Science, 1988. **36**(5): p. 1097-1106.

89. Jonas, A. and R. Legras, *Thermal stability and crystallization of poly(aryl ether ether ketone).* Polymer, 1991. **32**(15): p. 2691-2706.

90. Hoffman, J.D. and J.J. Weeks, *Melting Process and Equilibrium Melting Temperature of Polychlorotrifluoroethylene.* Journal of Research of the National Bureau of Standards Section a-Physics and Chemistry, 1961. **66A**(1). p. 13-28.

91. Marand, H., J. Xu, and S. Srinivas, *Determination of the Equilibrium Melting Temperature of Polymer Crystals: Linear and Nonlinear Hoffman–Weeks Extrapolations.* Macromolecules, 1998. **31**(23): p. 8219-8229.

92. Herrod-Taylor, A.J., *The crystallisation of Poly (aryl ether etherketone) (PEEK) and its carbon fibre composites.* M.Res. Thesis, University of Birmingham, 2011. p. 79-80.

93. Deslandes, Y., et al., *Crystallization of poly(aryl-ether-ether-ketone): Effect of thermal history of the melt on crystallization kinetics.* Polymer Composites, 1989. **10**(5): p. 360-366.

94. Medellin-Rodriguez, F.J., P.J. Phillips, and J.S. Lin, *Application of Secondary Nucleation Theory to Semirigid Macromolecules: PEEK, PET, and PEN.* Macromolecules, 1995. **28**(23): p. 7744-7755.

95. de Carvalho, B. and R.E.S. Bretas, *Crystallization kinetics of a PEEK/LCP blend.* Journal of Applied Polymer Science, 1995. **55**(2): p. 233-246.

96. Yang, Y., et al., *Crystallization kinetics of compatibilized blends of liquid crystalline polymer with PEEK.* Polymer Composites, 2006. **27**(6): p. 642-650.

97. Cole, K.C. and I.G. Casella, *Fourier transform infra-red spectroscopic study of thermal degradation in poly(ether ether ketone)-carbon composites.* Polymer, 1993. **34**(4): p. 740-745.

98. Kodera, Y. and B.J. McCoy, *Distribution Kinetics of Polymer Thermogravimetric Analysis: A Model for Chain-End and Random Scission.* Energy & Fuels, 2002. **16**(1): p. 119-126.

99. Hay, J.N. and D.J. Kemmish, *Thermal decomposition of poly(aryl ether ketones).* Polymer, 1987. **28**(12): p. 2047-2051.

100. Patel, P., et al., *Investigation of the thermal decomposition and flammability of PEEK and its carbon and glass-fibre composites.* Polymer Degradation and Stability, 2011. **96**(1): p. 12-22.

101. Vasconcelos, G.d.C., et al., *Evaluation of decomposition kinetics of poly (ether-ether-ketone) by thermogravimetric analysis.* Materials Research, 2014. **17**: p. 227-235.

102. Naffakh, M., et al., *Thermal decomposition of technological polymer blends 1. Poly(aryl ether ether ketone) with a thermotropic liquid crystalline polymer.* Polymer Degradation and Stability, 1999. **66**(3): p. 405-413.

103. Liu, S.J., et al., *Kinetic study of the thermal degradation of poly9aryl ether ketone)s containing 2,7-naphthalene moieties.* Journal of applied polymer science, 2008.

104. Nam, J.-D. and J.C. Seferis, *Generalized composite degradation kinetics for polymeric systems under isothermal and nonisothermal conditions.* Journal of Polymer Science Part B: Polymer Physics, 1992. **30**(5): p. 455-463.

105. Beehag, A. and L. Ye, *Consolidation and Interlaminar Fracture Properties of Unidirectional Commingled CF/PEEK Composites.* Journal of Thermoplastic Composite Materials, 1996. **9**(2): p. 129-150.

106. Deslandes, Y. and F. Boudreau, *Microindentation study of the surface mechanical properties of poly(ether-ether-ketone) films: effect of thermal degradation in the melt.* Journal of Materials Science Letters, 1990. **9**(11): p. 1274-1277.

107. Phillips, R., T. Glauser, and J.-A.E. Månson, *Thermal stability of PEEK/carbon fiber in air and its influence on consolidation.* Polymer Composites, 1997. **18**(4): p. 500-508.

108. Salek, H., S.V. Hoa, and J. Denault, *Viscous Behaviour Of Resin and Flow Through the Fiber Network of Carbon/PEKK Based Thermoplastic Composite.* The 9th International Conference on Flow Processes in Composite Materials, 2008.

109. Lee, Y. and R.S. Porter, *Crystallization of poly(etheretherketone) (PEEK) in carbon fiber composites.* Polymer Engineering & Science, 1986. **26**(9): p. 633-639.

110. Lee, Y.C. and R.S. Porter, *Crystallization of Polyetheretherketone (PEEK) in Carbon Fiber Composites*, 1985, DTIC Document.

111. McLauchlin, A.R., O.R. Ghita, and L. Savage, *Studies on the reprocessability of poly(ether ether ketone) (PEEK).* Journal of Materials Processing Technology, 2014. **214**(1): p. 75-80.

112. Kashiwagi, T., *Polymer combustion and flammability—Role of the condensed phase.* Symposium (International) on Combustion, 1994. **25**(1): p. 1423-1437.

113. Knauth, P., et al., *Thermogravimetric analysis of SPEEK membranes: Thermal stability, degree of sulfonation and cross-linking reaction.* Journal of Analytical and Applied Pyrolysis, 2011. **92**(2): p. 361-365.

114. Lu, S.X., P. Cebe, and M. Capel, *Thermal stability and thermal expansion studies of PEEK and related polyimides.* Polymer, 1996. **37**(14): p. 2999-3009.

115. Pingping, Z. and M. Dezhu, *Study on the double cold crystallization peaks of poly(ethylene terephthalate) (PET): 2. Samples isothermally crystallized at high temperature.* European Polymer Journal, 1999. **35**(4): p. 739-742.

116. Pingping, Z. and M. Dezhu, *Study on the double cold crystallization peaks of poly(ethylene terephthalate) 3. The influence of the addition of calcium carbonate (CaCO3).* European Polymer Journal, 2000. **36**(11): p. 2471-2475.

117. Zhu, P. and D. Ma, *Double cold crystallization peaks of poly(ethylene terephthalate)—1. Samples isothermally crystallized at low temperature.* European Polymer Journal, 1997. **33**(10–12): p. 1817-1818.

118. Sharon Xin, L. and P. Cebe, *Effects of annealing on the disappearance and creation of constrained amorphous phase.* Polymer, 1996. **37**(21): p. 4857-4863.

119. Sandler, J., et al., *Carbon-nanofibre-reinforced poly(ether ether ketone) composites.* Composites Part A: Applied Science and Manufacturing, 2002. **33**(8): p. 1033-1039.

120. Chalmers, J.M., W.F. Gaskin, and M.W. Mackenzie, *Crystallinity in poly(aryl-ether-ketone) plaques studied by multiple internal reflection spectroscopy.* Polymer Bulletin, 1984. **11**(5): p. 433-435.

121. Jonas, A., R. Legras, and J.P. Issi, *Differential Scanning Calorimetrt and Infrared Crystallinity Determinations of Poly(aryl ether ether ketone).* Polymer, 1991. **32**(18): p. 3364 - 3370.

122. Papkov, V.S., M.V. Gerasimov, and I.I. Dubovik, *Disordering of crystalline PEEK upon mechanical treatment.* Polymer Engineering & Science, 1997. **37**(8): p. 1280-1285.

123. Zhang, M., et al., *Effect of transcrystallinity on tensile behaviour of discontinuous carbon fibre reinforced semicrystalline thermoplastic composites.* Polymer, 1996. **37**(23): p. 5151-5158.

124. Jeng, C.-C. and M. Chen, *Flexural failure mechanisms in injection-moulded carbon fibre/PEEK composites.* Composites Science and Technology, 2000. **60**(9): p. 1863-1872.

125. Hachmi, B.D. and T. Vu-Khanh, *Crystallization Mechanism in PEEK/Carbon Fiber Composites.* Journal of Thermoplastic Composite Materials, 1997. **10**(5): p. 488-501.

126. Waddon, A.J., et al., *On the crystal texture of linear polyaryls (PEEK, PEK and PPS).* Journal of Materials Science, 1987. **22**(5): p. 1773-1784.

127. Medellin-Rodriguez, F.J. and P.J. Phillips, *Crystallization and structure-mechanical property relations in poly(aryl ether ether ketone) [PEEK].* Polymer Engineering & Science, 1990. **30**(14): p. 860-869.

128. Vu-Khanh, T. and S. Frikha, *Influence of Processing on Morphology, Interface, and Delamination in PEEK/Carbon Composites.* Journal of Thermoplastic Composite Materials, 1999. **12**(2): p. 84-95.

129. Gao, S.-L. and J.-K. Kim, *Cooling rate influences in carbon fibre/PEEK composites. Part II: interlaminar fracture toughness.* Composites Part A: Applied Science and Manufacturing, 2001. **32**(6): p. 763-774.

130. Jar, P.Y.B., et al., *A study of the effect of forming temperature on the mechanical behaviour of carbon-fibre/peek composites.* Composites Science and Technology, 1993. **46**(1): p. 7-19.

131. Gao, S.-L. and J.-K. Kim, *Cooling rate influences in carbon fibre/PEEK composites. Part III: impact damage performance.* Composites Part A: Applied Science and Manufacturing, 2001. **32**(6): p. 775-785.

132. Díez-Pascual, A.M., et al., *Influence of carbon nanotubes on the thermal, electrical and mechanical properties of poly(ether ether ketone)/glass fiber laminates.* Carbon, 2011. **49**(8): p. 2817-2833.

133. Uralil, F.S., G.M. Newaz, and A. Lustiger, *Processing effects and damage tolerance in poly(etheretherketone) composites.* Polymer Composites, 1992. **13**(1): p. 7-14.

134. Lustiger, A., F.S. Uralil, and G.M. Newaz, *Processing and structural optimization of PEEK composites.* Polymer Composites, 1990. **11**(1): p. 65-75.

135. Lustiger, A. and G.M. Newaz, *Interlamellar Fracture and Craze Growth in PEEK Composites under Cyclic Loading.* Journal of Composite Materials, 1990. **24**(2): p. 175-187.

136. Wang, X., C. Mayer, and M. Neitzel, *Some issues on impregnation in manufacturing of thermoplastic composites by using a double belt press.* Polymer Composites, 1997. **18**(6): p. 701-710.

137. Salek, H., S.V. Hoa, and J. Denault, *Viscous Behaviour Of Resin and Flow Through the Fiber Network of Carbon/PEKK Based Thermoplastic Composite.* The 9th International Conference on Flow Processes in Composite Materials, 2008.

138. Šimáček, P. and S.G. Advani, *Permeability model for a woven fabric.* Polymer Composites, 1996. **17**(6): p. 887-899.

139. Gibson, A.G. and J.A. Månson, *Impregnation technology for thermoplastic matrix composites.* Composites Manufacturing, 1992. **3**(4): p. 223-233.

140. Kim, H., et al., *Mechanical Characterization of PEEK/IM7 Fabricated Using an Automated Tape Placement Processing System.* 18th International Conference on Composite Materials, Jeju Island, Korea, 2011.

141. Mayer, C., X. Wang, and M. Neitzel, *Macro- and micro-impregnation phenomena in continuous manufacturing of fabric reinforced thermoplastic composites.* Composites Part A: Applied Science and Manufacturing, 1998. **29**(7): p. 783-793.

142. Mullins, B.J., et al., *Effect of Fibre Orientation on Fibre Wetting Processes.* J Colloid Interface Science, 2004. **269**(2): p. 449-58.

143. De Almeida, O., E. Bessard, and G. Bernhart, *Influence of processing parameters and semi-finished product on consolidation of carbon/PEEK laminates*. 15th European Conference on Composite Materials, 2012.

144. Jar, P.Y., W.J. Cantwell, and H.H. Kausch, *Study of the crystal morphology and the deformation behaviour of carbon fibre reinforced PEEK (APC-2).* Composites Science and Technology, 1992. **43**(3): p. 299-306.

145. Beehag, A. and L. Ye, *Role of cooling pressure on interlaminar fracture properties of commingled CF/PEEK composites.* Composites Part A: Applied Science and Manufacturing, 1996. **27**(3): p. 175-182.

146. Kuo, M.C., et al., *Fabrication of High Performance Magnesium/Carbon-Fiber/PEEK Laminated Composites.* MATERIALS TRANSACTIONS, 2003. **44**(8): p. 1613-1619.

147. Jar, P.Y.B. and H.H. Kausch, *The influence of moulding conditions on delamination behaviour of carbon-fibre/peak composites.* Composites Science and Technology, 1994. **52**(3): p. 349-359.

148. Unger, W.J. and J.S. Hansen, *The Effect of Cooling Rate and Annealing on Residual Stress Development in Graphite Fibre Reinforced PEEK Laminates.* Journal of Composite Materials, 1993. **27**(2): p. 108-137.

149. Manson, J.-A.E. and J.C. Seferis, *Autoclave Processing of PEEK/Carbon Fiber Composites.* Journal of Thermoplastic Composite Materials, 1989. **2**(1): p. 34-49.

150. Fujihara, K., et al., *Influence of processing conditions on bending property of continuous carbon fiber reinforced PEEK composites.* Composites Science and Technology, 2004. **64**(16): p. 2525-2534.

151. Zalaznik, M., M. Kalin, and S. Novak, *Influence of the processing temperature on the tribological and mechanical properties of poly-ether-ether-ketone (PEEK) polymer*. Vol. 94. 2016. 92-97.

152. Nazem, N., *Preparation of Highly Reflective Films by Supercritical Infusion of a Silver Additive into Poly(ether ether ketone).* 1997. p. 38-41.

153. Ye, L. and K. Friedrich, *Processing of thermoplastic composites from powder/sheath-fibre bundles.* Journal of Materials Processing Technology, 1995. **48**(1–4): p. 317-324.

154. Ye, L., et al., *Manufacture of CF/PEEK composites from powder/sheath fibre preforms.* Composites Manufacturing, 1994. **5**(1): p. 41-50.

155. Ye, L., et al., *Consolidation of unidirectional CF/PEEK composites from commingled yarn prepreg.* Composites Science and Technology, 1995. **54**(4): p. 349-358.

156. Nygard, P. and C.-G. Gustafson, *Continuous Glass Fiber–Polypropylene Composites Made by Melt Impregnation: Influence of Processing Method.* Journal of Thermoplastic Composite Materials, 2004. **17**(2): p. 167-184.

157. Peltonen, P., et al., *The Influence of Melt Impregnation Parameters on the Degree of Impregnation of a Polypropylene/Glass Fibre Prepreg.* Journal of Thermoplastic Composite Materials, 1992. **5**(4): p. 318-343.

158. Seo, J.W. and W.I. Lee, *A Model of the Resin Impregnation in Thermoplastic Composites.* Journal of Composite Materials, 1991. **25**(9): p. 1127-1142.

159. Mallick, P. and J. Ragone. *The Effect of Process Parameters on the Quality of Resin Infused Thermoplastic Matrix Prepregs*. in *17th International Conference on Composite Materials, Edinburgh, Scotland*. 2009.

160. Peltonen, P. and P. Törmälä, *Melt impregnation parameters.* Composite Structures, 1994. **27**(1–2): p. 149-155.

161. Manson, J.-A.E., T.L. Schneider, and J.C. Seferis, *Press-forming of continuous-fiber-reinforced thermoplastic composites.* Polymer Composites, 1990. **11**(2): p. 114-120.

162. Cogswell, F.N., *Processing and application of thermoplastic structural composites.* Makromolekulare Chemie. Macromolecular Symposia, 1991. **48-49**(1): p. 165-180.

Appendix 1

Appendix 1

“A covalently linked hydroxyapatite and poly (ether ether ketone) composite”

Erik A. B. Hughes [a], Andrew Parkes [b], Richard L. Williams [a], Michael J. Jenkins [b], and Liam M. Grover [a] *

[a] School of Chemical Engineering, University of Birmingham, Edgbaston, B15 2TT

[b] School of Metallurgy and Materials, University of Birmingham, Edgbaston, B15 2TT

ABSTRACT

Novel composites based on poly (ether ether ketone) (PEEK) are now used as commercially available spinal fusion devices. In this work, the interfacial interactions between hydroxyapatite (HA) and PEEK are improved beyond mechanical interlocking and physiochemical interactions by creating a direct chemical link between these dissimilar material phases. HA particulates were coated with (3-Mercaptopropyl) triethoxysilane (MPTES) introducing thiol moiety (-SH), and the ketone groups (C=O) of PEEK were reduced to hydroxyl groups (-OH), resulting in HA-SH and PEEK-OH respectively. HA–SH and PEEK–OH were then linked with a heterobifunctional linking reagent. Chemically linked HA and PEEK composites (HA_L_PEEK) loaded with 2.5 wt% HA displayed less extensive particulate debonding and microcrack propagation than the same composition of material without bonding. Furthermore, the flexural modulus of HA_L_PEEK was enhanced compared with non-linked HA and PEEK composites (HA_PEEK). We find no significant difference between PEEK and HA_L_PEEK ($p = 0.127$), however, HA_PEEK was significantly weakened ($p = 0.026$), suggesting enhanced load transfer between HA and PEEK phases that maintains the ductile flow of the polymeric matrix of HA_L_PEEK.

INTRODUCTION

Poly (ether ether ketone) (PEEK) is a high performance semi-crystalline engineering polymer that has been implemented across a range of industry sectors, including oil and gas, electronics, aerospace, automotive and medical [1-3]. One of the major uses of PEEK in the medical sector is in the fabrication of spinal fusion cages [2, 3]. Spinal cages have been in clinical use since the 1990's and were first shown to be successful in the treatment of horses suffering from compressive root compression [2, 4]. The cage facilitates the fusion of adjacent vertebrae whilst maintaining correct alignment and foraminal height of the spine.

PEEK is an attractive material for this role as it is light-weight, strong and well suited for high load-bearing application as demonstrated through computer modeling and in practice [5-7]. It exhibits a modulus of 3 GPa to 4 GPa which falls within the range of cancellous and cortical bone of 0.05 GPa to 30 GPa [2]. Metallic spinal cage implants, such as those fabricated from titanium alloy (Ti-6Al-4V), are considerably heavier and exhibit a higher modulus (approximately 110 GPa) compared with polymeric counterparts [8, 9]. This modulus mismatch with hard tissue can lead to a phenomena referred to as stress shielding, where bone does not experience required mechanical stimuli due to the high modulus material bearing a considerable fraction of the applied load. In addition, titanium based cages are typically associated with a high occurrence of subsistence for both lumbar and cervical devices, hard tissue weakening and porosity development [10-12].

Despite PEEK's physical advantages over titanium alloy, improving its integration into surrounding tissues has been recognized as essential in order to guarantee successful fusion [10, 13, 14]. In a side-by-side study of stand-alone devices, titanium cages were been shown to be 100 % successful in facilitating fusion, whereas

PEEK cages attain only a 76 % success rate in comparison [10]. The tradeoff between mechanical properties with poor fusion originates from PEEK surfaces being both hydrophobic and chemically inert, limiting direct bone attachment and osseointegration of newly forming hard tissue compared to Ti-6Al-4V [13, 15, 16].

In order to improve the osteointegration of PEEK, researchers have extensively developed and characterized both surface and bulk porosity, coatings, surface modifications, and composite formulations [14, 16-26]. Of these solutions, however, it appears that novel composite structures are beginning to play a more prominent role in commercially available medical implants as alternatives to metallic materials such as Ti-6Al-4V and stainless steel [2, 18]. These materials typically contain bioactive calcium phosphate particulates, including hydroxyapatite (HA, $Ca_5(PO_4)_3(OH)_2$) and beta tricalcium phosphate (β-TCP, $Ca_3(PO_4)_2$), which have been shown to improve the osseointegration of PEEK with increasing loading level [14, 17-21, 26]. Invibio® currently manufacture a medical grade HA in PEEK matrix composite fusion device, PEEK-OPTIMA™ HA Enhanced, which has FDA approval for orthopaedic devices and recently acquired the European CE mark of approval [27]. PEEK-OPTIMA™ HA Enhanced devices out-perform PEEK-OPTIMA™ Natural devices (HA free) in terms of bone ongrowth and fusion, demonstrated in a sheep model [28].

Under loading, however, particulate inclusions can act as stress initiators and risers that diminish the mechanical properties of these materials [29]. Moreover, dissimilarity between HA and PEEK leads to poor interfacial interactions between the two phases, limiting the level of biologically beneficial inclusion. Failure can arise due to HA particulates becoming debonded from the polymeric matrix of PEEK [17, 21]. High inclusion levels of HA also increases the brittleness of composites as the ductile

flow of the matrix is disrupted, decreasing the required energy to initiate fracture [20, 21, 30].

Up until now, approaches to improve additive interactions with polymeric matrices have focused on improving physical or physiochemical interlocking [17, 31, 32]. Further gains may be possible through achieving chemical bonding interactions, as has been demonstrated between modified PEEK linked with carbon nanotube fillers [33, 34]. Chemical interactions may facilitate more effective load transfer between composite components. This could allow for high levels of loading with bioceramic to improve osteointegration and fusion capability of composite devices whilst avoiding shortfalls in mechanical properties that may hamper performance and lead to catastrophic failure during load bearing.

With spinal fusion cage application in mind, we aim to overcome the weak interfacial interactions between HA and PEEK by chemically linking these phases. We demonstrate the chemical linking of HA and PEEK by functionalizing HA with (3-Mercaptopropyl) triethoxysilane (MPTES) and chemically modifying PEEK by a reduction reaction, producing HA-SH and PEEK-OH respectively. A chemical linker, p-Maleimidophenyl isocyanate (PMPI), was then used to link both HA-SH to PEEK-OH to produce a HA_L_PEEK additive, before processing composite materials by the heat-press method. Extensive characterization of bioceramic and polymer starting materials is provided, as well as physiochemical of analysis of PEEK, HA_PEEK and HA_L_PEEK composite materials to evidence the potential benefits of chemically linking both HA and PEEK components within composite formulations.

EXPERIMENTAL

Materials. Hydroxyapatite (20 µm agglomerations from SEM analysis, ≥97 %, synthetic), (3-Mercaptopropyl) triethoxysilane (MPTES) (≥ 95 %), Propan-2-ol

(puriss, p.a., ACS reagent, ≥ 99.8 % (GC)), HCl (ACS reagent, 37 %), Potassium hydroxide (reagent grade, 90 %), Methanol (CHROMASOLV®, ≥ 99.9 %), p-Maleimidophenyl isocyanate (purum, ≥ 97 %) and Sodium borohydride (99.99 % trace metals basis) were acquired from Sigma Aldrich Ltd (U.K.). Ethanol (absolute, analytical reagent grade), dimethyl sulfoxide (DMSO) (analytical reagent grade) and Ellman's reagent (5,5'-Dithio-bis-(2-nitrobenzoic acid)) were acquired from Fisher Scientific (U.K.). Acheson Silver DAG was acquired from Agar Scientific (U.K.). VICTREX® PEEK 450PF (25 µm, easy fine flow) was acquired from Victrex plc (U.K.). Kapton® polyimide film was acquired from DuPont™(U.S.A). Loctite® Frekote® 44-NC mold release agent was acquired from Henkel (Germany). Distilled water acquired from an arium® advance EDI pure water system by Sartorius (Germany).

Chemical methodologies

Synthesis of HA-SH derivative. Three reaction vessels containing 200 mL 90/10 (vol %) propan-2-ol/water solutions were prepared. 2 mL MPTES, 250 mg HA and a further 200 mL reaction media were added initially and at 40 minute intervals thereafter under stirring (250 rpm) on a MR stirrer hotplate (Heidolph, Germany). Reaction pH was adjusted to between 3 and 6 at the start of the reaction, and between 9 and 11 after 20 minutes, and the pattern repeated at 40 minute intervals in coordination with the addition of MPTES, reaction media and HA. pH profiles for each reaction were acquired manual tracking of pH values with a Mettler Toledo SevenCompact™ pH/ion meter equipped with InLab Expert Pro-ISM probe (Mettler Toledo, U.S.A). Stirring was maintained for 4.67 h (7 cycles). HA-SH powder from each vessel was then combined, washed in 5 mL ethanol, recovered by centrifugation

with a CR4.22 centrifuge (Jouan SA, France) at 4000 rpm for 10 minutes and the process repeated five times before being dried at 60 ^{o}C for 30 minutes to ascertain full curing of MPTES to HA surfaces, yielding HA-SH.

Synthesis of PEEK-OH derivative. 5 g of PEEK 450PF was dispersed in 120 mL DMSO charged with 1.5 g $NaBH_4$ under inert argon (Ar) atmosphere. The suspension was heated to 120 °C and the reaction suspension allowed to react for 24 hours, after which the heating source was removed and the contents allowed to cool to room temperature. The reaction product was filtered and washed with excess ethanol, distilled water and 0.1 M HCl (diluted from concentrate), then dried at 80°C under vacuum.

Synthesis of PEEK_L_ HA linked additive. 5 g HA-SH was dispersed in 10 mL DMSO charged with 50 mg of PMPI under constant agitation. After 15 min, 5 g of PEEK-OH was added to the reaction mixture, and the reaction allowed to proceed for a total of 3 h. The resulting product was then washed in methanol, water and methanol again.

Composite fabrication and acquisition of test specimens for mechanical testing. PEEK, HA_PEEK and HA_L_PEEK powder batches were prepared at a total mass of 50 g. Regarding HA containing batches, the bioceramic content was 2.5 wt%. Prior to processing, batches were kept at 140 ^{o}C overnight period in order to remove residual moisture. Plaques were fabricated in a Moore Hydraulic Press retrofitted with heating plates (JRD Bipel, U.K.) to attain temperatures of 400 ^{o}C. A spacer was placed between the plates in order to act as a frame for the plaque providing 27.9 cm^3 of

volume to be filled with powder. Powders were spread evenly within the press volume and heated to 125 ^{o}C at minimal plate contact to remove air pockets. Contact pressure was then applied and the temperature increased to 400 ^{o}C. After 4 h, heating was turned off and the apparatus allowed cooling fully to room temperature to obtain plaques with dimensions 180 mm x 150 mm x 1.2 mm. Test specimens with dimensions of 60 mm x 12 mm x 1.2 mm were then cut out from the plaques using a band saw.

Chemical and physical characterization methods

Raman spectroscopy. Raman spectroscopy data were collected using an inVia Raman microscope (Renishaw, U.K.). The instrument was equipped with a 532 nm laser. Each spectrum was collected over 3 acquisitions between 100 cm^{-1} and 4100 cm^{-1} and the data normalised between sets.

Powder X-ray diffraction (XRD). Powder XRD patterns were acquired using a Powder Diffractometer D8 Auto sampler (Bruker, U.S.A.) with Cu Kα line (0.154 nm). Pattern data was collected between 2θ values of 5 ^{o} and 60 ^{o} with a 0.02 ^{o} step-size and a step time of 0.5 s/^{o}. Patterns were matched to patterns within The International Centre for Diffraction Data (ICDD) database.

Thiol group (-SH) quantification. Quantification of thiol groups was undertaken using an Ellman's reagent (DTNB, 5,5'-Dithio-bis-(2-nitrobenzoic acid)) assay protocol [35]. Briefly, a buffer solution was prepared (distilled water, 100 mM Na_3PO_4, 1 mM EDTA, pH 8). 0.05 mL of Ellman's solution (4 mg DTNB in 1 mL buffer solution) was added to 2.5 mL of buffer solution to produce a reaction solution. 5 mg

of HA-SH was dispersed in a 0.25 mL of buffer solution and added to the reaction solution. The solution was kept agitated for 15 minutes to develop an assay solution. Upon reacting with free thiol groups, DTNB is converted to 2-nitro-5-thiobenzoic acid (TNB). TNB has a molar absorption coefficient of 14150 M^{-1} cm^{-1} at 412 nm. 1 mL of this solution was then transferred to a cuvette and the absorbance read at 412 nm with a Cecil CE7500 spectrophotometer (Buck Scientific, U.S.). The absorbance reading for unmodified HA sample was used as a control, and was automatically taken away from the reading acquired from the HA-SH samples. Equations 1-3 were followed in order to determine the molar concentration of –SH groups present in the sample [35].

$$C = \frac{A}{Eb} \qquad \text{(Equation 1)}$$

$$M = 2.80\ mL\ x\ \left(C\ x\ \frac{1\ L}{1000\ mL}\right) \qquad \text{(Equation 2)}$$

$$C_{sample} = \left(\frac{M}{0.25\ mL}\right)\ x\ \frac{1000\ mL}{1\ L} \qquad \text{(Equation 3)}$$

Where: C = -SH concentration as measured (mol L^{-1}), E = TNB molar absorption coefficient, 14150 (M^{-1} cm^{-1}), b = path length of cuvette (1 cm), M = -SH concentration as measured (mol), and C_{sample} = -SH concentration of the sampled volume 0.25 mL containing HA-SH (mol L^{-1}).

The concentration of –SH groups was then converted from units of mol L^{-1} to mol g^{-1} by calculating the equivalent mass in grams of HA-SH sample in 1 L and dividing C_{sample} by this number (e.g. 20 g HA-SH in 1 L so 20).

Differential scanning calorimetry (DSC). DSC analysis was undertaken using a DSC 6000 N520-0116 instrument (Perkin Elmer, U.S.A). Approximately 10 mg of sample was held for two minutes at 20 ^{o}C for temperature stabilisation of the equipment. Samples were then heated to 400 ^{o}C at a ramp rate of 10 ^{o}C/min before cooling back down to 20 ^{o}C at the equivalent ramp rate.

Scanning electron microscopy (SEM). For Figure 4a-d and 7a-c, specimens were placed upon double-sided sticky carbon discs that had been secured onto aluminum stubs. Specimens were then gold sputter coated using a K550X sputter coater (Quorum Technologies, U.K.). SEM images were then acquired using an EVO MA 10 scanning electron microscope (Carl Zeiss AG, Germany). For Figure 7d-f, specimen test pieces were placed in liquid nitrogen to allow for cryogenic fracture and exposure of a clean internal surface. Upon the underside of each specimen, a small amount of silver Acheson Silver DAG was applied in order to reduce charging. Double-sided sticky carbon discs and adhesive were used to secure specimens firmly to aluminum stubs. Specimens were then gold sputter coated using a Polaron SC7640 sputter coater (Quorum Technologies, U.K.). SEM images were then acquired using a 6060 scanning electron microscope (JOEL, U.S.A.).

Thermal gravimetric analysis (TGA). TGA was carried out using a STA 449 F3 Jupiter instrument (Netzsch, Germany). Samples were heated to 700 ^{o}C at a ramp rate

of 10 °C/min. Further analysis was carried out directly on the data to calculate hydroxylation degree (HD) of the PEEK-OH derivative (Equations 4-9).

$$M_{250^oC} = \left(\frac{M_S}{100}\right) x\ \%\ M_{250^oC} \quad \text{(Equation 4)}$$

$$M_{400^oC} = \left(\frac{M_S}{100}\right) x\ \%\ M_{400^oC} \quad \text{(Equation 5)}$$

$$M_{OH} = \%\ M_{400^oC} - M_{250^oC} \quad \text{(Equation 6)}$$

$$mol_{OH} = \frac{M_{OH}}{Mr_{OH}} \quad \text{(Equation 7)}$$

$$M_{PEEK-OH} = mol_{OH}\ x\ Mr_{PEEK-OH} \quad \text{(Equation 8)}$$

$$HD = \left(\frac{M_{PEEK-OH}}{M_{250^oC}}\right) x\ 100 \quad \text{(Equation 9)}$$

Where: M_s = TGA sample mass (g), M_{250^oC} = TGA sample mass at 250 °C (g), $\%\ M_{250^oC}$ = % TGA sample mass remaining at 250 °C (%), M_{400^oC} = TGA sample mass at 400 °C (g), $\%\ M_{400^oC}$ = % TGA sample mass remaining at 400 °C (%), M_{OH} = Mass of OH groups lost from PEEK-OH between 250 °C and 400 °C (g), mol_{OH} = Moles of OH groups lost from PEEK-OH between 250 °C - 400 °C (g), Mr_{OH} = Molar mass of OH group (g mol^{-1}), $M_{PEEK-OH}$ = Mass of PEEK-OH in sample (g), $Mr_{PEEK-OH}$ = Molar mass of PEEK-OH group (g mol^{-1}), and HD = PEEK-OH hydroxylation degree (%).

Fourier transform infrared spectroscopy (FT-IR). FT-IR spectra were collected using a Nicolet 380 FT-IR spectrometer (Thermo-Scientific, U.S.A.), fitted with a Golden Gate ATR attachment (Specac, U.K.). Measurements were collected between 100 cm^{-1} and 4100 cm^{-1} wavenumbers. A background scan was acquired was acquired

before each scan and subtracted in order to minimize the appearance of H_2O and CO_2 molecular modes contaminating each spectrum of interest.

Micro- fluorescence spectroscopy (μ-XRF) - Scans were performed in mapping mode on sections of PEEK composites materials with exposed areas of HA using a M4 Tornado instrument (Bruker, U.S.A.). Measurements settings of 20 ms/pixel were employed with the instrument operating at 50 kV with anode current of 300 mA. The chamber was maintained at 20 mbar during measurements.

Mechanical characterization methods. A schematic of the mechanical testing set-up is provided (Figure S1). Specimens were cut from plaques with dimensions of approximately 60 mm in length, 12 mm width and depth of 1.2 mm. The span to depth ratio was calculated as outlined in ASTM D790/ISO 178, ensuring specimens fail through compression stress whilst minimising shear stress. Tests were performed with an 5566 testing rig (Instron, U.K.) at a rate of 1 mm/min. Flexural strength and modulus were calculated using equations 10 and 11.

$$\sigma_f = \frac{3Fl}{2bd^2} \qquad \text{(Equation 10)}$$

Where: σ_f= Flexural strength (MPa), F= Max force before yielding or fracture (N), l= Test specimen support separation length (mm), b= Test specimen width (mm), and d= Test specimen thickness (mm).

$$E_f = \frac{Fl^3}{4bd^3\delta} \qquad \text{(Equation 11)}$$

Where: E_f = Flexural modulus (MPa), F = Force (N), l = Test specimen support separation length (mm), b = Test specimen width (mm), d = Test specimen thickness (mm), and δ = Test specimen displacement (V_{DC}).

Statistical analysis. One-way ANOVA and corresponding Holm-Sidak post-hoc tests were performed upon mechanical testing data using SigmaPlot v13.0 software environment. All data sets where deemed fit for statistical analysis by passing a Normality test (Shapiro-Wilk) and Equal Varience test (Brown-Forsythe). Values where $p<0.05$ was satisfied were deemed to signify statistical significance.

RESULTS AND DISSCUSSION

Synthesis of HA-SH. MPTES attaches to substrates through hydrolysis and subsequent condensation reactions (Figure 1a, b). For the attachment of MPTES to HA, the pH was controlled over several hours to promote favorable thermodynamic environments for both reactions (Figure 1c) [36]. Acidic regions between pH values of 3 and 7 were used to promote hydrolysis of siloxy groups (R-Si-$(OCH_3)_3$) to silanol (R-Si-$(OH)_3$). Adjustment of the pH to above 9 was used to promote silanol condensation upon the surface of HA.

Figure 1d shows the Raman spectra of HA prior to and after surface modification with APTMS to produce HA-SH. In both spectra, peaks relating to the vibrations of the tetrahedral PO_4^{3-} anion associated with HA, including symmetric stretching ($PO_4\,v_1$), symmetric bending ($PO_4\,v_2$), asymmetric stretching ($PO_4\,v_3$) and asymmetric bending ($PO_4\,v_4$) [37-41]. Peaks are present at 435 cm^{-1} ($PO_4\,v_2$), 590 cm^{-1} ($PO_4\,v_4$), 960 cm^{-1} ($PO_4\,v_1$) and 1050 cm^{-1} ($PO_4\,v_3$). A degree of carbonate substitution

into the HA crystal lattice of both materials is also suggested by a peak at approximately 1070 cm^{-1} (CO_2 v_1) [40, 41].

Peaks relating to the grafting APTMS upon the surface of HA were found in the spectrum of HA-SH, evidencing attachment of silane molecules [35, 42-45]. Firstly, a medium intensity peak indicative of Si-C stretching appears at 652 cm^{-1}. A low intensity peak at 864 cm^{-1} is present due to CH_2 rocking. Furthermore, peaks at 1262 cm^{-1}, 1301 cm^{-1}, 1342 cm^{-1} and 1431 cm^{-1} are indicative of $–CH_2$ twisting modes. Strong overlapping peaks at 2804 cm^{-1}, 2891 cm^{-1} and 2918 cm^{-1} are due to $–CH_2$ vibrations. The peak at 2569 cm^{-1}, representative of –SH stretching, confirms presence of thiol groups on the surface of HA-SH [35]. Oligimerisation is likely to have occurred between silane molecules before attachment, as indicated by the Si-O-Si stretching peak located at 809 cm^{-1}. Therefore, a network of MPTES molecules may be present on the surface of HA-SH, as opposed to monolayer coverage.

Subtle broadening of PO_4 v_{1-4} peaks in the spectrum HA-SH indicates alterations of P-O bonding environments on the surface of HA [40]. Broader Raman peaks tend to indicate structural disorder, whilst sharper peaks are provided by more ordered environments [40]. Such differences could be due to the dynamic reaction environment experienced by HA during surface modification with MPTES, which may be capable of promoting dissolution and re-precipitation of alternative calcium phosphate phases, as well as the bonding of MPTES to the surface HA in the final product. Promisingly, analysis of X-ray diffraction patterns indicates that HA remains the sole bioceramic phase (Figure 1e). Both the pattern of HA and HA-SH were successfully matched to ICDD pattern number 01-076-0694 (synthetic HA, * quality, with formula $Ca_5(PO_4)_3(OH)_2$), with no other phases detected. In addition, crystalline regions of HA are minimally disrupted by the reaction procedure with MPTES, as

there is a non-substantial decrease in crystallinity from 77.0 % to 76.6 %, further evidencing that the widening of PO_4 peaks seen in the Raman spectrum of HA-SH is likely due to successful grafting of MPTES to HA particulate surfaces.

Quantification of thiol groups upon the surface of HA-SH was undertaken with an Ellman's reagent assay, confirming attachment of MPTES to the surface of HA [35]. Using un-modified HA as a control, the content of thiol groups associated with the surface of HA was approximated at $5.9 \times 10^{-6} \pm 8.2 \times 10^{-8}$ mol g^{-1}.

Synthesis of PEEK-OH. PEEK was converted to PEEK-OH via a reduction reaction (Figure 2a) [46, 47]. The crystal structures of PEEK and PEEK-OH were assessed by acquisition of powder XRD patterns (Figure 2b). The main peaks of both patterns were located at 2θ values of 19 °, 21 °, 23 ° and 29 °, suggesting that the lattice parameters are preserved during hydroxylation. These peak positions are representative of orthorhombic unit cell PEEK crystal planes of 110, 111, 200 and 211 respectively in both samples [46]. Introducing –OH groups to PEEK facilitates a reduction in crystallinity from 46.1 % to 38.4 % after conversion to PEEK-OH. When PEEK undergoes reduction, the C=O affiliated carbon goes from having three different bonded groups (the C=O group, the rest of that PEEK subunit and the adjoining PEEK subunit) to having four bonded groups (the newly introduced hydroxyl group and hydrogen, the rest of that PEEK subunit and the adjoining PEEK subunit), which introduces chirality. Given the random introduction of –OH groups along the polymer backbone and chirality about each carbon atom associated with a –OH moiety, it is expected that symmetry within crystallites is disrupted leading to an increase in the amorphous nature of PEEK-OH compared to PEEK (Figure S2).

Thermal transitions of PEEK and PEEK-OH were examined by analysis of differential scanning calorimetry (DSC) curves (Figure 2c). The melting temperature (T_M) of PEEK was found to be 347.8 ^oC, which was approximately 4 ^oC greater than the T_M possessed by PEEK-OH of 343.7 ^oC. On cooling, PEEK-OH appears to undergo minimal crystallization, possessing no clear peak to define crystallization temperature (T_C), whilst PEEK possesses a T_C of 306.47 °C. This could indicate that on cooling from 400 ^oC, PEEK-OH becomes fully amorphous due to thermal treatment. The -OH moiety introduced along the polymer chain may inhibit crystallization by creating irregularity in forming crystalline regions. Moreover, hydrogen bonding mediated by –OH groups may be extensive enough to suppress polymer chain mobility that is a requirement for crystallization to take place, making it more difficult for PEEK-OH to crystallize unlike the parent PEEK structure [46].

Figure 2d shows the thermal gravimetric analysis (TGA) curves collected for PEEK and PEEK-OH. PEEK undergoes a one step degradation beginning at approximately 550 ^oC. The steep drop off in mass with temperature is indicative of main chain polymer degradation [48]. PEEK-OH undergoes a loss in mass before undergoing main chain degradation at approximately 500 °C. Due to the increased hydrophilic properties of PEEK-OH, the loss in mass between 100 ^oC and 250 ^oC is attributed to loosely bound H_2O associated with the particle surfaces. Main chain degradation occurs at approximately 500 ^oC, suggesting that the thermal stability of PEEK-OH is lesser in comparison to PEEK. Promisingly however, the polymer remains intact with respect to processing temperatures for PEEK of between 380 ^oC and 400 ^oC.

The calculation of hydroxylation degree (HD), expressed as the percentage of =O groups converted to –OH groups, requires knowledge of the approximate mass of

-OH groups lost from PEEK-OH on heating. It has been shown previously by TGA coupled to mass spectrometry that hydroxyl group fragments are primarily lost from PEEK-OH between 250 °C and 400 °C [49]. From Equations 4-9, HD of PEEK-OH was calculated as 37.6 %. The result is inconsistent with values previously reported for this reaction at varying reaction times (Figure S3) [46].

Synthesis of chemically linked HA_L_PEEK. PMPI molecules used to link HA-SH and PEEK-OH contain two termini, one consisting of maleimide moiety and the other of isocyanate. Thiol groups upon HA-SH are able to react with maleimide to produce a thioether linkage (C-S-C) (Figure 3a). The reaction between PMPI isocyanate and hydroxyls of PEEK-OH produces a carbamate bond (R-O-C(=O)-NH-R) (Figure 3b). Following the linking reaction between HA-SH and PEEK-OH with PMPI, the composite components and newly formed chemical bonds between them were assessed by FT-IR spectroscopy (Figure 3c).

PO_4 stretching and bending modes associated with the structure of HA-SH are located at 470 cm^{-1}, 608 cm^{-1}, 962 cm^{-1} (as a shoulder), and 1033 cm^{-1} in accordance with reported spectra [35, 38, 41]. Peaks associated with C-H stretching that originate from MPTES on the HA surface are observed at 2920 cm^{-1} [35, 45]. Importantly, FT-IR confirms the formation of C-S-C bonds with PMPI by the symmetric and asymmetric peaks of which are detected at 677 cm^{-1} and 771 cm^{-1} [50]. The peak at 2546 cm^{-1} is representative of –SH stretching, and is suggestive of unreacted thiol groups present on the surface of HA-SH [35].

Characteristic peaks belonging to the structure of PEEK identified PEEK-OH content, namely out of plane aromatic hydrogen (O.A.H.) modes at 840 cm^{-1} and 860 cm^{-1}, a diphenyl ketone band at 927 cm^{-1}, asymmetric C-O-C bending at 1182 cm^{-1} and

1278 cm^{-1}, C-C(=O)-C bending at 1307 cm^{-1}, aromatic skeletal vibrations (A.S.V.) at 1412 cm^{-1} and 1493 cm^{-1}, and C=O stretching at 1650 cm^{-1} [51-55]. Identification of peaks relating to the formation of carbamate bonds between PEEK-OH and PMPI was made, but was difficult due to peak overlapping [56-58]. COO^- and C=O stretching modes expected at 1600 cm^{-1} and 1650 cm^{-1} respectively are overlapped by peaks relating to C=C and C=O stretching due to the structure of PEEK. However, peaks due to C-N stretching are found at 1220 cm^{-1} and 1703 cm^{-1}. Additionally, N-H stretching peaks are located at 1550 cm^{-1} and 3370 cm^{-1}. Peaks at 1495 cm^{-1} and 2194 cm^{-1} are evident due to NH_3^+ modes. Unreacted N=C=O groups are evidenced by the peak at 2341 cm^{-1}. Minimal evidence of –OH stretching bands in the region between 3200 cm^{-1} and 3550 cm^{-1} also indicates the formation of carbamate bonds as hydroxyls upon PEEK-OH are used up in the formation of these bonds.

SEM micrographs further evidenced the success of the linking procedure. Figure 4a shows that HA-SH particulates are in the approximate size range of between 25 μm and 50 μm in diameter and furthermore possess textured surfaces and sharp interfaces. Particles of PEEK-OH were between 10 μm and 30 μm in diameter, and possessed smooth surfaces (Figures 4b). HA-SH and PEEK-OH powder particulates do not appear to interact strongly when mixed (Figure 4c). Mixing alone therefore does not appear to facilitate interactions between the dissimilar phases. After chemical linking with PMPI however, the resulting HA_L_PEEK appears to consist of agglomerates of both powders (Figure 4d). Larger HA-SH particles appear to act as a substrate for bonding interactions with PEEK-OH particles, made possible through the chemical linking procedure. This is also consistent with our experimental method, whereby the maleimide groups of PMPI firstly react with the –SH groups of

HA-SH, allowing the then presented isocyanate groups of the linker to react with the –OH groups of PEEK-OH following its addition to the reaction mixture.

Characterisation of PEEK, HA_PEEK and HA_L_PEEK composites. Physical properties of the composites were gauged from the results of 3-point bend testing, the set-up of which is shown in Figure 5a and Figure S1. Load displacement curves acquired for PEEK and PEEK composites show that PEEK specimens underwent ductile failure without fracture, and demonstrated plastic deformation at extension beyond the elastic region (Figure 5b). All of the PEEK specimens remained whole after testing. Both HA_PEEK and HA_L_PEEK specimens containing 2.5 wt% HA content underwent brittle failure immediately following elastic deformation, resulting in test specimens snapping (Figure 5b).

PEEK exhibited a flexural strength of 201.2±8.3 MPa, which was significantly greater that the flexural strength of HA_PEEK and HA_L_PEEK being 170.7±5.4 MPa ($p < 0.001$) and 171.7±14.8 MPa ($p < 0.001$) respectively (Figure 5c). Importantly, chemical linking provides HA_L_PEEK with a slightly greater flexural strength, although this was not found to be significant ($p = 0.851$), presumably due to the due of variation of the results expected from brittle failure. The flexural modulus of PEEK was 5.3±0.3 GPa (Figure 5d). Interestingly, there was no statistical difference between PEEK and HA_L_PEEK materials in terms of flexural modulus, the former possessing a value of 5.0±0.3 GPa ($p = 0.127$). However, the flexural modulus of HA_PEEK was significantly lower in comparision to PEEK ($p = 0.026$). Therefore, HA_L_PEEK substantially improved upon HA_PEEK in terms of flexural modulus.

The linking chemistry possessed by HA_L_PEEK may facilitate the improvement to both flexural strength and flexural modulus compared to HA_PEEK

through the provision of enhanced interfacial interactions between HA and PEEK components that is greater than mechanical interlocking alone. Analysis of the linking chemistry after fabrication of prototype composites was undertaken by comparing elemental maps of HA inclusions within HA_PEEK and HA_L_PEEK materials. The main elemental constituents of the HA inclusions were expectedly calcium (Ca) and phosphorous (P) as indicated by Kα signals at 3.7 KeV and 2.0 KeV respectively (Figure 6a-b). Elemental silicon (Si) was also detected in HA_L_PEEK by a peak at 1.75 keV, but was absent in HA_PEEK (Figure 6c). The silicon signal originates from the presence of the MPTES molecules grafted to HA as part of chemical linking formulation. Mapping of the Ca Kα and P Kα signals show that elemental Ca and P are localised to the HA particulates in both composites (Figure 6d). During processing, harsh temperatures and mobile PEEK chains during melt are most likely to disrupt and distribute components of the linking chemistry throughout the wider polymeric matrix. Given that the Si content of HA_L_ PEEK remains localised to HA particulates, it can be taken as evidence that the chemical linking chemistry remains intact during the processing of composites to provide enhanced interactions between HA and PEEK (Figure 6e). Additionally, DSC data acquired for HA_PEEK and HA_L_PEEK loaded with 5-50 wt% HA content suggests that increased levels of HA lower the re-crystallisation temperature, a trend which is further pronounced regarding HA_L_PEEK composites, which may be due to the covalent bonding between HA and PEEK in this system (Figure S4).

Firstly, we consider that the established chemical interactions appear to lessen the development of HA debonding as well as the formation of micro-cracks (Figure 7a-c). Pre-existing microcracks can promote crack initiation, leading to premature failure of materials under load [59]. Although PEEK contains some surface

imperfections, HA inclusions within HA_PEEK surfaces appear to promote micro cracks spanning several 10's of microns (Figure 7 a, b). In contrast, HA inclusions visible on the surface of HA_L_PEEK were not associated with any visible debonding from the polymer matrix or crack development prior to mechanical testing (Figure 7c).

Secondly, mechanical failure of these composites is partly dependent on the presence of flaws within the brittle HA component, as well as the HA particulates themselves. Similar to other ceramics, HA is a relatively stiff material that when introduced to a polymeric matrix can provide the resulting composite with an enhanced modulus [21, 60]. However, these gains are dependent on both loading level and the nature of the filler particulates [29, 60]. Lower levels of loading are generally favoured using both micro- and nano- scale particulates, as filler agglomeration that occurs at high loading levels, can reduce the gains in mechanical properties [26, 29, 60, 61]. This is because as particulate inclusions become smaller, they are less liable to contain flaws or act as a flaw themselves [59, 60, 62, 63]. Griffith's law states that the stress concentration at the tip of a defect depends on the defects size [62, 63]. Thus, the combined stress concentration will be greater for and within larger HA particulates.

A downside of the chemically linked HA and PEEK additive is that the particle shape and size distribution is difficult to control due to the additive itself existing as an agglomeration of bioceramic and polymeric materials. For instance, HA particulates appear to agglomerate within the polymeric matrix of HA_PEEK and HA_L_PEEK. Important to note, is that the effect is exacerbated to a greater extent in the case of HA_L_PEEK composites (Figure 7d-f). Therefore, the resulting particle size range of HA within HA_PEEK is between 62.5 µm to 219 µm, and between 125 µm to 1219 µm within HA_L_PEEK. It is therefore evident that the linking chemistry

is effective at maintaining mechanical properties of composite possessing larger inclusions, considering that there is no significant difference in flexural modulus between PEEK and HA_L_PEEK materials, whilst the properties of HA_PEEK are significantly lessened despite HA_L_PEEK containing larger particulates. Chemical linking interactions appear to advantageously improve load transfer between HA and PEEK phases as to arrest crack growth and propagation at the interface, benefiting the ability of HA_L_PEEK to resist failure under load by increasing fracture energy [20, 21, 30]. Comparatively poorer mechanical locking interactions present in HA_PEEK likely promotes brittle failure at lower force loadings due to the high stiffness possessed by HA not effectively being transferred to the surrounding polymeric matrix, reducing regions of ductile flow about bioceramic irregularities [20, 21, 30].

Further work will look to reduce inclusion particle size, lessen agglomeration, increase the range of HA loadings and assess *in vitro* cytotoxicity in order to realize further advantages of chemically linking additive and polymeric phases within medically relevant materials. Ideally, smooth nano-scale spherical particulates should be introduced to both improve increase the surface area of interaction with the matrix in addition to the benefit of chemical linking HA and PEEK [26, 30, 60]. Such particulates will also ensure more homogeneous distribution of fillers, reducing the variation between localized areas of composition and ultimately allow higher loadings of HA to be included for purposed of enhancing bone ongrowth. We intend the materials chemistries generated herein may serve as a stepping-stone toward a composite system that can be adjusted both in terms of physical properties and osteogenic performance to be utilized in spinal cage devices.

CONCLUSIONS

We demonstrate formulation of a PEEK composite containing HA particulates that are chemically linked to the polymeric matrix. Chemical linking HA and PEEK facilitates significant improvements to the mechanical properties of HA_L_PEEK over HA_PEEK at equivalent 2.5 wt% HA loading, despite the former possessing larger inclusions of HA due to agglomeration effects. The mechanism by which these gains are constituted is three-fold:

1) Lessening HA particle debonding - HA particles that are chemically linked to PEEK are fully integrated within the polymeric matrix and show no evidence of delamination at the filler to matrix boundary.

2) Lessening the development of microcracks - The development of microcracks in the vicinity of HA inclusions within HA_L_PEEK is limited. In comparison, microcracks of 10's of microns in length are present on the surface of HA_PEEK emanating from exposed HA.

3) Facilitating enhanced load transfer between phases – The flexural strength and flexural modulus of HA_L_PEEK is enhanced compared to HA_PEEK due to the enhanced transfer of stiffness between bioceramic and polymeric phases, which improves the ductile flow of the material.

Advantages of HA_L_PEEK composites may be further improved over conventional HA_PEEK systems by facilitating homogeneous distribution of filler and lowering the degree of additive agglomeration. This may potentially allow for greater loadings of HA within PEEK suitable for next generation PEEK based spinal fusion devices that can out perform metallic alternatives (i.e. Ti-6Al-4V) in terms of

fusion capacity, whilst avoiding additive particle debonding and diminishment of mechanical properties that currently hamper HA and PEEK composite systems.

ASSOCIATED CONTENT

Supporting Information

Specimen dimensions and 3-point bend testing set-up (Figure S1)

Explanation of PEEK-OH derivative chirality as a contributing factor to the distruption of crystallite formation (Figure S2)

Effect of reaction time on HD of PEEK-OH derivatives (Figure S3)

DSC data acquired for HA_PEEK and HA_L_PEEK loaded with 5-50 wt% HA as evidence of covalent linking between HA and PEEK phases (Figure S4)

AUTHOR INFORMATION

Corresponding author

*Email: l.m.grover@bham.ac.uk

Notes

The authors declare no competing financial interest.

ACKNOWLEDMENTS

We would like to thank the EPSRC for funding the work in association zwith industrial sponsors TWI Ltd (Project number 1294393 - Medical Materials). We are spectroscopy and XRD data. SEM was undertaken with the help of Jianguo Liu in the School of Dentistry at the University of Birmingham. We also wish to extend thanks to the team at TRS Engineering located in Bloxwich (West Midlands, UK) for cutting out the composite specimens.

REFERENCES

1. Shukla, D.; Negi, Y. S.; Uppadhyaya, J. S.; Kumar, V., Synthesis and Modification of Poly(ether ether ketone) and their Properties: A Review. *Polymer Reviews* **2012,** 52, (2), 189-228.

2. Kurtz, S. M.; Devine, J. N., PEEK Biomaterials In Trauma, Orthopedic, And Spinal Implants. *Biomaterials* **2007,** 28, (32), 4845-4869.

3. Kurtz, S. M., Chapter 1 - An Overview of PEEK Biomaterials. In *PEEK Biomaterials Handbook*, Kurtz, S. M., Ed. William Andrew Publishing: Oxford, 2012; pp 1-7.

4. Bagby, G. W., Arthrodesis by the distraction-compression method using stainless steel implant. *Orthopedics* **1988,** 11, (6), 931-934.

5. Ferguson, S.; Visser, J. A.; Polikeit, A., The long-term mechanical integrity of non-reinforced PEEK-OPTIMA polymer for demanding spinal applications: experimental and finite-element analysis. *Eur Spine J* **2006,** 15, (2), 149-156.

6. Mastronardi, L.; Ducati, A.; Ferrante, L., Anterior cervical fusion with polyetheretherketone (PEEK) cages in the treatment of degenerative disc disease. Preliminary observations in 36 consecutive cases with a minimum 12-month follow-up. *Acta neurochirurgica* **2006,** 148, (3), 307-312; discussion 312.

7. Ni, J.; Zheng, Y.; Liu, N.; Wang, X.; Fang, X.; Phukan, R.; Wood, K. B., Radiological evaluation of anterior lumbar fusion using PEEK cages with adjacent vertebral autograft in spinal deformity long fusion surgeries. *Eur Spine J* **2015,** 24, (4), 791-799.

8. Wu, S. H.; Li, Y.; Zhang, Y. Q.; Li, X. K.; Yuan, C. F.; Hao, Y. L.; Zhang, Z. Y.; Guo, Z., Porous titanium-6 aluminum-4 vanadium cage has better

osseointegration and less micromotion than a poly-ether-ether-ketone cage in sheep vertebral fusion. *Artificial organs* **2013,** 37, (12), E191-201.

9. Herrera, A.; Yanez, A.; Martel, O.; Afonso, H.; Monopoli, D., Computational study and experimental validation of porous structures fabricated by electron beam melting: A challenge to avoid stress shielding. *Materials science & engineering. C, Materials for biological applications* **2014,** 45, 89-93.

10. Cabraja, M.; Oezdemir, S.; Koeppen, D.; Kroppenstedt, S., Anterior cervical discectomy and fusion: Comparison of titanium and polyetheretherketone cages. *BMC Musculoskeletal Disorders* **2012,** 13, (1), 172.

11. Chen, Y.; Wang, X.; Lu, X.; Yang, L.; Yang, H.; Yuan, W.; Chen, D., Comparison of titanium and polyetheretherketone (PEEK) cages in the surgical treatment of multilevel cervical spondylotic myelopathy: a prospective, randomized, control study with over 7-year follow-up. *Eur Spine J* **2013,** 22, (7), 1539-1546.

12. Nemoto, O.; Asazuma, T.; Yato, Y.; Imabayashi, H.; Yasuoka, H.; Fujikawa, A., Comparison of fusion rates following transforaminal lumbar interbody fusion using polyetheretherketone cages or titanium cages with transpedicular instrumentation. *Eur Spine J* **2014,** 23, (10), 2150-2155.

13. Almasi, D.; Iqbal, N.; Sadeghi, M.; Sudin, I.; Abdul Kadir, M. R.; Kamarul, T., Preparation Methods for Improving PEEK's Bioactivity for Orthopedic and Dental Application: A Review. *International journal of biomaterials* **2016,** 2016, 8202653.

14. Zhao, M.; Li, H.; Liu, X.; Wei, J.; Ji, J.; Yang, S.; Hu, Z.; Wei, S., Response of Human Osteoblast to n-HA/PEEK--Quantitative Proteomic Study of Bio-effects of Nano-Hydroxyapatite Composite. *Sci Rep* **2016,** 6, 22832.

15. Williams, D. F., On the mechanisms of biocompatibility. *Biomaterials* **2008,** 29, (20), 2941-2953.

16. Evans, N. T.; Torstrick, F. B.; Lee, C. S.; Dupont, K. M.; Safranski, D. L.; Chang, W. A.; Macedo, A. E.; Lin, A. S.; Boothby, J. M.; Whittingslow, D. C.; Carson, R. A.; Guldberg, R. E.; Gall, K., High-strength, surface-porous polyether-ether-ketone for load-bearing orthopedic implants. *Acta biomaterialia* **2015,** 13, 159-167.

17. Ma, R.; Weng, L.; Bao, X.; Song, S.; Zhang, Y., In Vivo Biocompatibility and Bioactivity of In Situ Synthesized Hydroxyapatite/Polyetheretherketone Composite Materials. **2013,** 127, (4), 2581-2587.

18. Ma, R.; Tang, T., Current strategies to improve the bioactivity of PEEK. *Int J Mol Sci* **2014,** 15, (4), 5426-5445.

19. Green, S., Chapter 3 - Compounds and Composite Materials. In *PEEK Biomaterials Handbook*, Kurtz, S. M., Ed. William Andrew Publishing: Oxford, 2012; pp 23-48.

20. Wang, L.; Weng, L.; Song, S.; Sun, Q., Mechanical properties and microstructure of polyetheretherketone–hydroxyapatite nanocomposite materials. *Materials Letters* **2010,** 64, (20), 2201-2204.

21. Abu Bakar, M. S.; Cheng, M. H. W.; Tang, S. M.; Yu, S. C.; Liao, K.; Tan, C. T.; Khor, K. A.; Cheang, P., Tensile properties, tension–tension fatigue and biological response of polyetheretherketone–hydroxyapatite composites for load-bearing orthopedic implants. *Biomaterials* **2003,** 24, (13), 2245-2250.

22. Lee, J. H.; Jang, H. L.; Lee, K. M.; Baek, H. R.; Jin, K.; Hong, K. S.; Noh, J. H.; Lee, H. K., In vitro and in vivo evaluation of the bioactivity of hydroxyapatite-coated polyetheretherketone biocomposites created by cold spray technology. *Acta biomaterialia* **2013,** 9, (4), 6177-6187.

23. Barkarmo, S.; Andersson, M.; Currie, F.; Kjellin, P.; Jimbo, R.; Johansson, C. B.; Stenport, V., Enhanced bone healing around nanohydroxyapatite-coated polyetheretherketone implants: An experimental study in rabbit bone. *Journal of Biomaterials Applications* **2014,** 29, (5), 737-747.

24. Johansson, P.; Jimbo, R.; Kozai, Y.; Sakurai, T.; Kjellin, P.; Currie, F.; Wennerberg, A., Nanosized Hydroxyapatite Coating on PEEK Implants Enhances Early Bone Formation: A Histological and Three-Dimensional Investigation in Rabbit Bone. *Materials* **2015,** 8, (7), 3815-3830.

25. Landy, B. C.; VanGordon, S. B.; McFetridge, P. S.; Sikavitsas, V. I.; Jarman-Smith, M., Mechanical and in vitro investigation of a porous PEEK foam for medical device implants. *J Appl Biomater Funct Mater* **2013,** 11, (1), 35-44.

26. Wang, L.; Weng, L.; Song, S.; Zhang, Z.; Tian, S.; Ma, R., Characterization of polyetheretherketone–hydroxyapatite nanocomposite materials. *Materials Science and Engineering: A* **2011,** 528, (10-11), 3689-3696.

27. Invibio, Invibio Biomaterial Solutions Announces Global Launch of “PEEK-OPTIMA HA Enhanced Polymer” - A new PEEK-based biomaterial designed for superior bone apposition. In Online, 2013.

28. Walsh, W. R.; Pelletier, M. H.; Bertollo, N.; Christou, C.; Tan, C., Does PEEK/HA Enhance Bone Formation Compared With PEEK in a Sheep Cervical Fusion Model? *Clin Orthop Relat Res* **2016,** 474, (11), 2364-2372.

29. Michler, G. H.; von Schmeling, H.-H. K.-B., The physics and micro-mechanics of nano-voids and nano-particles in polymer combinations. *Polymer* **2013,** 54, (13), 3131-3144.

30. Kuo, M. C.; Tsai, C. M.; Huang, J. C.; Chen, M., PEEK composites reinforced by nano-sized SiO2 and Al2O3 particulates. *Materials Chemistry and Physics* **2005,** 90, (1), 185-195.

31. Sousa, R. A.; Reis, R. L.; Cunha, A. M.; Bevis, M. J., Coupling of HDPE/hydroxyapatite composites by silane-based methodologies. *Materials in medicine* **2003,** 14, 475-487.

32. Ma, R.; Li, Q.; Wang, L.; Zhang, X.; Fang, L.; Luo, Z.; Xue, B.; Ma, L., Mechanical properties and in vivo study of modified-hydroxyapatite/polyetheretherketone biocomposites. *Materials science & engineering. C, Materials for biological applications* **2017,** 73, 429-439.

33. Díez-Pascual, A. M.; Martínez, G.; Martínez, M. T.; Gómez, M. A., Novel nanocomposites reinforced with hydroxylated poly(ether ether ketone)-grafted carbon nanotubes. *Journal of Materials Chemistry* **2010,** 20, (38), 8247.

34. Díez-Pascual, A. M.; Martínez, G.; González-Domínguez, J. M.; Ansón, A.; Martínez, M. T.; Gómez, M. A., Grafting of a hydroxylated poly(ether ether ketone) to the surface of single-walled carbon nanotubes. *Journal of Materials Chemistry* **2010,** 20, (38), 8285.

35. Williams, R. L.; Hadley, M. J.; Jiang, P. J.; Rowson, N. A.; Mendes, P. M.; Rappoport, J. Z.; Grover, L. M., Thiol modification of silicon-substituted hydroxyapatite nanocrystals facilitates fluorescent labelling and visualisation of cellular internalisation. *Journal of Materials Chemistry B* **2013,** 1, (35), 4370-4378.

36. Savard, S.; Blanchard, L. P.; Léonard, J.; Prud'homme, R. E., Hydrolysis and condensation of silanes in aqueous solutions. *Polymer Composites* **1984,** 5, (4), 242-249.

37. Markovic, M.; Fowler, B. O.; Tung, M. S., Preparation and Comprehensive Characterization of a Calcium Hydroxyapatite Reference Material. *Journal of Research of the National Institute of Standards and Technology* **2004,** 109, (6), 553-568.

38. Ciobanu, C. S.; Iconaru, S. L.; Le Coustumer, P.; Predoi, D., Vibrational Investigations of Silver-Doped Hydroxyapatite with Antibacterial Properties. *Journal of Spectroscopy* **2013,** 2013, 1-5.

39. Khan, A. F.; Awais, M.; Khan, A. S.; Tabassum, S.; Chaudhry, A. A.; Rehman, I. U., Raman Spectroscopy of Natural Bone and Synthetic Apatites. *Applied Spectroscopy Reviews* **2013,** 48, (4), 329-355.

40. Esmonde-White, K.; Esmonde-White, F., Raman spectroscopy in biomineralization. In *Biomineralization Sourcebook: Characterization of Biominerals and Biomimetic Materials*, DiMasi, E.; Gower, L. B., Eds. CRC: 2014.

41. Koutsopoulos, S., Synthesis and characterization of hydroxyapatite crystals: A review study on the analytical methods. *Journal of Biomedical Materials Research* **2002,** 62, (4), 600-612.

42. Wang, S.; Wen, S.; Shen, M.; Guo, R.; Cao, X.; Wang, J.; Shi, X., Aminopropyltriethoxysilane-mediated surface functionalization of hydroxyapatite nanoparticles: synthesis, characterization, and in vitro toxicity assay. *International journal of nanomedicine* **2011,** 6, 3449-3459.

43. de Campos, R. P.; Yoshida, I. V.; Breitkreitz, M. C.; Poppi, R. J.; Fracassi da Silva, J. A., Raman imaging spectroscopic characterization of modified poly(dimethylsiloxane) for micro total analysis systems applications. *Spectrochim Acta A Mol Biomol Spectrosc* **2013,** 100, 67-71.

44. Schmitt, M., Analysis of silanes and of siloxanes formation by Raman spectroscopy. *RSC Advances* **2014,** 4, (4), 1907-1917.

45. Kim, D.; Dhand, V.; Rhee, K.; Park, S.-J., Study on the Effect of Silanization and Improvement in the Tensile Behavior of Graphene-Chitosan-Composite. *Polymers* **2015,** 7, (3), 527-551.

46. Díez-Pascual, A. M.; Martínez, G.; Gómez, M. n. A., Synthesis and Characterization of Poly(ether ether ketone) Derivatives Obtained by Carbonyl Reduction. *Macromolecules* **2009,** 42, (18), 6885-6892.

47. Conceicao, T. F.; Bertolino, J. R.; Barra, G. M. O.; Mireski, S. L.; Joussef, A. C.; Pires, T. N., Preparation and Characterization of Poly(Ether Ether Ketone) Derivatives. *J. Braz. Chem. Soc.* **2008,** 19, (1), 111-116.

48. Naffakh, M.; Ellis, G.; Gómez, M. A.; Marco, C., Thermal decomposition of technological polymer blends 1. Poly(aryl ether ether ketone) with a thermotropic liquid crystalline polymer. *Polymer Degradation and Stability* **1999,** 66, 405-413.

49. Molnár, G.; Botvay, A.; Pöppl, L.; Torkos, K.; Borossay, J.; Máthé, Á.; Török, T., Thermal degradation of chemically modified polysulfones. *Polymer Degradation and Stability* **2005,** 89, (3), 410-417.

50. Rao, C. N. R.; Venkataraghavan, R.; Kasturi, T. R., Contribution to the Infrared Spectra of Organosulphur Compounds. *Canadian Journal of Chemistry* **1964,** 42, 36-42.

51. Ellis, G.; Naffakh, M.; Marco, C.; Hendra, P. J., Fourier transform Raman spectroscopy in the study of technological polymers Part 1: poly(aryl ether ketones), their composites and blends. *Spectrochima Acta Part A* **1997,** 53, 2279-2294.

52. Lv, M.; Wang, Y.; Wang, Q.; Wang, T.; Liang, Y., Effects of individual and sequential irradiation with atomic oxygen and protons on the surface structure and

tribological performance of polyetheretherketone in a simulated space environment. *RSC Advances* **2015,** 5, (101), 83065-83073.

53. Al Lafi, A. G., The sulfonation of poly(ether ether ketone) as investigated by two-dimensional FTIR correlation spectroscopy. *Journal of Applied Polymer Science* **2015,** 132, (2).

54. Henneuse, C.; Goret, B.; Marchand-Brynaert, J., Surface carboxylation of PEEK film by selective wet-chemistry. *Polymer* **1998,** 39, (4), 835-844.

55. Henneuse, C.; Boxus, T.; Duliere, E.; Pringalle, C.; Tesolin, L.; Adriaensen, Y.; Marchand-Brynaert, J., Surface amination of PEEK film by selective wet-chemistry. *Polymer* **1998,** 39, (22), 5359-5369.

56. Mioč, U. B.; Ribnikar, S. V., Carbamates of the Lower Aliphatic Amines in Aprotic Solvents. I. Vibrational Spectra *Bulletin de la Société chimique Beograd* **1978,** 43, (9), 603-612.

57. Chen, G. C.; Rowell, M.; Ellis, W. D., Fungal Resistance of Southern Pine Impregnated with Methyl Fluorophenyl Carbamates or Reacted with Fluorophenyl Isocyanates. *Wood and Fiber Science* **1990,** 22, (2), 165-172.

58. Robinson, K.; McCluskey, A.; Attalla, M. I., An ATR-FTIR study on the effect of molecular structural variations on the CO2 absorption characteristics of heterocyclic amines, part II. *Chemphyschem* **2012,** 13, (9), 2331-2341.

59. Loughran, G. M.; Versluis, A.; Douglas, W. H., Evaluation of sub-critical fatigue crack propagation in a restorative composite. *Dent Mater* **2005,** 21, (3), 252-261.

60. Rodrigues Jr., S. A.; Zanchi, C. H.; de Carvalho, R. V.; Demarco, F. F., Flexural strength and modulus of elasticity of different types of resin-based composites. *Braz Oral Res* **2007,** 21, (1), 16-21.

61. Parvaiz, M. R.; Mohanty, S.; Nayak, S. K.; Mahanwar, P. A., Polyetheretherketone (PEEK) Composites Reinforced with Fly Ash and Mica. *Journal of Minerals and Materials Characterization and Engineering* **2010,** 9, (1), 25-41.

62. Launey, M. E.; Ritchie, R. O., On the Fracture Toughness of Advanced Materials. *Advanced Materials* **2009,** 21, (20), 2103-2110.

63. Gao, H.; Ji, B.; Jager, I. L.; Arzt, E.; Fratzl, P., Materials become insensitive to flaws at nanoscale: lessons from nature. *Proc Natl Acad Sci U S A* **2003,** 100, (10), 5597-5600.

Figures

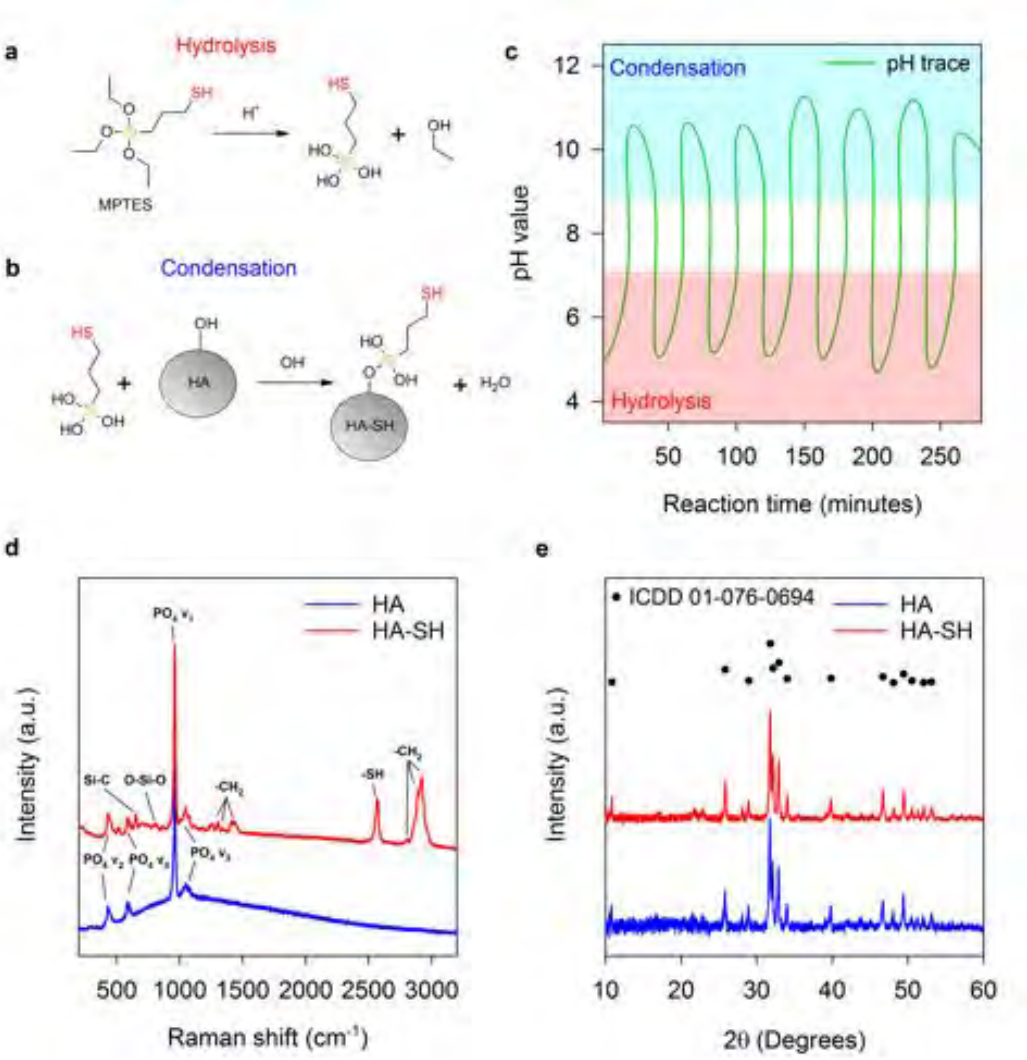

Figure 1. Synthesis of HA-SH: (a) Hydrolysis of MPTES molecules under acidic conditions results in silanol groups about the central silicon atom. (b) Condensation reactions are promoted under alkali conditions, facilitating coupling of MPTES onto the surface of HA via surface presented hydroxyl groups to produce HA-SH. (c) For the modification of HA particulates with MPTES molecules, the pH value was carefully monitored and adjusted over time in order to promote hydrolysis and condensation reactions accordingly. (d) Raman spectra for HA and HA-SH. (e) XRD patterns for HA and HA-SH.

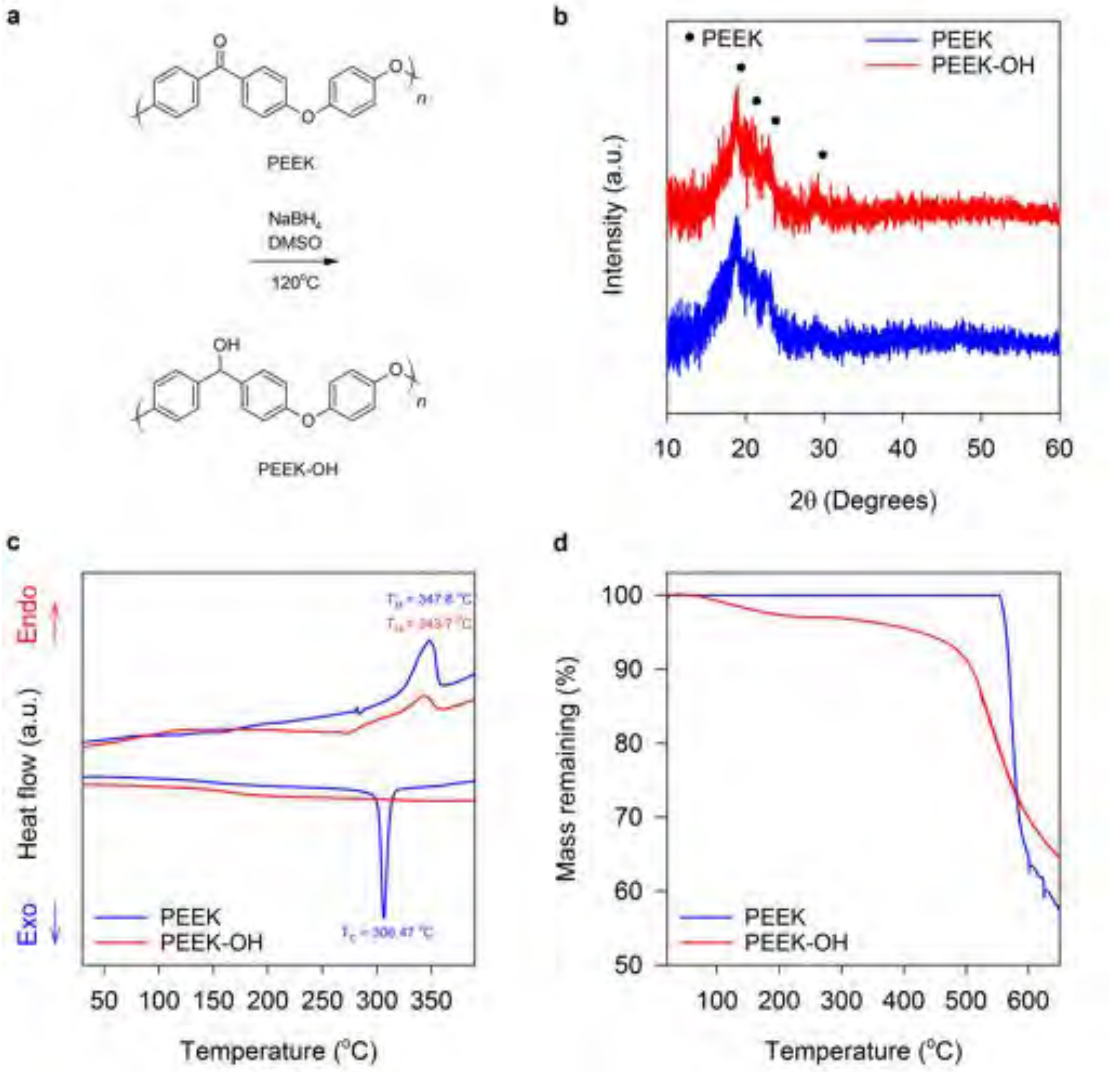

Figure 2. Synthesis of PEEK-OH: (a) Reduction of PEEK with $NaBH_4$ reagent produces PEEK-OH. (b) XRD patterns for PEEK and PEEK-OH. (c) DSC traces for PEEK and PEEK-OH. (d) TGA traces for PEEK and PEEK-OH.

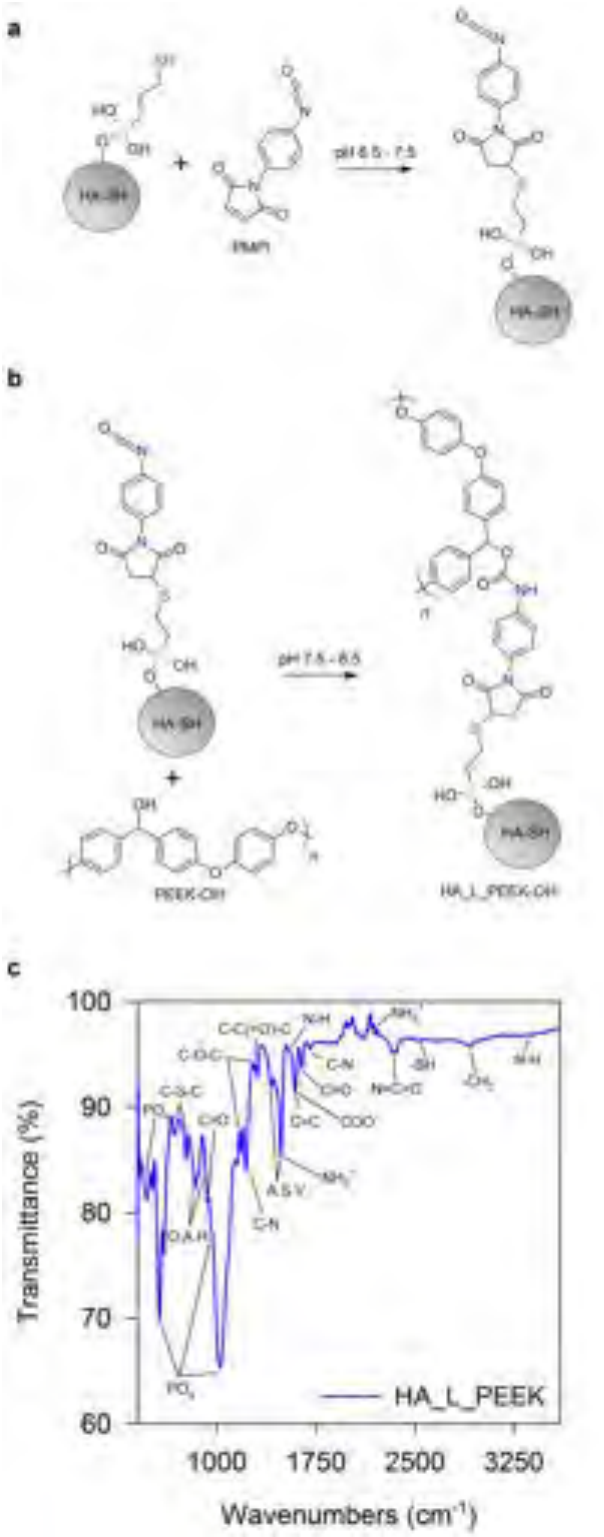

Figure 3. Chemical linking of HA-SH and PEEK-OH: (a) Reaction between thiol groups upon HA-SH and the maleimide terminus of PMPI chemical linker occurs between pH 6.5 - 7.5 to form a thioether (C-S-C) linkage. (b) Reaction between hydroxyl groups upon PEEK-OH and the isocyanate terminus of PMPI chemical

linker occurs between pH 7.5 - 8.5 to form a thioether (C-S-C) linkage. (c) FT-IR spectrum for HA_L_PEEK.

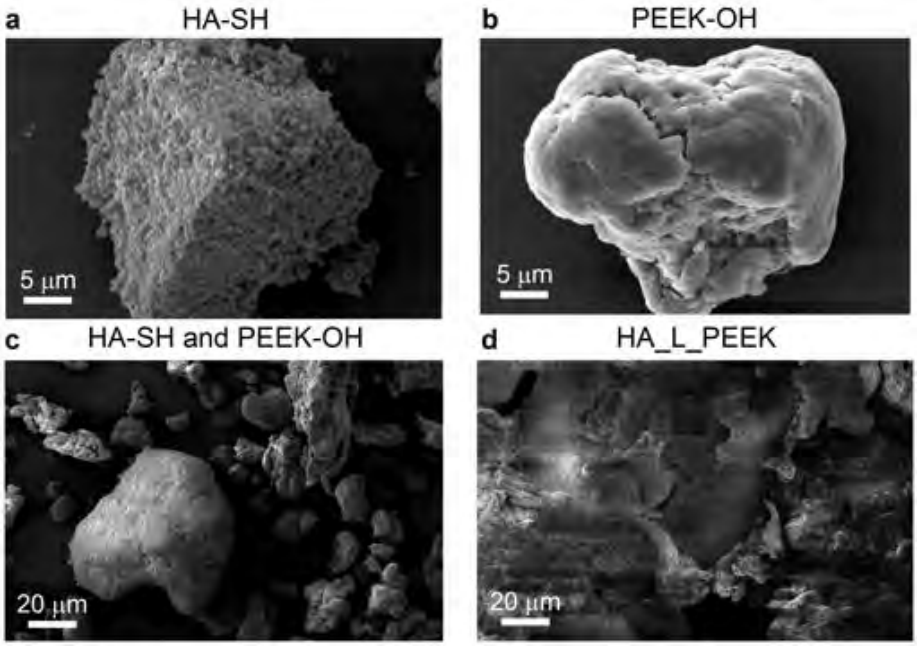

Figure 4. SEM imaging of HA-SH and PEEK-OH particulates: (a) HA-SH. (b) PEEK-OH. (c) Mixed HA-SH and PEEK-OH particulates demonstrating no fundamental interactions exist prior to chemical linking. (d) Chemically linked HA-SH and PEEK-OH (additive material for HA_L_PEEK composites).

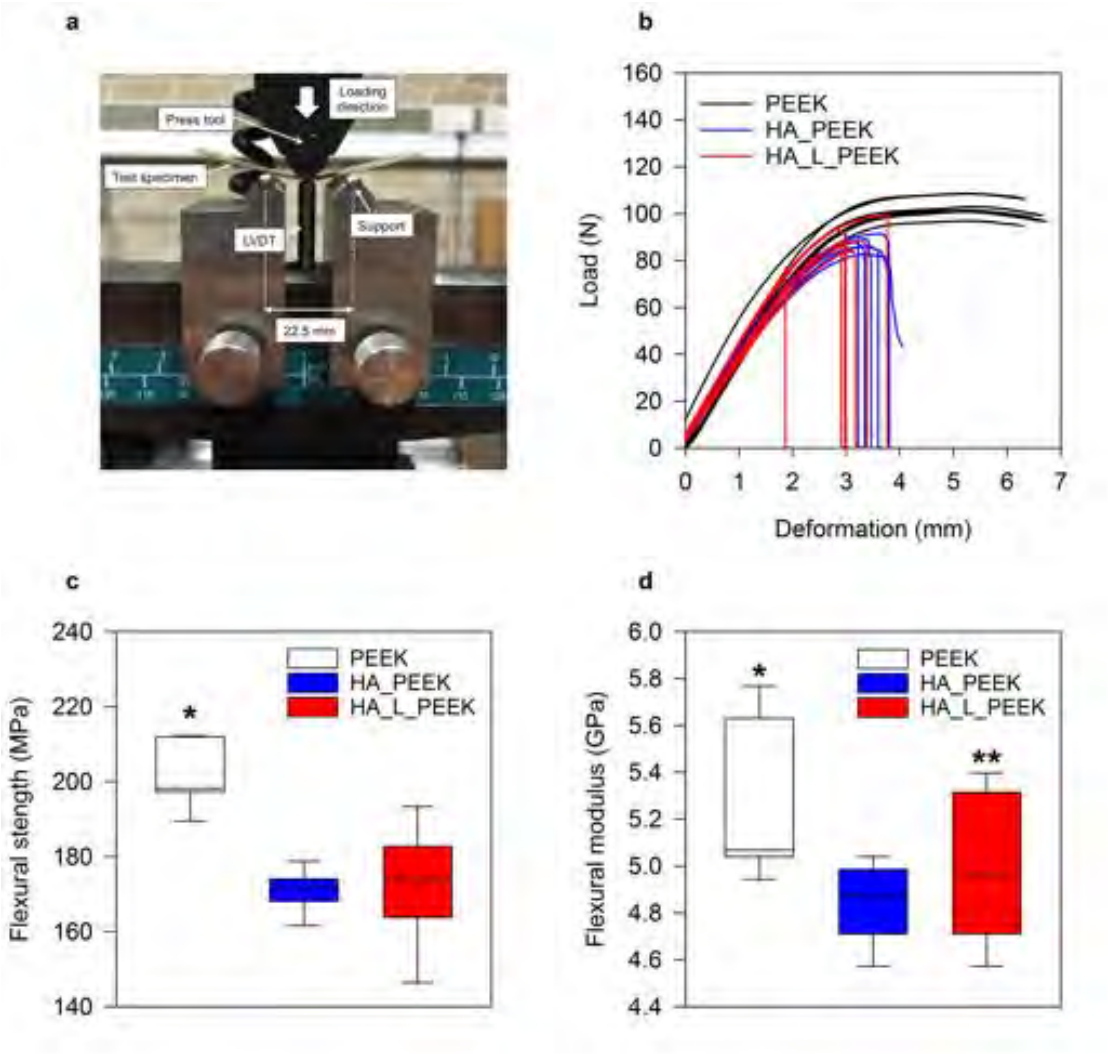

Figure 5. Mechanical testing of prototype PEEK and PEEK composite materials through 3-point bend: (a) 3-point bend test set-up (LVDT = Linear variable Displacement Transducer). (b) Load displacement curves for all groups. (c) Flexural strength box-plot for all groups (* = $p < 0.05$ for PEEK vs. HA_PEEK and for PEEK vs. HA_L_PEEK). (d). Flexural modulus box-plot for all groups (* = $p < 0.05$ for PEEK vs. HA_PEEK, ** = $p > 0.05$ for PEEK vs. HA_L_PEEK).

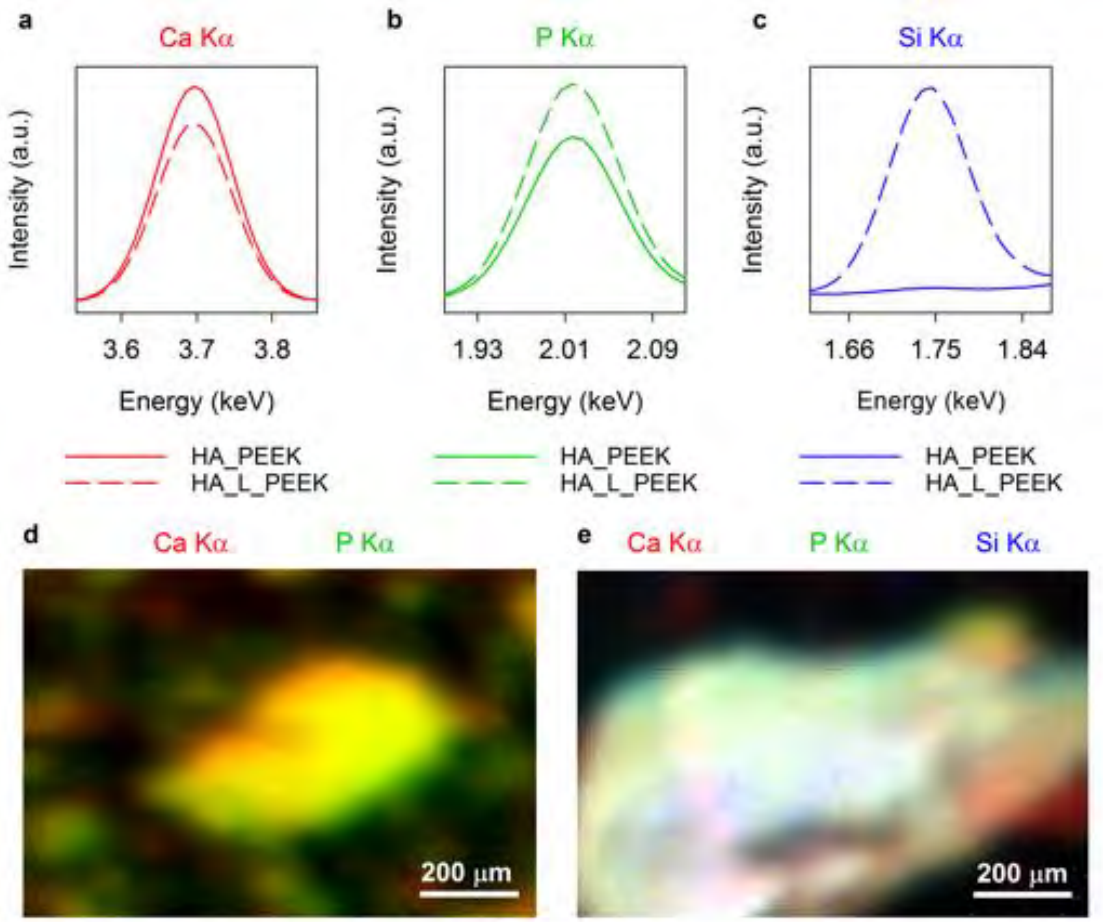

Figure 6. μ-XRF elemental mapping of HA particulates within HA_PEEK and HA_L_PEEK materials following composite fabrication: (a) μ-XRF spectrum central to the Ca Kα signal. (b) μ-XRF spectrum central to the P Kα signal. (c) μ-XRF spectrum central to the Si Kα signal. (d) Elemental map for a fracture surface of HA_L_PEEK with Ca and P Kα channels shown. (e) Elemental map for a fracture surface of HA_L_PEEK with Ca, P and Si Kα channels shown.

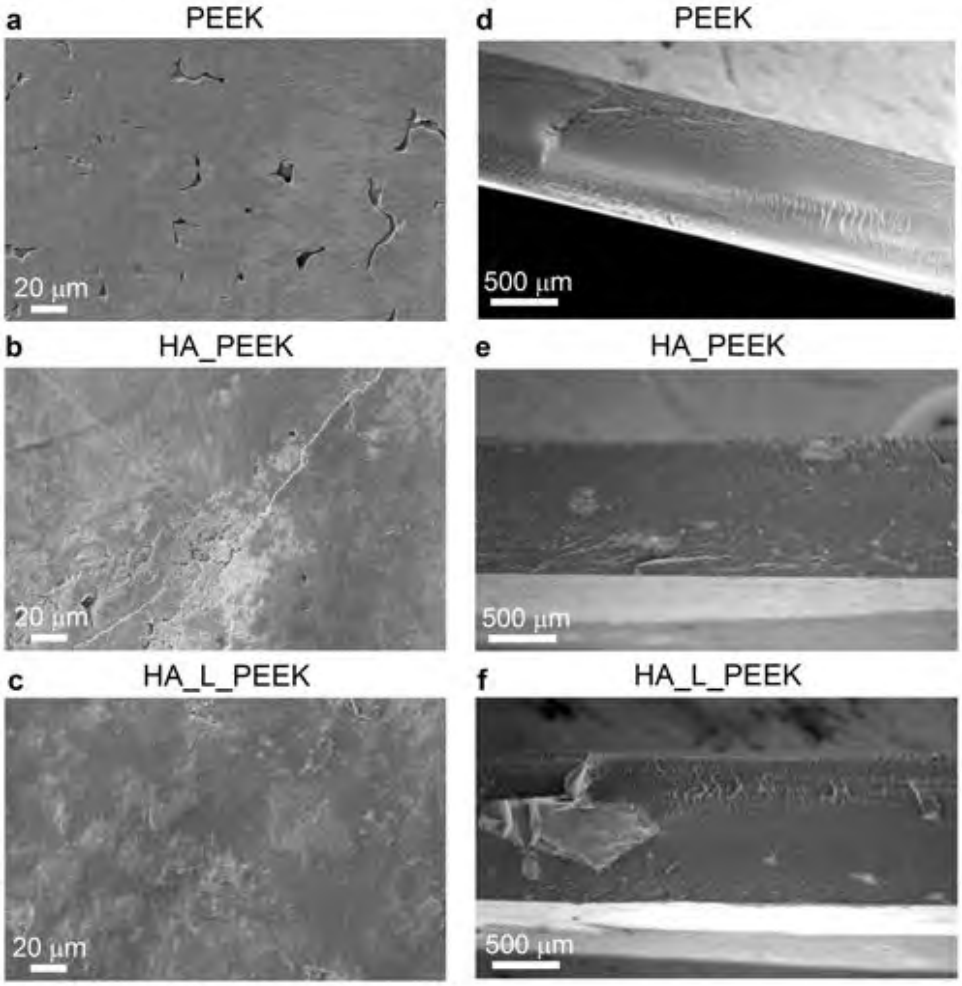

Figure 7. SEM images of PEEK and PEEK composites as manufactured and fracture surfaces: (a) PEEK as manufactured surface. (b) HA_PEEK as manufactured surface. (c) HA_L_PEEK as manufactured surface. (d) PEEK fracture surface. (e) HA_PEEK fracture surface. (f) HA_L_PEEK fracture surface.

TOC image